Wallonia-Europe University Academy
Faculty of sciences
Environmental sciences and management department
BEMS - Building Energy Monitoring and Simulation

Analysis of solar air-conditioning systems and their integration in buildings

Sébastien THOMAS

July 2013

Thesis submitted in fulfilment of the requirements for the degree of
Doctor (Ph.D.) in Sciences (Environmental sciences and management)

Jury members:

President:	Pr. Jean-Marie Hauglustaine (ULg, Belgium)
Supervisor:	Pr. Philippe André (ULg, Belgium)
Co-supervisor:	Dr. Rahal Boussehain (INSA Strasbourg, France)
Members:	Pr. Ursula Eicker (Hochschule für Technik Stuttgart, Germany)
	Pr. Michel Feidt (Université de Lorraine, France)
	Pr. Lieve Helsen (KULeuven, Belgium)
	Pr. Vincent Lemort (ULg, Belgium)
	Pr. Stefan Maas (UNI.LU, Luxembourg)

Abstract

Due to economical and environmental concerns, the energy efficiency of buildings nowadays has proven to play an increasingly important role. To satisfy the occupants comfort, the cooling of buildings generally involves a considerable consumption of electricity. Solar radiation, which is a free and renewable resource, is linked to the cooling needs of buildings.

This work consists in the evaluation, from an energy-saving and economical point of view, of a potential use of solar energy for air-conditioning in residential and office buildings. It includes an integral approach of solar air-conditioning, involving the analysis of the buildings cooling needs, the cold production devices, the solar collector fields and climates. This analysis is supported by simulations and experimental setups.

The study of solar air-conditioning systems already available on the market or in laboratories reveals their operational principles as well as their main performance indicators. Two main solar cooling paths are investigated: a thermal and a photovoltaic conversion of solar energy. Besides this, the performance of the entire air-conditioning system broadens the question of the energy performance to the interactions between the different parts of the system.

The building thermal loads (heating, cooling, domestic hot water) of some theoretical residential and office buildings are computed in a part of this work dealing with the influence of the comfort model, the building energy performance level and the climate. What comes across through this analysis is that, the location of the buildings put aside, the cooling load is greatly influenced by the envelope thermal performance and the internal gains.

The cooling systems involving absorption or adsorption or vapour compression chiller cooling machines are simulated for the previously defined building cases. The use of solar energy through thermal collectors for heating meets higher primary energy savings than for cooling. In all cases, the thermally driven system achieves a lower energy and economical performance than a vapour compression chiller partially supplied with a photovoltaic field.

Some real scale testing of solar air-conditioning systems was carried out in Arlon (Belgium). A thermally driven adsorption chiller and a vapour compression chiller with a photovoltaic grid-connected field were operated during the cooling season. The measurements made during this experiment and their analysis manage to discover every thermal and electrical energy flows of the systems leading to a new adsorption chiller model. Concerning the comparison with the simulations, the main point of interest is the consumption of electricity dedicated to thermally driven systems, which is two times higher in real scale conditions. The results obtained from the monitoring campaigns corroborate the simulation results about system comparison.

De nos jours, l'utilisation de l'énergie dans les bâtiments joue un rôle important pour des considérations économiques et environnementales. Afin de satisfaire le confort des occupants, le refroidissement des bâtiments implique une consommation d'électricité considérable. Le rayonnement solaire qui est une ressource gratuite et renouvelable est lié aux besoins de froid des bâtiments.

Ce travail concerne l'évaluation énergétique et économique du potentiel d'utilisation de l'énergie solaire afin de climatiser les bâtiments résidentiels ou de bureaux. Une approche intégrée est proposée, elle rassemble l'analyse des besoins des bâtiments, des dispositifs de production de froid, des champs de capteurs solaires et des climats. L'analyse des systèmes de climatisation solaire est alimentée par des simulations et des campagnes de mesures.

La revue bibliographique des systèmes de climatisation solaire sur le marché et au stade laboratoire révèle leurs principes de fonctionnement ainsi que leurs principaux indicateurs de performances. Les deux principaux modes de conversion de l'énergie solaire sont couverts: thermique et photovoltaïque. Par ailleurs, la performance du système de climatisation complet étend la notion de performance aux interactions entre ses différentes parties.

Les besoins (chaleur, froid, eau chaude sanitaire) de bâtiments théoriques (résidentiels et de bureaux) sont calculés. Ce travail présente l'influence du modèle de confort sélectionné, du niveau de performance énergétique du bâtiment ainsi que du climat. Mis à part la région dans laquelle est située le bâtiment, la charge de froid est largement influencée par la performance de l'enveloppe et les gains internes.

Les machines à froid classiques (compression mécanique de vapeur) ainsi que la production de froid par absorption et adsorption sont simulées pour les bâtiments précédemment définis. L'utilisation de l'énergie solaire à travers des panneaux solaires thermiques pour chauffer le bâtiment ou l'eau chaude sanitaire atteint de plus grandes économies d'énergie primaire que si on l'utilise pour refroidir. Dans tout les cas, les systèmes à absorption et adsorption ont une plus faible performance économique et énergétique que les systèmes classiques alimentés partiellement par un champ de capteurs photovoltaïques.

Des tests en conditions réelles ont été menés à Arlon (Belgique). Une machine à adsorption alimentée par des capteurs solaires thermiques ainsi qu'une machine classique combinée à un champ de capteurs photovoltaïque ont fonctionné en période estivale. Les mesures effectuées et leur analyse aboutissent à la dévouverte de tout les flux thermiques et électriques des systèmes. Il en découle un nouveau modèle de machine à adsorption. Concernant la comparaison avec les simulations, le point crucial est la consommation électrique des auxiliaires mesurée qui est deux fois supérieure à celle calculée. Les résultats obtenus dans les diverses campagnes de mesure confirment les résultats obtenus en simulation au sujet de la comparaison des systèmes.

When you're finished changing, you're finished.

Benjamin Franklin,

Acknowledgements

I would like to thank Professor Philippe André for his trust, his inhexaustible optimism and the opportunity he offered to integrate his research team and to start a PhD. He proposed me a new subject for the research team, and left me adequate freedom in my investigations about solar cooling systems. Moreover, he gave me many occasions to broaden my knowledge by taking part to international conferences and trainings in various countries and involving me in many other tasks of the research team.

I am grateful to Lieve Helsen, Stefan Maas and Rahal Boussehain who supervised my work. They also gave me the necessary freedom but they were available for any requested help. I would like to thank them for the remarks improving this document.

This work could not have been completed without my colleagues from the BEMS research team in Arlon. Special thanks to Laurent Collard for the technical support for the numerous experimental works (whatever their complexity). I would also thanks a lot Pierre-Yves Franck for involving me in the very exciting so called *Opal Systems* project. The other members of the *Solar Team*, Samuel Hennaut and Elisabeth Davin were very helpful for many solar energy concerns. Nicolas Pignon, Vincent Dolisy, Julien Minet and Jacques Nicolas solved so many issues related to softwares or statistical analysis. I would also like to thank my colleagues Fabien Claude, Corinne Rogiest, Bertrand Fabry, Youness Ajaji, Gilles Adam, Christophe Cerisier and Julien Carton for their friendship and unconditional support. I am grateful to the administrative staff, Chantal Bartholomé, Liliane Carpentier, Marie-Claire Domasik and Catherine Heyman to have expanded my horizons.

The supervision of students projects consented to assist me in discovering the solar cooling field mysteries. My thanks go to Romain Dubois, Anne-Sophie Bogaert, Mahamadou Dao, Nicolas Deconinck, Jean-François Sosson, Julien Collot and Maria-José Dominguez.

I also wish to thank my family and friends for supporting me in so many ways during the good and hard times. They have boundless capacity of ideas and a great inspiration for me. My special thanks go to Benoît, Emilie, Cécile, Pauline and Sophie for attempting to improve my written English.

Finally, I would like to thank the people, whenether during these six years, never stop to ask technical and more philosophical questions. They reconsidered continuously my way of thinking and made me realized what scientific research is.

Contents

Nomenclature and abbreviations

Symbols

If no other units are mentioned in the text, the following units are used.

A	Collector aperture area $[m^2]$
a_0	Thermal collector optical efficiency $[-]$
a_1	Thermal collector linear heat loss coefficient $[W/(m^2K]$
a_2	Thermal collector quadratic heat loss coefficient $[W/(m^2K^2]$
C	Costs [€]
c_p	Specific heat at constant pressure $[kJ/(kg\,K)]$
$COP_{Carnot\,VCC}$	Carnot Vapour compression chiller coefficient of performance $[-]$
$COP_{el\,chill}$	Thermally driven chiller electrical coefficient of performance $[-]$
$COP_{el\,chill\,pump}$	Electrical coefficient of performance of the thermally driven chiller and its three pumps $[-]$
$COP_{el\,cold\,chill}$	Electrical coefficient of performance of the thermally driven chiller, its three pumps and the rejection device $[-]$
$COP_{elec\,tot}$	Electrical coefficient of performance of the complete thermally driven system $[-]$
COP_{therm}	Thermal coefficient of performance (for thermally driven chillers)$[-]$
COP_{rej}	Rejection device electrical coefficient of performance $[-]$
$COP_{solar\,loop}$	Solar loop electrical coefficient of performance $[-]$
COP_{VCC}	Vapour compression chiller coefficient of performance $[-]$
$CPES$	Cost of primary energy savings [€/kWh]
$E_{elec\,tot}$	Total electricity consumption of the thermally driven system $[kWh]$
$E_{prim\,tot}$	Building primary energy use for heating and cooling $[kWh/m^2]$
$Elec_{red}$	Yearly electricity consumption decrease $[kWh/year]$
f_{sav}	Fraction of energy savings $[-]$
Gas_{red}	Yearly gas consumption decrease $[kWh/year]$
I	Investment cost [€]
I_{tot}	Incident total (beam and diffuse) radiation $[W/m^2]$
i	Annuity factor [%]
i_{elec}	Annual electricity price increase [%]
i_{gas}	Annual gas price increase [%]
k_θ	Incidence angle modifier constant $[-]$
M	Collector effective thermal capacitance $[J/(m^2K)]$
NPV	Net Present Value [€]
Nu	Nusselt number $[-]$
OSR	Only Solar Ratio $[-]$

P_{fan}	Fan power $[W]$
PER	Primary Energy Ratio $[-]$
Pr	Prandtl number $[-]$
Q	Thermal energy $[kWh]$
$\dot{Q}$	Thermal power $[kW]$
$Q_{coll\ yield}$	Solar energy collected per year per collector area $[kWh/(m^2\ year)]$
Q_C	Cold source energy $[kWh]$
Q_M	Rejection energy at medium temperature $[kWh]$
Q_H	Hot source energy $[kWh]$
R	Receipts [€]
Re	Reynolds number $[-]$
$SF_{cooling}$	Solar fraction cooling $[-]$
STR	System thermal ratio $[-]$
T_{amb}	Ambient temperature $[K]$
T_{coll}	Average fluid temperature in thermal collector $[K]$
T_C	Cold source temperature $[K]$
T_M	Rejection temperature $[K]$
T_H	Hot source temperature $[K]$
T_{RM80}	Running mean outside temperature $[^\circ C]$
P_{elec}	Inverter alternating power output $[W]$
W	Vapour compression chiller electrical energy $[kWh]$
W_{aux}	Thermally driven chiller auxiliaries consumption $[kWh]$
δ	Interest rate [%]
ϵ	primary energy factor $[kWh/kWh]$
η_{boiler}	Boiler efficiency $[-]$
$\eta_{cold\ sto}$	Cold water storage efficiency $[-]$
$\eta_{hot\ sto}$	Hot water storage efficiency $[-]$
η_{PV}	Photovoltaic field efficiency $[-]$
$\eta_{PV\ coll}$	Photovoltaic collector efficiency $[-]$
$\eta_{solar\ loop}$	Solar loop efficiency $[-]$
$\eta_{thermal\ collector}$	Solar thermal collector efficiency $[-]$
θ	Incidence angle $[^\circ]$
λ	Inflation related to the harmonized indices of consumer prices [%]
€$_{elec}$	Electricity price [€$/kWh$]
€$_{gas}$	Gas price [€$/kWh$]

Subscripts

boil	Boiler
bui	Building
coll	Collector
DCT	Dry cooling tower
elec	Electricity
gas	Gas
in	Inlet
mean	Mean value on one half-cycle
out	Outlet

p	Photovoltaic collector or field peak power
pe	Primary energy
PV	Photovoltaic system
ref	Reference value
$therm$	Thermally driven system
VCC	Vapour compression chiller

Abbreviations

A-C	Air-Conditioning
ACA	Adaptive Comfort Algorithm
ACM	Absorption or Adsorption Cooling Machine
AHU	Air Handling Unit
ADS	ADSorption cooling machine
CDD	Cooling Degree Day
ClAC	Classical Air-Conditioning
COP	Coefficient Of Performance
DEC	DEsiccant Cooling system
DCT	Dry Cooling Tower
DHW	Domestic Hot Water
ECBCS	Energy Conservation in Buildings and Community Systems
EER	Energy Efficiency Ratio
ESEER	European Seasonal Energy Efficiency Ratio
ETC	Evacuated Tube Collector
FPC	Flat-plate Collector
FRC	FResnel Collector
FREE	FREE floating cooling set point
HDD	Heating Degree Day
HICP	Harmonized Indices of Consumer Prices
IAM	Incidence Angle Modifier
IEA	International Energy Agency
ORC	Organic Rankine Cycle
PMV	Predicted Mean Vote
PPD	Percentage of persons dissatisfied
PTC	Parabolic Trough Collector
PV	PhotoVoltaic
RH	Relative Humidity
RMSE	Root Mean Square Error
SAC	Solar Air-Conditioning
SH	Space Heating
SHC	Solar Heating and Cooling
SPF	Seasonal Performance Factor
TMY	Typical Mean Year
VCC	Vapour Compression Chiller
WCT	Wet Cooling Tower

List of Figures

List of Tables

Introduction

Background

The present energy context is characterized by the imminent end of the era of fossil fuels and the negative environmental impact of their operation. Energy demand growth, local pollution, global climate change... are problems that must be addressed. It seems urgent to reconsider our way of life and design equipments as to minimize their energy use.

Most air-conditioning equipments are electrically driven vapour compression systems. It can be considered that, in the 90's, 15% of the world's electricity is used for refrigeration and cooling (Pridasawas, 2006). The electricity is mainly produced by fossil fuels or nuclear energy also involving negative environmental impact.

For example, the electricity consumption due to air-conditioning in the Brussels-Capital Region in 2004 accounts for 7% (400 GWh) of the total annual electricity use. In this region, 70% of the offices have air-conditioning installation (IBGE, 2006). With 20 million square meters of offices, this represents a consumption of around 30 $kWh/m^2/year$ for air-conditioned areas.

While cooling of buildings seems to be important for occupants' comfort, the electricity consumption reduction must be tackled. Moreover, electricity network failures occur in regions were cooling demand is high. A lower electricity dependent cooling technology could restrain this phenomenon (Henning, 2011).

One possible solution could be thermally driven air-conditioning systems, **cooling space using a heat source**. Depending on the heat source required temperature level, cooling energy can be obtained from a variety of renewable energy sources. The absorption and adsorption chillers as well as desiccant cooling systems open the door to **solar energy exploitation to produce cold**. In addition, the photovoltaic effect enables the electricity production with solar energy.

Solar energy is a free resource, it is the largest renewable energy resource. The solar radiation is generally linked in time to the cooling needs of buildings. One particular asset of solar energy is the coincidence of cooling load and solar energy availability on a yearly basis as well as on a daily basis. This is shown on figure 1 dealing with simulation of an office building in Paris. The daily graph describes a hot summer day.

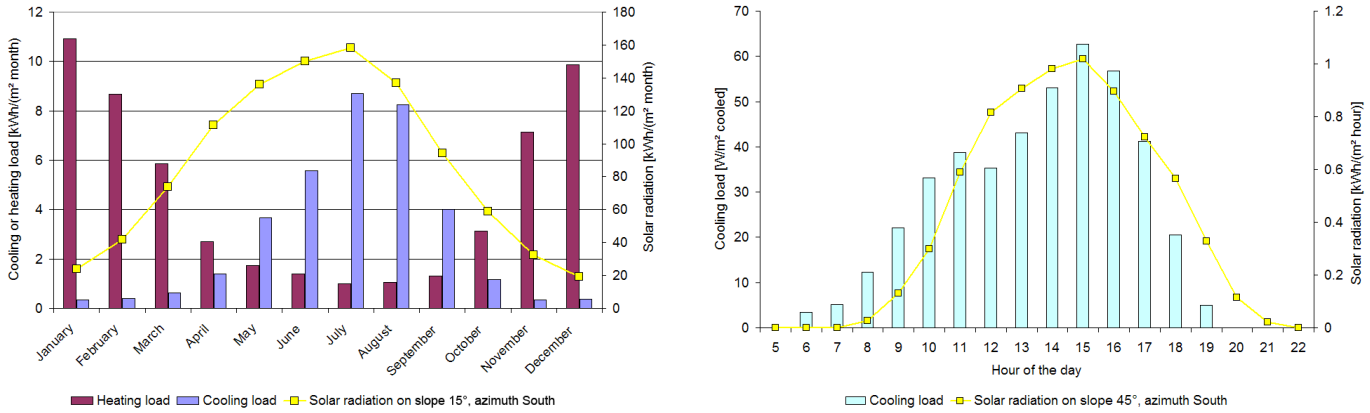

Figure 1: Coincidence of cooling load and solar radiation on a yearly and daily basis for an office building in Paris

Many research projects have been carried out this hot topic. The International Energy Agency inaugurated the *Solar Heating and Cooling* program in 1976. This program is still going on and three recent tasks involve solar air-conditioning. The task 25, *Solar Assisted Air Conditioning of Buildings* was set up in 1999. From 2006 to 2011, the task 38 *Solar air-conditioning and Refrigeration* aimed to implement measures for an accelerated market introduction of solar cooling systems. Recently, in 2011, the task 48 *Quality Assurance and Support Measures for Solar Cooling* was launched. Among its objectives, this project attempts to develop quality requirements targets.

In this work *solar cooling* or *solar air-conditioning of buildings* both describe the same thing: the use of solar energy to maintain comfortable conditions for the occupants of the buildings.

Scope of the thesis

This thesis aims at evaluating, on an energy and economic basis, alternative ways to cool buildings and the possibility to use solar energy for air-conditioning in residential and office building sectors. Several aspects are to be addressed in order to provide an energy-efficient and economically competitive solution. The main physical elements of solar air-conditioning systems are illustrated here below (figure 2). More than the elements themselves, the links between them are crucial to evaluate the global energy performance. As a consequence, the work performed aims to study the links between the various parts of a solar cooling system.

This global objective can be distributed in several specific objectives.

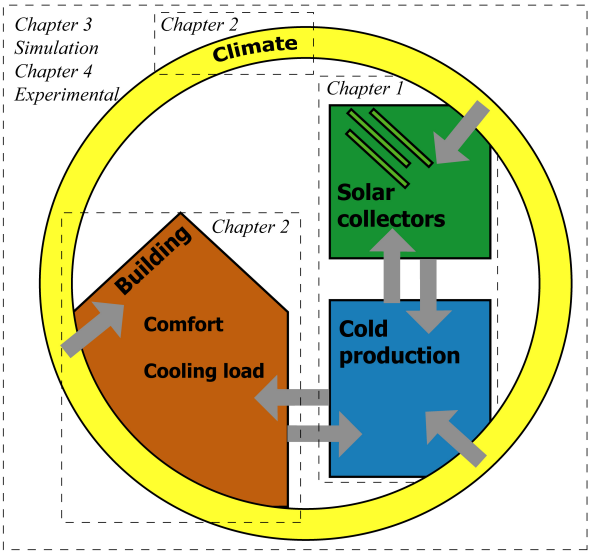

Figure 2: Links between the four elements of solar air-conditioning

- to evaluate the main parameters impacting the cooling load of a building;
- to compute the energy use of buildings containing a solar air-conditioning system. This involves an entire modelling and simulation approach including all the energetic systems (e.g., distribution system, rejection loop, water storages, fans, pumps);
- to evaluate accurately the energy and economical performance of solar cooling systems, namely absorption cooling machine, adsorption cooling machine, combination of vapour compression chiller and photovoltaic field;
- to compare experimental (obtained from an intensive monitoring campaign performed in a laboratory building) and simulation energy performance of the adsorption cooling system and combination of vapour compression chiller and photovoltaic field. This comparison emphasizes the key points to be addressed in solar air-conditioning simulations;

This last objective points out the main concern of current solar air-conditioning field. The recent project of the international energy agency focuses on the solar air-conditioning quality assurance because many systems do not fulfil the expected energy performance. **For two solar air-conditioning systems in real scale operation, the experimental part of this work assesses each heat and electrical energy consumption field to discover the discrepancies between the commonly made assumptions and the measured energy performance.**

Outline of the thesis

Chapter 1 starts with a description of the solar cooling technologies. The theoretical background is presented and the main performance indicators of solar cooling systems are described. The focus is put on market available technologies but other laboratory level technologies are briefly introduced for sake of completeness.

Chapter 2 deals with building cooling load and solar energy availability. The occupant comfort theory is detailed as it is crucial to understand the reason why buildings are cooled. The solar energy availability and the cooling load are analysed in relation to the type of cooled building (residential or office building), the climate, the envelope and internal gains. Both cooling load and solar energy availability characteristics influence the design and performance of solar cooling systems.

In Chapter 3, the entire cooling system is simulated for residential and office building cases. The main elements of the system are deeply investigated. The building is modelled as well as the occupants influence on thermal behaviour: internal gains, light and ventilation requirements, solar protection operation. The solar collector field and cold production with absorption or adsorption chiller, distribution, emission devices are modelled. The performance figures are presented for the different combinations of systems, climates and buildings. In addition to energy performance, the economical viability is evaluated.

Chapter 4 is dedicated to the analysis of the experimental setups installed in a laboratory building. On the one hand, the small scale adsorption chiller is coupled with a solar thermal collector field, a cooling tower, storages and emissions systems. On the other hand, a vapour compression chiller and an on-grid photovoltaic field are in operation in the same laboratory. Both systems are monitored and the energy performances figures are measured on various time scales (10 seconds to one month). A fair comparison of the systems is presented using the common energy indexes and a new one, more appropriate to evaluate the solar conversion quality. Moreover, the adsorption chiller and cooling tower behaviour are more investigated resulting in the creation of a new model of the adsorption chiller.

Finally, a summary of the main findings of this thesis and perspectives for future researches in solar cooling applications are drawn in the conclusion of the thesis.

Chapter 1

Solar cooling options and technologies

In this chapter, the description and explanation of market available solar cooling systems are carried out. Before going into details for each solar cooling path, some important basic features and thermodynamic limitations are defined. Then, a synthetic summary of each available system depicts the main advantages and disadvantages. Finally, the performance indicators are described.

1.1 Solar cooling basics

1.1.1 Short history of solar refrigeration

Producing cold with solar energy is not recent. From the 1850's to the 1870's, the French government decided to subsidize the development of solar applications because of the energy crisis. During the world exposition 1878 in Paris, *Augustin Mouchot* aided by his assistant *Abel Pifre* produced the first ice block with solar energy using the periodical absorption machine of *Ferdinand Carré* (SACE, 2003). They won the Gold medal for this work which was drawn in pen and ink on figure 1.1.

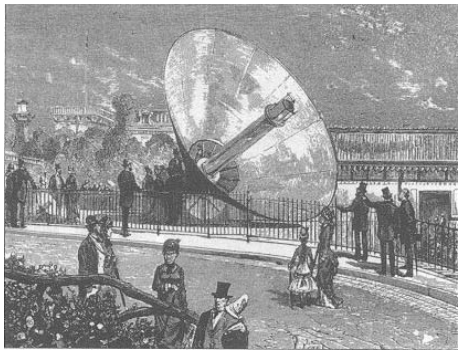

Figure 1.1: Solar energy receiver of *Augustin Mouchot* (Bolocan and Boian, 2010)

During the 20^{th} century, thanks to a good and cheap electricity grid provided worldwide, the mechanical compression of fluid had a large development. After the Oil crisis in 70 and 80's, non-conventional ways to produce cold reappeared. Solar energy became once again a popular energy source. Research and development grew rapidly and many paths to produce cold energy with solar radiation (re)appeared. Among these, the World Health Organization initiated the development of solar refrigeration (for medical use) by photovoltaics in 1979.

Several world events later and after an incredible energy price rise (see figure 1.2), thinking about alternative sources for cooling is not sufficient any more and many systems are designed and used all over the world. Future fossil fuel price increase will certainly disseminate clean energy technologies for the general interest. This vision fortunately includes the development of solar cooling systems. The current price of oil has not yet reached the peak of *Mouchot, Pifre* and *Carré* marvellous period...

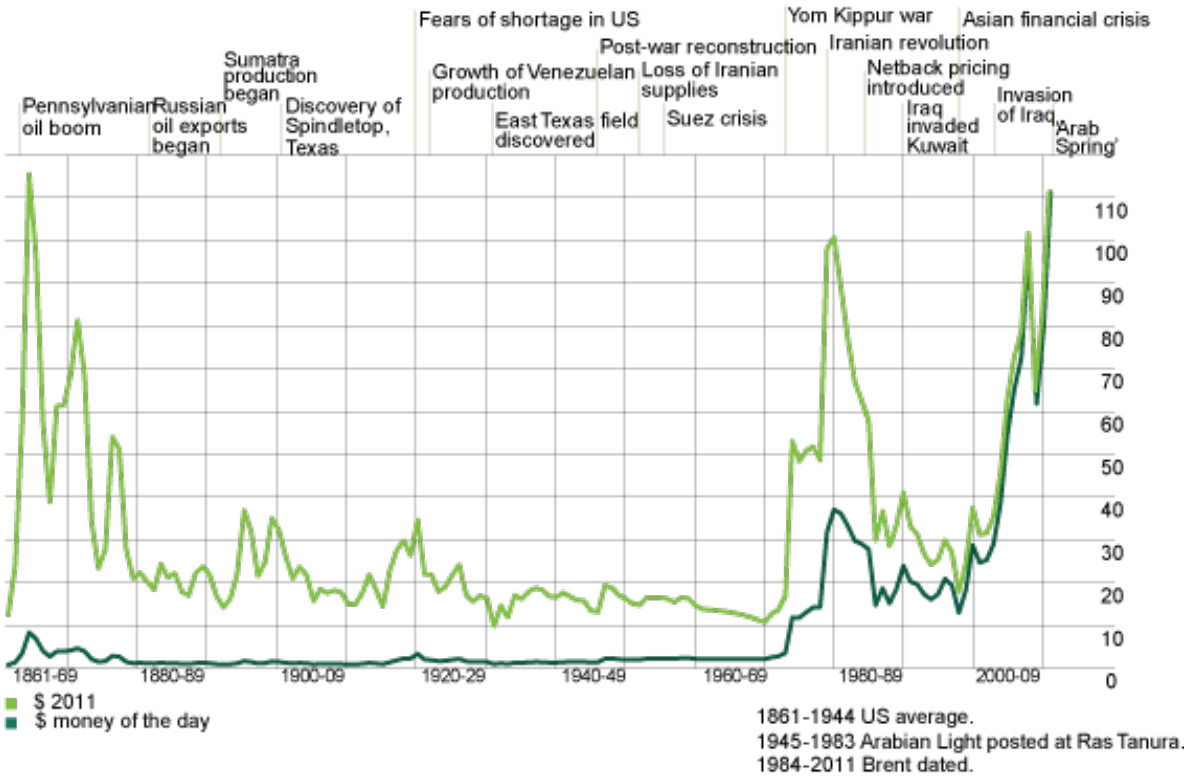

Figure 1.2: Crude oil prices 1861-2011 and worlds events (BP, 2012)

1.1.2 Solar cooling paths

The identification of different solar cooling processes delivers a clear overview of the subject. Many processes can be found in work from Pridasawas (2006) or Henning (2007a), focus is put on systems available on the solar air-conditioning market. For these few solar cooling paths a deeper search has been completed.

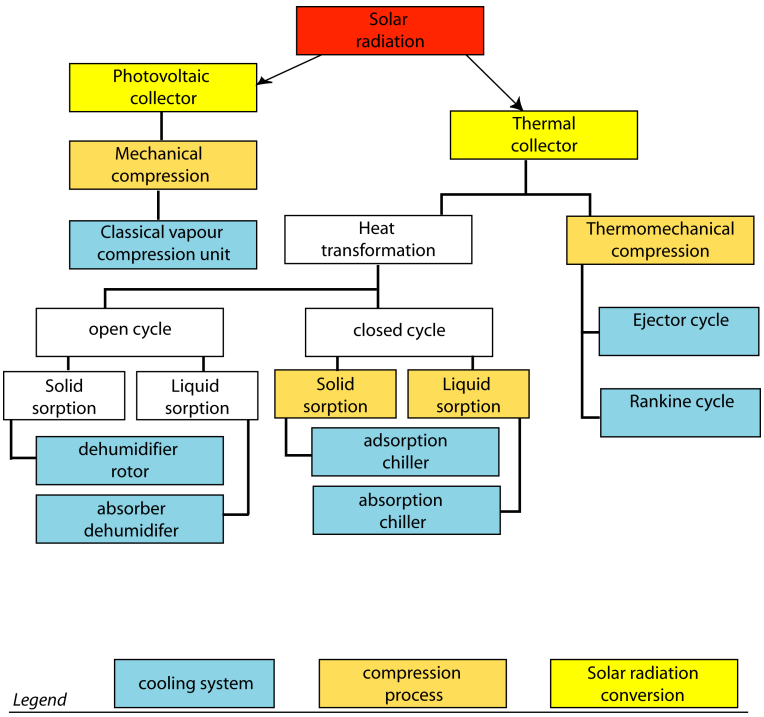

Figure 1.3: Solar cooling paths, inspired by Henning (2007b)

Processes selected are *firstly* divided into two paths (figure 1.3) depending on the way solar energy is converted:

1. **PhotoVoltaic (PV) conversion**: from solar radiation to electricity;
2. **Thermal conversion**: from solar radiation to thermal energy;

Depending on the kind of collector (air, flat-plate, evacuated tube or concentrating collector) a certain temperature level can be reached. Some technologies (cooling system on figure 1.3) are more suitable for low or high temperature. In most cases, the production of cold is the result of condensation-evaporation cycle of a fluid called refrigerant. The compression-expansion of this fuild makes possible the condensation-evaporation.

The various cooling systems can be *secondly* sorted by the compression driving force:

1. **Mechanical compression** with any kind of compressor (piston, screw, scroll...);
2. **Sorption compression** is a reversible physical reaction that ejects and absorbs a gas from a solid matrix (adsorption chiller) or from a liquid (absorption chiller);
3. **Thermomechanical compression** is the compression of a fluid with a heat source and a possible expansion with a nozzle;

The cooling systems are nearly all linked with a fluid compression except for the **desiccant** cooling systems. These systems use the water contained in the ambient air as a refrigerant. Therefore no compression driving force is needed. To dehumidify the air, the sorption material can either be in a liquid or a solid phase. A dehumidifier rotor uses a solid sorbent while a counter flow heat exchanger uses a liquid one.

The different technologies cited below can also be sorted by the hot water temperature needed or the cold temperature reached by the system. This will be explained in the section 1.3.

Thermomechanical compression (extreme right part of figure 1.3) is only used in demonstration plants but not in market available technologies. The first mentioned is the ejector cycle using a nozzle for the refrigerant expansion and a boiler for the compression. The second one is a Rankine cycle (with an organic fluid) driven by solar energy to produce mechanical work. It is finally transmitted to a vapour compression chiller. These two technologies are also explained in section 1.3.

This paragraph about solar cooling paths seems to depict a general view of the solar cooling systems. Nevertheless a fracture exists between PV driven systems (*left branch*) and thermally driven systems (*right branch*). When speaking about buildings linked to the electricity grid, the first branch is de facto a juxtaposition of two technologies that can operate independently. The second branch seems to be more complex because of the interaction between the heat source (solar thermal collectors) and the cooling system. The two systems are more or less in competition with their own detractors. The result is that the international projects cited in the introduction (page 1) mainly focused on the thermally driven systems. Generally, literature about solar air-conditioning comes down to the thermally driven technologies.

1.1.3 Still a niche market?

For the reasons just mentioned, only thermally driven systems will be taken into account in the following lines.

In Europe, around 200 solar cooling plants were in operation in 2007. Solar air-conditioning data base counted 300 systems all over the world in the end

of 2009 (Sparber *et al.*, 2009b) for a total of 16 MW cold production. They are mainly small scale systems (<15kW cold). The estimated number of solar cooling installations was 700 in 2011. The system number evolution is drawn by Stryi-Hipp *et al.* (2012) and displayed on figure 1.4. In current days (2013), it can be considered that around 1000 systems are installed all over the world (Stryi-Hipp *et al.*, 2012). This is clearly still a niche market compared to the huge vapour compression chiller market progression of around 75 millions units per year (Mugnier, 2011).

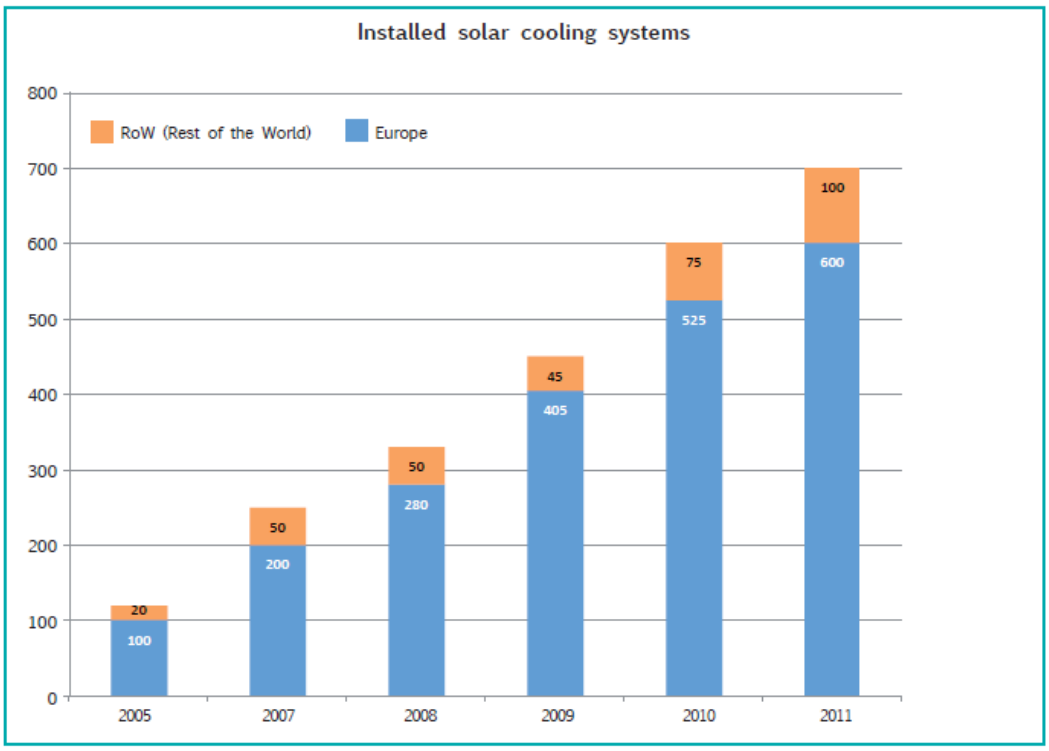

Figure 1.4: Estimation of number of solar cooling installations worldwide (Stryi-Hipp *et al.*, 2012)

Coming back to the solar cooling paths, the absorption cooling systems are still dominating the market (71% of chillers). Adsorption 13% and Desiccant (solid 14%,liquid 9%) still play a smaller role in cooling systems (Sparber *et al.*, 2009b). From a solar collector point of view, the flat-plate collector and evacuated tube collectors have a considerable importance. Other kinds of collectors (concentrating collectors) stand for unusual high temperature systems.

Some installations stand out of the crowd because of their huge capacity or their specific use. The largest system in the world is installed in Singapore in

the United World College of South East Asia (East Campus - Tampines). 3900 m^2 solar collectors produce hot water and feed a 1.575 MW absorption cooling machine (Holter, 2012). Another example is the football world cup in Qatar in 2018. A demonstration stadium is already built in Qatar and cooled with a double effect absorption chiller with 750 kW cold power. Heat is provided by Fresnel concentrating collectors (Zahler *et al.*, 2011).

The main current barriers to solar cooling systems dissemination are the high price and the lack of technical skills at system level. This technology includes many subsystems with their own control and electrical consumptions. In most cases, the electricity consumption was greater than what was planned (Wiemken *et al.*, 2010). The quality of systems is also an obstacle which couldS be soon overcome with a large development of solar cooling.

1.2 Definitions and thermodynamic limitations

1.2.1 Cycles efficiencies

Thermodynamic schemes and limits

The **conventional cooling machine** (mechanical compression) satisfies the Carnot refrigeration cycle on figure 1.5 (a). The useful cold energy (Q_C) and the condenser heat (Q_M) are driven by the work provided by the compressor. The cycle efficiency is characterized by the electrical COP (Coefficient Of Performance) and the Carnot thermodynamical limit are respectively defined in equations 1.1 and 1.2. The subscript *VCC* stands for Vapour Compression Chiller. This acronym will be used in the text to indicate a conventional cooling machine. W indicates the power absorbed by the cooling machine; which includes the compressor work and the auxiliaries consumptions of electrical devices dedicated to the cooling machine.

$$COP_{elec\,VCC} = COP_{VCC} = \frac{Q_C}{W} \tag{1.1}$$

$$COP_{Carnot\,VCC} = \frac{T_C}{T_M - T_C} \tag{1.2}$$

The **thermally driven machines**, namely absorption, adsorption and desiccant, deal with three thermal energy flows at three different temperature levels as displayed on figure 1.5 (b). This differs a little from the widely used thermal systems (Rankine Cycle, Electrically driven heat pumping and cooling machines) that use two thermal energy flows. The driving heat (Q_H) is, in a sense, the engine of a heat transfer from a low temperature level (Q_C heat flow) to an intermediate temperature level (Q_M heat flow). Two COP's are defined, they quantify the system global performance (COP_{elec} in equation 1.3) and the machine thermal performance (COP_{therm} in equation 1.4). Moreover, the

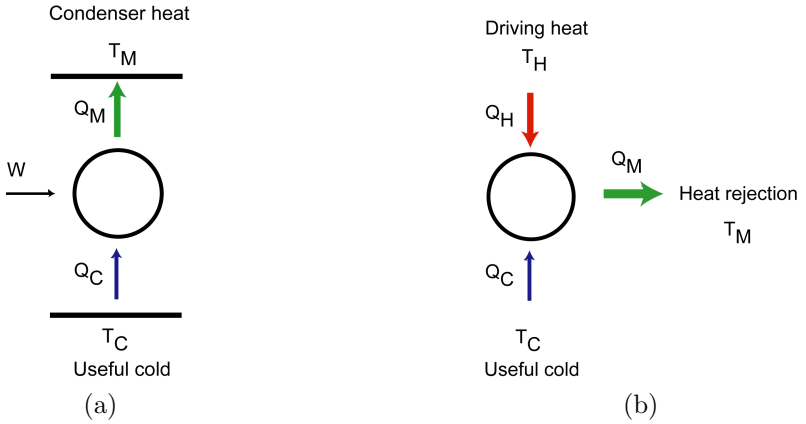

Figure 1.5: Mechanical compression cooling (a) and thermally driven cooling (b) thermodynamic schemes

Carnot thermodynamic limit of those machines can be defined (equation 1.5). It results from the combination of the two Carnot cycles (figure 1.6).

$$COP_{elec} = \frac{Q_C}{W_{aux}} \tag{1.3}$$

$$COP_{therm} = \frac{Q_C}{Q_H} \tag{1.4}$$

$$COP_{Carnot\ therm} = \frac{T_C}{T_H} \cdot \frac{T_H - T_M}{T_M - T_C} \tag{1.5}$$

The electrical COP (equation 1.3) reveals the factor W_{aux} counting for the auxiliaries only. In comparison with conventional cooling machines, the driving force is here not a mechanical work but an energy flow. For this reason the only electrical consumptions are auxiliary devices (pumps, fans, electronic cards).

Section 1.4 reveals what is taken into account in W_{aux}. Those equations raise the question of machine and system definition. The **cooling machine** counts for the chiller itself (absorption or adsorption chiller) while the **cooling system** covers other devices installed to assist the chiller: the thermal collector, the cooling tower, the back-up system.... Depending on the selected system, some devices are included or not. When analysing one particular system, it is therefore important to identify its boundaries.

The three temperature levels will influence the thermal performance of the machine. For some thermally driven systems, figure 1.7 shows the thermal COP for common cold and rejection temperature levels. The difference between the single-effect and double-effect chiller is detailed in section 1.3. The thermal COP grows as much as the driving temperature increases. The name *driving*

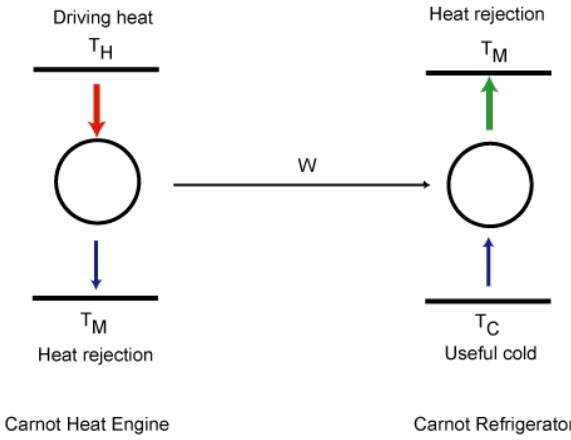

Figure 1.6: Carnot basis of the thermally driven cooling machine

is therefore properly chosen.

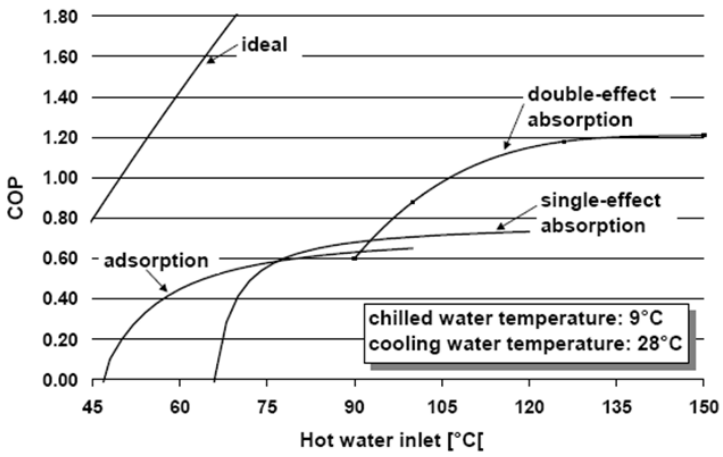

Figure 1.7: Thermal COP of sorption chiller (Henning, 2007a)

1.2.2 PV Collectors efficiency

The PV module efficiency can be defined by the collector electric power divided by the incident total solar irradiation on the collector surface (equation 1.6). Direct current is provided by the collector, an inverter is used to produce

alternating current for the grid. For a given PV collector, the Current-Voltage curve (on figure 1.8) varies with the irradiation level and the cells temperature. The voltage allowing maximum peak power also varies according to the previous variables. The collector shading widely influences the efficiency too.

$$\eta_{PV\ coll} = \frac{P_{elec\ DC}}{A\ I_{tot}} \tag{1.6}$$

Where

$P_{elec\ DC}[W]$ = Collector direct current production

$A\ [m^2]$ = the aperture area

$I_{tot}\ [W/m^2]$ = incident total (beam and diffuse) radiation on the collector plane

Market available collectors can reach efficiency up to 17.55% (Green *et al.*, 2011)) in standard conditions (IMT-Solar, 2009). Nevertheless, Suri *et al.* (2007) say that the yearly efficiency of a photovoltaic system (PV modules, cables and inverter) varies from 800 to 1500 kWh_{elec} per kW peak installed power and per year for Western Europe. Taking the amount of solar radiation and the collector area (7.5 m^2 per kW installed) into account gives a global approximate efficiency of 10% . Main market technologies are Silicium Mono-crystalline and Poly-crystalline cells (IEA-PVPS, 2011).

The global efficiency is used in following chapters, it includes PV modules, cables and inverter losses. It is defined as follows:

$$\eta_{PV} = \frac{P_{elec}}{A\ I_{tot}} \tag{1.7}$$

Where

$P_{elec}[W]$ = Inverter alternating power output.

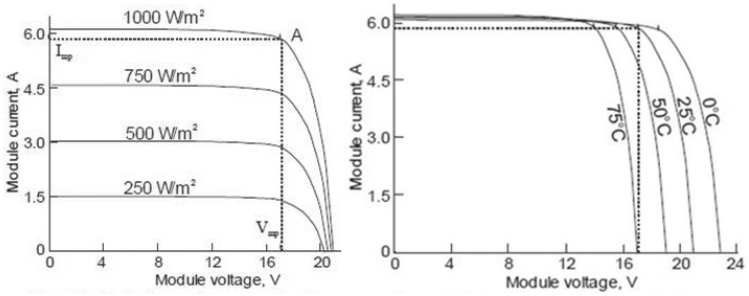

Figure 1.8: Dependence of current and voltage collector curve on incident irradiation and temperature (IMT-Solar, 2009)

1.2.3 Thermal collectors efficiency

This paragraph focuses on thermal collector technologies that are specific to solar cooling applications. The solar collector efficiency is defined as the thermal energy received by the fluid (air, water ...) divided by the incident solar energy (equation 1.8).

$$\eta_{thermal\ collector} = \frac{\dot{Q}_{useful}}{A\ I_{tot}} \tag{1.8}$$

Where

$\dot{Q}_{useful}$ $[W/m^2]$ = increase of fluid energy between collector inlet (T_{in}) and outlet (T_{out})

A $[m^2]$ = the aperture area (for tests regarding the EN12975 norm)

I_{tot} $[W/m^2]$ = incident total (beam and diffuse) radiation on the collector plane

The energy gain from collector comes from solar radiation in a large spectrum (see figure 1.9). The energy flows through a glazed collector is pictured in figure 1.10. The quantity of energy absorbed by the absorber (useful energy) is influenced by the incident radiation and by the losses. These are infra-red radiation from the collector, convective heat transfer and conduction losses through the rear and sides of the collector. A generic equation for all kind of collectors can be written as equation 1.9.

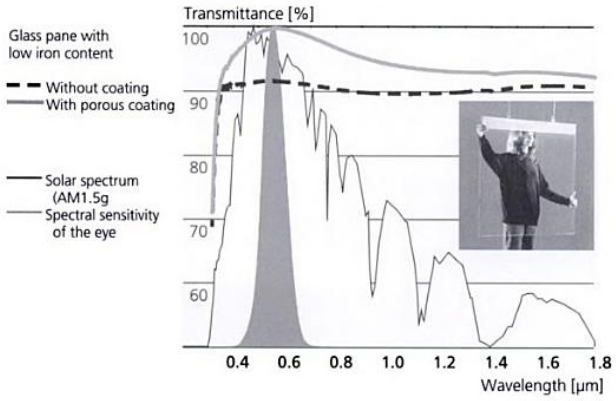

Figure 1.9: Solar radiation wave length, glass transmittance and influence of coating (Santamouris, 2003)

$$\eta_{thermal\ collector} = k(\theta)a_0 - a_1\frac{(T_{coll} - T_{amb})}{I_{tot}} - a_2\frac{(T_{coll} - T_{amb})^2}{I_{tot}} \tag{1.9}$$

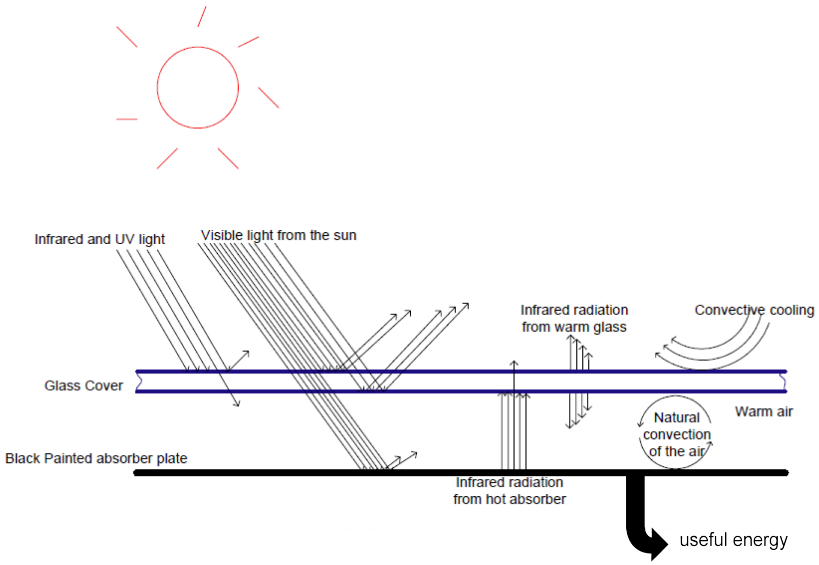

Figure 1.10: Energy flows in glazed collector (Pridasawas, 2006)

Where

$k(\theta)$ $[-]$ = incidence angle modifier (IAM), it takes the influence of non perpendicular incident radiation into account. It is the ratio between the intercept efficiency (a_0) at current incidence angle θ and its value at normal incidence ($k(0) = 1$)

a_0 $[-]$ = intercept or optical efficiency (sometimes written η_0) is approximately the product of the glass transmissivity by the absorptivity of the absorber

a_1 $[W/(m^2K)]$ = linear heat loss coefficient

a_2 $[W/(m^2K^2)]$ = quadratic heat loss coefficient

I_{tot} $[W/m^2]$ = incident total (beam and diffuse) radiation on the collector plane

T_{amb} $[K]$ = ambient temperature near the collector

T_{coll} $[K]$ = average fluid temperature in the collector $(T_{in} + T_{out})/2$

Those parameters are given in collector test reports such as the ones from "Solar Keymark" quality label. For the use in solar air-conditioning systems, different kinds of collectors can be selected depending on the medium (water or air) and the required temperature level:

- **Flat-plate collector (FPC)** is the mostly used collector type in solar cooling system. The absorber stands behind a flat (simple or double) glazing and is cooled by a pipe network (figure 1.10),

- **Air collector (AIR)** has similar operation principle as for FPC, the absorber is cooled by air instead of water (figure 1.13). It is used only for desiccant cooling systems,
- **Evacuated tube collector (ETC)** benefits from lower convection losses due to the vacuum (lower than 1 kPa) between the absorber and outside air. Various types of tube collector can be found depending on piping technology and on tube geometry. The collector contains few parallel tubes whose cross section is displayed on figure 1.11. In some cases, a reflector is installed behind the tube, however it is not considered as a concentrating collector,
- **Parabolic trough (PTC)** is a line axis concentrating collector (figure 1.13). Concentrating collectors generally produce steam in a tube similar to ETC collector. Moreover, they can stay stationary or can have a tracking system,
- **Fresnel collector(FRC)** is another kind of single axis concentrating collector using Fresnel lens geometry that reduces the material compared to conventional lenses (figure 1.12).

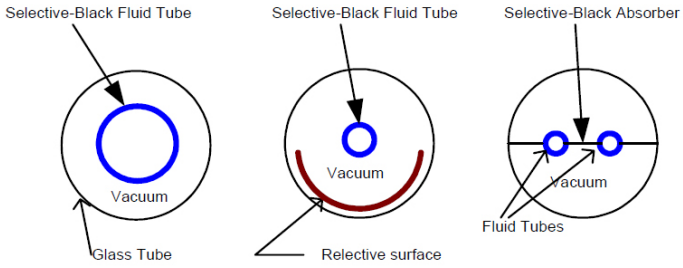

Figure 1.11: Evacuated tube collector : cross section of the available tube designs (Pridasawas, 2006)

The required temperature for various solar cooling systems and the different collector efficiencies are displayed on figure 1.14 while the numerical values of equation 1.9 parameters are presented in table 1.1.

Incidence angle modifier influence

The incidence angle is the angle between the beam radiation and the normal onto the collector. As the incidence angle increases, the glass transmittance diminishes. It involves an efficiency degradation that is emphasized by the factor $k(\theta)$ in equation 1.9. For Evacuated Tube Collectors, this factor is split into two therms (θ longitudinal and θ transversal) because of the collector geometry. The $k(\theta)$ values can easily be found from test data and is displayed on figure 1.15 where the evacuated tube collector has no reflector. The $k(\theta)$ for ETC is the product of $k(\theta_{longitudinal})$ and $k(\theta_{transversal})$

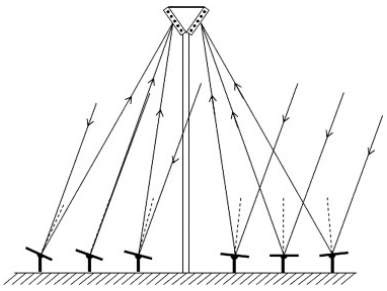

Figure 1.12: Fresnel collector scheme (Abbas *et al.*, 2012)

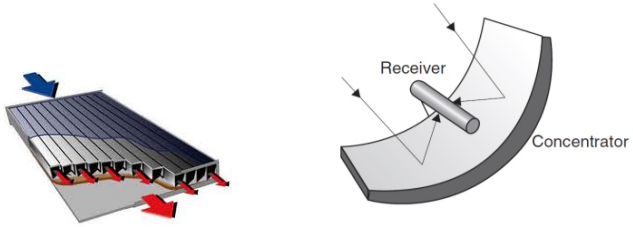

(a) (b)

Figure 1.13: Air collector (a) and parabolic trough collector (b) schemes

Non nominal mass flow

The efficiency equation 1.9 could be rewritten involving a **non nominal mass flow**. For water systems, the efficiency is given for a certain mass flow specified in test conditions. As stated by Duffie and Beckman (1991), decreasing the mass flow also decreases the efficiency. This effect will be taken into account into the various simulations.

Collector inertia influence

The previous collector efficiency explanation is a static definition. The collector has nevertheless a significant thermal mass. In equation 3.1, an additional term has to account for the dynamic behaviour of the collector:

$$\eta_{thermal\ collector} = k(\theta)a_0 - a_1\frac{(T_{coll} - T_{amb})}{I_{tot}} - a_2\frac{(T_{coll} - T_{amb})^2}{I_{tot}} - M\frac{\partial T_{coll}}{\partial t} \tag{1.10}$$

The effective thermal capacitance M $[J/(m^2K)]$ is defined in European standard EN12975-2 and present in collector certificate (DINCERTO, 2011). A model including this inertia effects as well as other features (Fischer *et al.*, 2001) has been recently developed in TRNSYS (Haller, 2012) but is not used in this work because it was discovered in the mean time of running the simulations.

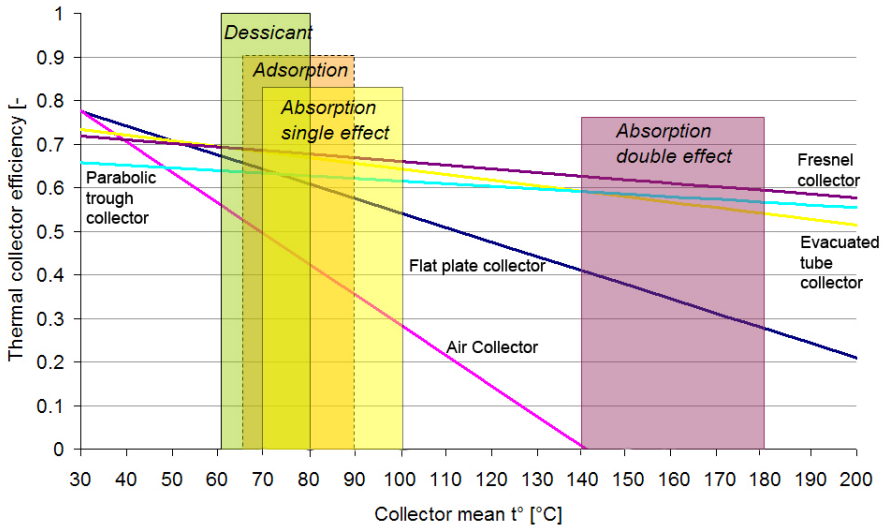

Figure 1.14: Thermal efficiencies for the different kinds of collector (numerical values and sources in table 1.1) and range of operating temperatures for solar cooling technologies coming from Henning (2011). The ambient temperature, solar radiation and $k(\theta)$ are respectively $25°C$, $1000\ W/m^2$ and 1

1.2.4 Reference efficiency of the conventional system

In order to design the best performing solar cooling system we must compare them to the conventional ones. The conventional heat and cold production efficiencies must be defined at least for comparison purpose. The numerical values given in this paragraph come from Napolitano *et al.* (2011). The main conventional systems used in this work are the gas boiler and the vapour compression chiller. As a rough approximation, the annual mean efficiency is given. They are respectively efficiency (equation 1.11) and Seasonal Performance Factor (equation 1.12) for gas boiler and vapour compression chiller. These values are often used in the literature and make the comparison easier. In this work, if no other value is specified, these values will be taken into account. The boiler efficiency addresses the ratio between the thermal energy produced and the gas lower heating value.

$$\eta_{boiler}\ ref = 0.95 \left[\frac{kWh_{thermal}}{kWh_{gas}}\right] \tag{1.11}$$

$$SPF_{ref} = 2.8 \left[\frac{kWh_{thermal}}{kWh_{elec}}\right] \tag{1.12}$$

Collector type	a_0 [−]	a_1 $[W/(m^2K)]$	a_2 $[W/(m^2K^2)]$	**Source**
FPC	0.791	3.307	0.016	Keymark test report DINCERTO (2011)
AIR	0.81	7	0	Average data from Henning (2007a)
ETC	0.74	1.28	0.007	Keymark test report DINCERTO (2008b)
PTC	0.66	0.6	0	Average data from Kalogirou (1998)
FRC	0.723	0.838	0	Model from Singh *et al.* (2010) with a concentration factor of 10

Table 1.1: Collector efficiencies numerical values

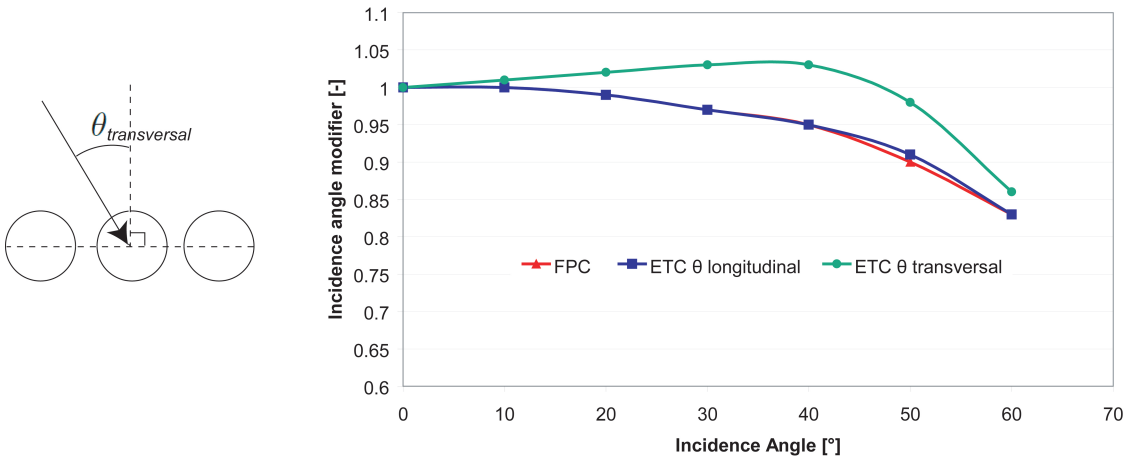

Figure 1.15: Incidence angle modifier for flat-plate (DINCERTO, 2011) and evacuated tube collector (DINCERTO, 2008b). The figure also shows the incidence angle definition for ETC (cross section)

1.2.5 Other definitions

Some other definitions give interesting keys to the reader.

Chiller temperatures

For each flow of any chiller, the temperatures are named as follows

$T_{H\ in}$ = Temperature of driving supply flow to the chiller.

$T_{H\ out}$ = Temperature of driving return flow from the chiller.

$T_{M\ in}$ = Temperature of rejection supply flow to the chiller (or from cooling tower).

$T_{M\ out}$ = Temperature of rejection return flow from the chiller (or to cooling tower).

$T_{C\ in}$ = Temperature of cold supply flow to the chiller.

$T_{C\ out}$ = Temperature of cold return flow from the chiller.

T_H, T_R, T_C are the thermodynamic cycle temperatures, logarithmic mean value between the inlets and outlets (equation 1.13).

$$T = \frac{T_{in} - T_{out}}{\ln \frac{T_{in}}{T_{out}}} \tag{1.13}$$

Primary energy factor

It is important to fix the primary energy factors for the main energy carriers used in installations, i.e. electricity and fossil fuels (oil and natural gas). They describe the conversion "quality" between primary energy and the energy vector. The primary energy conversion factors are defined according to EN 15603 standard.

$$\epsilon_{elec} = 0.4 \left[\frac{kWh_{elec}}{kWh_{pe}} \right] \tag{1.14}$$

$$\epsilon_{fossil} = 0.9 \left[\frac{kWh_{gas}}{kWh_{pe}} \right] \tag{1.15}$$

1.3 Solar cooling technologies overview

1.3.1 Introduction

This section details the operating principles of the main available technologies for solar cooling of buildings. It deals with the "cooling system" boxes shown on figure 1.3 on page 7. The focus is put on thermally driven technologies. The encountered values of chiller performance and temperature levels are mentioned for each technology.

The solar cooling systems generally have a back-up system when the sun is not shining enough to satisfy the cooling load. That is the reason we sometimes name those systems as *Solar ASSISTED air conditioning system*. The back-up system can stand either on the hot side (heat production for feeding the thermally driven system) or on the cold side (generally a vapour compression chiller). Two kinds of systems are encountered : **autonomous** and **assisted**.

The combination of PV and vapour compression chiller does not need back-up because it is considered as grid connected.

1.3.2 Absorption cooling machine

The absorption cooling system is the most widespread solar cooling system in the world. This thermally driven technique benefits from the largest experience feedback. It is on the market for a large range of powers. To describe the absorption chiller operation, these previous works were very useful: Henning (2007b), CLIMASOL (2002), Mugnier (2002), Schaefer (2000), Energieplus (2012), Tozer and James (1997).

The operating principle is based on pressure variation while refrigerant (e.g. water) is absorbed or desorbed by working fluid (eg: lithium bromide). The governing equation of the sorption compression is written for Lithium Bromide - Water couple. The description below also stands for other absorbent-refrigerant (mainly Water-Ammonia) used in absorption cooling systems. Nevertheless, the temperature and pressure levels are varying depending on the couple used.

$$Li\,OH_{(l)} + HBr_{(l)} \rightleftharpoons LiBr_{(l)} + H_2O_{(g)} \tag{1.16}$$

The direct endothermal reaction is called the **desorption**, water vapour is rejected. The reverse reaction (exothermal) is called the absorption, the hygroscopic material absorbs the water vapour. Those two equations involve pressure variation : direct reaction increases pressure while the reverse decreases it.

Four steps are used to run this closed cycle technique (figure 1.16).

In the Evaporator which is a vacuum recipient ($\approx 0.01\ bar$), water evaporates. Water heat vaporisation cools water coil (cooling effect). In the absorber, the refrigerant is absorbed by the working fluid, and low pressure is thus maintained in both absorber and evaporator. In the Generator, the refrigerant and

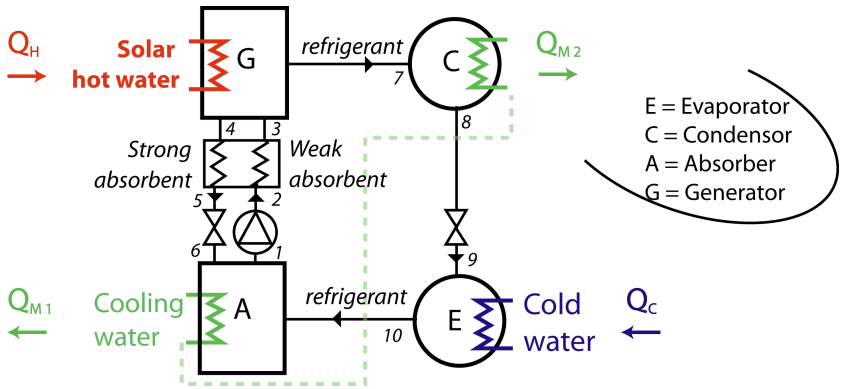

Figure 1.16: Absorption chiller description scheme (e.g. absorbent Lithium Bromide - refrigerant Water)

working fluid forming together the weak absorbent solution are separated by consuming solar heat (or other heat source). Water vapour is brought to condenser and then cooled while the absorbent strong solution is driven back to the absorber. The condensed water comes back to the Evaporator. The high pressure steps are Generator and Condenser (≈ 0.1 *bar*) recipients. The cycle states are displayed on the Oldham ($\ln P - T$) diagram for the Lithium-Bromide - Water cycle (figure 1.17). The weak (strong) solution means a high (low) concentration of refrigerant in the absorbent material.

To enhance the thermal performance, a heat exchanger is implemented between the generator (high temperature step) and the absorber. Moreover, the absorber and condenser must be respectively cooled to favour the direct reaction (equation 1.16) and to evacuate the water latent heat.

Three energy flows (colour lines on figure 1.16) at different temperature levels are needed: cold, hot and heat rejection. The challenge is to keep those energy sources and sinks in a proper temperature range to operate the chiller with a good thermal COP.

For a single effect absorption chiller, a typical value of thermal COP is 0.7. We should be careful with the given value of COP as it mostly depends on the fluid temperatures of hot, cold and rejection circuit. Moreover, it is a steady state value. The single stage absorption chiller performance is generally given for one nominal point. Sometimes, some manufacturers give a set of operating points (figure 1.18) including the nominal (or rated) one. Moreover, the figure provides the chiller capacity meaning the cold water energy flow Q_C on equation 1.4.

As a variant to the described technique, "double effect" or "double stage" absorption chiller can be introduced (Tozer and James, 1997). It consists of

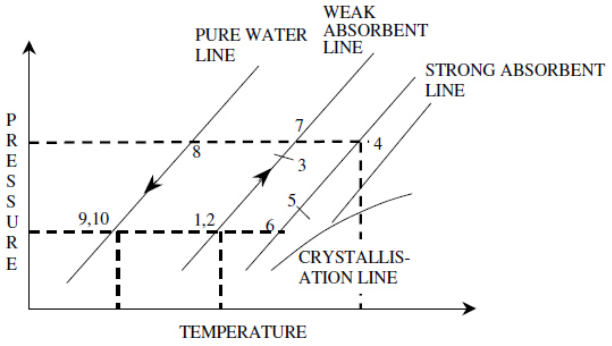

Figure 1.17: Oldham diagram for a theoretical single effect absorption chiller (Florides *et al.*, 2003).

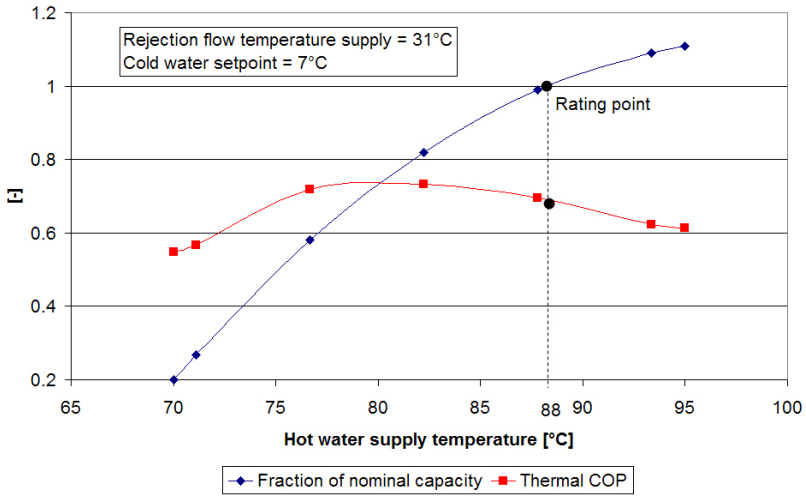

Figure 1.18: Absorption chiller thermal COP and capacity curves (Thomas and André, 2010)

two absorption cycles, where the heat rejected from the condenser of the high temperature stage 2, is used to supply heat to the generator of the low temperature stage 1. This means that the low temperature generator 1 is also the high temperature condenser 2 (figure 1.19). It implies a higher temperature driving source (140-180°C) but reaches a higher thermal COP (around 1.2). The main used double effect cycle is displayed on figure 1.19 (Castaing-Lasvignottes, 2001). Based on the same principle, some "triple stage" absorption chiller could be set up. It is yet available on the market for waste heat driven cooling ap-

plications (Deng *et al.*, 2011) but not especially dedicated to solar cooling.

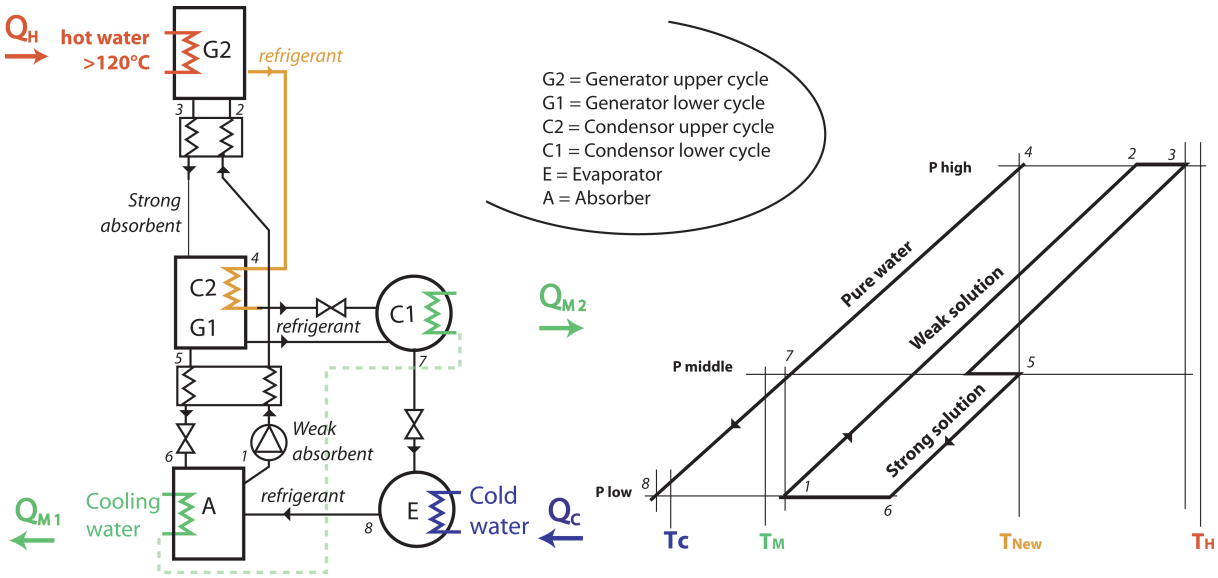

Figure 1.19: Double effect absorption chiller description scheme and Oldham diagram for a theoretical cycle.
Inspired by Castaing-Lasvignottes (2001)

The minimal cold temperature for Lithium Bromide-Water cycle is around 5°C to avoid its crystallization (figure 1.17). The other market available couple Ammonia-Water can reach lower temperatures that enable freezing process (for food conservation for example). The rejection temperature is in any case up to 35-40°C.

A continuous cycle was described in this paragraph. It could also be intermittent on some cases (e.g. triple phase absorption).

The advantages of absorption chillers (this applies to adsorption too) are that they have very few moving parts, leading to low noise and vibration levels, and they do not emit ozone depleting substances. Moreover, absorption has the highest thermal COP values among all solar cooling technologies.

Finally the absorption chillers are widely used for many applications besides the solar cooling systems: combined heat-power production, process heat recovery, mobile home chiller... The special features of the machines dedicated to solar cooling are the temperature range and level of the three energy flows, especially the hot one.

1.3.3 Adsorption cooling machine

The adsorption chillers form a less significant part of the solar cooling systems installed worldwide. The description of this technology is based on previous work accurately detailing the adsorption cooling systems and written by Ait-Taleb (2002), Lachance *et al.* (2002), Wang and Oliveira (2006) and Ziegler (2002).

This machine type is based on the same principle as the single effect absorption chiller. The major difference is that adsorption chiller is intermittent while absorption chiller is generally continuous. The adsorption process brings together a solid and a gas (it was liquid and gas for absorption).

To operate an adsorption cycle, four successive steps and three recipients are used (displayed on figure 1.20 where the sorption reaction is written for any kind of reacting material). An adsorption chiller includes the **Adsorber** (containing solid sorbent e.g. silica gel), the **Condenser** and the **Evaporator**. To describe the cycle, it is initially considered that the adsorber is "loaded" with refrigerant (e.g. water).

- During the first step, (constant volume compression) both valves are closed, the adsorber is heated to increase its pressure,
- The second step begins when adsorber pressure reaches condenser pressure. The Desorption with constant pressure takes place, the condenser valve is opened, refrigerant is desorbed and condenses. Adsorber is still heated with hot water, condenser is cooled with heat rejection circuit,
- The third step consists in lowering pressure at constant volume (two valves closed). When cooling the adsorber, a part of the gas is adsorbed and pressure falls,
- The last step begins when adsorber and evaporator pressures are equivalent. This constant pressure adsorption step brings the cooling effect to the building. When the evaporator valve is opened, the condensed refrigerant is sprayed and evaporates. Adsorber adsorbs refrigerant and keeps the low pressure in the two recipients. The rejection circuit is feeding adsorber to remove heat of adsorption. The adsorber is now "loaded" and a new cycle can start,

The four steps are represented on an Oldham diagram on figure 1.21 for a theoretical cycle.

This operation only involves one cooling step. To overcome this problem in real chillers, two adsorbers are installed in phase opposition (figure 1.23). It creates two useful steps instead of one, the cold production is more continuous. Besides, the use of two adsorbers allows the heat recovery between the two adsorbers.

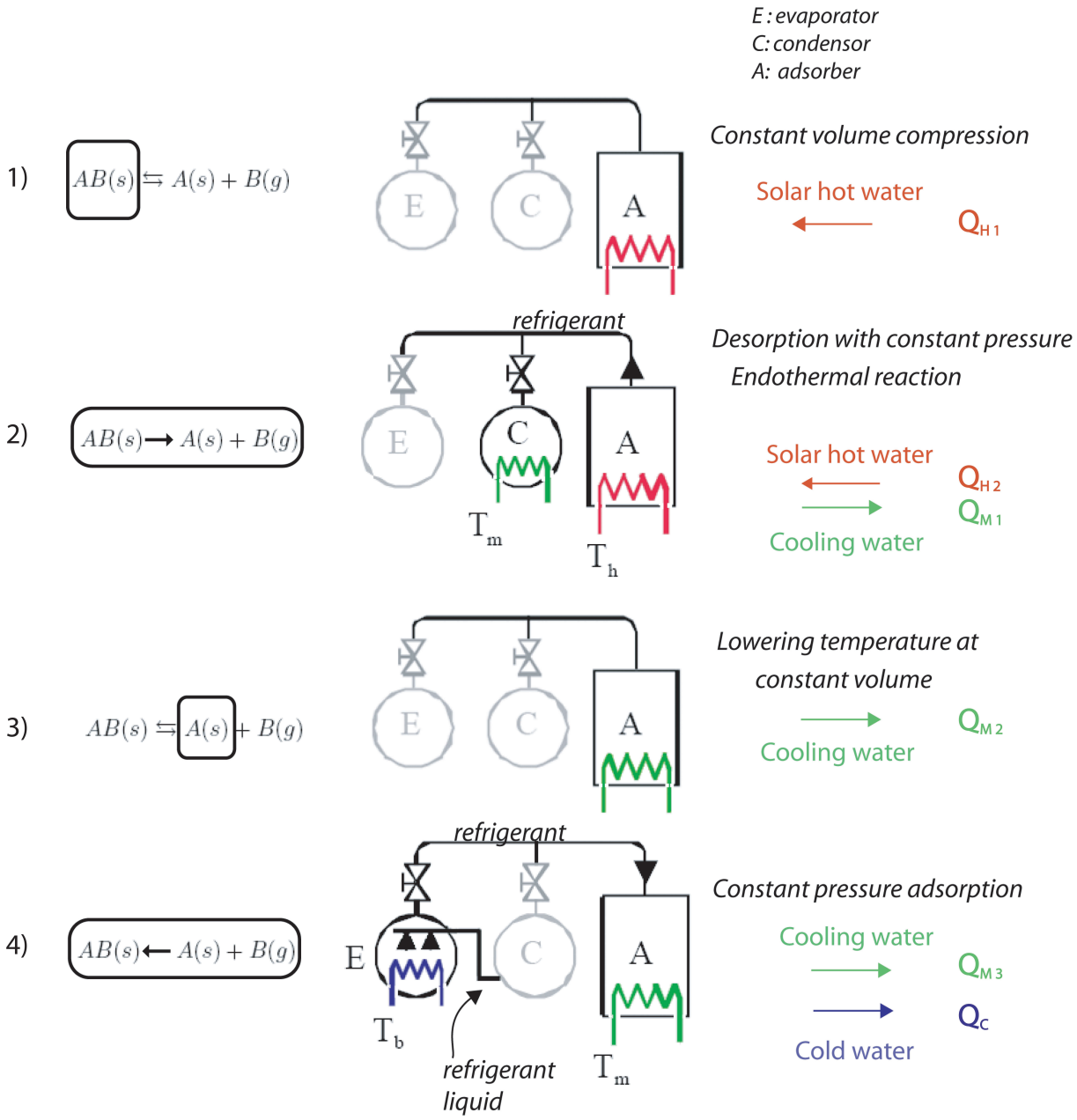

Figure 1.20: Adsorption chiller operation, the four successive steps. Inspired by Lachance *et al.* (2002)

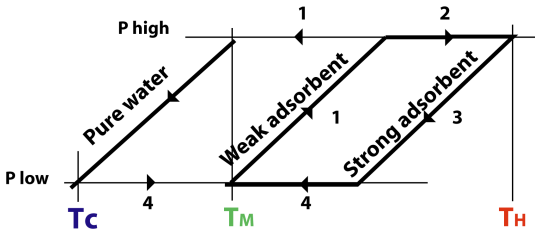

Figure 1.21: Oldham diagram for theoretical adsorption cycle

Two couples of adsorbent-refrigerant are mainly used in adsorption chiller: Silica-gel - Water and Zeolite-Water. Many sorts of zeolites exist, they belong to the aluminosilicate minerals. The important feature is the water affinity of the material.

The typical thermal COP is 0.6 and the operating temperature is between 55 and 75°C. This is slightly lower than the absorption cycles. The cold water temperature produced is higher than 8°C while the rejection temperature should be lower than 37°C. Figure 1.22 displays the thermal COP and cooling capacity of an adsorption chiller. For the small scale chillers studied (INVENSOR and SORTECH), the adsorption cycle duration goes from 6 to 20 minutes depending on the machine and on the temperatures levels.

Non negligible advantages of this technology are the availability of small capacity systems down to 8 kW_C (SORTECH, 2008) and the slightly lower driving temperature compared to absorption systems. Some disadvantages are also pointed out. An intermittent cycle successively heats and cools the same material, unfortunately implying some thermal losses. Moreover, in comparison to the absorption cycle, the heat exchangers are bringing liquid face to face with solid in contrast to liquid/liquid heat exchangers. It induces higher temperature gradients between the heat source and the desorption process.

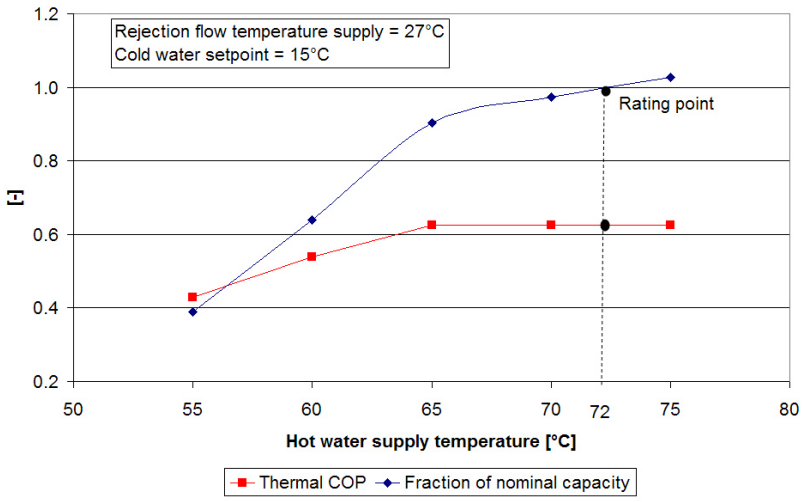

Figure 1.22: Adsorption chiller COP and capacity curves from manufacturer's data (INVENSOR, 2010)

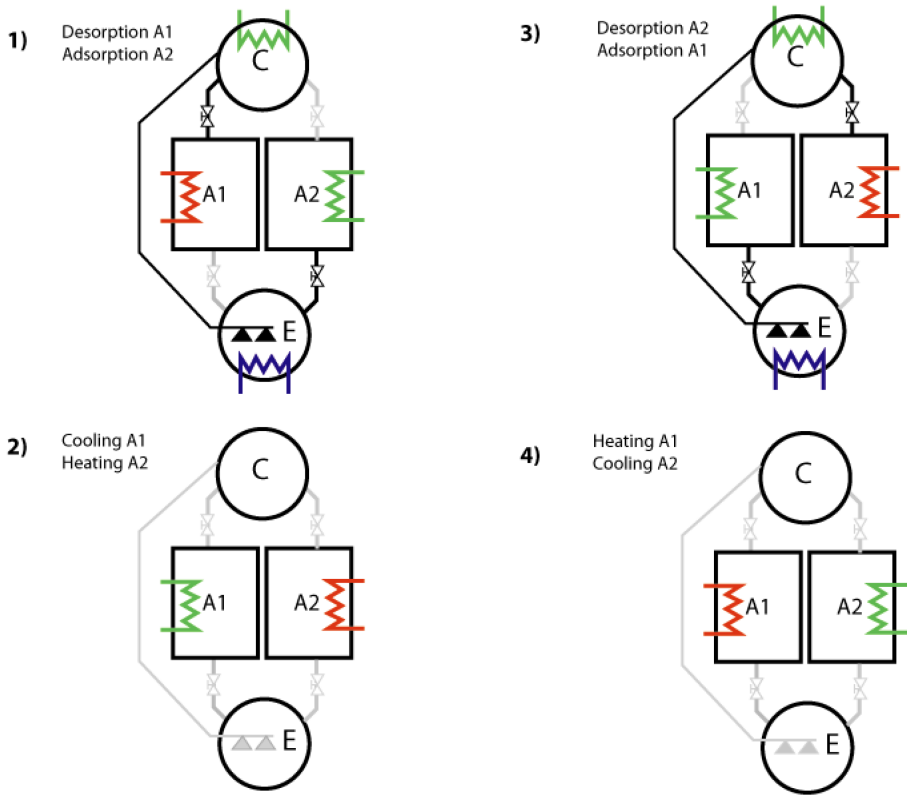

Figure 1.23: Adsorption chiller operation with two adsorbers

1.3.4 Desiccant cooling systems

Desiccant cooling also uses sorption material but in an open cycle instead of a closed cycle (as for ab-adsorption chiller see figure 1.3). In such an open cycle, the refrigerant is the moisture contained in supply air for room ventilation. The general principle of this technique is to cool ventilation air by spraying water in the air flow. Cooling effect is important if supply air is dry enough. To provide dry air, sorbent material ab-adsorbs (liquid or solid) moisture contained in ambient air. In this technique, heat is needed to desorb (regenerate) the sorbent material. There are mainly two ways to remove moisture: using a dehumidifier rotor with solid sorbent or a fixed bed dehumidified with liquid sorbent.

This cooling technique is suitable for buildings where there is a mechanical ventilation (it is plugged on the ventilation system). The maintenance of the

cooling system is then linked to the air handling unit, it implies water treatment, moving parts and filters management. Moreover, in many cases, the air flow will be greatly higher than the hygienic required volume flow. Depending on the humidity the satisfied cooling load is around 3 to 5 W_C/m^3h^{-1} ventilation flow. Finally, the minimal air supply air temperature is around 18°C.

Desiccant cooling technique is not currently developed for small scale application. Cooling powers from 10 kW_C to 350 kW_C are available on the market. The typical thermal COP scale is 0.6 to 1.1 (greatly depending on humidity contained in ambient air). The operating temperature ranges from 60 to 85°C. This system does not need a heat rejection circuit as heat is removed by exhaust ventilation air.

Some useful documentation made the system description possible: SONNENKLIMA (2002), Daou *et al.* (2004), Henning *et al.* (2000), Mavroudaki *et al.* (2002), Jalalzadeh-Azar (2005) and Vitte (2007).

Solid sorption

General scheme of a desiccant system (solid sorbent - desiccant wheel) is displayed on figure 1.24. It also includes the different humid air states in the Mollier diagram. Its operation is detailed by enumerating the successive air transformations. The system is also designed to use solar energy to heat the air flow during the heating season.

The **cooling season** operation can be described as follows (refer to figure 1.24):

1-2 Dehumidification of the ambient air by the desiccant wheel (or dehumidifier wheel). The solid sorbent (generally Silica-gel) adsorbs moisture and releases the sorption heat.

2-3 The supply air flow is firstly cooled by a heat exchanger.

3-4 Humidification up to around 50% relative humidity (to keep comfortable conditions) decreases the air flow temperature.

5-6 Air is slightly heated by the fan.

6-7 Air flow satisfies the cooling load.

7-8 The return flow is humidified to cool it down as much as possible (nearly 100% relative humidity).

8-9 The return flow cools the supply flow without any moisture content exchange.

9-10 The desorption taking place at the next step needs high temperature. So, the air flow is heated by solar collectors or by any other heat source. Due to the use of air as heating medium, the desiccant cooling system enables the installation of air collectors.

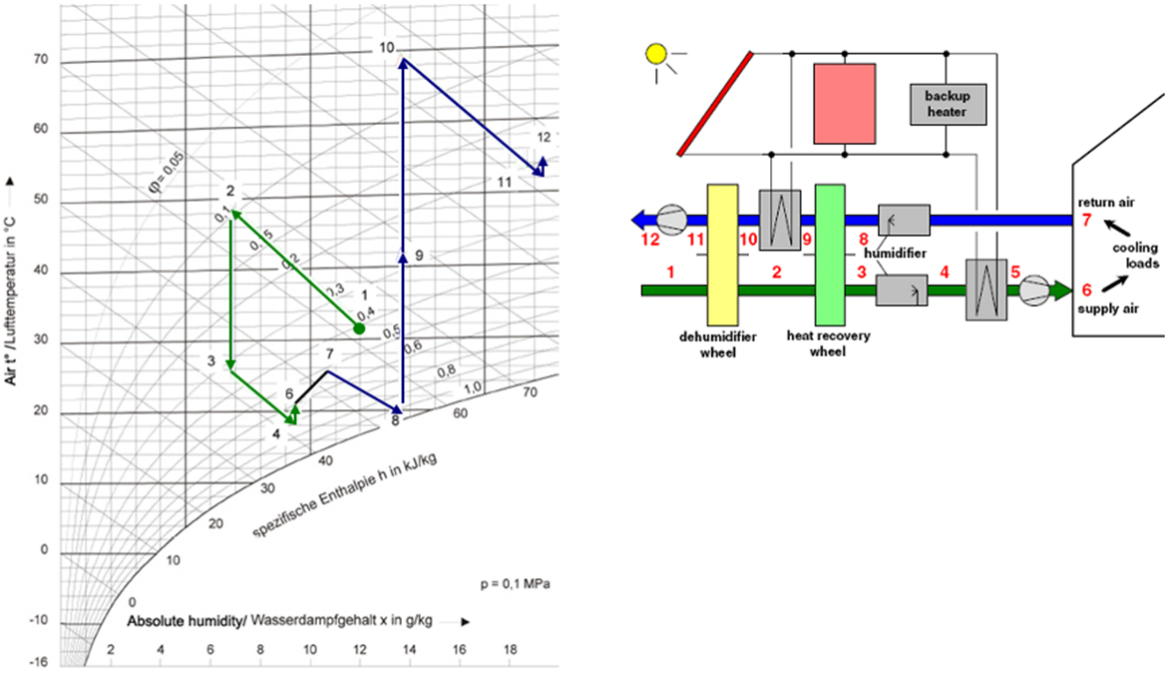

Figure 1.24: Desiccant system operation from SONNENKLIMA (2002) and Henning (2007b)

10-11 Finally the desiccant wheel is regenerated by rejecting the moisture to the return air flow.

During **heating season** the operation is a little bit different:

2-3 The outdoor air is heated by the heat exchanger.

3-4 Humidification up to reach comfortable conditions.

4-5 Air is heated by solar energy or by any other heat source.

5-6 Air is slightly heated by the fan.

6-7 Air flow satisfies the heating load.

8-9 The return flow heats the supply flow.

12 The air flow returns outdoor.

A number of systems similar to the one pictured in figure 1.24 exists (Daou *et al.*, 2004). The represented system also has different control possibilities. Depending on ambient and building air and humidity, the desiccant wheel, the heat exchanger and the humidifiers can be either switched on or off. Moreover

the desiccant wheel speed can be controlled. In short, the control of the air handling unit is difficult because of the ambient air humidity variation.

One operating mode which is considered as passive cooling is interesting to introduce here, it is called *Adiabatic Cooling*. This mode consists in using the two humidifiers but no desiccant wheel nor solar energy. If the ambient air is dry enough and the cooling load slightly low, the humidification (steps 3-4 and 7-8 on figure 1.24) is sufficient to reach comfortable conditions in the building. It is actually a combination of *direct* and *indirect* adiabatic cooling. On the one hand, *direct* implies the water is directly sprayed into the process air stream (step 3-4). On the other hand, the *indirect* adiabatic cooling consists in using another air stream cooled directly with evaporation and exchange energy with the process air stream trough a heat exchanger (steps 7-8 and 8-9).

Liquid sorption

The principle is globally the same as for solid sorption. The liquid sorption system used for drying the air basically consists of an absorber and a regenerator (figure 1.25) instead of a desiccant wheel. The humidity is absorbed from the process air into the hygroscopic solution in the absorber (replaces step 1-2 in solid desiccant cooling system figure 1.24). Then the diluted sorbent solution is regenerated by achieving the moisture desorption in the regenerator (as in step 9-10).

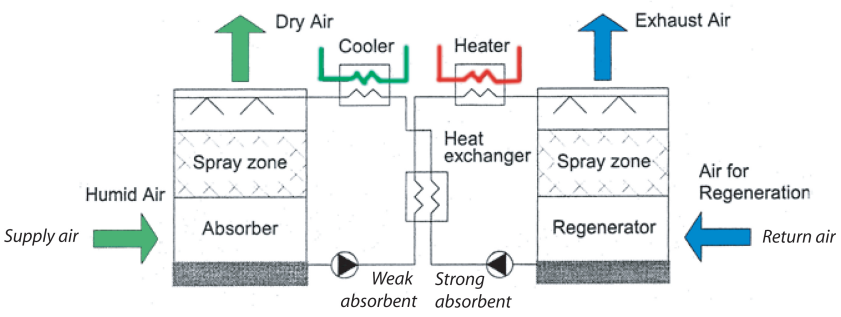

Figure 1.25: Liquid desiccant cooling system operation principle (CLIMASOL, 2002)

The solution is sprayed into the absorber, it flows by gravity to the vessel (some vertical plates could be installed). The absorbent used can be Lithium Chloride or Calcium Chloride, it requires a regeneration temperature from 60 to 85°C.

The major problems concerned with liquid desiccant cooling systems are corrosion caused by inorganic salts and transport of liquid desiccant into the

air-stream (Conde-Petit, 2007).

The desiccant technologies will no longer be studied in this work as the focus will now be put on absorption and adsorption systems.

1.3.5 Triple phase absorption chiller

Another system based on absorption technology is interesting to introduce here (Bales and Nordlander, 2005) for sake of completeness. It is a triple-phase absorption chiller (using the Lithium Chloride Water couple). This makes it significantly different from the traditional absorption processes as it is a three phases process (solid, solution and vapour). On the Oldham diagram on figure 1.17 (page 23), the cycle widens to the crystallization line. The system benefits from two main advantages: high energy density storage in the solid crystals and good heat and mass transfer, as this occurs with a liquid solution. The other originality of this product is to combine a solar cooling system with energy storage as it is an intermittent cycle.

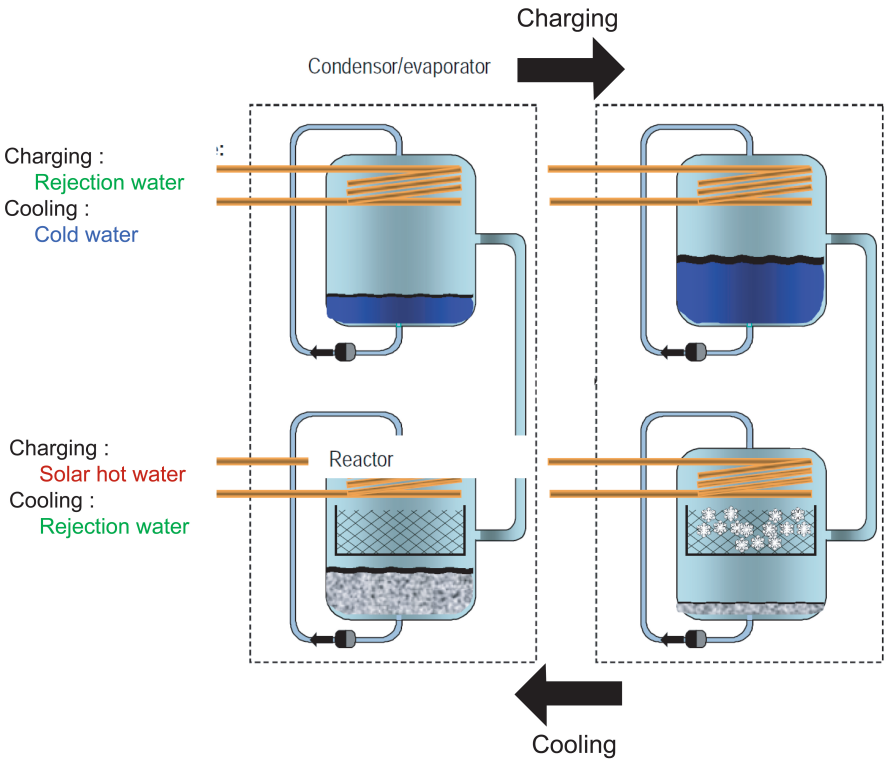

Figure 1.26: Triple phase absorption cooling system operation principle (ICOGEN, 2009)

The machine consists of two barrels that can alternatively be charged and discharged (independently). The charging mode is presented in figure 1.26. Left side represents the beginning of the charging phase while right side is the end of phase.

The hot water from thermal source heats the mix of Lithium Chloride and water contained in reactor (desorption reaction). Water condensates in condenser to maintain an appropriate pressure level in reactor (helped by the rejection circuit). Lithium Chloride, when heated enough, returns to crystalline phase. A basket is put in the bottom of the reactor to avoid pumping crystals. So, the reactor is charged for the next phases where water will be absorbed.

The cooling mode (figure 1.26) includes the evaporation of refrigerant and absorption of the Lithium Chloride. The right side represents the beginning of cooling phase while the left side is the end of the phase. As the absorption progresses, the Lithium Chloride returns to the liquid phase (the crystals are dissolved). The evaporated water (bringing the cooling effect) is absorbed in the reactor. The cycle lasts few hours (compared to few minutes for adsorption chiller) and allows short to long term energy storage.

The Thermal COP for cooling is 0.68 in nominal conditions ($T_{H\,in} = 83$, $T_{M\,in} = 30$, $T_{C\,out} = 15$). Recently the company who patented this technology in 2000 went bankrupt. It sold a machine with $10kW_C$ cooling power (per barrel) and $28\,kWh$ stored energy (per barrel) (ICOGEN, 2009).

1.3.6 Miscellaneous technologies and systems

This paragraph goes through some systems or technologies that are still at laboratory level but very promising.

Double effect absorption machine for heating and cooling

The main issue of solar-assisted air-conditioning dissemination is the system costs. Taking advantage of the same device for Heating and Cooling could bring in more attractive systems.

A new double effect absorption heat pump for both heating and cooling seems to be interesting to introduce here. It is in operation since 2010 in South Germany and surveyed by Riepl *et al.* (2011). Previously, the same kind of system was built in 2009 in Japan for cooling only (Onda *et al.*, 2009).

The driving idea is straightforward; by using a higher driving temperature (200°C instead of 60-90°C) it is possible to use a double effect absorption machine which has a higher thermal COP (1.2 instead of 0.6-0.7). Solar hot water scarcely accomplishes so high temperatures while it is not a problem for a back-up heat source (e.g. gas burner). This system is able to operate in single effect or double effect mode. The operation is described on figure 1.27 (where SE

means Single Effect, DE means Double Effect).

Firstly, in the summer, three cases can be encountered (from the left to the right in figure 1.27):

- *C1* for a sunny day: operation similar to any single effect absorption chillers. (thermal COP = 0.7),
- *C2* for a quite sunny day: hot water mass flow at 90°C not sufficient to satisfy the cooling load; The gas burner drives the high temperature cycle while the lower temperature cycle is partially driven by the solar loop,
- *C3* for a cloudy day: back-up system is the only source for driving the absorption chiller. Double effect machine leads to a thermal COP of 1.2.

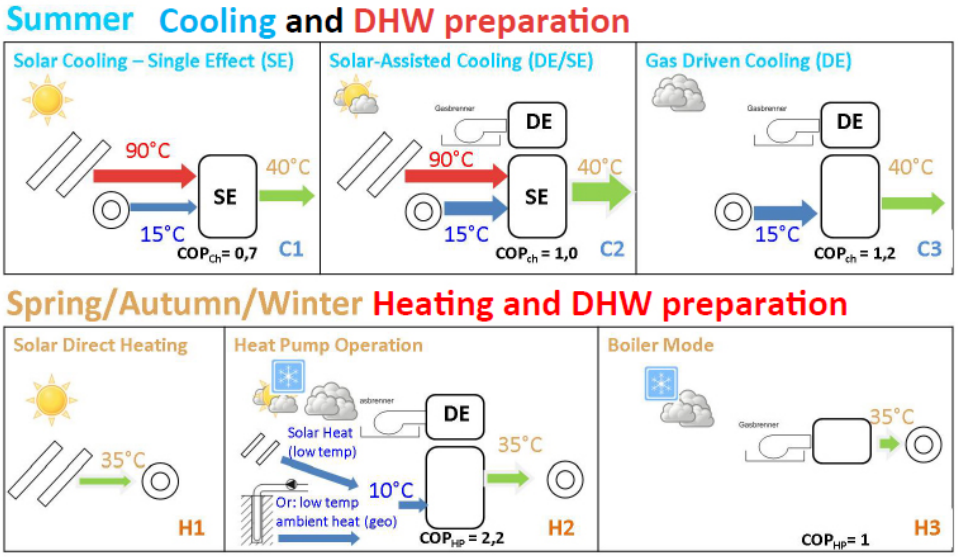

Figure 1.27: Operation modes of double effect absorption chiller for heating and cooling (Riepl *et al.*, 2012)

Secondly, in other seasons, the system can heat the building:

- *H1* direct solar heating,
- *H2* solar assisted heating where the absorption machine acts as a heat pump. The cold source is provided by the solar collectors. The thermal heat pump coefficient of performance target is 2.2 but the real measured value is 1.5 (Riepl *et al.*, 2012),
- *H3* classical gas burner heater is used when no cold source is available. The energy performance is limited by the gas burner efficiency.

Where the thermal heat pump COP is defined as the ratio between the useful heat (rejection flow) and the driving heat (hot water flow).

This system has the advantage of an all-in-one system. The reduction of the complexity of the system could decrease its costs and increase its reliability. Heating and cooling with the same integrated system appears to be a convenient solution for the implementation of renewable energies in building.

Contacts with Mr Riepl gave some measured system performances. In the summer 2011, the system mostly operated in single effect with a thermal COP of 0.6. The partial load is very frequently met. After the summer operation, some adjustments and optimization have been undertaken. During the winter 2010-2011, the heat pump operation did not operate. Direct solar heating led to a solar fraction of heat demand of 14% and a mean collector efficiency of 27%. In winter 2011-2012, the double effect heat pump operated some times and the reached thermal COP was 1.5. Those results show the importance of experimentation and better knowledge of dynamic effects and partial loads. Nevertheless, this system seems to be interesting on both energy and economical aspects.

Steam jet ejector system

The ejector technology is presented in figure 1.3 as a system driven by thermomechanical compression. The main advantage is the system simplicity that could decrease its costs. Ejector systems have been investigated for solar cooling applications for a while (Chunnanond and Aphornratana, 2004) but no system is available on the market yet (Abdulateef *et al.*, 2009).

The ejector is in fact a pipe with a shape similar to a jet engine. Its operation can be described following (figure 1.28) Chunnanond and Aphornratana (2004).

The high pressure steam(P), known as "primary fluid", expands and accelerates through the primary nozzle (i), it fans out with supersonic speed to create a very low pressure region at the nozzle exit plane (ii) and hence in the mixing chamber. According to the differences of pressure of two positions, higher-pressure vapour, which, can be called the secondary fluid (S), can be entrained into the mixing chamber. The primary fluids expanded wave was thought to flow and form a converging duct without mixing with the secondary fluid. At some cross-section along this duct, the speed of secondary fluid rises to sonic value (iii) and chokes. The ejector is indeed a way to create a pressure difference (thus a compression) into a fluid. The rest of the system includes a condenser and an evaporator such as in ab-adsorption cooling systems. There is no need for a couple of materials, only one refrigerant is required. Figure 1.29 displays the a typical ejector system.

As heat is added to the boiler, the high pressure and temperature refrigerant vapour is evolved and used as the primary fluid for the ejector. The ejector draws low pressure refrigerant from the evaporator as its secondary fluid. This

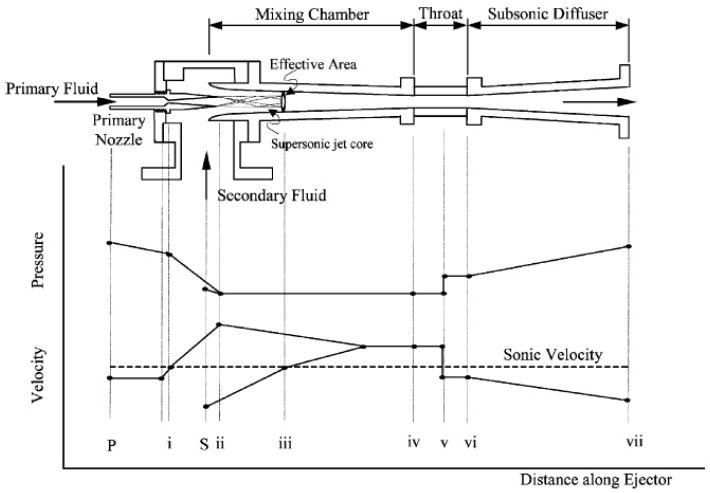

Figure 1.28: Schematic view and the variation in stream pressure and velocity as a function of location along a steam ejector (Chunnanond and Aphornratana, 2004).

causes the refrigerant to evaporate at low pressure and produce the useful refrigeration. The ejector discharges its exhaust to the condenser where it is liquefied at the ambient temperature. Part of the liquid refrigerant is pumped back to the boiler whilst the remainder is returned to the evaporator via a throttling device.

Some heat exchangers could be added for example to transfer energy from the ejector exhaust to the boiler supply.

One example of ejector system is interesting to describe, it is developed by Pollerberg *et al.* (2012). The analysis does not deal yet with experimental setup. The main idea is to use water only in the whole cooling system without hydraulic separation. By using the same fluid in collectors (able to produce steam), cooling water loop, cold loop and in the ejector (figure 1.30) the heat exchanger temperature lifts disappear and some pumps can be avoided. The solar cooling system is simple in design and a high reliability of operation can be expected. A solar-driven steam jet ejector chiller with a cooling capacity of 80 kW_C will be realised as demonstration plant in Germany.

Organic Rankine Cycles

Solar cooling systems could be implemented in another way. An Organic Rankine Cycle (ORC) could be implemented to produce mechanical work driven by solar thermal energy. The compressor of a vapour compression chiller could directly be installed on the expander transmission shaft (Pridasawas, 2006).

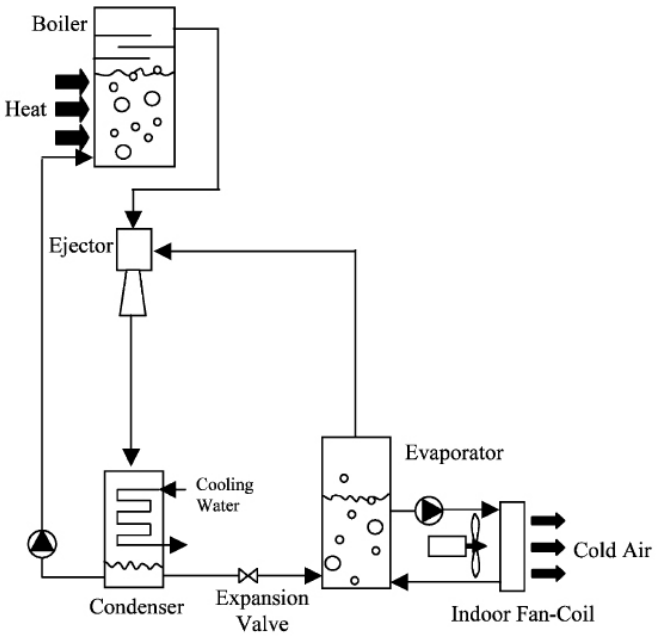

Figure 1.29: Typical ejector cycle (Chunnanond and Aphornratana, 2004)

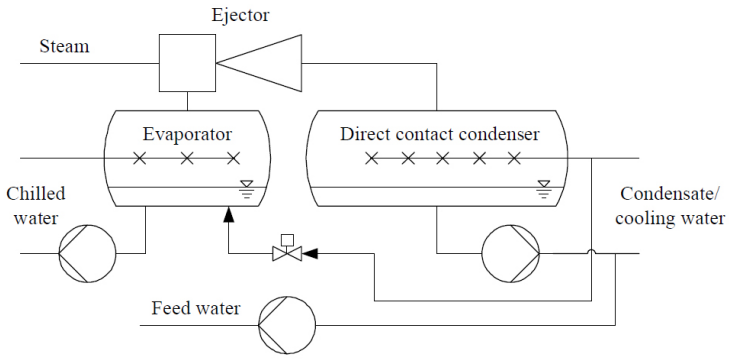

Figure 1.30: Open loop ejector cycle (Pollerberg *et al.*, 2012)

Generally those cycles are connected to an electricity generator.

This technology requires a certain level of temperature depending on the working fluid. A solar thermal application already implemented has to reach 200°C (Canada *et al.*, 2005). The efficiency (electricity generation compared to the solar energy collected) of such system in this temperature range ended up

with around 10-12% (Quoilin, 2007) which is comparable to the PV efficiency.

1.3.7 Technologies summary

The key informations of the market available technologies are summarized on figure 1.31. The $EER_{thermal}$ corresponds to the thermal COP and *Driving Temperature Range* corresponds to $T_{H\,in}$. The types of systems cover all the thermally driven systems dedicated to solar cooling of buildings. The triple-phase absorption chiller described below is classified in the solid sorption class in this figure.

The systems could also operate in heating mode during the heating season as depicted on figure 1.27. Firstly the solar collector could directly satisfy the heating or domestic hot water demand. Secondly, the thermally driven chiller could operate in heating mode. The rejection temperature ($T_{M\,out} \approx 30-35°C$) is able to heat a building with low temperature emission devices such as floor heating. In that way, the driving heat could come from an auxiliary heater while the cold sink could be either solar collectors or geothermal heat exchanger.

Type of system	**Water chillers (closed thermodynamic cycles)**						**Direct air treatment (open thermodynamic cycles**	
Physical phase of sorption material	Liquid			Solid			Liquid	Solid
Sorption material	Water	Lithium-bromide		Zeolite	Silica gel	Lithium-chloride	Lithium-chloride	Silica gel (or zeolite), cellulose matrix with lithium-chloride
Refrigerant	Ammonia	Water		Water	Water	Water	Water	Water
Type of cycle(1)	1-effect	1-effect	2-effect	1-effect	1-effect	1-effect	Cooled sorption process	Desiccant rotor
$EER_{thermal}$ range	0.5-0.75	0.65-0.8	1.1-1.4	0.5-0.75	0.5-0.75	0.5-0.75	0.7-1.1	0.6-0.8
Driving temperature range, °C	70 … 100 120 …180(2)	70 … 100	140 … 180	65 … 90	65 … 90	65 … 90	60 … 85	60 … 80
Solar collector technology(3)	FPC, ETC SAT(2)	FPC, ETC	SAT	FPC, ETC	FPC, ETC	FPC, ETC	FPC, ETC, SAHC	FPC, ETC, SAHC

Comments:
1 1-effect: single-effect thermodynamic cycle (no internal heat cascade); 2-effect: double-effect thermodynamic cycle (with internal heat cascade)
2 Valid for production of cold at temperatures significantly below the freezing point of water, i.e. < 0°C
3 Abbreviations for solar thermal collector types: FPC = flat plate collector; ETC = evacuated tube collector; SAT = single-axis tracking solar collector (e.g. parabolic trough collectors or Fresnel type collectors); SAHC = solar air heating collector

Figure 1.31: Overview on thermally driven cooling systems based on sorption technology available on the market (Henning, 2011)

For each market available technology, figure 1.31 could be completed with other interesting information. The tables 1.2 to 1.5 summarize each technology with main advantages and disadvantages as well as other key figures.

Sorption material	*Refrigerant*	*Operating temperature range* $T_{H\,in}$	$T_{M\,in}$	$T_{C\,out}$	Typical nominal thermal COP and temperature conditions $(T_{H\,in}, T_{M\,in}, T_{C\,out})$
Lithium-Bromide	Water	$55-95$	<37	>6	$0.78\,(85, 27, 15)$ [a]
Lithium-Bromide	Water (double effect)	$140-180$		>6	$1.2\,(175, 29.4, 6.7)$ [b]
Water	Ammonia	$65-110$	<36	>-3	$0.73\,(75, 24, 15)$ [c]
Lithium-Chloride	Water	$85-110$	<30	>10	$0.68\,(83, 30, 15)$ [a]

Nominal power	$>10kW_C$
Advantages	Widespread technology (more operation feedback)
	Few moving parts (one pump at least), increase the machine lifespan
	Environmentally friendly materials
	Keep high thermal COP values while meeting low cold temperature (6°C)
	No noise nor vibrations
Disadvantages	Part load operation decreasing the thermal COP
	Low pressure process, leakages could appear
	Three energy flows to drive involve higher auxiliaries consumption

Table 1.2: Absorption chiller technology summary.
The numerical values are given for existing cooling machine:
[a] Hallström *et al.* (2010), [b] THERMAX (2012) , [c] Pink (2010)

Sorption material	*Refrigerant*	*Operating temperature range* $T_{H\,in}$	$T_{M\,in}$	$T_{C\,out}$	Typical nominal thermal COP and temperature conditions $(T_{H\,in}, T_{M\,in}, T_{C\,out})$
Zeolite	Water	$55-95$	<40	>8	$0.6\,(72, 27, 15)$ [a]
Silica gel	Water	$55-95$	<37	>8	$0.6\,(72, 27, 15)$ [b]

Nominal power	$>8kW_C$
Advantages	Lowest driving temperature
	Few moving parts (valves only), increase the machine lifespan
	Environmentally friendly materials
	No noise nor vibrations
Disadvantages	Part load operation decreasing the thermal COP
	Low pressure process, leakages could appear
	Three energy flows to drive involve higher auxiliaries consumption
	Lower thermal COP compared to absorption chillers (due mainly to intermittent cycle)

Table 1.3: Adsorption chiller technology summary
The numerical values are given for existing cooling machines [a] INVENSOR (2010), [b] SORTECH (2009)

		Operating temperature range			
Sorption material	*Refrigerant*	$T_{H\,in}$	$T_{M\,in}$	$T_{C\,out}$	Typical nominal thermal COP
Solid sorbent	Water	$60-80$	–	>18	$0.6-0.8$
Liquid sorbent	Water	$60-85$	–	>18	$0.7-1.1$

Nominal power	$>10kW_C$
Advantages	Quite low driving temperature
	Does not require rejection loop
	Environmentally friendly materials
	Can be integrated in the Air Handling Unit
Disadvantages	Control more difficult if high relative humidity
	Thermal COP depends strongly on ambient conditions
	Desiccant system involves water consumption
	Water treatment must be carried out (energy use)
	Maintenance due to moving parts and water spraying

Table 1.4: Desiccant cooling technology summary
The numerical values come from Henning (2011)

	Typical nominal electrical COP and temperature conditions $(T_{M\,in}, T_{C\,out})$
Water cooled chiller	$\approx 4\,(30, 7)$
	Electrical COP includes compressor and other miscellaneous chiller consumptions
Nominal power	For any cooling power
Advantages	
	Mature technology
	Two energy flows to drive
	High electrical COP
Disadvantages	
	Refrigerant havs a larger environmental impact
	Noise and vibrations, maintenance due to moving parts
	High pressure process, leakages could appear

Table 1.5: Vapour compression chiller (grid connected) technology summary

1.3.8 Solar cooling systems implementation schemes

The solar cooling systems studied in this work follow the general schemes presented in figures 1.32 and 1.33 respectively for thermally driven system and PV driven systems. This work focuses on cooling needs but also covers heating load and domestic hot water demand (depending on the case study).

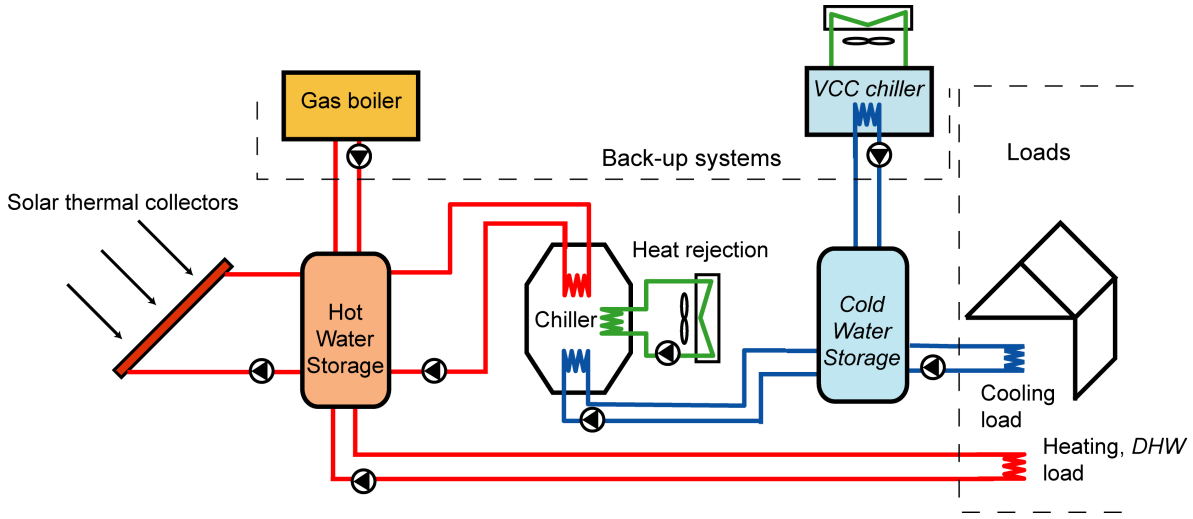

Figure 1.32: Thermally driven solar cooling system general scheme (mandatory and *optional* devices)

The thermally driven systems contain an absorption or adsorption chiller. The back-up systems connections could be modified as explained in section 1.4. The figure shows mandatory and *optional* devices. Depending on the case study, the back-up devices and/or cold storages can be removed. The main rejection devices used in solar cooling systems are dry cooling tower (with or without spraying kit), wet cooling tower, geothermal heat exchanger or swimming pool (Besana *et al.*, 2009). These sinks have to dissipate a heat flow at 30-35°C temperature level. The rejection loop could also contain a storage tank to delay the heat sink use (Helm *et al.*, 2009).

Water storage tanks are displayed but this is obviously not the only technology to store energy. Among all thermal energy storages (Evliya, 2007), the latent heat or cold storage is sometimes selected to increase the energy storage density (Zetzsche *et al.*, 2009). The research on those phase change materials (Tatsidjodoung *et al.*, 2013) achieves numerous new techniques for heat and cold storages (Liu, 2010). The collector and storage designs are really impacting the overall system performance and thus comfort conditions.

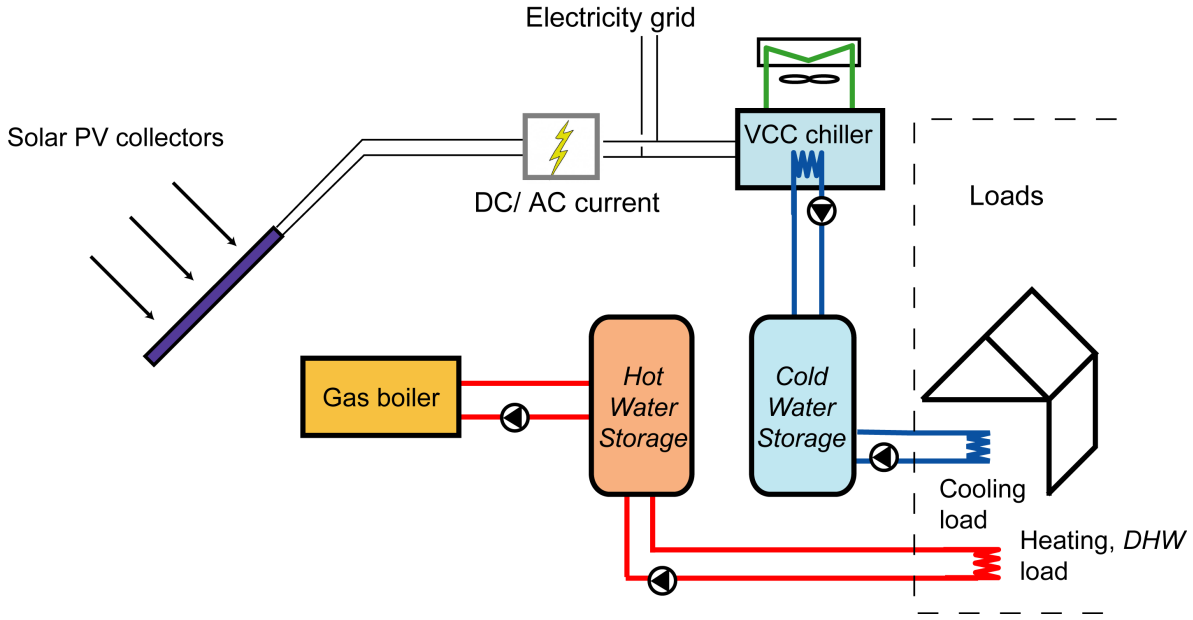

Figure 1.33: PV driven solar cooling system general scheme (mandatory and *optional* devices)

The PV driven system general scheme is described in figure 1.33. This cooling system includes a grid connected PV field and a vapour compression chiller (VCC). Depending on the case study, the cold water storage is used or not. Moreover, the VCC could be a direct expansion machine that does not deal with water loops (evaporator and/or condenser). A gas boiler back-up satisfies the heating and/or domestic hot water load. Furthermore, the possibility to use a reversible heat pump for building heating could be investigated.

1.4 Solar cooling system performance indicators

The previous paragraphs detailed the different solar cooling systems. This paragraph will tackle the performance indicators definition. For the subsystems, the COP and other efficiencies have already been defined in section 1.2. Some of the overall system performance indicators are defined in previous work performed by Nowag *et al.* (2012) or Napolitano *et al.* (2011). In the frame of IEA-SHC Task 38, a unified monitoring procedure has been developed. For thermally driven systems, the global seasonal performance can be defined with the help of figure 1.34 displaying the most complete solar cooling system to enable any system analysis. Desiccant system part of the scheme has been removed because this technology is not tackled any more in this work. Besides, the solar energy is not only used for cooling but also for domestic hot water

(DHW) and for space heating (SH). The description of each variable is presented in table 1.6. This scheme has to be adapted to the analysed systems.

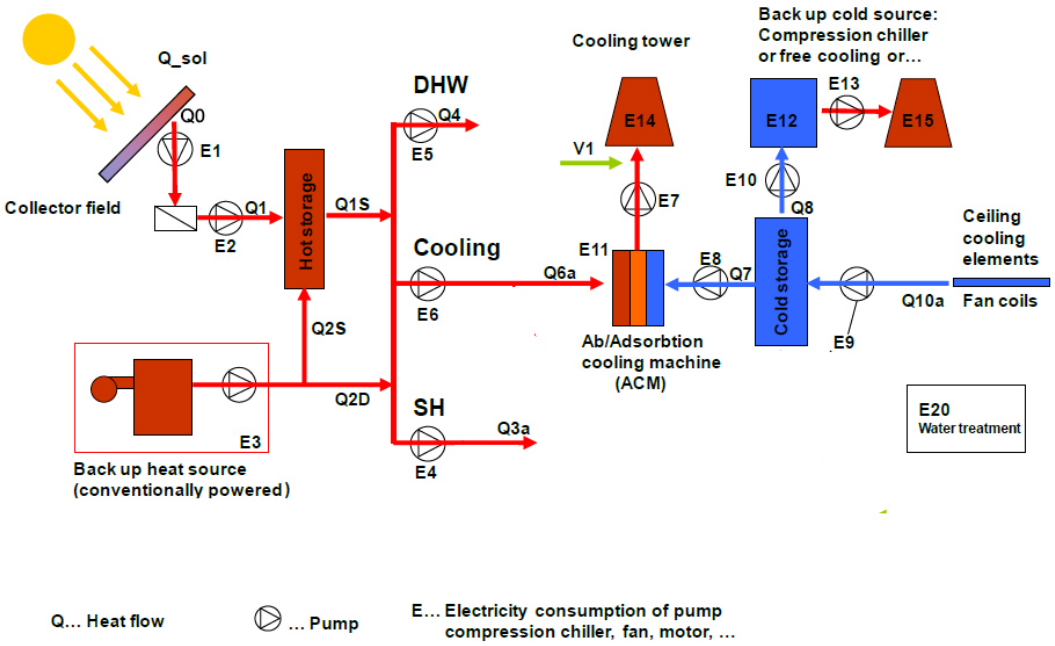

Figure 1.34: Solar cooling system variables (Napolitano *et al.* (2011) with minor modifications)

1.4.1 Energy indexes

These definitions essentially come from Napolitano *et al.* (2011) and Nowag *et al.* (2012) where the unnecessary variables for our study are removed (mainly desiccant cooling system variables). Definitions below include solar energy used for the domestic hot water and for heating as explained in section 1.3. They can be computed for various periods.

Chiller Thermal COP

In accordance with equation 1.4, the thermal performance of the chiller can be defined as follows:

$$COP_{therm} = \frac{Q_7}{Q_{6a}} \tag{1.17}$$

It has an instantaneous value varying with the operating conditions. The manufacturer usually gives the steady-state thermal COP with selected chiller inlet/outlet temperatures and mass flows (INVENSOR, 2010). The order of

Label	**Electricity consumer [kWh]**
	Heating System
E_1	pump collector field (primary loop)
E_2	pump collector field (secondary loop)
E_3	pump boiler hot-storage (including internal boiler consumption)
E_4	pump hot-storage to space heating (SH)
E_5	pump hot-storage to domestic hot water (DHW)
	Cooling System
E_6	pump hot-storage to cooling machine
E_7	pump cooling machine (ACM) to cooling tower
E_8	pump cooling machine (ACM) to cold-storage
E_9	pump cold storage to cold distribution
E_{10}	pump back-up source - cold storage
E_{11}	absorption/adsorption cooling machine (ACM)
E_{12}	compression chiller (back-up system)
E_{13}	pump compression chiller to fan (back-up system)
E_{14}	fan, cooling tower
E_{15}	fan of compression chiller (back-up system)
	Water treatment System
E_{20}	water treatment for wet cooling tower
	Thermal flows [kWh]
Q_{sol}	solar irradiation on total collector aperture area
Q_0	collector solar thermal output
Q_1	solar thermal output to hot storage
Q_{1s}	heat output from hot storage
Q_{2S}	boiler thermal output (fossil) into storage
Q_{2D}	fossil boiler thermal input (fossil) bypassing hot storage (directly used)
Q_{3a}	space heating (SH) consumption (conventional)
Q_{3b}	space heating (SH) consumption (ventilation system)
Q_4	domestic hot water (DHW) consumption
Q_{6a}	hot storage input to cooling machine (ACM)
Q_{6b}	hot storage input to DEC-system (sorption regeneration)
Q_7	cold output ACM to cold-storage
Q_8	cold output back-up chiller or free cooling to cold-storage
Q_{10a}	cold storage output to cold-distribution
Q_{10b}	cold storage to Air Handling Unit (AHU)
	Water Consumption [Litre]
V_1	water consumption for wet cooling tower

Table 1.6: Energy or water consumer fields and thermal flows of solar cooling systems (Napolitano *et al.*, 2011)

magnitude of this index for the different technologies is displayed in figure 1.31 where the thermal COP is named $EER_{thermal}$.

Electrical COP's

For the thermally driven system, the definition of electrical COP is crucial. Various indexes could be defined depending on the auxiliaries consumption incorporated. As we consider an entire system, the electrical COP has to entail space heating load and domestic hot water. The COP represents the useful effect divided by the electricity consumed to produce it. The definitions below are successively including more auxiliary devices.

First of all, the electrical COP of the chiller itself from equation 1.18

$$COP_{el\ chill} = \frac{Q_7}{E_{11}} \tag{1.18}$$

The mandatory pumps (1 for each chiller flow) is included in the next COP definition on equation 1.19

$$COP_{el\ chill\ pump} = \frac{Q_7}{E_6 + E_7 + E_8 + E_{11}} \tag{1.19}$$

The cooling tower generally has a significant impact on energy use (Henning, 2011). For rejection device comparison, it is interesting to introduce the heat rejection COP (equation 1.20).

$$COP_{rej} = \frac{Q_{6a} + Q_7}{E_{14} + E_{20}} \tag{1.20}$$

For the same reason, the solar loop electrical performance is defined by equation 1.21.

$$COP_{solar\ loop} = \frac{Q_0}{E_1 + E_2} \tag{1.21}$$

Then the cold production is rated on the sum of all the electricity consumptions relevant with the thermally driven chiller (equation (1.22)), i.e. pump hot-storage to cooling machine, pump cooling machine to cooling tower, pump cooling machine to cold-storage, absorption/adsorption cooling machine and cooling tower.

$$COP_{el\ cold\ chill} = \frac{Q_7}{E_6 + E_7 + E_8 + E_{11} + E_{14}} \tag{1.22}$$

Finally, the total electrical COP ($COP_{elec\ tot}$ on equation 1.23) computes the ratio of useful heat and/or cold in relation to the entire electricity consumption needed but exclude the electrical consumption of pumps and fans which are used to distribute heat and/or cold in the building by pumping water or blowing air. This index could also be computed for a conventional system by removing the missing flows and electricity consumptions in equation 1.23.

$$COP_{elec\ tot} = \frac{Q_{3a} + Q_{10a} + Q_4}{\underbrace{E_{1\to4} + E_{6\to8} + E_{10\to15} + E_{20}}_{E_{elec\ tot}}} \tag{1.23}$$

To be complete, the electrical COP of a vapour compression chiller (included in figure 1.34) must be also defined (equation 1.24).

$$COP_{VCC} = \frac{Q_8}{E_{10} + E_{12} + E_{13} + E_{15}} \tag{1.24}$$

Primary Energy Ratio and Fraction of energy savings

The primary energy ratio (PER in equation 1.25) is the ratio of useful heat and/or cold in relation to the primary energy demand. The primary energy factors (ϵ) were previously defined in equations 1.14 and 1.15 on page 20. If the PER is high, the system uses less primary resources to generate the same useful effect. The PER could also be defined for a reference system (equation 1.26) and a PV driven system (equation 1.27) where Q_{PV} is the energy produced by the PV field.

$$PER_{therm} = \frac{Q_{3a} + Q_{10a} + Q_4}{\frac{Q2_S + Q2_D}{\epsilon_{fossil}\,\eta_{boiler}} + \frac{E_{elec\,tot}}{\epsilon_{elec}}} \tag{1.25}$$

$$PER_{ref} = \frac{Q_{3a} + Q_{10a} + Q_4}{\frac{Q_{boiler\,ref}}{\epsilon_{fossil}\,\eta_{boiler}} + \frac{Q_{VCC\,ref}}{SPF_{ref}\,\epsilon_{elec}} + \frac{E_{boiler\,ref}}{\epsilon_{elec}}} \tag{1.26}$$

Where

$Q_{boiler\,ref} = Q_{3a} + Q_4 +$ the tank losses if reference system contains a hot water storage

$Q_{VCC\,ref} = Q_{10a} +$ the tank losses if reference system contains a cold water storage

$SPF_{ref} = 2.8$ if no other value is provided as defined in equation 1.12

$E_{boiler\,ref} =$ the boiler electricity consumption $= 0.02\,Q_{boiler\,ref}$ if no other value is provided

$$PER_{PV} = \frac{Q_{3a} + Q_{10a} + Q_4}{\frac{Q_{2S} + Q_{2D}}{\epsilon_{fossil}\,\eta_{boiler}} + \frac{E_{elec\,tot} - Q_{PV}}{\epsilon_{elec}}} \tag{1.27}$$

Another index uses the primary ratio to check whether there are energy savings by installing a solar cooling system instead of a conventional (reference) system. The fraction of energy savings is written in equations 1.28 and 1.29 in case of thermally driven system or PV driven system. A positive value involves energy savings while a negative one means energy waste.

$$f_{sav} = 1 - \frac{PER_{ref}}{PER_{therm}}[-] \tag{1.28}$$

$$f_{sav} = 1 - \frac{PER_{ref}}{PER_{PV}}\,[-] \tag{1.29}$$

Solar efficiency

The solar efficiency can be defined in two ways, it respectively expresses the energy conversion quality of the collectors (including or not solar loop) and the energy collected by the collector per square meter aperture area. The first definitions are similar to collector efficiency defined before by equation 1.8. They are specified for the collector only (equation 1.30) and for the whole solar loop including collector and pipes (equation 1.31). The second one tells the quantity (per year) of stored solar energy per collector area (equation 1.32).

$$\eta_{thermal\ collector} = \frac{Q_0}{Q_{sol}} \tag{1.30}$$

$$\eta_{solar\ loop} = \frac{Q_1}{Q_{sol}} \tag{1.31}$$

$$Q_{coll\ yield} = \frac{Q_1}{Collector\ Aperture\ Area} \left[\frac{kWh}{m^2\ year}\right] \tag{1.32}$$

Solar fraction

When the studied system is an "assisted system" meaning a back-up is put in place, the sharing between solar energy and back-up energy must be exploited. This becomes quite complex to evaluate when the system can deal with two different back-ups.

First a back-up on the hot side is considered (typically gas boiler), the vapour compression machine does not stand any more in the system. Three sub-cases must be cited:

- *DIRECT STO* sub-case: back-up heat source is **only** connected to the storage ($Q_{2D} = 0$),
- *NO STO* sub-case: back-up heat source is **not** connected to the storage ($Q_{2S} = 0$),
- *COMBI* sub-case: back-up heat source is connected on **both** sides ($Q_{2D}$and$Q_{2S} \neq 0$).

The solar fraction (SF) is the ratio between the solar heat and the total heat consumed.

$$SF_{DIRECT\ STO} = \frac{Q_1}{Q_1 + Q_{2S}} \tag{1.33}$$

$$SF_{NO\ STO} = \frac{Q_{1S}}{Q_1 + Q_{2D}} \tag{1.34}$$

$$SF_{COMBI} = \frac{Q_{1S}\left(\frac{Q_1}{Q_1+Q_{2S}}\right)}{Q_1 + Q_{2S} + Q_{2D}} \tag{1.35}$$

$$\tag{1.36}$$

These factors (SF) describe as well the ratios between:

- The space heating load covered by solar energy and the entire space heating load
- The domestic hot water load covered by solar energy and the entire domestic hot water load
- The cooling load covered by solar energy and the entire space cooling load

To have a more accurate idea of the solar contribution for heating or cooling separately, this index could be computed on a monthly basis.

Secondly, the cold back-up is considered to satisfy the cooling load complementary to the thermally driven chiller. The sub-case called *NO STO* is the only one making sense for the description below. There is no need to heat the storage if the sorption cooling machine can be replaced by the vapour compression chiller. The solar fraction can now be defined separately for cooling while heating and domestic hot water solar fractions still satisfy equation 1.35.

$$SF_{cooling} = \frac{Q_7}{Q_7 + Q_8} \tag{1.37}$$

Storage efficiency

The two storage (hot and cold) efficiencies can be defined by:

$$\eta_{hot\ sto} = \frac{Q_{1S}}{Q_1 + Q_{2S}} \tag{1.38}$$

$$\eta_{cold\ sto} = \frac{Q_{10a}}{Q_7 + Q_8} \tag{1.39}$$

System Thermal Ratio and Only Solar Ratio

The **System thermal ratio (STR)** is outlined by Pridasawas (2006) as the ratio of the refrigerating effect Q_C and solar radiation input on the collector field (definition in equation 1.40). It describes the conversion quality of solar energy into cold. It could be used to compare solar systems globally. It has the advantage to compare PV driven and thermally driven systems. The calculation is simple and straightforward but needs to be enhanced.

$$STR = \frac{Q_C}{A\, I_{tot}} \tag{1.40}$$

It can be computed for both systems: PV driven - single effect chiller (rough numerical values). An approximation is given:

$$STR_{PV} = \eta_{PV} \cdot COP_{VCC} = 0.12 \cdot 2.8 \approx 0.34 \tag{1.41}$$

$$STR_{therm} = \eta_{thermal\ collector} \cdot \eta_{hotsto} \cdot COP_{therm} = 0.6 \cdot 0.9 \cdot 0.6 \approx 0.32 \tag{1.42}$$

Unfortunately this index does not include the electrical consumption of thermally driven systems. A new ratio, similar to the previous one is set up. The **Only Solar Ratio (OSR)** depicts the quality of a system using solar energy as the only energy source. In other words, the auxiliaries electrical consumption for thermally driven technologies are considered to be produced by PV. Such as the STR, it allows to globally compare systems. It answers the question : *What is the cold energy that could be produced with 1 kWh solar energy?*

$$OSR_{PV} = STR_{PV} \tag{1.43}$$

$$\begin{aligned} OSR_{therm} &= Thermal\ fraction \cdot \eta_{thermal\ collector} \cdot \eta_{hotsto} \cdot COP_{therm} \\ &= (1 - Thermal\ fraction) \cdot \eta_{PV} \cdot COP_{elec\ tot} \end{aligned} \tag{1.44}$$

Where
$Thermal\ fraction$ is the fraction of the solar field dedicated to thermal collector. Its value can be found by solving the equation 1.44.

The seasonal OSR reaches the following value for a targeted single stage system:

$$\begin{aligned} OSR_{therm} &= 0.77 \cdot 0.5 \cdot 0.9 \cdot 0.6 \\ &= (1 - 0.77) \cdot 0.09 \cdot 10 \\ &\approx 0.21 \end{aligned} \tag{1.45}$$

This index allows to evaluate the ratio between thermal and PV collectors assuming the system is entirely driven by solar energy. It could be evaluated for a given operation point or for the entire cooling season.

1.4.2 Economical indexes

The economical profitability computation of solar system is important in an integrated approach. The main indexes for any kind of investment are the Net Present Value (NPV) and the payback time. Besides, the cost of primary energy savings index in $€/kWh$ allows to evaluate the system profitability under the environmental aspect. More information about economical indexes will be given in chapter 3.

1.4.3 Building comfort indicators

The solar cooling systems are used to cool the building. Some indicators have to be defined to evaluate the system capacity to meet required comfort conditions. A fraction of time of uncomfortable conditions index is set up. More information about comfort and its indexes will be given in chapter 2.

1.4.4 Indexes summary

Table 1.7 reminds the most important solar cooling system indexes, some common measured values (on good systems) and the minimal values for quality insurance (Nowag *et al.*, 2012). The numerical value can be seen as plausible values representative of common solar cooling systems. Their performance clearly varies depending on many features such as the climate, the building load, the collector surface, the piping...

Index	**Time scale**	**Value**	**Source**	**Minimal requirement**	**Source**
COP_{therm}	Instant.	$0.5 - 0.8$ [−]	figure Henning (2011)	0.5	Wiemken *et al.* (2010)
COP_{therm}	Cool. seas.	$0.5 - 0.6$ [−]	Rosiek and Batlles (2009) Neyer and Streicher (2011)	$0.8 * COP_{nominal}$	Nowag *et al.* (2012)
$COP_{elec\,tot}$	Cool. seas.	5.4 [−]	Vukits *et al.* (2011)	10	Wiemken *et al.* (2010)
PER_{therm}	Cool. seas.	[−]		1	Nowag *et al.* (2012)
$Q_{coll\,yield}$	Yearly	350 $[\frac{kWh}{m^2\,year}]$	*Simulation* Thomas and André (2012)	350	Nowag *et al.* (2012)
COP_{VCC}	Instant.	> 4 [−]	EUROVENT (2012)		
$SPF_{VCC\,ref}$	Cool. seas.	2.8 [−]	Napolitano *et al.* (2011)		

Table 1.7: Measured and minimal requirements of the most important energy indexes

1.5 Discussions

There are various ways to convert solar energy into cooling power. Some of the technologies are already available on the market for a wide range of cooling power. The distinction between thermally and electrically driven chillers is essential as the two techniques imply different thermodynamic cycles and solar energy conversion (respectively PV and thermal collectors).

For thermally driven systems, the choice of technology and system is driven by the cooling load and the required temperature levels:

On the hot side, the choice of collector must suit the chiller requirements (for example concentrating collector for high temperature $> 120°C$),

On the rejection side, the chosen recooling device must cope with the chiller rejection temperature level and the ambient temperature. For example, a wet cooling tower is preferred to a dry cooling tower if the chiller rejection temperature is close to the ambient temperature. A compromise must be found between the rejection temperature to attain and the electricity consumption of rejection device. Desiccant systems do not require any recooling unit.

On the cold side, the temperature level has to be consistent with the building cold emission devices. On the one hand, fan coil units involving sensible and latent load handling must be supplied by cold water temperature (around 7°C). On the other hand, surface cold emitting devices are fed with water temperature of around 15°C to avoid condensation. Finally, cooling by ventilation also requires appropriate set points to satisfy the cooling load.

The thermal performance of the chiller and the global performance (thermal and electrical) of the cooling system mainly depend on the choice of the three temperature levels and the appropriate selection of the devices used to reach these temperatures.

For electrically driven systems, namely PV driven systems in case of solar air-conditioning, the approach of this work is summarized as the conventional grid connected cooling system. A grid connected PV field comes additionally to feed the grid. There is no consideration about any impact of electricity transfer from/to the grid. This strong hypothesis is discussed in chapters 3 and 4 and leads to simple PV driven systems rather than thermally driven ones requiring more devices.

Thermally driven systems can also be used with solar energy or other thermal source. The particularity of the solar cooling system is its low driving temperature which is adapted to the use of solar collectors. Nevertheless, this is the same temperature level as for industrial low-grade waste heat or district heating. Solar cooling and waste heat cooling are then two topics that are related. This work focuses on the solar cooling technologies but the same

principle could be kept for waste heat cooling. Generally, the waste heat is less intermittent than the solar energy which is a considerable advantage. Moreover, the low-grade waste heat accounts for 50% or more of the total heat generated by industry (Hung *et al.*, 1997) leading to the possibility of a huge market. Besides, as the solar collector costs are non negligible in thermally driven systems, they ranges from 20 to 40 % (Preisler, 2008). The economical analysis carried out in chapter 3 collector corroborates this range. The collectors replacement by a free heat source could improve the economical profitability of such a project.

To conclude, energy performance evaluation of solar cooling systems is quite complex. In addition to the energy (thermal and electrical) performance of each separate device, the entire system energy performance must be analysed. The interactions between the different parts of the system subject to variable weather conditions (temperature, radiation, humidity) imply a non-nominal system operation. A yearly evaluation could lead to system energy performance far from the one planned in nominal operation.

Chapter 2

Building heating and cooling loads

2.1 Introduction

The use of energy in buildings can be split into five main sectors: heat & cold production, ventilation, lighting, domestic hot water production and equipments. This last category includes all possible devices involved by the occupants activity (cooking, television, computers ...). Above all, the energy is used in order to satisfy the occupants comfort. It is not only the thermal environment but also the visual comfort (lighting) and the air quality (ventilation). The heating and cooling loads are the energy quantity required to maintain thermal comfort in buildings. More than the building envelope and its air tightness, it has to include all other energy use cited above because they all involve heat production. Besides, the persons heat and vapour production must be taken into account to evaluate the building heat balance.

Concerning some countries such as Belgium, well-designed residential buildings should not have too high cooling load to install an active cooling system. Nevertheless, the increase of production and sales of small scale cooling applications exhorts to pay attention to residential buildings. This chapter is dedicated to the analysis of the building heating and cooling energy loads in European residential and office buildings. Moreover, it handles the solar energy availability for different locations in Europe. Three buildings are selected, the definition of essential parameters for heating and cooling (H&C) load computation is detailed. The simulations of solar air-conditioning systems in chapter 3 use the buildings detailed below.

2.2 Comfort basics

2.2.1 Thermal comfort

Comfort models

Buildings are heated or cooled to satisfy the thermal comfort of the occupants. The underlying question is how to reach the optimal occupants thermal comfort. There are two prevailing comfort models (Pagliano, 2010):

- the comfort model originally proposed by Fanger (1970) or **Predicted Mean Vote (PMV)** model
- and the model which takes into account the adaptation to the prevailing climate of occupants of buildings: **Adaptive comfort model** (Ferrari and Zanotto, 2012)

The standard ISO7730 (2005) standardizes an analytical method based on the PMV and PPD indexes including the six main parameters (with their units) which are summarized in one value.

activity $[met]$

clothing thermal resistance $1[clo] = 0.155[m^2K/W]$

air temperature $[°C]$

radiant temperature $[°C]$

air velocity $[m/s]$

relative humidity [%]

This is called the energy balance model which was developed by Fanger in the seventies (Fanger, 1970). It allows the comfort estimation based on the seven-point-scale which is the occupants answer to the question: how do you feel at this moment?

+3 hot

+2 warm

+1 slightly warm

0 neutral

-1 slightly cold

-2 cool

-3 cold

The energy balance can be written as follows :

$$H = W + S + K + C + R + E + E_{res} + C_{res} \tag{2.1}$$

Where H is the metabolic heat production, W is the work done and S is heat stored in the body (assumed zero over time). K,C and R are the heat losses (or gains) from the clothing or skin conduction, convection and radiation. E is the heat loss from the skin by evaporation. E_{res} and C_{res} are the evaporative and convective heat exchanges through respiration.

Equations can be derived for all of these individual contributions to the heat balance equation since the metabolic rate, the clothing insulation and the

environmental parameters are known. In all these terms, except H, a negative value will constitute a heat gain to the body. The heat balance is essentially steady-state calculation.

The PMV is however a mean value to be expected from a group of people. Fanger extended the PMV to predict the proportion of any population that will be dissatisfied with its environment. Those who vote outside the central three scaling points (-1, 0, +1) are counted as dissatisfied. **The percentage of persons dissatisfied (PPD)** is directly linked to the PMV (figure 2.1).

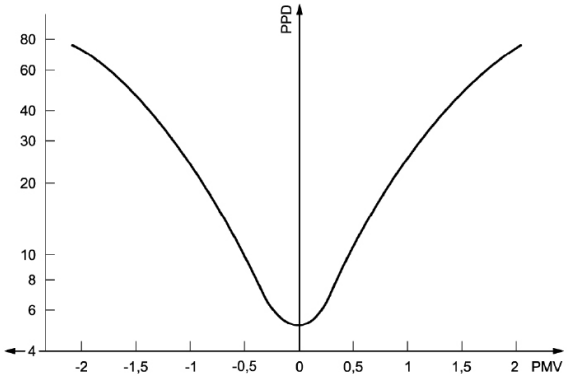

Figure 2.1: Correlation between PMV and PPD according to Fanger

Since the model is often used assuming typical values of clothing and metabolic rates, it might lead to specify a static, narrow band of comfortable room temperatures to be applied uniformly through space and time. In these cases it may disfavour the use of passive technologies and increase the cooling energy demand. The comfort level evaluation completely decouples the indoor environment from the external one. In addition, the steady state approach is not consistent with real behaviour (the body adapts to its environment).

The PMV model, in spite of being largely employed, meets some important limitations. It will be used in this work but it has to be extended to more up to date comfort models.

The **Adaptive comfort model** proposes a correlation between comfort temperature for occupants of a building with the temperature of external air (or more precisely with a moving average of past outside temperatures). The underlying concept is the adaptation of the body and the metabolic rate to the recent climate variations. This model is closer to real-life comfort requirements (Pagliano, 2010) and its use in a simulation reduces the computed cooling energy demand. Today, the EN15251 (2007) norm proposes the use of the adaptive approach only for non mechanically conditioned buildings. Nevertheless it

is suggested to implement an adaptive approach to the cooled buildings analysed in this work. Some other research (McCartney and Nicol, 2002) showed improvements regarding comfort and energy use even in actively cooled buildings when using the adaptive comfort model.

Required building temperatures

The **PMV model** implemented into standard EN15251 involves the definition of comfortable temperatures depending on the chosen building category and type. The building categories are defined with regard to the percentage of dissatisfied people:

- category I, which corresponds to a high level of expectation ($PPD < 6\%$ or $-0.2 < PMV < 0.2$), recommended in case of very sensitive and fragile occupants,
- category II, which corresponds to a normal level of expectation ($PPD < 10\%$ or $-0.5 < PMV < 0.5$), recommended in case of new buildings and renovations,
- category III, which corresponds to a moderate level of expectation ($PPD < 15\%$ or $-0.7 < PMV < 0.7$) and can be used in case of existing buildings.

Table 2.1 shows the minimal and maximal operative temperature for a given building use, clothing and activity. The category II is considered for further calculations because it is suited to the studied buildings. Note that the spaces with brief occupancy in residential buildings do not require any cooling energy.

Space use and *activity*	**Category**	**Operative Temperature [$°C$]**	
		Minimum (heating) Clothing 1 clo	Maximum (cooling) Clothing 0.5 clo
Residential building (bedrooms, kitchen, living room), *Sedentary activity (1.2 met)*	I	21	25.5
	II	**20**	**26**
	III	18	27
Residential building (other rooms), *Standing (1.6 met)*	I	18	–
	II	**16**	**–**
	III	14	–
Offices, *Sedentary activity (1.2 met)*	I	21	25
	II	**20**	**26**
	III	19	27

Table 2.1: Recommended temperature for conception of HVAC systems (EN15251, 2007)

The category II assumes a relative humidity between 25 and 65% and a low air velocity (< 0.2 m/s).

The **Adaptive comfort model** proposes a larger comfortable temperature band. The standard EN15251 details the comfortable temperature range for summer comfort only (figure 2.2). The *outdoor reference temperature* is a running mean temperature calculated for a time interval of 7 days.

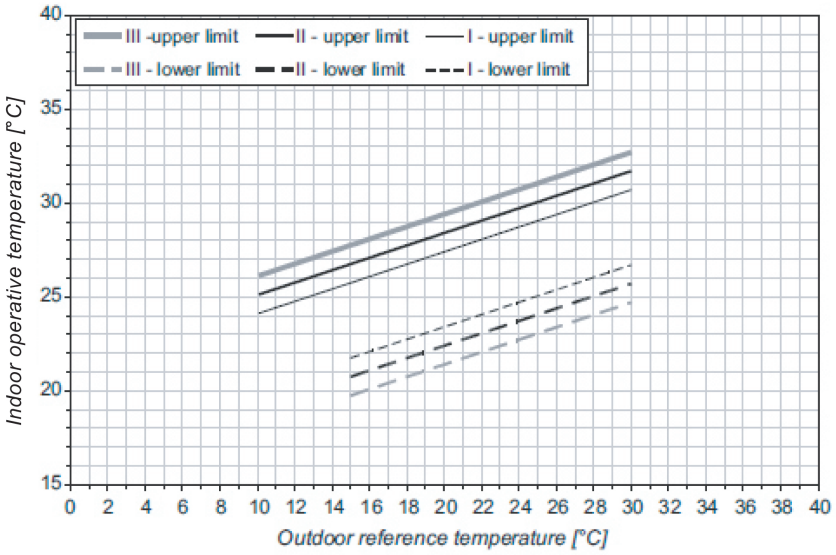

Figure 2.2: Acceptability ranges calculated for naturally ventilated non cooled buildings according to the CEN index (EN15251, 2007)

With this model, the acceptable high temperature is higher than with the PMV model, it could reach 30°C (instead of 26°C) depending on the category and on the reference temperature. Important energy savings could be met if this index describes correctly the occupants comfort. Even though, in accordance to the standard, the applicability of the curves of the figures 2.2 is limited to the following buildings:

- buildings used for low metabolic rate activities (<1.3 MET); buildings without any HVAC system,
- buildings where occupants can freely operate windows and change their clothing level;

Those two last conditions do not match with the topic of this work which deals with active cooling of buildings. However, Ferrari and Zanotto (2012), Gail Brager and Baker (2008) put forward the fact that adaptation takes place also in conditioned buildings. It seems reasonable to extend the adaptive approach to all kinds of buildings. Ferrari and Zanotto (2012) suggest to use another index to evaluate the comfort in buildings with HVAC system in Europe. It is called ACA for *Adaptive Comfort Algorithm* and it has been developed in

the frame of the Smart Control and Thermal Comfort project (McCartney and Nicol, 2002). The upper and lower limits are showed on figure 2.3 where there are no more building categories. This index works for European buildings for both heating and cooling seasons. This index is implemented in the cooling load simulations. Its mathematical basis is described as follows (McCartney and Nicol, 2002).

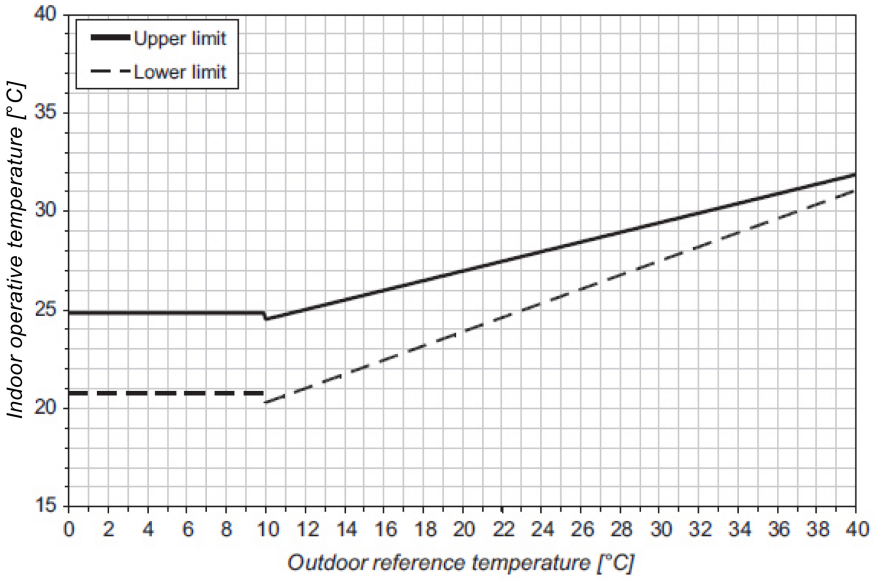

Figure 2.3: Acceptability ranges calculated according to the ACA index (Ferrari and Zanotto, 2012)

$$T_{op\ comf} = 0.302\, T_{RM80} + 19.39, \quad T_{RM80} > 10[^{\circ}C] \tag{2.2}$$

$$T_{op\ comf} = 22.88, \quad T_{RM80} \leq 10[^{\circ}C] \tag{2.3}$$

With $T_{op\ comf}[^{\circ}C]$ the operative comfort temperature and T_{RM80} the Running Mean outside temperature computed according to the following equation leading to a "half life" of 3.5 days.

$$T_{RM80}\,|_{day\ D} = 0.8\, T_{RM80}\,|_{day\ =D-1} + 0.2\, T_{DM}\,|_{day\ =D-1} \tag{2.4}$$

Where

D represent the current day and $D-1$ the previous one,

T_{DM}, the daily mean external temperature term translates the adaptation to external temperature.

The acceptability range amplitude is determined by equation 2.5. It is equally distributed on either side of the operative comfort temperature $T_{op\ comf}$ and leads to the limits displayed on figure 2.3.

$$T_{upper\ limit} - T_{lower\ limit} = 2 \cdot (-0.189\, T_{op\ comf} + 6.35) \tag{2.5}$$

The clothing is assumed to be adapted by the building occupants but the effects of humidity and air velocity are neglected in these adaptive models. The air velocity considered in our buildings is less then 0.1 m/s. In case of higher air velocity (v_a) the following correlation could be used (Ferrari and Zanotto, 2012). A high air velocity compensates an air temperature rise.

$$T_{op\ comf\ high\ air\ velocity} = T_{op\ comf} + 7 - \frac{50}{4 + 10\sqrt{v_a}} \tag{2.6}$$

According to Ferrari and Zanotto (2012), the increase of humidity affects the width of the acceptability range around the ideal comfort temperature, but there is still no simple equation available to link it with temperature. In this work the relative humidity bounds are set to 25 and 60% for the adaptive model. The same is defined for PMV model.

Comfort indexes

In order to evaluate the thermal comfort on a long term (season, year), the computed temperature or PMV-PPD has to be compared to the required ones. Among the methods presented in EN15251 (2007), two global comfort indexes are chosen:

The **percentage of time outside of the temperature range** describes the period when the operative temperature is out of bounds defined in table 2.1 for PMV model or in the figure 2.3 for the adaptive one.

The **degree-hour index** is the duration when operative temperature is out of bounds weighted by the temperature gap between the computed temperature and the nearer bound.

Those two global comfort indexes could compare the buildings and their cooling strategies. The common criteria for the first index is 5% of the working period (office buildings).

Depending on the chosen model (PMV or adaptive), the global comfort index could encounter significant variation. Ferrari and Zanotto (2012) showed that the adaptive temperature range index ACA reaches a decrease between 25% and 50% of discomfort degree-hours compared to traditional 26°C cooling set point for offices in Italy. The model chosen influences greatly the required energy for cooling in the hot climate. Nevertheless, in more temperate climate, the operative temperature upper limit of the adaptive model is rarely higher than the PMV model limit (26°C). It implies a lower impact on cooling energy required for northern locations (Sourbron and Helsen, 2011).

2.2.2 Visual comfort

On the building thermal loads computation perspective, the visual comfort concerns windows and artificial lighting. The windows size and parameters influence the solar gains and modify the envelope thermal performance. During the occupancy period, the room illumination must be satisfied by the natural light, the artificial light or by a combination of both. The artificial lighting, when switched on, produces heat also modifying the heat balance.

The illumination unit is the LUX. The standard EN12464 recommends 500 LUX for offices, 100 LUX for corridors and toilets, 150 LUX for stairs. For the residential building, the recommended illumination is: 300 LUX for kitchen, 150 LUX for bathrooms and living room, 100 LUX for the rest of the house. Depending on the lamp efficiency, a lighting power is set. It varies from 1.58 to 3.6 $W/(m^2$ for 100 $LUX)$ for the studied buildings.

Other considerations such as Colour Rendering Index or glare ... should be tackled if the entire lighting system needs to be designed. This is not the case in the present work.

2.2.3 Air quality

Ventilation is required to evacuate the pollutants created by the occupants and other materials from the buildings. Moreover, some activities necessitate extra ventilation such as cooking. Each person in a building category II needs at least 25 m^3/h fresh air (EN15251, 2007). This accounts for occupancy period. One hour before occupancy, a volume flow equal to two times the volume flow required for occupancy must be blown.

Two kind of flows have to be distinguished: the fresh air flow and the extracted air flow. For dry rooms, the "fresh air" comes from outside while for humid rooms (bathrooms, toilets, kitchen) the air is extracted. It means the air can move from dry to humid rooms in a building.

For residential buildings, the table 2.2 specifies the required volume flows based on the standard EN15251 (2007). This is consistent for permanent ventilation during occupancy. There are no specifications about a higher ventilation flow during cooking. During absence, a minimal ventilation flow, 0.18 to 0.32 $m^3/(h\,m^2)$ corresponding to an air change rate of 0.075 to 0.15 vol/h (for a room height of 2.5 m) is required. Here as well, the infiltration could be included in this flow.

2.3 Climate influence on solar energy availability and loads

The objective of this work is to study the integration of solar air-conditioning in European buildings. To handle the climate influence on loads and on available

Dry rooms	**Fresh air flow**	**Unit**
Bedroom, living, dining rooms	25	$[m^3/(h\,pers.)]$
Wet rooms	**Extracted air flow**	
Toilets	36	$[m^3/h]$
Bathroom	48	$[m^3/h]$
Kitchen	72	$[m^3/h]$

Table 2.2: Recommended permanent ventilation during occupancy in residential buildings (EN15251, 2007)

solar energy, some representative locations have to be chosen for the selected building simulations.

2.3.1 Cooling load indexes

The common indexes to compute the cooling load are based essentially on the external temperature. The indexes are split into Heat index and Cold index. The degree-day method is used in both ECI-EHI and IEA-ECBCS indexes.

The **European Heating Index** and **Cooling Index** (EHI and ECI) has been defined in the frame of a European research project ECOHEATCOOL (2006). Their construction is detailed in figure 2.4. First, the heating index takes into account an increase of building temperature of 3°C due to the internal gains. The set point temperature is respectively 20°C and 22°C for heating and cooling. Secondly for the cooling index, 2°C are added to take the solar gains into account. The temperature set point for cooling increases as much as the outdoor temperature increases. A start up margin of 2°C is set before taking into account the heating and cooling degree days. The ECI and EHI are then deduced, a 100 index stands for Munich climate (ECOHEATCOOL, 2006).

In other words, the EHI is based on the heating degree day 13/17. The buildings should not be heated if the external mean daily mean temperature is higher than 13°C. The temperature to reach by the heating system is 17°C, the 3 other degrees are delivered by the internal gains.

This index summarizes the cooling load for given internal and solar gains. It makes possible the comparison between different locations. Nevertheless, the building load can remain far from this index depending on its thermal performance, the internal gains and the control of solar gains.

Another index is interesting to introduce here. It has been established within the **IEA-ECBCS** Annex 48 project (Stabat *et al.*, 2011). The indexes also use the heating degree day method with other transition temperatures. The heating degree days 15/15 are computed (HDD) and the cooling degree days (CDD) include the latent load. The daily mean temperature is the mean value of minimum and maximum daily temperatures. The cooling degree days

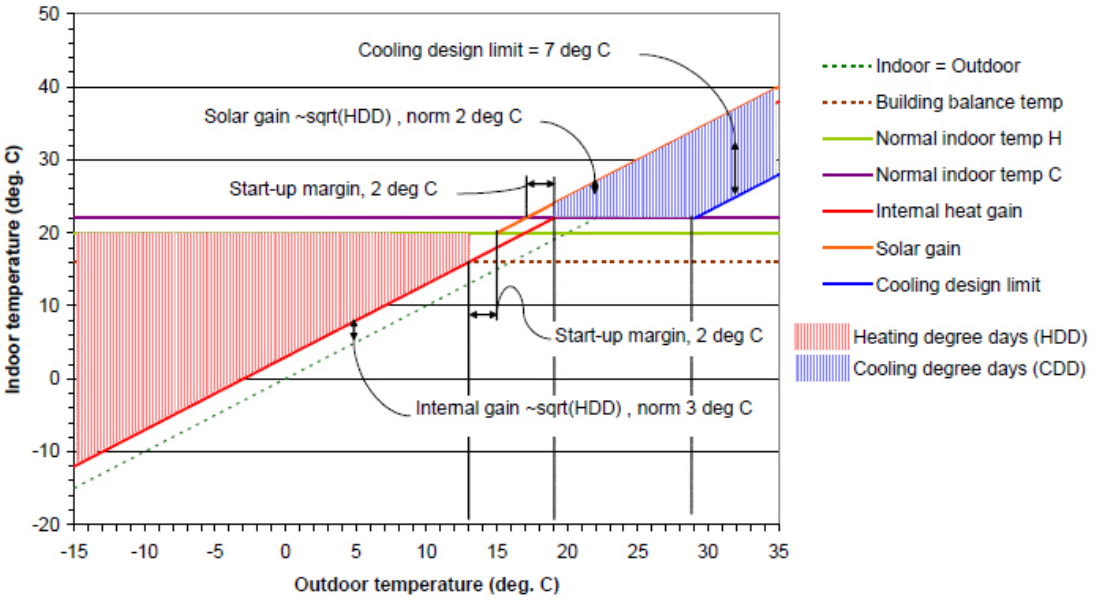

Figure 2.4: European Heating and Cooling index construction (ECOHEATCOOL, 2006)

take into account the days with a mean temperature higher than 15°C and humidity higher than 0.01066 kg water per kg dry air. The implementation of latent load for cooling is more accurate because of the importance of air dehumidification in many systems.

Based on the similarity of heating and cooling degree days, five climatic zones are defined (see figure 2.5):

- Zone 1: Low heating demand (HDD<1000), high cooling demand (CDD>1400) *Corresponds to south of Spain, south of Italy, French Mediterranean cost, Greece*
- Zone 2: Low heating demand (HDD<1000), medium cooling demand (700<CDD<1400) *Corresponds to Portugal, North West of Spain*
- Zone 3: Medium heating demand (1000<HDD<2300), medium cooling demand (700<CDD<1400) *Corresponds to North of Italy, South of France*
- Zone 4: Medium heating demand (1000<HDD<2300), low cooling demand (CDD<700) *Corresponds to North of France, Belgium, The Netherlands, South of UK, West of Germany*
- Zone 5: High heating demand (HDD>2300), low cooling demand (CDD<700) *Corresponds to the east of EU-15 and North East of EU-15*

This index, such as the previous ECI and EDI, does not explain the heterogeneity of building cooling loads for the same location but helps in defining some representative location in Europe.

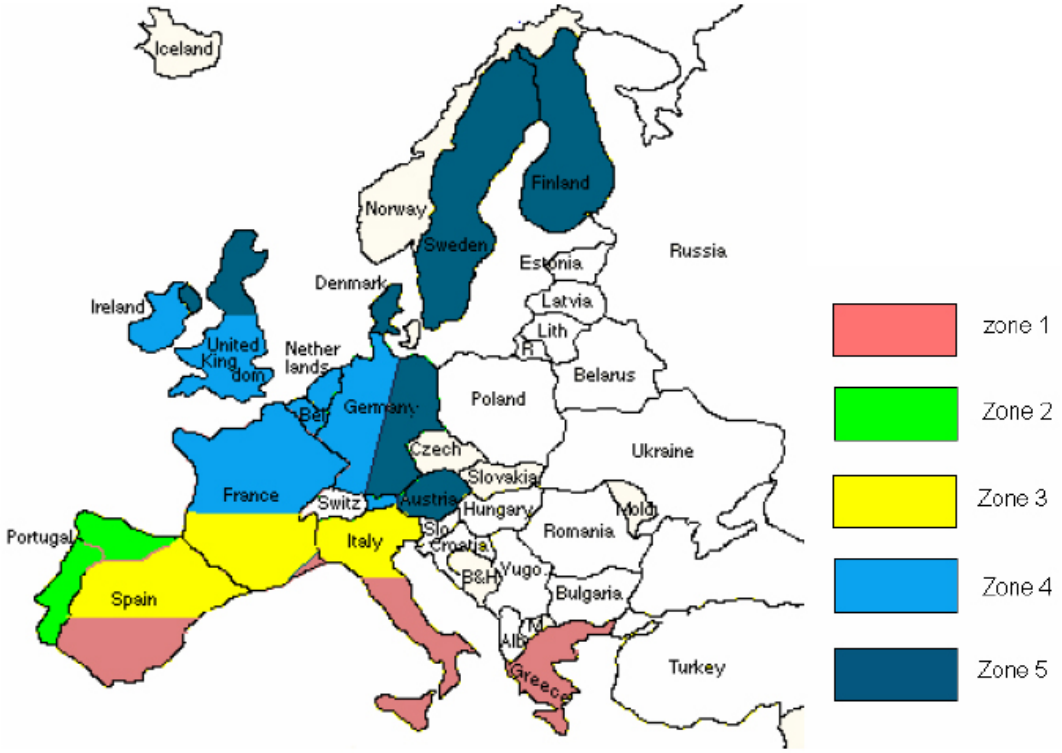

Figure 2.5: European climatic zones (Stabat *et al.*, 2011)

2.3.2 Solar availability

The solar radiation has an impact on the solar energy available for driving solar air-conditioning systems. The available solar energy radiation for Europe is represented in figure 2.6. The values for some selected locations are represented in table 2.3 for the most recent database (Huld *et al.*, 2012) and for the TMY2 data base which takes into account 1961-1990 period (TRNSYS, 2012). The meteorological data taken into account in this work is the TMY2 database. It is a one-year data construction gathering pieces of measurements picked up from 30 years of real measurements, in order to construct a mean year.

The optimal inclination considered on figure 2.6 allows a maximum global yearly radiation but does not emphasize any consideration for winter or summer

solar radiation. However, this consideration is interesting to investigate when analysing solar air-conditioning.

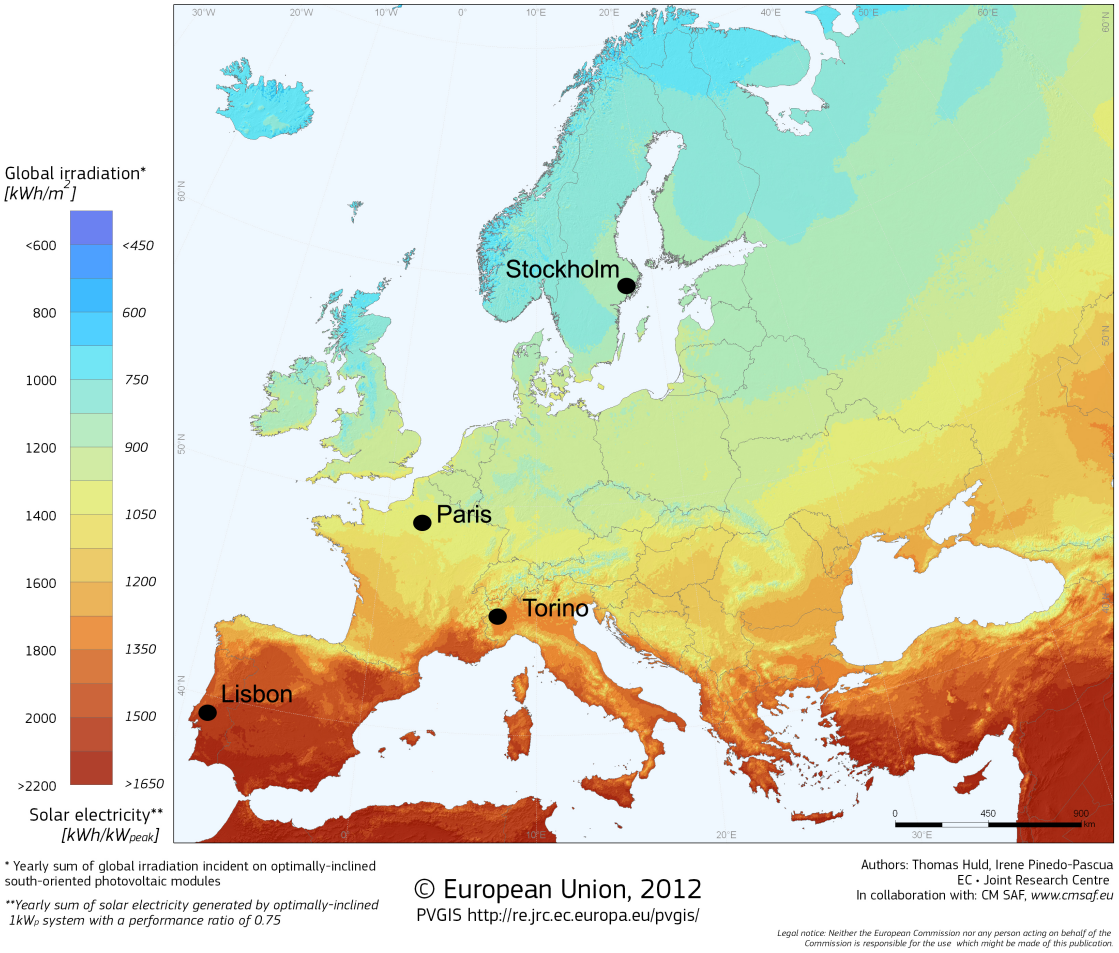

Figure 2.6: Solar yearly global radiation on an optimally-inclined plane facing south (Huld *et al.*, 2012)

Table 2.3 emphasizes the variation between the various measurements of solar radiation. Those variations are less then 8 % which is the order of magnitude of global radiation variation between years (APERE, 2011).

2.3.3 Meteorological database and real values discrepancies

Global warming has an effect on temperature. The climate data used in this study (TMY2) is quite old which could lead to a smaller computed cooling load compared to more actual values. No more recent mean year involving hourly

Location *Units*	**Mean Yearly radiation PVGIS** $[kWh/(m^2.year)]$		**Mean Yearly radiation TMY2** $[kWh/(m^2.year)]$		**Optimal inclination** [°]
	Horizontal plane	Optimal plane	Horizontal plane	Optimal plane	
Stockholm	937	1130	980	1230	41
Paris	1112	1265	1037	1171	35
Torino	1342	1582	1296	1521	37
Lisbon	1632	1892	1683	1915	33

Table 2.3: Yearly global radiation for four locations from two databases: PVGIS from Huld *et al.* (2012) and TMY2 from TRNSYS with Perez 1999 model

data is currently available for Europe.

2.3.4 Selected locations

Both cooling load and solar radiation have to be considered to select some locations. The cooling load (based on temperature) and solar energy (based on radiation) maps (figures 2.5 and 2.6) show discrepancies. Even if the North of Europe is colder, the solar radiation keeps close to the centre of Europe. For the South, high radiation leads to lower cooling load near the Atlantic ocean.

The simulations run in this work will deal with four locations representing four of the five radiation zones. The results of the solar air-conditioning simulations carried out in chapter 3 did not show any necessity to extend the analysis to the fifth zone. For a given high solar radiation, the energy benefits of solar cooling are important as long as the solar fraction is high. A too high cooling load could not reach easily high solar fraction, and thus lower energy benefits.

The selected cities are Stockholm, Paris, Torino and Lisbon (the solar radiation for these cities is written in table 2.3). These locations cover well the solar energy availability range in Europe.

2.3.5 Other impacts of the weather

More than the cooling load and available solar energy for driving the cooling system, the weather impacts the heat transfer of rejection thermal flow. The temperature of the heat sink significantly affects the performance of heat driven systems in general. The cooling tower electricity (and water consumption) depends on the external temperature (and humidity). A high ambient temperature and humidity imply higher electrical energy use. This will be emphasized in chapters 3 and 4.

2.4 New office building

The building has been defined in the frame of the EPICOOL project (EPICOOL, 2009). The envelope characteristics are representative of a new office building in Belgium. Three levels of energy performance are defined: "acceptable, good, very good". The "acceptable" case is the minimal requirements of the Brussels region energy performance directive translation. The "good" and "very good" increase the building energy performance by implementing a more insulated envelope and a more efficient lighting system decreasing the internal gains. The main characteristics are picked up from EPICOOL (2009) project and detailed in appendix (where it is called Belgian office building), while the most important assumptions about cooling load evaluation are detailed here under.

The three levels of this building are simulated in the four locations selected in section 2.3. The building energy balance is computed using TRNSYS, it allows the computation of the heating and cooling loads (sensible and latent). Domestic hot water consumption is not considered in this building.

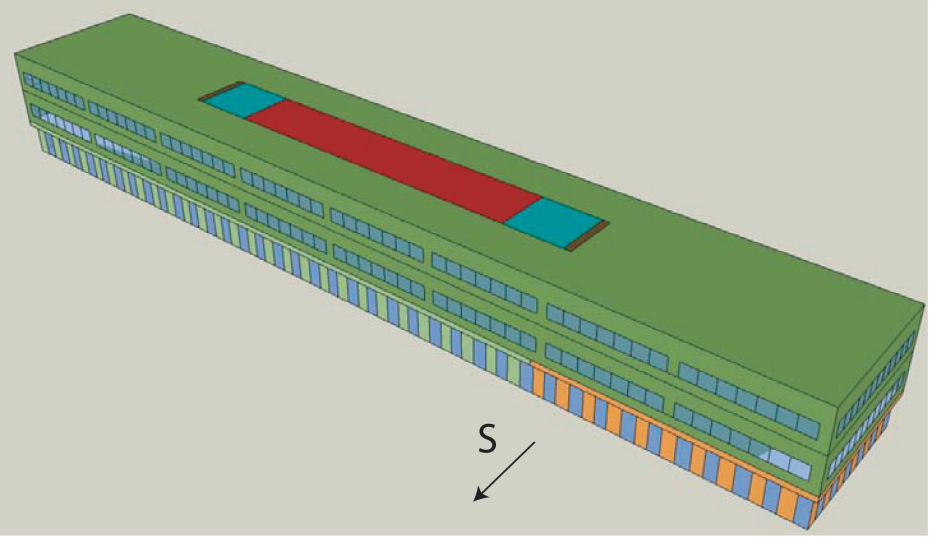

Figure 2.7: New office geometry (EPICOOL, 2009)

2.4.1 Building shape and space use

The small office building pictured in figure 2.7 consists of three floors and has main orientations north and south. It is a stand-alone building with a total available area 4403 m^2 (volume 18350 m^3) while the percentage of windows area is 19.8 % of available floor area, it is shared on all façades without any

orientation considerations. The ground floor is 50% glazed (vertical full height windows) and contains a cafeteria (E-side), lobby (W-side) and central dark zone with technical and storage area and sanitary. The first and second floor are identical: open space office at the area near the façade and central dark zone with sanitary and meeting rooms. Some more assumptions:

- All the zones can be heated or cooled.
- The occupancy of this building is limited to the weekdays between 8 am and 7 pm.
- The ventilation, heating and cooling are switched off during absence but start at 7 am.

2.4.2 Internal gains

The office building considered is designed to have around 250 occupants and has low internal gains due to equipment and lighting. For instance, the office and meeting zones which have the higher equipment internal gains reach respectively 7.52 and 9.43 W/m^2. Besides, the maximum installed lighting power is 1.84 W/m^2 for 100 LUX which leads to 9.19 W/m^2 for the office zone. Moreover, the lighting system involves dimming to decrease the electricity consumption and diminish internal gains. Other considerations such as the variation of internal gains throughout the day are described in appendix.

2.4.3 Solar protections

The solar protections use has a great impact on both heating and cooling loads. The shading devices efficiency has been analysed by Wall and Bülow-Hübe (2003). In these simulations, an external shading device is considered for each window. The selected device is a light beige pleated curtain which has a constant shading coefficient whatever the sun incidence angle. Its shading factor is 0.55 (Wall and Bülow-Hübe, 2003) meaning a decrease of available radiation on external window by 55%.

The movement of the solar protections is controlled by total radiation on the window wall. The thresholds for opening or closing the solar protection are 150 and 250 W/m^2 (total radiation on wall). These numerical values have been proposed by Saelens *et al.* (2009) for external automatic shading devices dedicated to office buildings in cooling period. For the heating period, the solar protections are used with a unique threshold of 300 W/m^2 to get more solar gains in the building. The criteria for the heating/cooling periods definition is a mean daily temperature RM80 (see equation 2.4) lower/higher than 15°C. This approach maximizes solar gains to decrease the heating load but does not affect significantly the cooling load.

2.4.4 Heating & cooling setpoints

The work investigates the two comfort models (see section 2.2): PMV and Adaptive. Moreover, a free-floating simulation describes the comfort indexes without any cooling set points. The operative temperature set points for the different cases are detailed in table 2.4. The humidity bounds are 25-65% but there is no upper bound for the free-floating simulation. The dehumidification takes place only when cooling is required (high internal temperature).

The operative temperature is used for set points and to compute the comfort indexes. In TRNSYS, the set point must be the air temperature which is connected to the mean surface temperature and the operative temperature set point as mentioned in the equation 2.7. This assumption is only valid for a small temperature gradient between the surfaces and a low air velocity.

$$T_{air\ set\ point} = 2 \cdot T_{operative\ set\ point} - T_{mean\ radiant} \tag{2.7}$$

The free-floating simulations determine the maximum temperature reached throughout the year as well as the overheating degree-hour and percentage of time with overheating discomfort. Those discomfort indexes are computed based on the ACA model set points for cooling. The degree hours are taken into account as soon as the operative temperature is higher than the cooling ACA set point plus 0.5 °C.

The three selected cooling set points in simulation are specified by the following acronym:

- PMV: PMV model
- ACA: adaptive model
- FREE: free floating cooling set point.

	PMV model		**ACA model**		**FREE-floating**	
	Heating	Cooling	Heating	Cooling	Heating	Cooling
Setpoint presence	20	26	21	25-28*	21	-
Setpoint absence	16	30	16	30	16	-

∗ Temperature varies according to figure 2.3

Table 2.4: Set points temperature for the new office loads simulations

2.4.5 Yearly loads

The yearly heating and cooling loads for the three energy performance levels ("acceptable", "good" and "very good") and four locations are represented in figure 2.8 and in table 2.5. The new office building has a non negligible yearly cooling load whatever the case, ranging from 5 to 59 kWh/m^2.

The impact of the building energy performance level is high on both heating and cooling loads. Firstly, for cooling, the "good" level has a better envelope and lower internal gains compared to the "acceptable" one. The cooling load is then slightly higher, the lower losses through the envelope are not totally counterbalanced by the decrease of internal gains. This is true whatever the location and the cooling set point used. To enhance the building from "good" to "very good" level, the envelope is more insulated and the glazing g-value is higher to provide more solar gains in the heating season. The effect on cooling load is extremely important as it is increased by nearly 100% for each location compared to the "acceptable" case.

Secondly, for heating, the best is the envelope, the lowest is the load. The "very good" level has at least 3 times lower heating load than the "acceptable" one for Stockholm. For the hotter climates with a significant heating load, it ranges from 4 to 6 times lower.

The comfort model also impacts the loads. The set point for heating is higher for the ACA model than for the PMV. The impact of this 1°C difference is high for Lisbon which has a low heating load. For other locations with significant heating load, the reduction ranges from 8 to 30%.The comfort model has also an impact on the cooling load because of the temperature set point. The ACA model has a higher cooling set point than the PMV model for high outdoor temperature. For Lisbon and Torino, the ACA model decreases the cooling load by 10-17 % for "acceptable" and "good" levels. For the "very good" level, the impact is not significant. For the colder climates of Paris and Stockholm the cooling set point of ACA model is very often between 25 and 26°C which implies a slightly higher cooling load than for the PMV model.

The solar protections installed have a huge impact on cooling load. For Lisbon "acceptable" case, a simulation run without any solar protections doubled the cooling load.

The part of the latent load is also computed. The dehumidification is computed to attain 65% relative humidity. The Sensible Heat Ratio for cooling is higher than 87% whatever the case. It is higher for Lisbon ($> 95\%$) than for Torino and Paris. The cooling latent load is not important in this building. The humidification of the air to reach 25% relative humidity is not significant, it reaches a Sensible Heat Ratio of (at least) 96% in each case. The Sensible Heat Ratio (SHR) is defined as the sensible heat or cooling load divided by the total heating or cooling load.

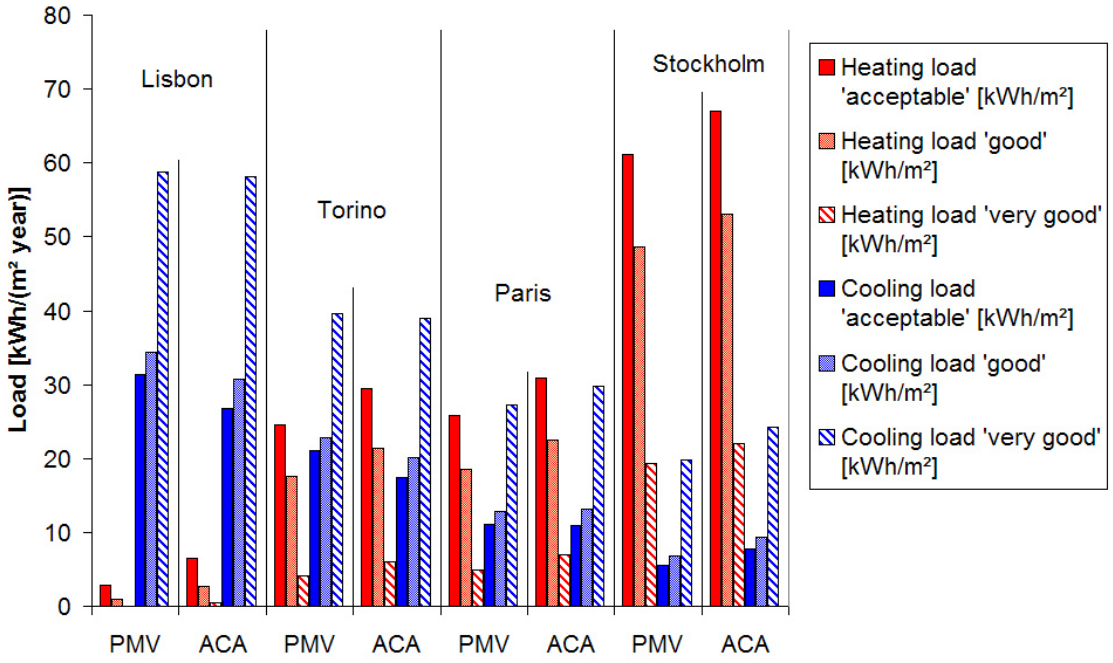

Figure 2.8: Small office yearly heating and cooling loads

Level	**'acceptable'**		**'good'**		**'very good'**	
Yearly loads *Test case*	**Heating** $[kWh/m^2]$	**Cooling** $[kWh/m^2]$	**Heating** $[kWh/m^2]$	**Cooling** $[kWh/m^2]$	**Heating** $[kWh/m^2]$	**Cooling** $[kWh/m^2]$
Lisbon PMV	2.8	31.3	0.9	34.4	0.1	58.8
Lisbon ACA	6.4	26.7	2.7	30.7	0.5	58.1
Torino PMV	24.6	21.0	17.7	22.9	4.2	39.6
Torino ACA	29.4	17.4	21.3	20.1	6.1	39.0
Paris PMV	25.8	11.1	18.5	12.9	4.9	27.3
Paris ACA	30.9	10.9	22.5	13.1	7.0	29.8
Stockholm PMV	61.2	5.5	48.7	6.8	19.4	19.7
Stockholm ACA	67.1	7.8	53.1	9.3	22.0	24.2

Table 2.5: Small office yearly heating and cooling loads

2.4.6 Comfort indexes

The load calculation results showed above support the installation of cooling systems in each case. The criterion of overheating duration is not respected in any case (the duration exceeds 5 % of working hours). The free-floating simulations without any cooling set points reach the comfort indexes displayed in table 2.6. The overheating degree-hours numbers are larger with higher build-

ing level. The Stockholm location with "very good" building has nearly the same overheating degree-hour value has the "acceptable" one in Lisbon. The climate has consequently a similar influence on overheating as the building energy performance level.

The maximum operative temperature mentioned in table 2.6 is the highest temperature reached in any zone during occupancy period. This temperature also justifies the installation of cooling systems.

Level	Degree-hour overheating $[Kh]$	Duration [%]	Maximum operative t° [°C]
Cooling 'acceptable'			
Lisbon FREE	9124	60	38.8
Torino FREE	5739	42	37.3
Paris FREE	3222	30	33.6
Stockholm FREE	2070	27	31.6
Cooling 'good'			
Lisbon FREE	11015	64	39.7
Torino FREE	7109	47	39.1
Paris FREE	4126	34	36.0
Stockholm FREE	2737	31	33.6
Cooling 'very good'			
Lisbon FREE	26034	90	48.7
Torino FREE	17039	66	44.9
Paris FREE	11496	56	41.1
Stockholm FREE	9499	46	38.8

Table 2.6: Small office comfort indexes in free-floating mode and maximum obtained operative temperature (3120h occupancy period is considered)

2.4.7 Night cooling

This paragraph emphasizes the possibility to decrease the loads by implementing an energy saving measure. The night cooling measure allows the ventilation system operation (without cooling) during the night to decrease its temperature.

Here are the three conditions for activating the night cooling:

- The *ventilation return temperature* must be higher than 24°C,
- The external temperature must be lower than the *ventilation return temperature* minus 4°C,
- The night cooling can be activated between 0 and 6 am.

Where *ventilation return temperature* means the temperature of the mixing of flow coming from the different ventilated zones.

The impacts of this energy saving measure are detailed in table 2.7. To include all the energy concerns of this measure, the impacts on both cooling, heating loads and electricity consumption has to be handled. In the analysed building, the installed power of the fans for the entire building is 9.047 kW . The simulations deal with some selected cases from previous analysis. For the three building energy levels, the two extreme locations are simulated with the set points from the ACA model.

	Cooling load		**Heating load**		**Night cooling**	
	initial	**decreased by**	**initial**	**increased by**	**duration**	**efficiency**
Units	$[kWh/m^2]$	$[kWh/m^2]$	$[kWh/m^2]$	$[kWh/m^2]$	$[h]$	[-]
"Acceptable"						
Lisbon	26.8	2.7	6.4	0.5	620	1.74
Stockholm	7.8	0.3	67.1	0.01	42	3.09
"Good"						
Lisbon	30.7	4.1	2.8	0.4	757	2.34
Stockholm	9.3	0.5	53.1	-0.02	84	2.85
"Very good"						
Lisbon	58.1	7.6	0.5	0.4	1039	3.37
Stockholm	24.2	2.8	22.0	0.02	255	5.31

Table 2.7: Yearly results for the implementation of night cooling in new office building

This measure decreases the cooling load by around 10% in the cases where the cooling load is relatively high ($> 10\ kWh/m^2$). The gain is not so important when the cooling load is low, Stockholm still needs a cooling system to satisfy occupants thermal comfort.

The night cooling efficiency is the ratio between the reduction of the total load (cooling and heating) and the electricity consumption of the saving measure. In other words it is the electrical COP of the energy saving measure. The efficiency includes the slight impact of night cooling on the heating load. The best values are encountered for the Stockholm "very good" case where the efficiency reaches 5.31. In the other cases the night cooling efficiency has the same order of magnitude as the COP of a chiller. Thus, from a global energy use point of view, this measure does not save much energy.

The impact on maximal cooling load is not significant except for the Stockholm "very good" case with a decrease of 8%. Nevertheless, it will not modify considerably the installed cooling power.

For this building, this measure does not impact significantly the cooling load and the short energy benefits vary within the cases. It is therefore pro-

posed to leave it out in the solar cooling systems simulations.

Other energy savings measures could be implemented and compared to the efficiency of the night cooling in the same way.

2.4.8 Daily loads

Hottest day

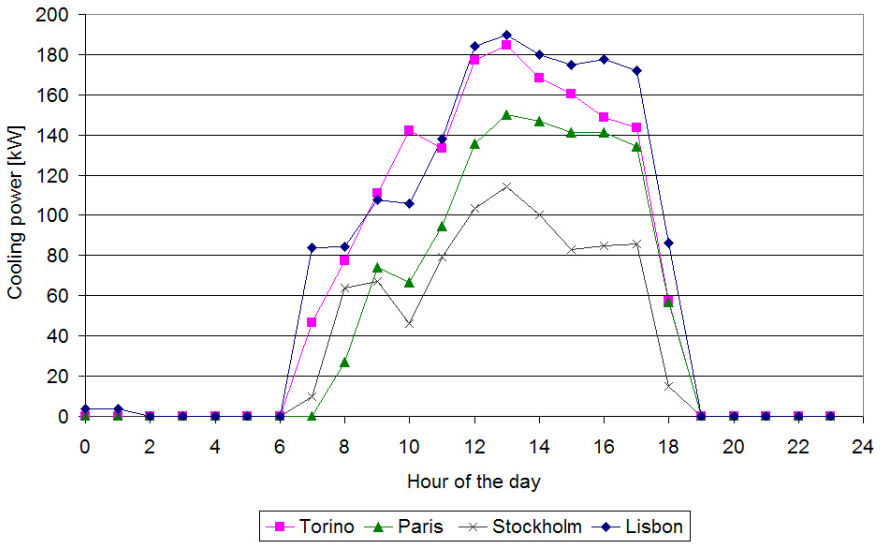

Figure 2.9: Day with the maximal cooling load for the new office "acceptable" in the four locations (ACA model)

Level	**'acceptable'**		**'good'**		**'very good'**	
Maximum cooling power	Power	Load	Power	Load	Power	Load
Daily cooling load	$[kW]$	$[kWh/day]$	$[kW]$	$[kWh/day]$	$[kW]$	$[kWh/day]$
LisbonPMV	221	2061	231	2151	270	2546
LisbonACA	190	1677	205	1767	250	2185
TorinoPMV	196	1686	210	1805	265	2367
TorinoACA	169	1362	185	1506	236	2004
ParisPMV	151	1184	175	1383	247	2137
ParisACA	150	1167	171	1342	243	2090
StockholmPMV	110	960	122	1043	197	1641
StockholmACA	114	812	131	835	210	1850

Table 2.8: New office maximum cooling power and its daily load

For the different locations, the day with the maximum power is emphasized in table 2.8 and on figure 2.9. The cooling load occurs almost entirely during the presence hours. The absence set point temperature (30°C) is reached during a very few hours only in Lisbon. It implies a cooling load during the weekend or during the night (Lisbon curve on figure 2.9). Torino and Lisbon have similar curve for the hottest day despite a smaller yearly cooling load for Torino (minus 34%). The cooling load sharing between the different seasons has consequently an importance while designing solar cooling systems.

The four locations have similar cooling load shapes, the cooling load is growing from 8 am to 1 pm. The load decreases slowly after 5 pm. The East and West side of the building having the same glazing percentage, the slow cooling load decrease is due to the higher external temperature during the afternoon.

The shape is quite similar for the "good" and "very good" levels. For these levels, the cooling load is scaled up for both locations. The night cooling load remains nearly zero except for Lisbon where it grows with the quality level of the building.

Sometimes, the cooling load is expressed in W/m^2 available area. For the whole buildings it is within the range of 25-60 W/m^2 for the maximum cooling load in the various cases.

Solar radiation is simultaneous to the cooling load. Around 7 kWh/m^2 hits an horizontal plane (new office roof) on sunny days in summer whatever the selected location. The available surface on the roof is around 1300 m^2, it could supply up to 2700 kWh cold energy (considering a collector yield of 0.5 and COP of thermally driven chiller equals 0.6). It has the same order of magnitude as the required cooling load for very hot days. The available surface on the roof will become crucial when designing a solar cooling system for such an office building.

The design of a cooling system is not restricted to the hottest day analysis, the origin of the gains inside the building is also important. The cooling load is not only linked to the solar radiation, internal gains have a considerable influence on the load. As there is cooling load even in winter, the focus is put in next paragraph on a day with significant cooling load in winter.

The cooling load is displayed on figure 2.10 for 7 consecutive cooling days in Torino. Even if the same cooling load curve is encountered, the highest load is 2 times higher than the lowest one. The variation between days is something important to take into consideration.

Colder days

For Lisbon, some days in winter encounter some small cooling load especially in the cafeteria zone where there are more people gains at midday. For the

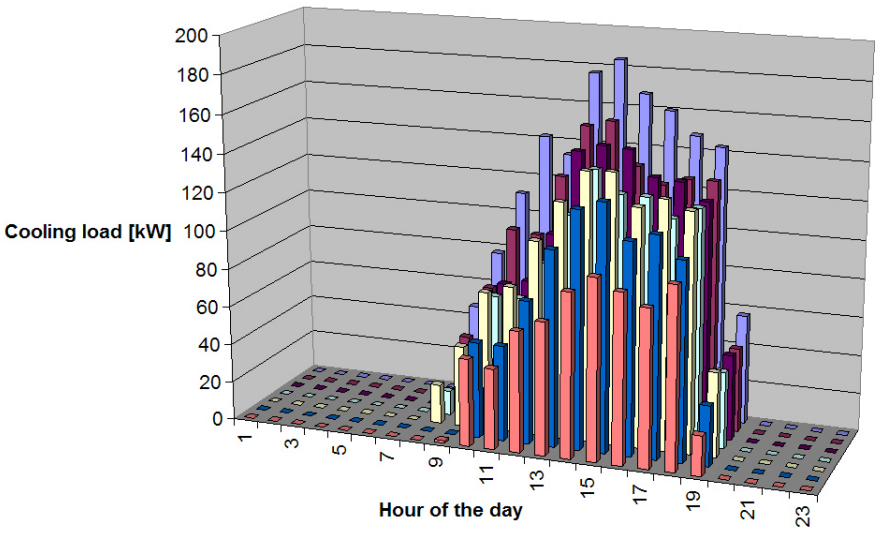

Figure 2.10: New office hourly cooling load for 7 days in Torino (ACA model - "acceptable" level)

"acceptable" building and ACA model, the cooling load attain 30 kW at 1 PM for the 19^{th} of January (cold day without high solar radiation). For the other locations, the tendency is the same but it occurs later in the year. The internal gains impact the cooling loads, but another fact explains this colder days cooling load.

The ventilation is centralized, the same air temperature is supplied to each zone. This is a real problem, for instance the cafeteria with highly varying internal gains could not be cooled by the ventilation air if the other zones require heating. A decentralized ventilation could avoid this. Moreover, the opposite problem is also encountered; there is sometimes heating load during summer. The bypass is only activated when the mixed flow is higher than 24°C (and the outdoor temperature is lower than the mixed flow).

2.4.9 Monthly loads

Despite the cooling load during winter and heating loads during summer, the main loads are encountered in the expected season. For the "acceptable" case, at least 90% of the heating and cooling loads occur respectively in the periods of October-March and April-September (figure 2.11). So the heating and cooling periods are nearly separated; it is a key point for the solar systems control. Otherwise, the "good" and "very good" cases are characterized by a longer cooling season and a shorter heating season.

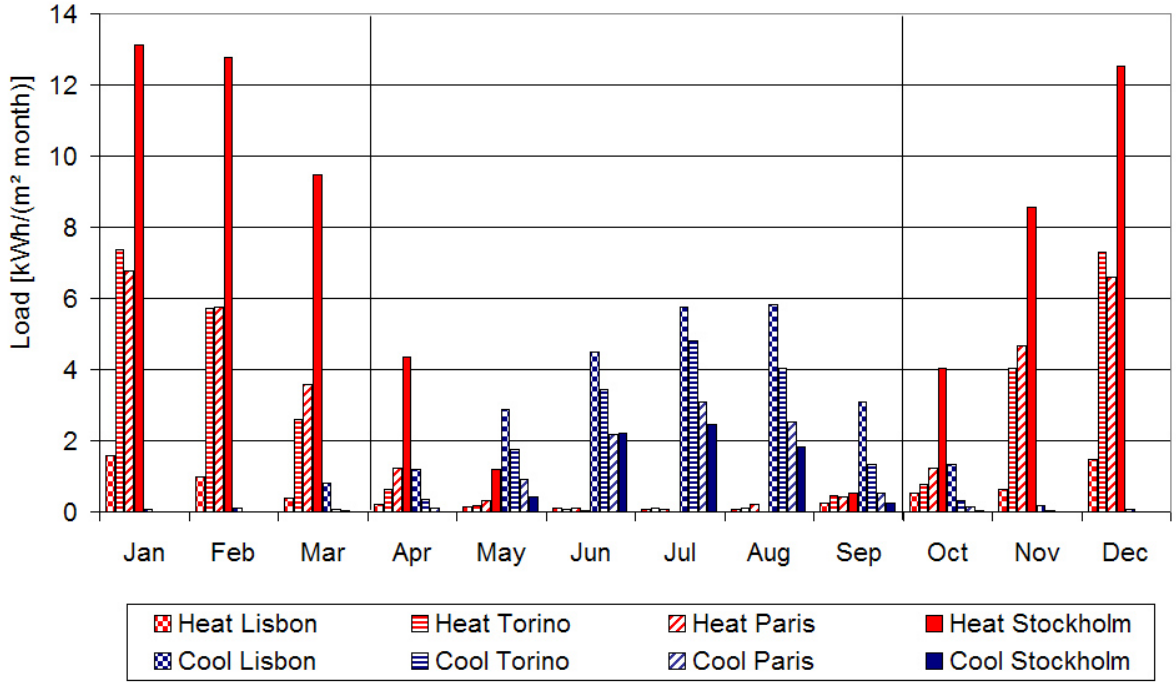

Figure 2.11: New office monthly loads (ACA model - "acceptable" level)

2.5 Typical existing European office building

The analysis deals with a theoretical building representative of existing large office buildings in Europe. It was defined in the framework of the IEA-ECBCS annex 48 project called Heating Pumping and Reversible air-conditioning (Stabat *et al.*, 2011). It is a twelve identical floors, 15000 m^2 building with an average occupancy of 1000 persons. From the modelling point of view, only one floor is considered but all floors can be treated similarly. The complete description of this building is given in appendix.

This building is defined in this work for comparison purposes with the new office building defined above. The lower thermal insulation and higher air leakages are characteristic of existing buildings. The other main differences between a new office building and the existing ones are defined in the next paragraphs. The chosen location for the simulations is Paris Montsouris meteorological station.

2.5.1 Building shape and space use

The geometrical description of one floor is presented on figure 2.12. Five zones are considered for a total of 1250 m^2. The glazed area is 26% of the floor area.

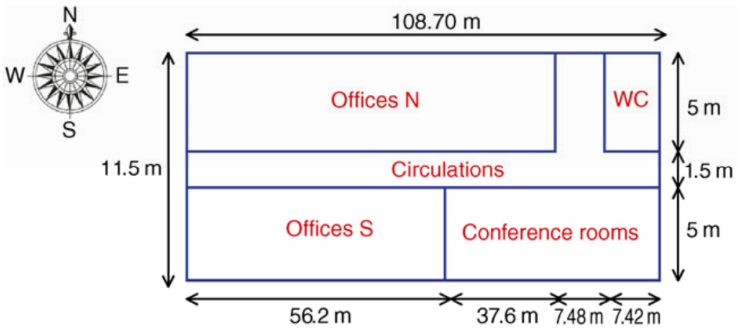

Figure 2.12: Office building floor geometry (Stabat *et al.*, 2011)

2.5.2 Internal gains

One floor is designed for around 80 persons which corresponds to 15 m^2 building area per person. It is nearly the same for the new office building described in previous section. The appliances have a high value: 13.35 W/m^2 at maximum occupancy rate in offices (7.5 W/m^2 in new building). A residual power (2.25 W/m^2) of appliances is kept during the night and the weekend. The installed light power is also quite high: 18 W/m^2 in offices (maximum 9.19 W/m^2 in new building). A correlation is implemented to adjust the lighting power in accordance to the available natural light.

The appliance gains and lighting installed power claim to be a mean value of existing office buildings (Stabat *et al.*, 2011) but some over study discovered a large disparity between the electricity consumption of these buildings (Thewes, 2011). Thus, it is not easy to summarize all buildings in one single case.

2.5.3 Solar protections

Some manual external solar protections are simulated. They implement the average behaviour of people in the zones (Alessandrini *et al.*, 2006). The solar protections shading factor is 80%. The opening of solar protections is activated by the user depending on the outside luminance, the solar protections are closed from 7 to 45% (percentage of the windows which is covered with the solar protection). The position of solar protections during non occupancy is defined as equal to those in the last hour of occupancy. More information about solar protections implementation can be found in appendix.

2.5.4 Heating & cooling set points

The encountered set points for heating-cooling in real office building are more often 21-24°C which do not indicate a real energy saving concern. A first set of set points is dedicated to a real building use while a second one is defined for comparison purposes with the PMV model (at least for cooling) explained below. The two sets of cooling set points used are:

- Heating 21°C RH 40% Cooling 24°C RH 60%
- Heating 21°C RH 40% Cooling 26°C RH 65%

The meeting room is occupied only 3 hours a day, it is not ventilated or cooled during the rest of the time. During non occupancy periods (before 7 am, after 8 pm, during the weekend), there is no cooling or ventilation. The night set point it 15°C.

2.5.5 Yearly loads

The typical existing building loads are displayed on figure 2.13 for one floor in Paris. The comparison is made with the new office building "acceptable" level defined in section 2.4. For the same set points, the loads are much higher for the Typical European existing building. Moreover, the cooling set point from 24°C to 26°C impacts largely the cooling load (- 30%). The building studied in this section has a lower energy peformance especially in terms of cooling demand compared to the new office building. The worst envelope thermal performance of typical building involves a higher heat transfer from inside to outside. Nevertheless, the higher glazed area, poorer solar protections and higher internal gains impact much more the cooling load.

These results highlight the benefits of new building regulations for decreasing the heating load. However, the cooling load could be higher in new buildings due to their better envelope. Besides, the cooling load is largely influenced by the quality of solar protections, their use and the internal gains which should be attentively studied in new buildings.

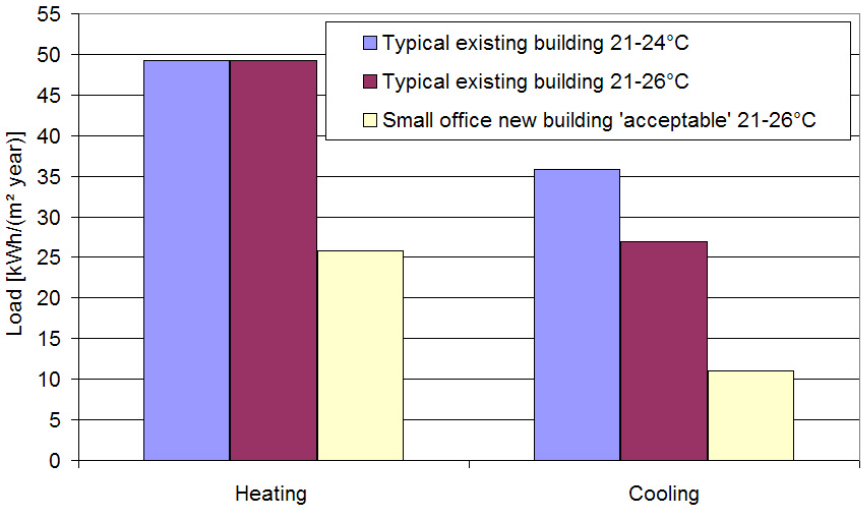

Figure 2.13: Typical European office building yearly loads

2.6 Detached house

The residential building has also been defined in the framework of the EPICOOL project (EPICOOL, 2009). The shape and size of this building is representative of Belgian stock family houses (4 people). Three levels of energy performance are defined: "acceptable, good, very good". The "acceptable" case is the minimal requirements of the Brussels region energy performance directive translation. The "very good" case get closer to the passive house standard. The main characteristics are picked up from EPICOOL (2009) and are detailed in appendix , while the most important assumptions about cooling load evaluation are detailed below.

The three levels of this building are simulated in the four locations selected in section 2.3. The cooling, heating (both latent and sensible) and domestic hot water loads are computed for those cases. The heating and cooling loads come from the building energy balance carried out by TRNSYS but they do not handle any heating and cooling system.

2.6.1 Building shape and space use

The building is a two floors detached house with an attic. The geometry is displayed in figure 2.14. The available area of the ground floor is 143 m^2 while the useful area for first floor is 74 m^2 (part of the zone which has not a Mansard roof). The attic zone is not considered in the floor area. The total glazing area is 29.6 m^2 corresponding to 14.1 % of available floor area and is located mainly on the south facade. There are three thermal zones; both ground and first floors are heated-cooled. The ground floor is occupied during the day while the

first floor is for night occupation.

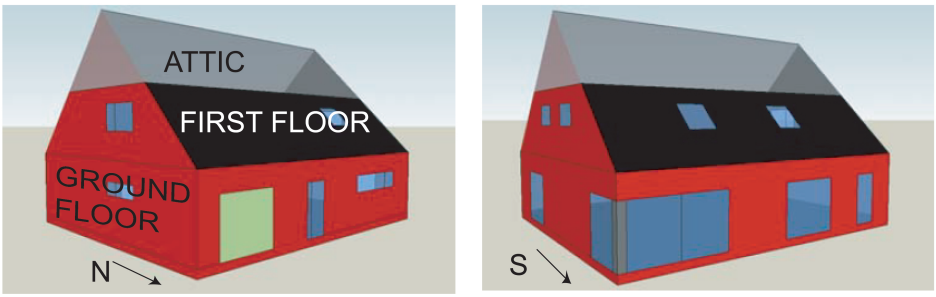

Figure 2.14: Detached house geometry (EPICOOL, 2009)

2.6.2 Internal gains

The internal loads are constant for the two periods for the three energy performance levels and they are presented in table 2.9 where considerations about schedules are also mentioned. The gains introduced in the building correspond to a four person family permanently at home. The total electricity consumption impacted by the equipment gains is around 3600 kWh per year (considering an electricity to heat conversion of 100%). This figure is the mean single household electricity consumption in Belgium.

	Weekday		**Weekend**	
	Day period *9 am-10 pm*	Night period	Day period *9 am-11 pm*	Night period
People load				
sensible	4.90	2.45	5.23	2.18
latent	2.64	1.32	2.82	1.17
Total people load	11.31		11.40	
Equipment	10.20		9.13	

Table 2.9: Detached house internal gains for 4 people occupancy in $[kWh/day]$ (EPICOOL, 2009)

2.6.3 Solar protections

Solar protections usage has a great impact on both heating and cooling loads. The shading devices efficiency has been analysed by Wall and Bülow-Hübe (2003). In these simulations, an external shading device is considered for each window. The selected device is a light beige pleated curtain which has a constant shading coefficient whatever the sun incidence angle. the shading factor

is 0.55 (Wall and Bülow-Hübe, 2003).

The movement of the solar protections is controlled by total radiation on window walls. The thresholds for opening or closing the solar protection are 150 and 250 W/m^2(total radiation on wall) as for the new office building. These numerical values have been proposed by Saelens *et al.* (2009) for external automatic shading devices dedicated to residential buildings. Besides, there is another control to implement the occupant behaviour. In the heating period, the shading devices are not used to receive maximum solar gains. The criteria for the heating/cooling periods definition is the same as defined for the new office building (section 2.4): a mean daily temperature RM80 lower/higher than 15°C. This approach maximizes solar gains to decrease heating load but does not affect significantly the cooling load.

2.6.4 Domestic hot water load

The domestic hot water load is computed based on a 45 litres per person per day hot water consumption. The temperature to reach is 45°C everywhere while the water mains temperature is different in each location and varies throughout the year, its computation is carried out by TRNSYS in relation with the mean air temperature. The daily power required to heat domestic hot water for 4 people is illustrated in figure 2.15.

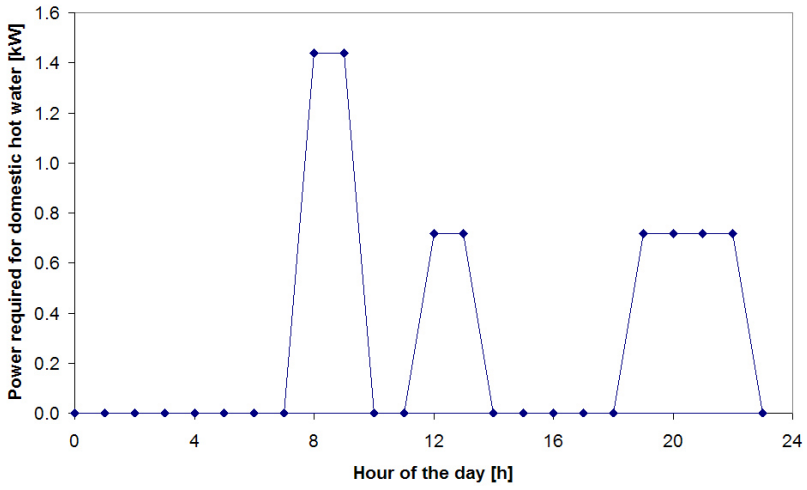

Figure 2.15: Power required to heat the detached house domestic hot water for Torino in winter.

The mains temperature is plotted on figure 2.16 for the four location. This comes from a correlation implemented into TRNSYS type 15, based on monthly mean outdoor temperatures (TRNSYS, 2012). It leads to significant variations

between the locations for the yearly load (table 2.10). An increase of 46% is encountered from Lisbon to Stockholm.

Domestic hot water load	Lisbon	Torino	Paris	Stockholm
Yearly load $[kWh/year]$	1898.5	2253.5	2327.0	2776.9
Yearly load $[kWh/(m^2\ year)]$	8.75	10.38	10.72	12.80

Table 2.10: Detached house yearly domestic hot water load for the four locations

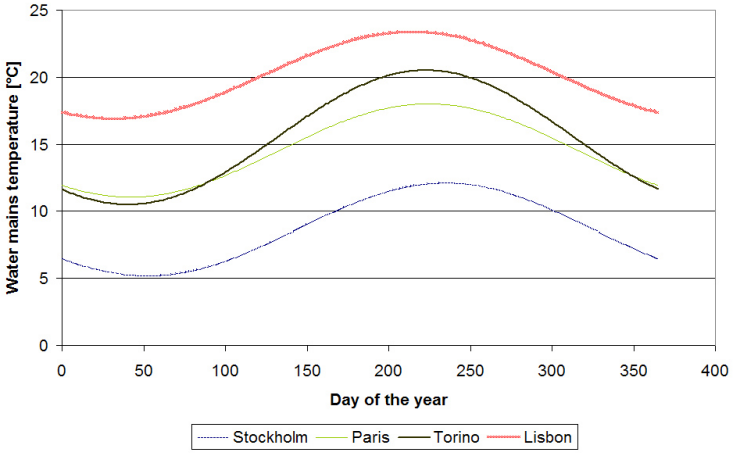

Figure 2.16: Water mains temperature throughout the year for the four locations

2.6.5 Heating & cooling set points

The work also considers the two comfort models: PMV and Adaptive. A free-floating simulation describes the comfort indexes without any cooling set points. The heating-cooling set points are the same as for new office building simulation (section 2.4). The operative temperature set points for the different cases are written in table 2.4 on page 70.

2.6.6 Yearly loads

The simulations were run using the previously described assumptions. The yearly heating and cooling loads for the three energy performance levels "acceptable", "good" and "very good" and four locations are represented in figure 2.17 and in table 2.11.

The building studied is characterised by lower heating load for "good" and "very good" levels. This is due to the better envelope and the heat recovery

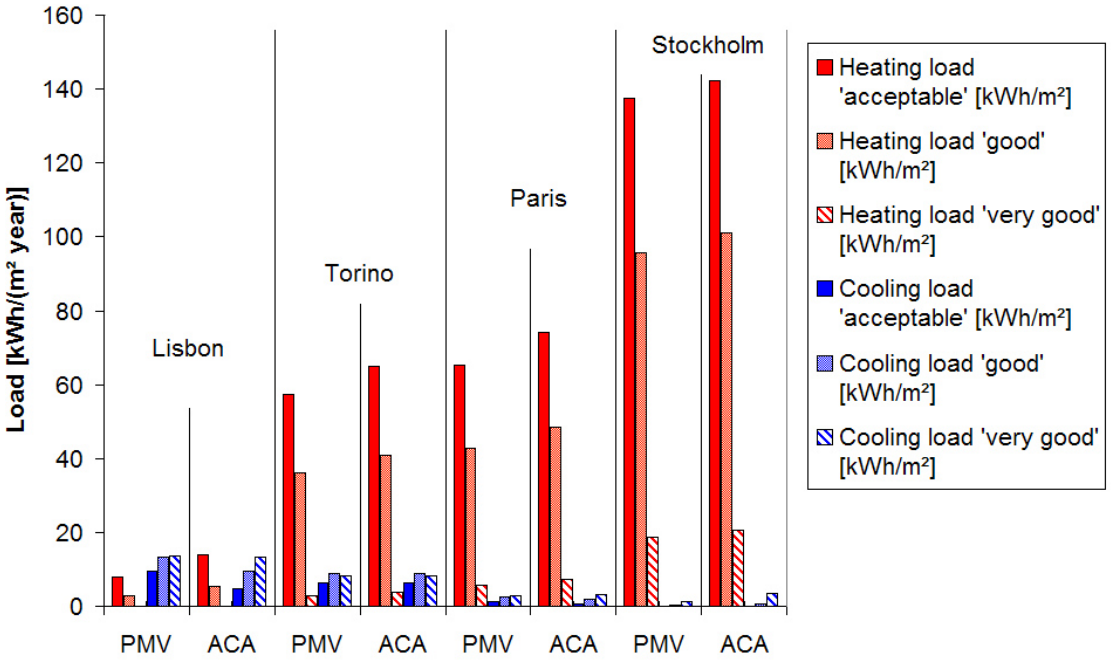

Figure 2.17: Detached house yearly heating and cooling loads

system for the "very good" level. A huge variation in heating load is observed between northern and southern Europe. The cooling load is low compared to the heating load, the maximum value reaches 13.6 $kWh/(m^2\,year)$ for the "very good" level for Lisbon. Torino reaches a lower cooling load value not higher than 8.1 $kWh/(m^2\,year)$ while the two northern locations have a very low cooling load. The cooling load grows with the quality level of the building. The house is indeed less able to evacuate heat with a higher insulation.

The importance of the comfort model is also emphasized in figure 2.17. The PMV model with the set points selected below allows a lower heating temperature (20°C instead of 21°C) and a higher cooling set point. It implies a lower cooling load and a higher heating load with the ACA adaptive model. On the cooling side, it is very significant for Lisbon where the ACA model has a cooling load nearly two times lower than the PMV model. High ambient temperature for successive days encountered for Lisbon justifies a higher cooling set point. The Torino location encounters some cooling loads even if the mean external temperature is not so high but the difference between cooling load to reach ACA or PMV model is negligible.

The solar protection influences greatly the cooling load, an increase of at least 67% of the cooling load is encountered when the solar protection are not

used for Lisbon. It is crucial to install some efficient solar protections to decrease the cooling load. The results below take into account solar protection which blocks 55% of the solar radiation. More efficient solar shading devices could achieve lower cooling loads but care has been taken to keep visible light coming inside the house.

The part of the latent load is also computed. The Sensible Heat Ratio is higher than 90% for Lisbon and a little bit lower for Torino (70-87%) due to the higher humidity in the ambient air. The humidication of the air to reach 25% is not significant; the Sensible Heat Ratio is minimum 97.5%.

Level	**'acceptable'**		**'good'**		**'very good'**	
Yearly loads *Test case*	**Heating** $[kWh/m^2]$	**Cooling** $[kWh/m^2]$	**Heating** $[kWh/m^2]$	**Cooling** $[kWh/m^2]$	**Heating** $[kWh/m^2]$	**Cooling** $[kWh/m^2]$
Lisbon PMV	7.9	9.6	2.7	13.4	0.0	13.6
Lisbon ACA	13.9	4.9	5.4	9.5	0.0	13.5
Torino PMV	57.2	6.2	36.2	8.9	2.8	8.1
Torino ACA	64.8	6.3	40.9	8.9	3.8	8.1
Paris PMV	65.3	1.1	42.8	2.5	5.7	3.0
Paris ACA	74.0	0.7	48.4	1.8	7.2	3.3
Stockholm PMV	137.5	0.0	95.5	0.4	18.7	1.3
Stockholm ACA	142.3	0.1	101.0	0.8	20.6	3.5

Table 2.11: Detached house yearly heating and cooling loads

2.6.7 Comfort indexes

The load computation of this residential building is particularly useful to decide whether a cooling system should be installed or not. The simulations run in FREE-float mode describe the comfort conditions if there are no cooling systems. The comfort indexes (degree-hour overheating and percentage of overheating period) can be observed in figure 2.18. It supports the fact that more insulated envelopes ("good" and "very good" levels) generate a much higher discomfort in summer period.

For the two sunniest locations, the degree-days overheating are three to four times higher for "very good" level compared to the "acceptable" one. In any case the discomfort period lasts at least 16% of the year to reach 45% for the most uncomfortable case. The maximum operative temperature reached in the building in this case (table 2.12) is 34°C. In a climate similar to Torino, a compromise should be made between the wall insulation decreasing the heating load and increasing the cooling one.

So, a cooling system should be installed in those locations for such a residential building. More efficient solar protection or night cooling ventilation could decrease the cooling load and avoid an active system installation. These decreasing load measures are briefly mentioned in the discussion section of this

chapter. Their implementation is out of the scope of this work.

For the two colder places, overheating appears only in the two “best” levels. The criteria of 5% overheating period is met in ”acceptable” and ”good” levels. A 10% duration (around 870 hours) overheating period is encountered for the ”very good” level. The maximum operative temperature is less than 30°C; the mean gap between upper limit comfort temperature and computed operative temperature is around 1.2°C. These facts added to the low ambient temperature in Paris (162 hours with temperature > 26°C) and Stockholm (13 hours with temperature > 26°C) explain that a cooling system is not essential in the studied residential building located in those places whatever the building level.

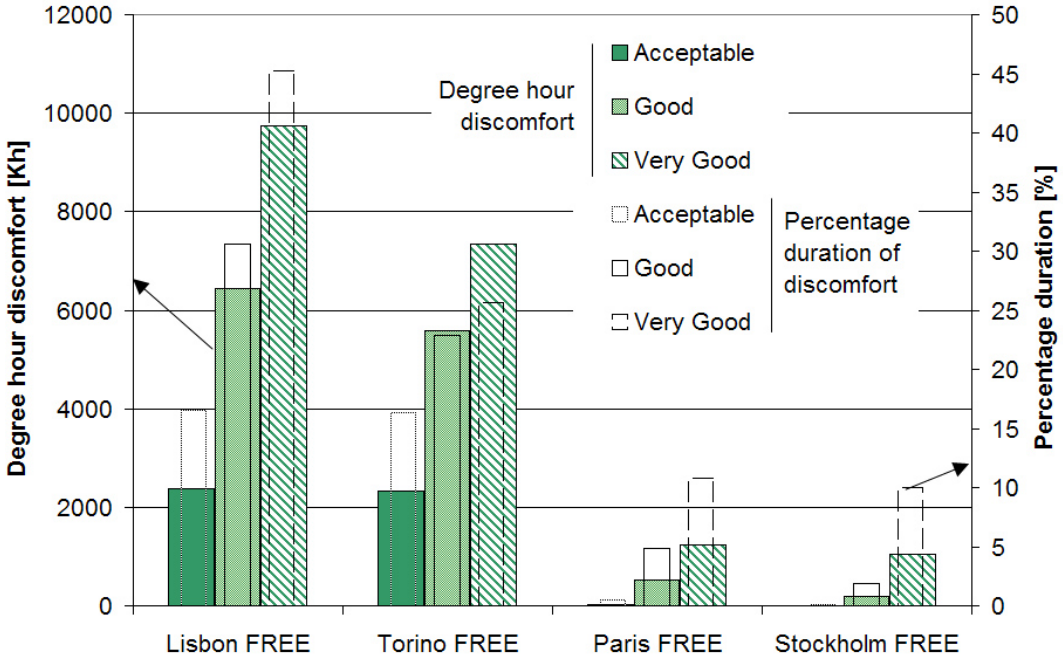

Figure 2.18: Detached house comfort indexes: overheating degree-hours and percentage duration of discomfort period

2.6.8 Cooling load shape on a hot day

For Torino and Lisbon where an active cooling system could be essential, the maximum cooling load is computed as well as the daily load when this maximum occurs (table 2.13). The shape of the load for a hot day in Lisbon (19^{th} of August in TMY2 data) is represented in figure 2.19. The nearly same shape

Level	Degree-hour overheating $[Kh]$	Duration [%]	Maximum operative t° [°C]
Cooling 'acceptable'			
Lisbon FREE	2381.1	16.6	32.0
Torino FREE	2319	16	30.0
Paris FREE	28	0.5	28.0
Stockholm FREE	10	0.1	27.1
Cooling 'good'			
Lisbon FREE	6446	31	33.7
Torino FREE	5578.6	23	31.7
Paris FREE	511	5	29.3
Stockholm FREE	198	2	29.0
Cooling 'very good'			
Lisbon FREE	9745	45	33.9
Torino FREE	7335	26	32.0
Paris FREE	1245	11	29.7
Stockholm FREE	1039	10	29.3

Table 2.12: Detached house comfort indexes in free-floating mode and maximum obtained operative temperature

is encountered for Torino (figure 2.20).

The cooling load reaches a peak at the end of the afternoon: the house has accumulated solar energy and internal gains during the hottest hours of the day. The cooling load encounters a sudden increase at 11 pm for the "good" and "acceptable" levels because of the shift between night and day zone occupation (weekend day). A quite important cooling load remains during the night but it goes down to a very low value before sunrise. The "very good" level has a more compact shape, the envelope and the glazing keep the solar radiation outside of the building. Generally the "very good" level building has lower peaks but higher mean cooling load throughout the year. This is not the case for Lisbon ACA simulation (table 2.13) which showed high peak cooling power. It comes from a high latent cooling load at the beginning of a day in Autumn. The temperature of the building remains high, so cooling is possible and the computation of latent load is done.

Concerning coincidence between solar energy and cooling load, the peak cooling power occurs with a delay compared to the solar energy on the south roof. It is interesting from the direct use of solar energy point of view. Nevertheless, to meet comfortable conditions during the night, the energy storage must be large enough to supply around one third of the daily cooling load during the night. On a yearly basis for Lisbon location with ACA model, 22% of

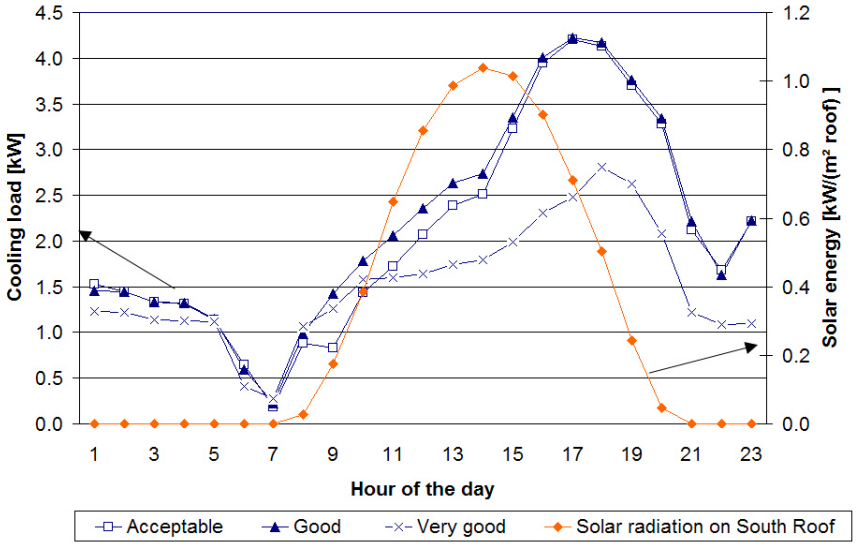

Figure 2.19: Detached house cooling load for a hot day in Lisbon for the three energy levels (ACA model) and the available solar energy on the south roof

the cooling load must be satisfied during the night (no solar radiation).

The solar energy displayed on figure 2.19 reaches 7.3 kWh/m^2 for this sunny day and deals with one square meter on the south roof. The available surface on this roof is around 90 m^2, it could supply up to 200 kWh cold energy (considering a collector yield of 0.5 and a COP of thermally driven chiller of 0.6). It is considerably higher than the required load ($\approx$ 50 kWh). The available space of roof is not the limiting criteria in this case.

Level	**'acceptable'**		**'good'**		**'very good'**	
Maximum cooling power	Power	Load	Power	Load	Power	Load
Daily cooling load	$[kW]$	$[kWh/day]$	$[kW]$	$[kWh/day]$	$[kW]$	$[kWh/day]$
Lisbon PMV	5.2	72.4	4.3	54.4	3.1	41.4
Lisbon ACA	4.2	49.6	4.2	52.1	4.8	17.2
Torino PMV	4.9	56.9	4.8	58.7	2.6	37.6
Torino ACA	4.9	56.9	4.8	58.8	2.6	37.6

Table 2.13: Detached house maximum cooling power and its daily load

Other load profiles can be encountered, figure 2.20 displays seven consecutive days hourly loads (sorted from the lower to the higher daily cooling load). The beginning of the day is still influenced by the accumulated energy of the previous day. The solar gains and external temperature impact the height of

the peak that occurs mainly at 6 pm. There are important variations from day to day, the cooling system will have to take care of these variations to be efficient.

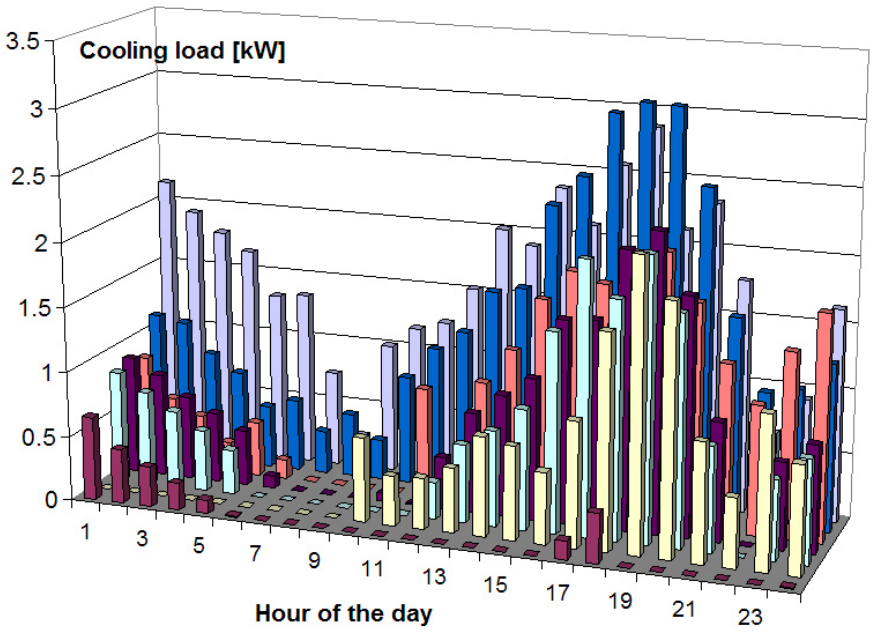

Figure 2.20: Detached house hourly cooling load for 7 days in Torino (ACA model - "acceptable" level)

2.7 Discussion

The heating, cooling and domestic hot water loads computation of three buildings in various conditions has been carried out. Those loads are the starting point of solar cooling systems energy performance evaluation detailed in the next chapter. Some points need to be discussed before proceeding to the system analysis:

Firstly, the comfort models try to convert the occupants feelings into some indexes. Depending on the model (PMV, ACA ...), the set points are chosen and the loads are computed. The energy use, which is linked to the load, is therefore considerably influenced by the chosen model (up to 17% less cooling load for ACA model than for PMV) for southern locations. From an energy point of view, in southern locations, the adaptive model seems to be more suitable as it does not separate completely the internal and external building conditions. Besides, the comfort models describing buildings where the occupants can control their environment involve larger comfort temperature range. Could it be the same for building with occupants aware of a cooling system driven by solar energy? Building energy use simulations depend largely on the hypothesis set for comfort requirements.

Secondly, the loads computed are based on a mean year which does not involve any hot waves. In an other context, the city center locations could reach different environmental conditions. This phenomenon is called the *heat island effect* (Santamouris, 2012) and involves an increase of air temperature as well as ground temperature (Menberg *et al.*, 2013). This effect would certainly lead to higher cooling loads and lower heating loads. Moreover, outdoor temperature and humidity greatly influence the performance of the rejection device used in any kind of chiller. The influence of outdoor temperature on the dry cooling tower electricity consumption is investigated in chapter 4.

Some building performance levels have been set, starting from Belgian typical buildings. Despite the different architectural habits over Europe, the same buildings were kept for the four location for comparison purposes. For example, the new office building 'very good' level will never be met in Lisbon, it is suited for a colder climate (glazing g-value is higher to get more solar gains...). Other buildings with regional specificities could be implemented to have a more accurate evaluation of the cooling load. This is out of the scope of this work. In this study, a higher building energy performance levels globally increase the envelope thermal resistance, thus the cooling load and respectively decrease the heating load. The best equilibrium will be found by evaluating the energy use of heat and cold production devices. The new office 'good' and 'very good' levels also have a more efficient lighting implying fewer thermal gains and electrical consumption. This leads to a decrease in the global building energy use.

Despite the fact that the selected buildings are not typical ones of southern regions, they represent well the loads that might be encountered in those

countries. Moreover, the improvements between building levels are consistent (except from 'very good' level for office building) with what can be implemented in reality to increase the building energy performance.

The loads are computed without taking the heating and cooling system into consideration which is a quite common method to evaluate the loads in solar air-conditioning (Henning, 2007a). Heat and cold distribution/emission as well as control are sources of thermal losses increasing the loads. For one building, next chapter shows the influence of distribution/emission on total computed loads. Moreover, it is hazardous to compare the loads computed here with the total energy use of the building. The figures addressing the building electricity and gas consumptions are presented in next chapter.

Finally, the cooling needs grow along the building energy performance level, even in northern locations. More and more buildings will lead to summer discomfort for the occupants if no cooling strategy is adopted. In new buildings, we really have to pay attention to the development of techniques that substantially improve the summer comfort without any significant increase in energy use. These techniques used could be active (such as solar air-conditioning) or passive (without any chiller). The main passives ones are:

- Night ventilation (natural or mechanical ventilation),
- Ground coupled heat exchanger for air ventilation or water cooling,
- Cooling tower coupled with thermally activated building structure.

Those passive techniques (Givoni, 2011) combined with architectural or urban considerations have been investigated by Hatamipour and Abedi (2008). As a passive technique could generate a supplementary electricity consumption, it is then important to analyse the energy performance by establishing its COP (Eicker *et al.*, 2006).

Chapter 3

Solar cooling systems simulation

This chapter details the simulation of thermally driven solar air conditioning systems and PV connected vapour compression chiller systems. The analysis of heating and cooling demand performed in chapter 2 must be extended to heat and cold production devices, as an integral approach is required to evaluate the energy savings. Therefore, the whole building energy use for heating and cooling in the previously selected locations will be handled in this chapter. This includes the energy required for heating, cooling, ventilation, auxiliaries and electrical needs for building use. The complete simulation environment is implemented in TRNSYS simulation software (TRNSYS, 2012). The various simulations are carried out with a 10-minute time step, which is consistent with the dynamics of the analysed system.

Three previously selected buildings entail some typical cases:

1. New office building
2. Typical European office building
3. Detached house

The second building includes a detailed analysis of heat and cold emission while the two others consider perfect emission devices (without any losses or inertia). The economical performance of the different simulated systems is also investigated to check both energy and economical benefits of solar cooling systems. The buildings are selected from those involving market opportunities (Henning, 2011).

The scheme of the simulated thermally driven systems depends on the building but is very similar to the general scheme displayed in chapter 1 in figure 1.32 (page 42). A solar collector field provides hot water to a storage tank to feed a sorption chiller (ab or adsorption), to satisfy the heating load and the domestic hot water load (for residential building only). Moreover, a gas boiler and a vapour compression chiller are used as back-up heat/cold production. Despite the differences between buildings, the vapour compression chiller prevails as cold back-up device. When there is not enough solar energy to cool the

building, the vapour compression chiller starts. Using a gas boiler as back-up for cold production is indeed not energy efficient in case of single effect sorption chillers (Henning and Döll, 2012).

In order to easily compare the energy uses, a reference case called "classical air-conditioning" is simulated. It includes an electricity driven vapour compression chiller for cold production and a boiler for heating but doesn't include solar panels or storage devices. The last case, namely "PV connected vapour compression chiller" system is simply the reference case where a PV field is added.

In TRNSYS software, the various existing models are named using a type number. In the following pages, the readers will be provided with the type number of each model used, which will enable them to find the model documentation more easily and directly recognize the models used.

3.1 New office building

3.1.1 Introduction

The Building modelling is described in section 2.4 of chapter 2 while the main building characteristics are detailed in appendix. The simulation considers the entire building displayed in figure 3.1 including around 4403 m^2 available area and both the absorption cooling system and the PV connected vapour compression system will be analysed. This kind of building is suited to the use of absorption chiller for cooling because of the lower cold temperature reached (7°C). This allows the use of fan coil unit for both sensible and latent load management. Large solar cooling systems generally involve absorption cooling systems (Sparber *et al.*, 2009b).

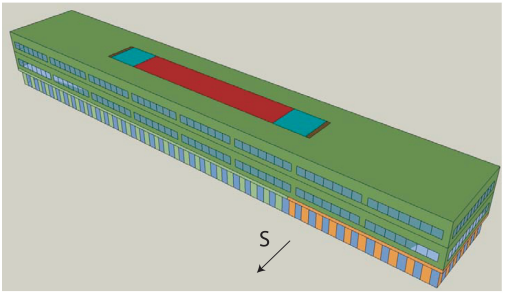

Figure 3.1: Newoffice geometry (EPICOOL, 2009)

The general scheme for the system simulation is displayed in figures 3.2 and 3.3 respectively for thermally driven and PV driven cooling. The simulations carried out in this section concern the systems displayed and the loads

computed in chapter 2. The different parts of the figures are detailed in the following paragraphs.

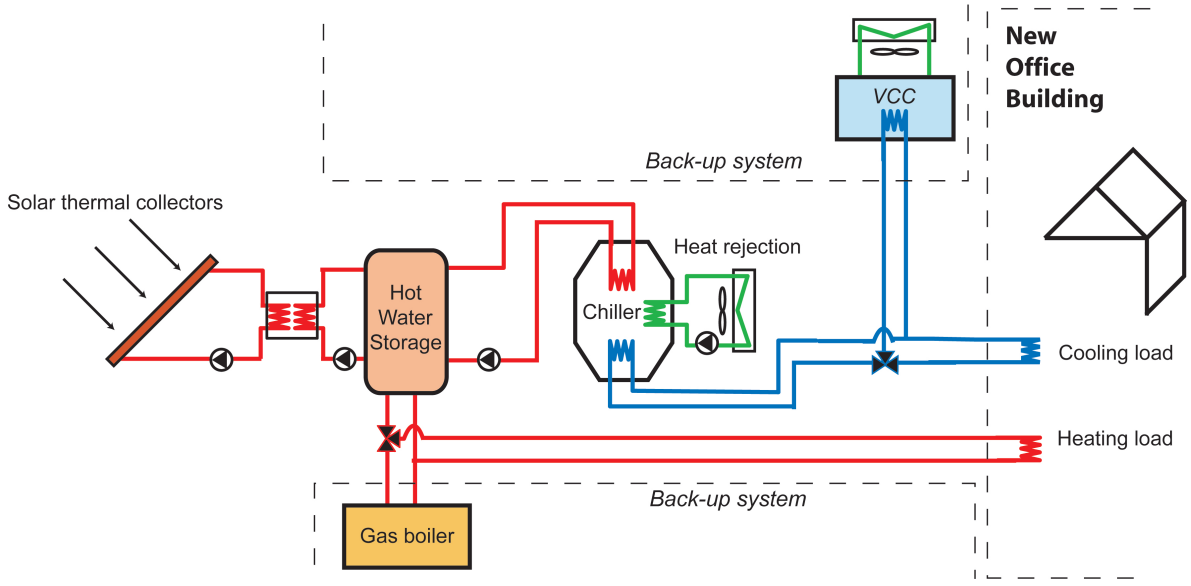

Figure 3.2: New office thermally driven solar air-conditioning scheme

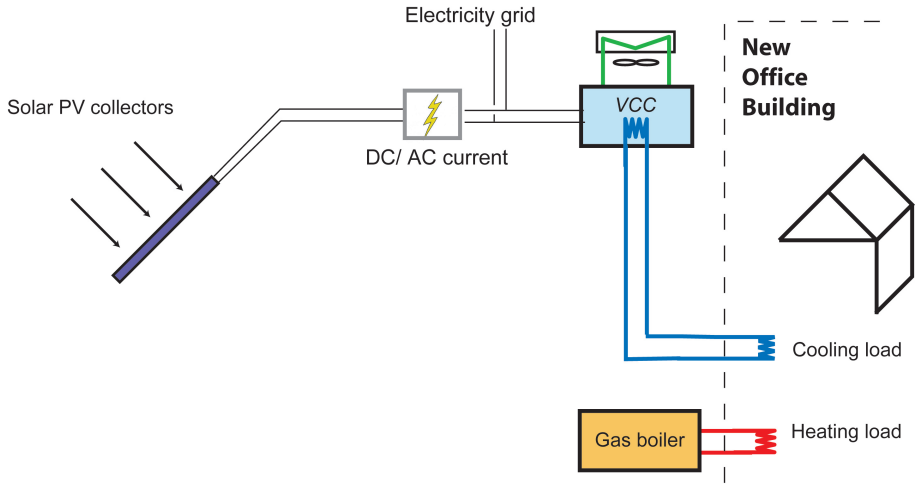

Figure 3.3: New office PV driven solar air-conditioning scheme

3.1.2 Thermal collector field

Evacuated tube collectors (ETC) are used because of the slightly high temperature they can reach compared to commonly used flat-plate collectors. The ETC collectors have a better efficiency in the absorption chiller operating temperature range (70 to 95 °C). TRNSYS type 71 has been chosen to implement the manufacturer's data including collector efficiency (see table 3.1), incidence angle modifier and mass flow variation. The general equation of a solar thermal collector has been detailed in chapter 1, it is presented in equation 3.1.

$$\eta_{thermal\ collector} = k(\theta)a_0 - a_1\frac{(T_{coll} - T_{amb})}{I_{tot}} - a_2\frac{(T_{coll} - T_{amb})^2}{I_{tot}} \tag{3.1}$$

Collector type	a_0 $[-]$	a_1 $[W/(m^2K)]$	a_2 $[W/(m^2K^2)]$
ETC16	0.773	1.09	0.0094

Table 3.1: Evacuated tube collector efficiency numerical values (SCHOTT, 2003)

The collector area is crucial for solar air-conditioning systems and its size is selected according to the following restrictions: the only available space is the flat roof of the building and the solar thermal energy production requirements are 350 kWh per net collector area per year that was given by Nowag *et al.* (2012) as a quality criterion. This second criterion is the most restrictive for all locations but Lisbon.

For example, the collector number to reach the "350 kWh per net collector area per year"criteria has been computed for Paris "acceptable" office building using the ACA comfort model (see chapter 2). The best design of the collector field includes four rows of 42 panels oriented to the south (the slope α in figure 3.4 depends on the location). It leads to an available solar absorption area of 136 m^2. A larger collector field would have reached a lower heat production per collector.

The collector (PV or thermal) field geometrical parameters are detailed in figure 3.4. For thermal collectors, the row spacing is 4 meters while the collector height is 1.7 meter. In the example, 33% of the roof length is reserved to solar collectors spanning the entire width of the roof. In a real situation this would reduce the thermal losses between collectors and storage. Moreover, this leaves available space on the roof for other purposes (terrace, equipment...).

In other words, the collector field has 1.27 square meter collector area per kW_{cold} absorption chiller nominal power. It is really low but does not reduce

the absorption chiller performance (see next paragraph about sorption chiller).

The shading between rows of collectors has to be taken into account by using a dedicated model (type 551). Finally, the solar loop is connected to the storage tank via a heat exchanger with 95% constant effectiveness. The collectors mass flow has been set to 30 kg per hour per collector area (Eicker and Pietruschka, 2009).

The thermal and PV fields design parameters are summarized for each location in table 3.2.

	Unit	**Lisbon**	**Torino**	**Paris**	**Stockholm**
Thermal field					
number of rows	-	4	4	4	4
d	m	4	4	4	4
h	m	1.70	1.70	1.70	1.70
α	°	0	15	15	30
net collector area	m^2	378.1	248.9	135.7	87.3
Minimal specific thermal prod.	$kWh/m^2_{absorber}$	350	350	350	350
Minimal specific thermal prod.	$kWh/m^2_{building}$	30.1	19.8	10.8	6.9
PV field					
Row number	-	12	12	12	10
d	m	1	1	1	1.25
h	m	0.7	0.7	0.7	0.7
α	°	10	10	10	20
net collector area	m^2	616.3	407.4	219.4	113.2
Specific elec.	kWh/m^2_{cells}	183	140	102	93
Specific elec.	$kWh/m^2_{building}$	25.7	13.0	5.1	2.4
Specific elec.	kWh/kW_p	1297	993	722	656
Common data					
Building length used	%	90	59	32	21

Table 3.2: New office building collector fields characteristics

3.1.3 PV collector field

The collector area also has a great impact on the electricity produced, the size of the roof available for PV collector is equivalent to the one reserved to thermal collectors (e.g 40% of roof area for Paris). As for thermal collectors, the number of rows is selected as a compromise between two extremes:

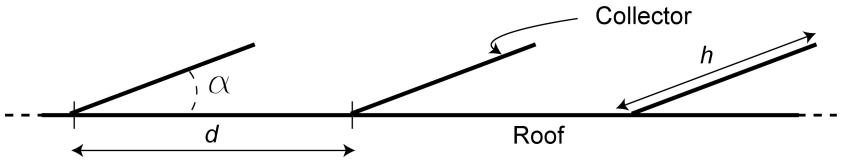

Figure 3.4: New office building collector field geometrical parameters

- Narrow space between the rows and a decreased electricity production per collector area.
- Larger space and lower number of collectors on the roof.

It is assumed that PV panels work at their optimal point (current-voltage curve) each time. Given the PV panel production, 17% losses are added due to cables, inverter and other reflectance effects (Suri *et al.*, 2007). The space between the rows and the collectors slope are chosen to achieve a maximum number of collectors and 90% solar production per collector compared to an optimal unshaded pannel. Horizontal collectors are avoided. Altough they have lower shading, the production per collector is a bit lower than for the optimal slope. Moreover, self-cleaning of the collectors requires a minimal slope of around 10° (Clean-Energy-Council, 2012).

The manufacturer's data (SHARP, 2006) is implemented in type 194 using a 5-parameter model presented by Kou *et al.* (1998). The current and voltage collector curve is used to build the five-parameter equivalent electrical circuit (Duffie and Beckman, 1991) seen on figure 3.5 where the shunt resistance (R_{sh}) is infinite in case of mono- or polycrystalline cells. This model handles a simple thermal model of the PV array. Here also, type 551 computes the collector shading according to figure 3.4. Besides, a conservative shading is computed to take the non-linearity of PV production affected by shading into account.

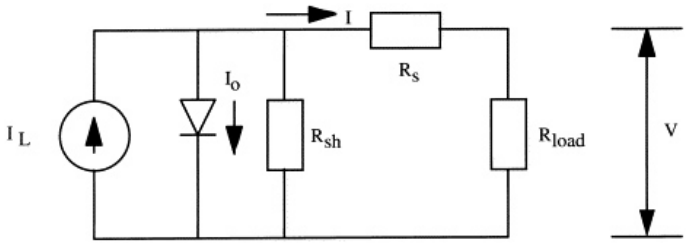

Figure 3.5: Equivalent circuit of a solar cell (Kou *et al.*, 1998) where I_L = light current; I_o = dark current; I = operation current; V = operation voltage; R_s = series resistance; R_{sh}= shunt resistance

Finally, the chosen PV collector field achieves a yearly production of electricity ranging from 10.5 to 112 MWh depending on the location. The PV field design parameters are also summarized for each location in table 3.2.

The area covered by the collectors is the same for thermal and PV fields which means a certain ratio of building length is dedicated to collectors (table 3.2). Nevertheless, the net collector area is greater for PV field. Two reasons explain this difference:

- The ratio of absorber area divided by the gross collector area is higher for PV (88%) than for evacuated tube collector (63%)
- The spacing between the rows is higher due to the shape of collectors. The evacuated tube collector should be placed in portrait view while the PV collectors can be placed in portrait or landscape view.

This explains the fact that the thermal collectors absorber area is around 61% of PV cells surface.

3.1.4 Absorption chiller

The heat provided by the solar collectors is stored and feeds an absorption chiller to produce cold water. Among all kinds of thermally driven chillers available on the market, a lithium bromide - water absorption chiller was chosen. Absorption chiller behaviour has been implemented in a new TRNSYS type 255 (nearly the same as existing TRNSYS type 107) based on manufacturer curves of a 105 kW_C absorption chiller ($COP_{rated} = 0.695$) (YAZAKI, 2008). The performance curve introduced in chapter 1 on figure 1.18 is extended by the figure 3.6 for other rejection temperatures.

The existing model (type 107) models the energy balance, but not the chiller internal dynamics which time constant is in the order of magnitude of 10 minutes as mentioned by Evola *et al.* (2013) or Zambrano *et al.* (2008). As detailed in chapter 1, the absorption chiller works with three energy flows (figure 1.5).

The model described in the following equations solves the energy balance. The relationship between the hot and cold flow is governed by the thermal Coefficient Of Performance. Furthermore, the maximum cold and hot flows are defined according to the current conditions of hot and rejection water temperatures. The model uses a normalized lookup table to compute the energy balance. Data file for types 107 and 255 requires fraction of rated capacity ($f_{rated\,cap.}$) and fraction of rated energy input ($f_{rated\,inp.}$). The absorption chiller selected for the study provides these two parameters as a function of hot water inlet temperature $T_{H\,in}$ and rejection inlet temperature $T_{M\,in}$. Only one cold water outlet temperature $T_{C\,out}$ is given: 7°C.

The maximal cooling capacity with given inlet temperatures and set point is named as *current* conditions. It is displayed in figure 3.6 for cooling. The

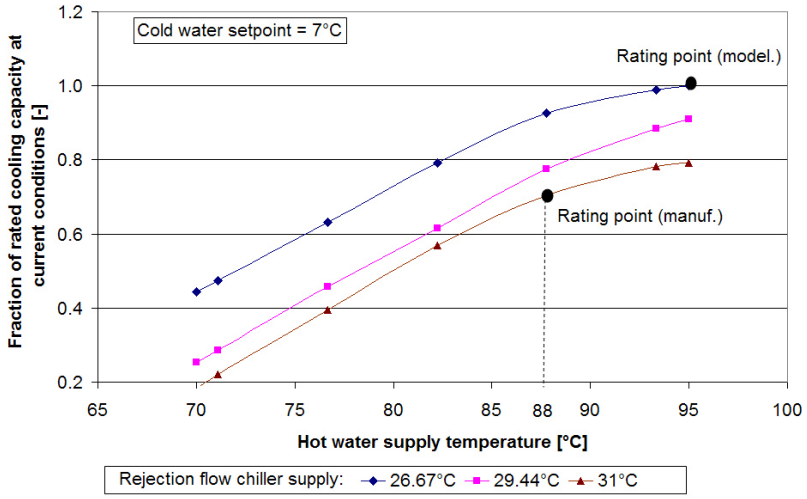

Figure 3.6: Absorption chiller cooling capacity for different rejection temperatures

same curves can be found for the heat energy input. The current conditions are computed using equations 3.2 and 3.3.

$$\dot{Q}_{C\,current} = \dot{Q}_{C\,rated} \cdot f_{rated\,cap.} \tag{3.2}$$

$$\dot{Q}_{H\,current} = \frac{\dot{Q}_{C\,rated}}{COP_{rated}} \cdot f_{rated\,inp.} \tag{3.3}$$

where $\dot{Q}_{C\,rated}$ and COP_{rated} must be given for the selected sorption chiller while $f_{rated\,cap.}$ and $f_{rated\,inp.}$ are read in the file.

The power required to reach the cold water set point is given by equation 3.4, it allows the part load fraction $f_{part\,load}$ calculation (equation 3.5).

$$\dot{Q}_{C\,required} = \dot{m}_C \cdot c_{p\,C} \cdot (T_{C\,in} - T_{C\,set\,point}) \tag{3.4}$$

$$f_{part\,load} = MIN(1, \frac{\dot{Q}_{C\,required}}{\dot{Q}_{cold\,current}}) \tag{3.5}$$

Finally, the absorption chiller power flows are computed using the three following equations:

$$\dot{Q}_C = f_{part\,load} \cdot \dot{Q}_{C\,current} \tag{3.6}$$

$$\dot{Q}_H = f_{part\,load} \cdot \dot{Q}_{H\,current} \tag{3.7}$$

$$\dot{Q}_M = \dot{Q}_C + \dot{Q}_H \tag{3.8}$$

Given the current conditions, equation 3.7 involves a constant thermal COP whatever the part load conditions. No absorption part load data have been found, the constant COP is henceforth considered. However, the model allows to add some part load performance data if available.

The analysis of the model revealed discrepancies in type 107. Firstly, in such chillers, the rated cooling power is generally not the highest cooling power. Nevertheless, in type 107, fraction of nominal capacity is computed based on the rated capacity and is limited to 1. It is then required to enter both parameters at maximum capacity conditions instead of manufacturer's rated conditions. The difference between manufacturer's rated capacity and the one required by the model is clearly shown in figure 3.6.

Secondly, the part load operation ($f_{part\,load}$) is independent of current conditions. It implies a non convenient way to create the data file. A new type numbered 255 was consequently developed; it has a second call to the external data file. The first call is used for discovering the maximum capacity at current conditions ($\dot{Q}_{cold\,current}$), the second call for the part load evaluation. This way, we are able to reproduce the behaviour described by the manufacturer's data.

There is still a lack of accuracy in the modelling and simulation of the absorption chiller. Due to the lack of manufacturer's data, the nominal water mass flows are assumed during the whole chiller operation. The thermal COP is computed based on the temperatures of the three input and on nominal mass flow conditions. Ortiz *et al.* (2009) modelled the effect of absorption chiller mass flow variation (between 50% and 120% of the nominal rating). The thermal COP variation encountered ranges from 0.65 to 0.75.

Additionally, when the cooling demand is lower than the cooling capacity, the chiller produces the exact quantity of cold to reach the set point (7°C in this case); it means there is no minimum cooling power.

The absorption chiller specifications used in those simulations are described in table 3.3.

Some additional comments must be addressed to the potential type 255 user:

- The routine reading the data file containing $f_{rated\,cap.}$ and $f_{rated\,inp.}$ achieves a linear interpolation between the different points. It does not extrapolate the data but uses the boundary value.
- This model also suits for adsorption chiller. Nevertheless, the reader should keep in mind it does not include any inertia effect.
- Type 107 and type 255 (and other TRNSYS models implementing absorption chillers in general) are able to enter auxiliary consumption due

	Manufacturer's rated conditions	Model rated conditions
$COP_{thermal}$	0.695	0.634
$\dot{Q}_{C\ rated}$	105 kW	138.3 kW
Temperature range		
$T_{H\ in}$	70-95 °C	
$T_{M\ in}$	26.67-31 °C	
$T_{C\ out}$	7°C	

Table 3.3: Thermal specifications of the absorption chiller (YAZAKI, 2008)

to chiller pumps in the model. This auxiliary power is added to the computed rejection flow (equation 3.8).

3.1.5 Other devices

Heat storage

The storage tank (type 534) shown in figure 3.2 is directly connected to three circuits (no heat exchanger in the tank): the solar collector, building heating network and absorption chiller hot water loop. The solar radiation is the only energy source supplying heat to the tank. A 0.2 m thick rock wool insulation has been modelled in order to decrease storage losses. The storage tank volume is 55 litres per square meter of solar absorber area, leading to a volume of around 10 m^3 (for the new office in Paris). This ratio is generally a good compromise between energy saving and cost (Henning and Döll, 2012).

Cooling tower

The absorption chiller requires a rejection circuit to evacuate the medium temperature energy flow. Heat rejection control is crucial to guarantee good performance of absorption chillers. The model used is type 510 representing a closed circuit wet cooling tower. According to the authors (Zweifel *et al.*, 1995), the model is able to find accurately the power rejected based on only one design point. This point has been found for an existing machine (AEC-FG 2004) with a nominal rejection thermal power of 263 kW (AEC, 2007). The control of outlet water temperature is done by modifying the cooling tower fan speed. The internal control of type 511 achieves an outlet cooling water temperature below 30°C all year around.

Vapour compression chiller

As mentioned before, the back-up system for cooling is a classical vapour compression chiller. A reversible air cooled heat pump WESPER VLH-HE804 was implemented into TRNSYS using type 655 (WESPER, 2005). The model consists in reading the manufacturer performance curves of cold energy produced and electrical consumption for various outdoor temperatures. To be consistent with the building and the absorption chiller specificities, this machine is used to

produce cold water at 7°C. Vapour compression chiller has cold power adapted to the building cooling load, its nominal COP(or EER) is 2.79, the seasonal index ESEER is 3.95. (including fans and pump) in steady state conditions. Those conditions are defined in standard (EN14511, 2004): the external air dry and wet bulb temperatures are respectively 35 and 24°C while the cold side inlet and outlet temperatures are 12 and 7°C.

Gas boiler

The gas boiler performance is defined according to Stabat *et al.* (2011): efficiency at 100 % load is 89.2 %; efficiency at 30% load is 88.2 %; losses at 0% load are 1.3 kW. A linear interpolation is done between these three points. The rated power is defined according to the maximal heating load. This device is switched OFF (i.e. no consumption) if there is no heating demand.

3.1.6 Electricity consumption

The electricity consumption of each device is evaluated. For the pumps, no typical pressure drop values are found for the different circuits. They are not modelled but their electricity consumption is taken into account. Common auxiliary energy use values of well designed systems are considered according to Henning (2008) and Napolitano *et al.* (2011):

- 0.02 kWh electricity per kWh thermal energy collected for the solar system,
- 0.03 kWh electricity per kWh thermal energy rejected for the cooling tower,
- 0.01 kWh electricity per kWh cold energy produced for the absorption chiller,
- 0.02 kWh electricity per kWh heat energy produced for the gas boiler,

The fans and pump of the vapour compression chiller are already included in the model presented above. The distribution pumps are not modelled as shown in figure 3.2 or 3.3. Their consumption has no impact on the choice of heat and cold production systems.

3.1.7 Heating and cooling loads management

The distribution and emission devices are not implemented. The heat ($\dot{Q}_{bui\ heat}$) and cold hourly loads ($\dot{Q}_{bui\ cold}$) from earlier simulations are directly used in the simulation. The building inlet temperatures are 7°C for cooling ($T_{bui\ cold\ in}$) and ranging between 45-90°C for heating ($T_{bui\ heat\ in}$), as shown in figure 3.7. The building outlet temperature is computed according to the following equations:

$$T_{bui\ heat\ out} = T_{bui\ heat\ in} - \frac{\dot{Q}_{bui\ heat}}{\dot{m}_{bui\ heat} \cdot c_{p\ water}} \tag{3.9}$$

$$T_{bui\ cold\ out} = T_{bui\ cold\ in} + \frac{\dot{Q}_{bui\ cold}}{\dot{m}_{bui\ cold} \cdot c_{p\ water}} \tag{3.10}$$

where the two mass flows are computed using maximum heating and cooling loads.

$$\dot{m}_{bui\ heat} = \frac{\dot{Q}_{bui\ heat\ max}}{20 \cdot c_{p\ water}} \tag{3.11}$$

$$\dot{m}_{bui\ cold} = \frac{\dot{Q}_{bui\ cold\ max}}{5 \cdot c_{p\ water}} \tag{3.12}$$

20°C is a conventional value for the temperature gap between the supply and return temperature of a radiator (NBN-EN442, 2004) while 5°C is consistent with the cold distribution-emission temperature increase (Energieplus, 2012).

3.1.8 System control

For the PV or classical air-conditioning systems, the heating and cooling loads are respectively satisfied by the gas boiler and vapour compression chiller. For the thermally driven solar air-conditioning, the control affects three parts of the system.

Solar collectors

The solar collectors are operated when the shaded collector temperature is 5°C higher than the bottom tank temperature. A hysteresis controller is implemented: the collectors stop collecting solar energy if the difference drops below 2°C. Finally, the maximum operating temperature of the collector outlet is set to 140°C.

Heating

The gas boiler is used as back-up when the storage tank top temperature is lower than the temperature given by the heating curve shown in figure 3.7. The gas boiler directly feeds the building, it does not heat the water tank.

Cooling

Previous work about the solar cooling control strategies (Thomas and André, 2009) showed the importance of the absorption chiller control strategy. Firstly, the absorption chiller is switched OFF and the vapour compression chiller switched ON when the temperature of the water on the top of the storage is lower than the cooling curve showed in figure 3.8. Besides, the cooling curve is affected by the building return cold temperature ($T_{bui\ cold\ out}$) in relation with the cooling load. Basically, when the cooling load is not high, the absorption chiller does not require hot water at such high temperature. To avoid

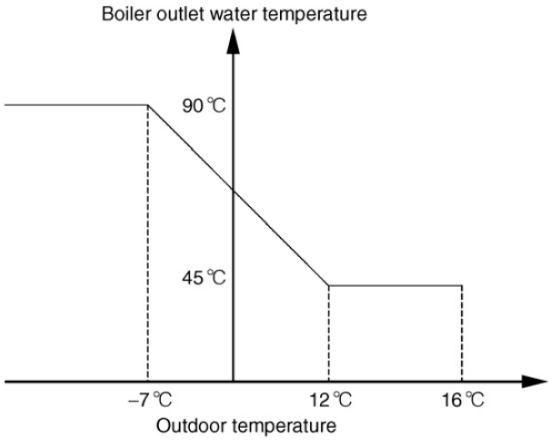

Figure 3.7: Gas boiler outlet water temperature set point (Stabat *et al.*, 2011)

ON/OFF switching between both chillers, a hysteresis controller with a 3°C dead band is implemented. Secondly, when the load is too important, both chillers are operated in series. The absorption chiller cools as much as it can and the vapour compression chiller does the rest.

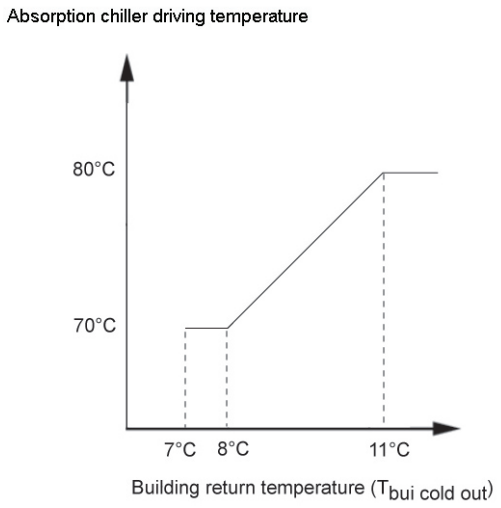

Figure 3.8: Required tank temperature to drive the absorption chiller

3.1.9 Appliances, light and ventilation consumption

The hypotheses made about the electricity consumption of the appliances, light and ventilations are detailed in appendix. For the three energy performance levels, the electricity consumption sharing is showed on table 3.4. The yearly electricity consumption reaches around 35 kWh/m^2 (meaning 87.5 kWh/m^2 primary energy), it has to be compared to the results about primary energy in the next paragraphs.

	Unit	"Acceptable"	"Good" and "Very Good"
Appliances	kWh/m^2	11.6	11.6
Light	kWh/m^2	17.2	14.8
Ventilation	kWh/m^2	6.4	6.4
Total	kWh/m^2	35.2	32.8

Table 3.4: Yearly net electricity consumption of appliances, light and ventilation for the new office building

3.1.10 Simulation results

The yearly simulation of the systems described above is carried out. It computes the key energy performance indicators for the different systems mentioned in the introduction:

- Thermally driven solar air-conditioning named *SAC therm*
- Classical air-conditioning named *Classical A-C*
- PV driven solar air-conditioning named *SAC PV*

The energy performance indicators are detailed in chapter 1, section 1.4. The Primary Energy Ratio definition (equations 1.25 to 1.27) is extended in this case, it handles now the current system boiler efficiency η_{boiler} and the VCC chiller performance SPF. The cold production performance is globally better than for the reference system ($SPF_{ref} = 2.8$). The current system SPF_{ref} ranges from 3.95 to 4.6 while η_{boiler} ranges from 0.83 to 0.88. The Primary Energy Ratio is used to compute the fraction of energy savings presented hereafter.

Comfort model influence

It is proposed to check the differences between the two models introduced in chapter 2, section 2.2: PMV (predicted mean vote) and ACA (adaptive). The heating and cooling loads of the building for the two comfort models are already described in section 2.4 in figure 2.8. The savings with thermally driven solar air-conditioning are now evaluated. Apart from the Lisbon case, the fraction of energy savings is not much influenced by the comfort model (figure 3.9). Lisbon's 'acceptable' and 'good' cases reach 15-20% more energy savings with an adaptive comfort model when using thermal solar air-conditioning. The cooling load decreases due to the use of ACA instead of PMV model with 10-15%

for these two cases (table 2.5). The energy savings showed in figure 3.9 come in addition to the cooling load decrease. So, for a building with a high cooling load, the use of an adequate cooling set point (coming from ACA model) wins on all fronts: building load and better solar system operation. This could be extended to the other simulation cases as the ACA model makes sense in solar air-conditioning because it links the internal and external environment. Consequently, for the following energy use investigations the results of the PMV model are removed from the analysis.

The PV driven system is not mentioned in this paragraph because the collector field operation is independent of the comfort model.

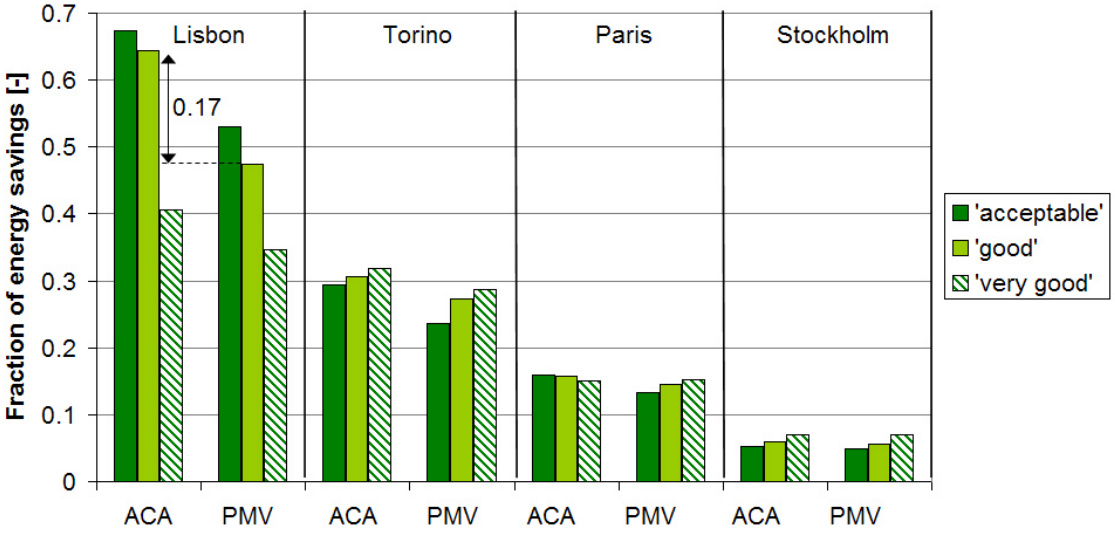

Figure 3.9: Comfort model influence on energy savings (SAC therm.)

Cold production system performance

The performance of the two chillers is linked to the cold water temperature and outdoor temperature. No part load performance correlation has been implemented for both VCC and absorption machines; the results are then based on full load data. Moreover the model does not take any dynamic effect into account. These two simplifications lead to discrepancies between the simulated and measured thermal COP values.

On the one hand, the simulated mean thermal COP of the absorption chiller ranges from 0.67 in Lisbon to 0.72 in Stockholm. These values are close to the nominal value ($COP_{rated} = 0.695$). For a similar system (lithium bromide - water absorption chiller), other studies revealed a lower thermal COP than the

nominal one. Rosiek and Batlles (2009) measured a COP of 0.53 for a three-month operation while Syed *et al.* (2005) proposes a value of 0.33. The part load operation is very often encountered in real operation and decreases the thermal performance (Zhai *et al.*, 2011). Moreover, the thermal COP is very sensitive to the water flow temperature (example for hot water temperature in figure 1.18 on page 23). An incorrect design of one of the water loop could lead to a significant thermal COP decrease. For well designed systems as studied by Vukits *et al.* (2011) or Neyer and Streicher (2011), a mean thermal COP of 0.53 to 0.62 has been measured. Therefore, the target given by Nowag *et al.* (2012) (mean thermal COP $\geq 0.8 \cdot COP_{rated}$) is a reachable goal for thermally driven cooling systems. So, the thermal COP computed is certainly a little bit overestimated.

On the other hand, the simulated electrical COP ($COP_{elec\,tot}$) is directly linked to the strong hypothesis made about the electrical consumptions. The consumption of solar air-conditioning devices has a default value regarding the thermal flow involved.

- 0.02 kWh electricity per kWh thermal energy collected for the solar system,
- 0.03 kWh electricity per kWh thermal energy rejected for the cooling tower,
- 0.01 kWh electricity per kWh cold energy produced for the absorption chiller,

This leads to $COP_{elec\,tot}$ values ranging from 17 to 24. This depends mainly on the fraction of solar heat used for cooling: high solar cooling fraction leads to low $COP_{elec\,tot}$ because of the electrical consumption of the chiller and cooling tower. These numerical values ($COP_{elec\,tot}$) depict the heating and cooling performance together. By focusing on cooling only, the COP would have reached 9.4 to 11.5. It is the order of magnitude of the target (10) given by Wiemken *et al.* (2010).

The fixed values of electrical consumptions taken in this study account for best practice installations. For cooling purpose, various measured monthly values are found in the literature for small and middle capacity installations (<30 kW_{cold}): 1.03 to 1.45 (Marc *et al.*, 2009), 1.81 (Neyer and Streicher, 2011), 3.6 (Agyenim *et al.*, 2010), 5.4 (Vukits *et al.*, 2011). Those values depend largely on hydraulics schemes and control (especially the cooling tower fans). Moreover, they are linked to the number of devices included in the analysis. The authors do not necessarily use the same index definitions as those defined in chapter 1. Thus, the comparison from the $COP_{elec\,tot}$ point of view is not so easy to establish. Nevertheless, Wiemken *et al.* (2010) gathered $COP_{elec\,tot}$ data on some real solar air-conditioning systems with absorption chiller and found values from 3 to 6.

The VCC chiller yearly simulated COP ranges from 3.95 in Lisbon to 4.6 in Stockholm (COP_{VCC}). Despite the large gap with the reference value (2.8), this is nevertheless consistent with the measured value for a small scale system (see chapter 4, section 4.2).

Primary energy use

The numerical results described in the following paragraphs are given in table 3.5.

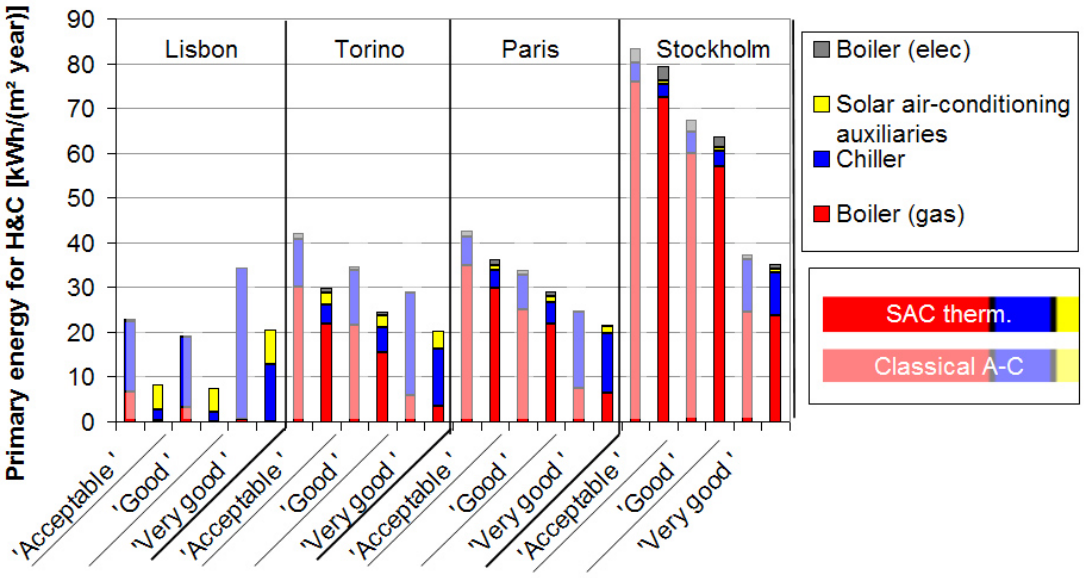

Figure 3.10: New office yearly primary energy use for heating and cooling (three building performance levels)

The yearly primary energy use for heating and cooling per building area is displayed in figure 3.10 for classical air-conditioning and thermally driven solar air-conditioning (*SAC therm.*). Solar air-conditioning auxiliaries stand for collectors, absorption chiller and cooling tower electricity consumption while the boiler consumption is separated into two parts: gas and electrical consumption.

"Good" and "very good" buildings significantly decrease the gas consumption while the "very good" ones particularly affect the primary energy used to produce cold water. Hot locations reach a higher energy decrease with solar air-conditioning due to the larger solar collector field.

In Lisbon, the primary energy use falls below 10 kWh/m^2 with *SAC therm* for two building levels. The "very good" building should be avoided, as it increases the primary energy use too much. Solar thermal collectors in Lisbon satisfy the entire heating load for "good" and "very good" cases. The gas

boiler is no longer required. In Lisbon, the solar air-conditioning auxiliaries consumption is around half of the primary energy use.

In Torino, where both heating and cooling loads are important, thermally driven air-conditioning shows a decrease of 10 kWh/m^2 whatever the case. The best building reaches 20 kWh/m^2 primary energy use. Paris location is characterized by a lower cooling load with a the decrease of around 5 kWh/m^2 due to thermally driven air-conditioning. As for Torino, the best case reaches around 20 kWh/m^2 primary energy use. In Stockholm, the decrease mentioned before is slightly lower ($\leq 5kWh/m^2$).

For the three most northern locations, the primary energy use is more impacted by the increase in building energy performance level than by the installation of thermally driven solar air-conditioning system. For Lisbon, the solar thermally driven air-conditioning is much more interesting from the primary energy point of view.

Fraction of energy savings

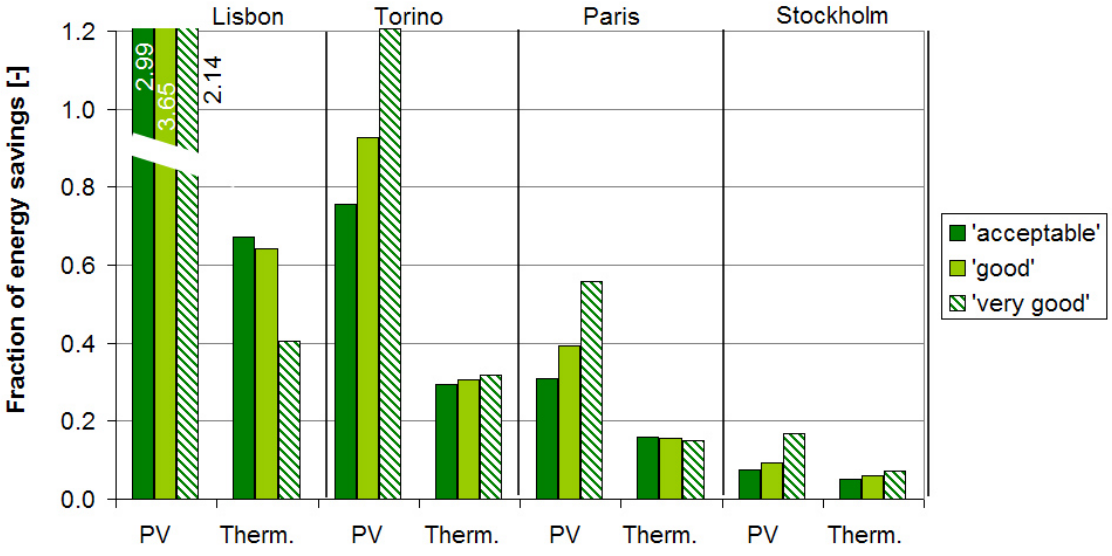

Figure 3.11: Fraction of energy savings for solar air-conditioning

The fraction of energy savings (f_{sav}) allows the comparison of solar air-conditioning systems with classical air-conditioning. It is displayed in figure 3.11 for all ACA cases. The savings higher than one entail cases where the PV field compensates for the entire heating and cooling primary energy use on a yearly basis. From a mathematical point of view, this leads to a a negative Primary Energy Ratio (PER). In table 3.5, the PER has no sense in the

cases where the fraction of energy is higher than 1 (there is no primary energy demand).

Stockholm "acceptable" and "good" cases put aside, the PV driven solar air-conditioning reaches a much higher fraction of energy savings than thermally driven system. The PV fraction of energy savings are higher for the highest building performance level (not the case for "very good" Lisbon). The fraction of energy savings is quite constant over the three building levels for the thermally driven system: around 5 % for Stockholm, 15 % for Paris, 30 % for Torino and more than 60% for Lisbon.

The given PV field size (table 3.2) enables 100% energy savings for well designed buildings in Lisbon and Torino. For Paris, a larger PV field (57% of the length of the building instead of 32%) would achieve the same result.

Solar fraction

As mentioned in chapter 1 (page 49), the solar fraction cooling ($SF_{cooling}$) is the ratio between the cold produced by the absorption chiller and the total cooling demand (displayed in figure 3.12). Lisbon location reaches a solar fraction of around 85% for the well designed building. The back-up system is still used for peak loads and days without high solar radiation. For Torino, a solar fraction of around 60% is reachable while Paris and Stockholm respectively reach 40% and 30%. Better insulated buildings generate higher cooling load and a lower solar fraction.

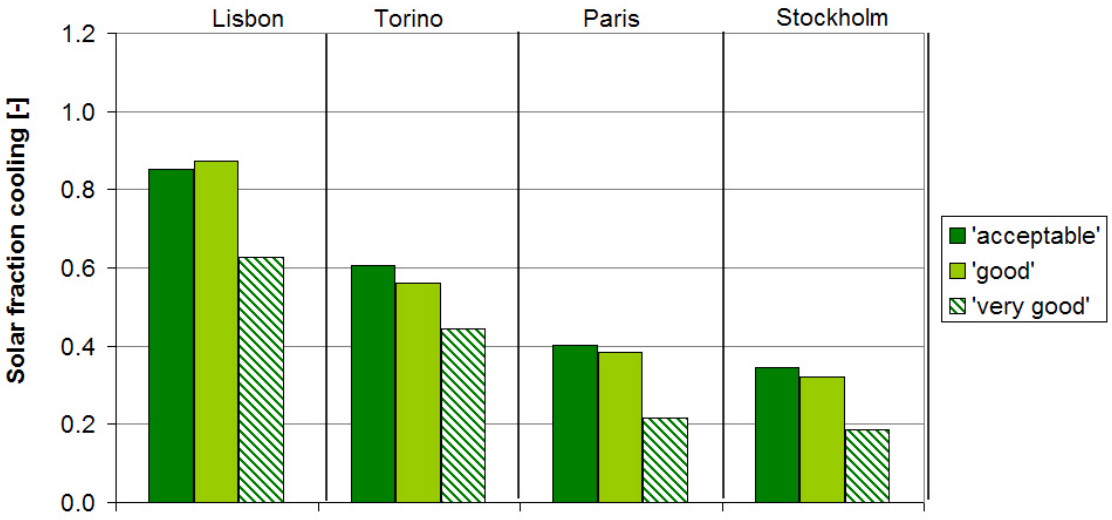

Figure 3.12: Solar fraction cooling for thermally driven solar air-conditioning

Primary energy savings per collector area

The primary energy savings per collector area detail the real primary energy benefits for each square meter collector (the absorption area is considered). The values for each case are listed in table 3.5. Firstly, the PV collectors generally have a better yield than the thermal. Sunnier locations reach higher savings because of the higher electricity production. Secondly, the thermal collector primary energy benefits increase proportionnally to the solar heat used to heat up the building (instead of driving the absorption chiller). This effect clearly occurs in Stockholm: the "acceptable" building has much more primary energy savings per collector area than the "very good" building, which has a lower heating demand and a larger cooling demand. Finally, the exclusive use of solar thermal collectors for cooling involves low energy savings per collector area despite the high solar irradiation. For Lisbon, the thermal collectors reach around three times less primary energy savings per collector area.

	'Acceptable'			**'Good'**			**'Very good'**		
	Cl AC	*SAC therm.*	*SAC PV*	*Cl AC*	*SAC therm.*	*SAC PV*	*Cl AC*	*SAC therm.*	*SAC PV*
Primary energy use for heating and cooling $E_{prim\,tot}[kWh/m^2]$									
Lisbon	24.3	8.2	-49.3	19.9	7.5	-53.7	34.3	20.6	-39.4
Torino	49.2	35.0	11.9	39.8	28.1	2.5	30.3	21.1	-6.9
Paris	46.5	39.5	31.9	36.5	31.4	22.0	25.6	22.2	11.0
Stockholm	91.9	87.4	85.0	73.9	70.0	67.1	40.0	37.7	33.2
Fraction of energy savings $f_{sav}[-]$									
Lisbon	0	0.67	2.99	0	0.64	3.65	0	0.41	2.14
Torino	0	0.29	0.76	0	0.31	0.93	0	0.32	1.21
Paris	0	0.16	0.31	0	0.16	0.39	0	0.15	0.56
Stockholm	0	0.05	0.07	0	0.06	0.09	0	0.07	0.17
Primary energy savings per collector absorption area $[kWh/m^2_{coll.}]$									
Lisbon	0	198	526	0	158	526	0	163	526
Torino	0	257	403	0	220	403	0	175	403
Paris	0	244	293	0	189	293	0	128	293
Stockholm	0	244	266	0	225	266	0	145	266
Primary Energy Ratio $PER[-]$									
Lisbon	1.36	4.02	-	1.49	3.96	-	1.70	2.85	-
Torino	0.95	1.34	3.88	1.04	1.48	14.21	1.48	2.13	-
Paris	0.90	1.06	1.29	0.97	1.14	1.58	1.44	1.66	3.19
Stockholm	0.81	0.86	0.88	0.84	0.88	0.92	1.09	1.15	1.29

Table 3.5: New office building results for ACA comfort model

3.1.11 Economical analysis

For the simulated building, the main significant economical indexes are presented: the economical payback period (simple and discounted), the net present value and the costs of primary energy savings. This analysis aims to compare both options of solar air-conditioning presented below over a 20 years period. This is generally the life time selected for such systems (Kohlenbach and Dennis, 2010), (Kalogirou, 2009).

Hypothesis

To perform the economical analysis, the energy cost must be firstly selected. Four locations over Europe have been simulated, the choice of energy price is not so easy to be consistent with each place. The energy prices in Europe (25 countries) for year 2011 have been recorded (EUROSTAT, 2011) for industrial customers, the three selected scenarios deal with mean and extreme values encountered. The highest energy prices recorded in Europe are named as **High** price energy scenario. The cheaper energy prices (**Low** scenario) and the mean values of the 25 countries (**Medium** energy scenario) are also handled in the analysis (the energy prices are listed in table 3.6) The energy price include all taxes, it is the price paid by the industrial customer.

Secondly some percentages addressing the money value and energy prices evolutions have to be set (they are also listed in table 3.6):

- The Harmonised Index of Consumer Prices (HICP) has been taken for Europe for year 2013.
- The interest rate is set to 3% (it corresponds to the current State notes rate in Belgium). The recent economical situation leads to a considerable decrease of the interest rate. Previous studies reached higher interest rates for Europe: 6% (Hartmann *et al.*, 2011) or 8% (Kalogirou, 2009).
- The Belgian mean price evolution for gas and electricity prices over 5 years is taken into account for this analysis.

Besides, the investment costs must be set to achieve the system comparison. The hypotheses are described in table 3.7 where all the prices are tax included and adapted to the system size. The design costs as well as maintenance costs are not included, they are considered similar for the two solar air-conditioning systems and do not modify the competitiveness of the systems. This last hypothesis is quite strong and favours a little bit the thermally driven system which requires much more devices. The replacement of PV inverter is nevertheless integrated in the analysis after 10 years. Moreover, there is no performance degradation considered on the system lifetime duration (20 years). Besides, the water consumption of the cooling tower (*SAC Therm* case) is not considered in the economical analysis. The simulation for Torino and Lisbon evaporate respectively 138 and 300 m^3 water per year, for the colder locations, it is much lower.

The value of 950 €/kW nominal cold power given in table 3.7 accounts for:

absorption chiller: 800 €/kW (Hartmann *et al.*, 2011) (for medium scale chillers $> 50\,kW_C$),

cooling tower: 50 €/kW (Hartmann *et al.*, 2011)

pumps: 100 €/kW (own guess).

The installed power and collector field size for investment cost computation has already been set in this section. For example, the considered cooling power for absorption cooling is 105 kW while the VCC cooling power relies to the table 2.8 on page 75 dealing with the maximum cooling load. The additional costs of solar air-conditioning are mentioned in table 3.7 and depending on the building case. The thermally driven Lisbon cases do not require any gas boiler, it is removed from the investment costs.

Finally, the analysis does not include any subsidies. It allows a fairly comparison between the energy saving measures. Subsidies can vary from countries to countries (even from city to city in the same country) and vary also over time. It would have been difficult to integrate them into the analysis.

Economical indexes computation

The net present value (NPV) presented in the analysis is computed as follows:

$$NPV = \left(\sum_{k=1}^{20} (1+i)^{-k} (R_k - C_k) \right) - I \ [€] \tag{3.13}$$

Where I means the extra investment of solar air-conditioning system. The annuity factor i is computed according to equation 3.14. The receipts (R_k) depend on the gas consumption decrease ($Gas_{red}\ [kWh/year]$) and the electricity consumption decrease ($Elec_{red}\ [kWh/year]$), they are defined in equation 3.15. The entire PV production counts for an electricity consumption decrease meaning it lowers the global building electricity bill (including lighting, appliances ...). The costs (C_k) are zero for every year except for SAC PV where C_{10} equals the PV inverter replacement amount.

$$i = \frac{\delta - \lambda}{1 + \lambda} \ [\%] \tag{3.14}$$

$$R_k = Gas_{red}\, €_{gas} (1 + i_{gas})^k + Elec_{red}\, €_{elec} (1 + i_{elec})^k \ [€] \tag{3.15}$$

The simple payback time does not include any prices variations nor inflation. It is defined in equation 3.16. where the value is rounded to the next integer. It is proposed to compare the different systems without any influence of the prices evolutions. The discounted payback time considers the annuity factor and energy prices increase; it occurs in the year when the Net Present Value

computed becomes positive.

$$Simple\,payback\,time = \frac{I}{R_1}\,[year] \tag{3.16}$$

The cost of primary energy savings ($CPES$) is defined as follows (the life time period is 20 years). It is another way to compare some energy savings measures. A negative value means a gain rather than a cost.

$$CPES = \frac{-NPV}{20 \cdot (E_{prim\,tot\,SAC} - E_{prim\,tot\,ClAC})}\,[€/kWh] \tag{3.17}$$

Energy price scenario	Symbol	**High**	**Medium**	**Low**	**Source**
Gas [€/kWh]	$€_{gas}$	0.062	0.038	0.021	EUROSTAT (2011)
Electricity [€/kWh]	$€_{elec}$	0.211	0.112	0.067	EUROSTAT (2011)
Yearly parameters			**Value**		
Inflation HICP	λ		1.84 %		Global-rates (2013)
Interest rate	δ		3 %		Own guess
Deduced annuity factor	i		1.1 %		
Gas price increase	i_{gas}		6.3 %		APERE (2012)
Electricity price increase	i_{elec}		4.5 %		APERE (2012)

Table 3.6: New office economical analysis parameters

Results

The economical analysis results are presented in table 3.8 and in figure 3.13 for discounted payback period.

First of all, the analysis is based on the extra investment costs of the two solar air-conditioning systems. The extra investment costs are detailed on the bottom right of table 3.7 while the complete air-conditioning system costs are presented in the "Amount" column. The installation of PV system is cheaper whatever the case. This further disadvantages the thermally driven system that had already reached a lower energy performance (see previously in this chapter).

The simple payback period does not take any energy price increase into account. The PV system reaches 12-24 years payback time while the thermal system has enormous values. The discounted payback period showed in figure 3.13 is a more realistic index and promotes the implementation of energy savings measures. Depending on low and medium energy price, the PV system becomes profitable within 20 years for each location. The payback time is very sensitive to the energy price, this is one of the most important parameters to fix when assessing a new project. The discounted payback time computation lead to values between 2 and 4 times higher for the thermal system than for

Investment by field	**Amount**	**Unit**	**Source**
Absorption chiller, wet cooling tower and hydraulics	950	€/kW$_C$	Hartmann *et al.* (2011) and own guess
Thermal installation	280	€/m^3	Hartmann *et al.* (2011)
PV collectors	2000	€/kW$_p$	Belgian PV installer
Inverter substitution	300	€/kW$_p$	Belgian PV installer
VCC	310	€/kW$_C$	Hartmann *et al.* (2011)
Gas boiler	100	€/kW$_{therm}$	Belgian heater installer
Hot water tank	1000	€/m^3	Belgian heater installer
Total investment	**Amount [€]**	**Extra costs (I) compared to Classical A-C [€]**	
Lisbon			
Classical A-C	73 900	0	
SAC therm	284 518	210 618	
SAC PV	248 064	174 164	
Torino			
Classical A-C	67 700	0	
SAC therm	250 642	182 942	
SAC PV	182 830	115 130	
Paris			
Classical A-C	61 500	0	
SAC therm	206 746	145 246	
SAC PV	123 502	62 002	
Stockholm			
Classical A-C	49 100	0	
SAC therm	178 794	129 694	
SAC PV	81 090	31 990	

Table 3.7: New office solar air-conditioning investment costs

PV. For a given case the payback time of a thermally driven system is never lower than a PV system. The most profitable case in thermally driven system has nearly the same payback period as the worst PV case.

The Net Present Value gives the present value of net cash inflows (over 20 years) generated by the investment. This is clearly linked to the discounted payback period. The investments having a discounted payback period shorter than 20 years have also a positive Net Present Value. For high energy price scenario, the PV system gets 2 and 3 times the investment for Torino and Lisbon respectively. For those two locations the installation of a PV system does not require any subsidies to be highly profitable.

The calculation of the cost of primary energy savings also enables the comparison between two energy saving measures. For a thermal system, the cost stands around 10 c€ per kWh primary energy savings for best cases. A higher price is encountered for less profitable systems up to 60 c€ per kWh. For PV systems, the primary energy savings generate generally a gain due to high primary energy savings and lower investment.

Finally, it is reasonable to treat the case where the costs of thermally driven system is decreased. The target price of thermally driven system is 400 € per kW_C (Hartmann *et al.*, 2011). In this case the analysis gives a discounted payback period of 33 years for medium energy price scenario (Lisbon 'acceptable' building). It is still three times longer than the PV case.

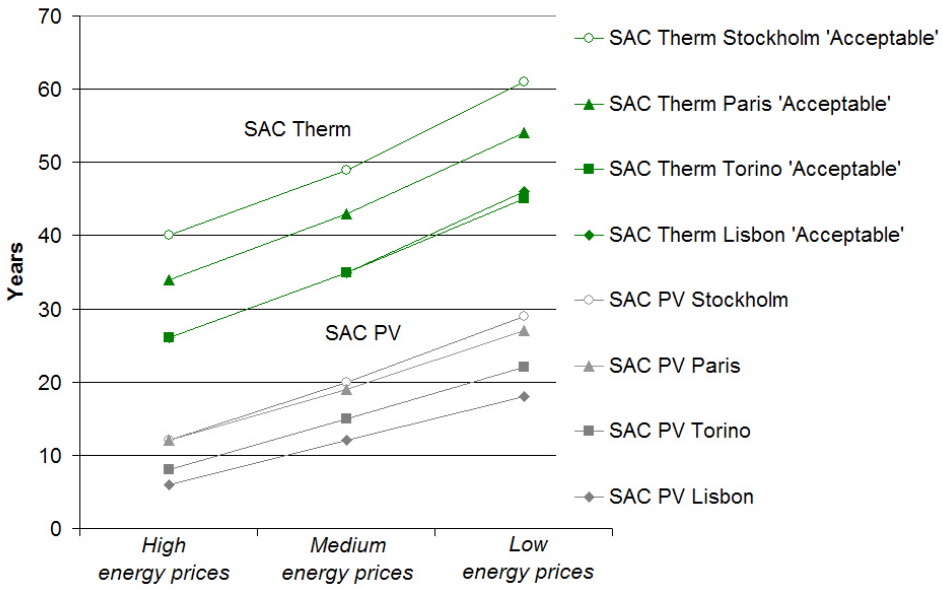

Figure 3.13: New office solar air-conditioning discounted payback time

	'Acceptable'			**'Good'**			**'Very good'**			*PV*		
	SAC therm			*SAC therm*			*SAC therm*			*SAC PV*		
Energy price	*High*	***Med.***	*Low*	*High*	***Med.***	*Low*	*High*	***Med.***	*Low*	*High*	***Med.***	*Low*
Payback period												
[*year*]												
Lisbon		**75**			**94**			**79**			**12**	
Torino		**80**			**94**			**110**			**16**	
Paris		**129**			**170**			**244**			**22**	
Stockholm		**182**			**208**			**326**			**24**	
Discounted payback period												
[*year*]												
Lisbon	26	**35**	46	30	**41**	52	27	**40**	49	6	**12**	18
Torino	26	**35**	45	29	**38**	49	33	**44**	56	8	**15**	22
Paris	34	**43**	54	39	**49**	61	48	**60**	73	12	**19**	27
Stockholm	40	**49**	61	42	**52**	64	54	**66**	78	12	**20**	29
Net present value (20 years operation)												
[k€]												
Lisbon	-62	**-127**	-162	-92	**-145**	-172	-72	**-137**	-149	554	**202**	41
Torino	-60	**-111**	-142	-79	**-123**	-149	-95	**-134**	-155	250	**71**	-10
Paris	-85	**-110**	-125	-100	**-119**	-130	-114	**-128**	-135	79	**9**	-23
Stockholm	-91	**-107**	-117	-96	**-110**	-119	-109	**-118**	-123	34	**1**	-14
Cost of primary energy savings (20 years operation)												
[c€/kWh]												
Lisbon	4.4	**9.0**	11.5	8.5	**13.3**	15.8	5.9	**11.3**	14.5	-8.5	**-3.1**	-0.6
Torino	4.9	**9.0**	11.5	7.7	**12.0**	14.5	11.8	**16.6**	19.1	-7.6	**-2.2**	0.3
Paris	13.8	**17.8**	20.4	21.9	**26.1**	28.7	38.8	**43.5**	46.0	-6.1	**-0.7**	1.8
Stockholm	23.3	**27.2**	29.7	28.5	**32.5**	35.0	54.4	**59.0**	61.5	-5.6	**-0.1**	2.3

Table 3.8: New office solar air-conditioning economical profitability

3.2 Typical existing European office building

This section summarizes the published article *Numerical simulation and performance assessment of an absorption solar air-conditioning system coupled with an office building* (Thomas and André, 2012). The main energy indexes are represented as for detached house and new office building.

3.2.1 Introduction

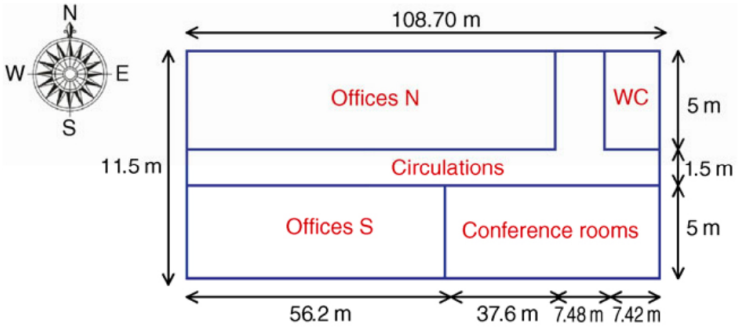

Figure 3.14: Office building floor geometry (Stabat *et al.*, 2011)

The building modelling is described in section 2.5 of chapter 2 while the main building characteristics are listed in appendix. The simulation considers one building floor (figure 3.14 representing 1250 m^2 area) while around 150 m^2 solar collectors (absorber area) are available due to the roof area. The thermal collector field design copes with the minimal requirements of 350 kWh of solar thermal energy production per net collector area per year. A three floor building is taken into account to share the roof area between the floors. The office building is simulated in Paris location only.

In comparison with the other buildings studied, the analysis deals here with heat and cold distribution and emission devices (pumps, fans, fan coil units). This involves higher loads than the loads computed in chapter 2 for the same building. A 10 and 13% increase have been reached respectively for heating and cooling loads due to the implementation of distribution and emissions losses. These percentages should be put in perspective with the additional thermal energy brought in the building by the fans and pumps driving the thermal flows in the building (see electrical consumptions below).

The heat and cold production scheme is similar to the new office building (figure 3.2). The hypotheses are almost identical to those presented in section 3.1 for the new office building. Two differences can be noticed:

- The gas primary energy factor (ϵ_{fossil}) defined in equation 1.15 is 1 instead of 0.9.

- The boiler electricity consumption is not considered.

The results presented in this section are then consistent with the results already published. Besides, these two differences do not alter considerably the results.

3.2.2 Distribution and emission modelling

The modelling of those two parts of the heating and cooling systems are briefly explained. All the details about distribution and emission modelling are found in the published paper (Thomas and André, 2012).

On the one hand, two pipe networks enable the distribution of hot and cold water in the building. They involves pumps and pipe losses that are partially recovered by the building. On the other hand, fan coil units satisfy the heating and cooling loads. The simulation addresses fan power consumption and variable water flow in the coil to control the room temperature. The scheme of distribution and emission devices used to heat and cool the three zones are represented in figure 3.15. The TRNSYS type used are mentioned, the heating and cooling coils are polynomial approximations of the manufacturer curves. The heat and cold distribution implementation involves significant modifications in the simulation: thermal losses (pipes), control losses (the controller is not able to reach exactly the set points), electrical consumption (see below). Otherwise, the hygienic ventilation is also implemented without any heat recovery.

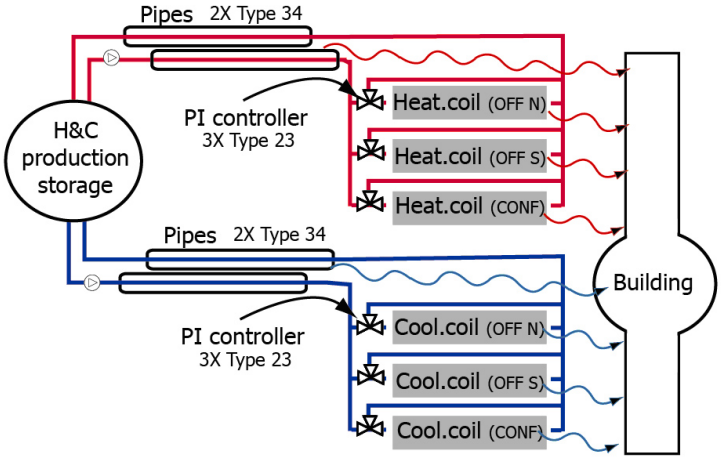

Figure 3.15: Distribution and emission implementation (Thomas and André, 2012)

3.2.3 Other electrical consumptions

The yearly electricity consumption of the devices is mentioned in table 3.9. The appliances and light consumption is substantially higher than for new office

building simulation. A wide range (30-300 kWh/m^2) of electricity consumption was measured in real existing office buildings in Luxembourg (Thewes, 2011) while the mean value for German office buildings built before 21^{st} century is 30 kWh/m^2 (Sajonz *et al.*, 2001). So, the studied existing office building does not claim to gather all office buildings. The yearly electricity consumption of the simulated building reaches around 62.4 kWh/m^2 (meaning 156 kWh/m^2 primary energy), it could be compared to the results about primary energy in the next paragraphs.

The electricity consumption dedicated to the heat and cold distribution and emission is pointed out. It reaches a significant value (around 13 kWh/m^2 for pumps and fan coils altogether). The cold pump consumption has particularly high value because of its permanent operation during occupancy. Otherwise, the heat losses of the electrical devices influence the heating and cooling loads.

Consumption field	kWh/m^2
Appliances	25.6
Light	20.4
Ventilation	3.7
Heat distribution pump	1.1
Cold distribution pump	3.6
Fan coil units	8.1
Total	62.4

Table 3.9: Yearly net electricity consumptions of auxiliaries in the typical existing office

3.2.4 Simulation Results

This building analysis handles *Classical A-C* and *SAC therm* simulations. There is no PV field evaluation in this section. The two set points introduced in chapter 2 section 2.5 are simulated, the key indexes computed are presented in table 3.10.

The primary energy use is higher than for the new office building. These results were foreseen in chapter 2, where considerably higher heating and cooling loads had been computed. The energy sharing between the different consumptions is presented in figure 3.16. The implementation of solar air-conditioning implies 25% of primary energy savings whatever the cooling set point. For the classical air-conditioning case, the cooling set point increased by 2°C leads to a 9% global reduction of primary energy use. This building could attain a 60 kWh/m^2 primary energy use for heating and cooling. This is considerably higher than the new office building which could meet 40 kWh/m^2.

The solar system also impacts the energy use for heating. On the whole year, the solar heat recovered by the collectors is split almost equally between the heating load (40%) and cooling load (60%) satisfaction. Previous work

about the same building (Thomas and André, 2009) emphasized that half of the energy savings were achieved in case of solar heating system only (without absorption chiller).

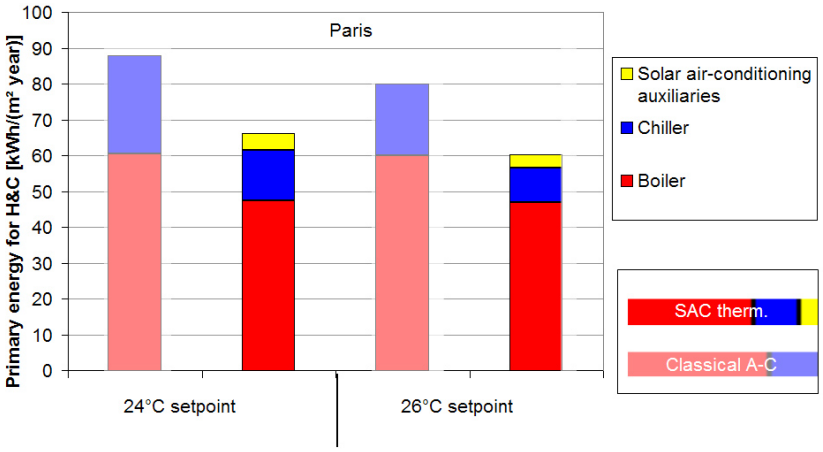

Figure 3.16: Yearly primary energy use for heating and cooling

The solar fraction for cooling is 0.41-0.43 (0.4 for new office acceptable). With nearly the same collector area, the same solar fraction cooling ($SF_{cooling}$) and a higher cooling load, the typical office building has a higher fraction of solar heat used for cooling than the new office. It implies lower primary energy savings per collector absorption area.

The criterion concerning the solar energy quantity recovered by the collector is respected (350 kWh/m^2). Besides, if this office building was occupied during the weekend the collector energy would reach 400 kWh per square meter collector (for 24°C set point). A seven-day operation would increase the solar energy use by 15%.

The simulated performance of the absorption chiller ($COP_{therm} = 0.67$-0.7) is close to the rated point. The system electrical COP has the same order of magnitude as in the new office ($COP_{elec\,tot} =$ 18-19 for both heating and cooling; 9-10 for cooling only). The difference between the two buildings lies more in the building loads than in the system implementation.

	'21-24°C set points'		**'21-26°C set points'**	
	Cl AC	*SAC therm.*	*Cl AC*	*SAC therm.*
Primary energy use for heating and cooling $E_{prim\,tot}[kWh/m^2]$				
Paris	87.9	66.1	80.1	60.4
Fraction of energy savings $f_{sav}[-]$				
Paris	0	0.25	0	0.25
Primary energy savings per collector absorption area $[kWh/m^2_{coll.}]$				
Paris	0	192	0	173
Primary Energy Ratio $PER[-]$				
Paris	1.06	1.44	1.02	1.40

Table 3.10: Typical office building yearly results

3.3 Detached house

3.3.1 Introduction

The building modelling is described in section 2.6 of chapter 2 while the main building characteristics are listed in appendix. The simulation considers the house displayed in figure 3.17 considering around 143 m^2 on the ground floor and 73 m^2 on the first floor. It is proposed to study both the adsorption cooling system and the PV connected vapour compression system. This kind of building is generally cooled with room air conditioners. The adsorption is chosen because of its low cooling power. The relatively high cold temperature reached by those chillers is more suited to the use of surface cooling emission devices handling the sensible load only.

The cooling load analysis carried out in chapter 2 for this building leads to remove any cooling system for Stockholm and Paris locations. This section only deals with Torino and Lisbon locations.

The general scheme for the system simulation is displayed in figures 3.18 and 3.19 respectively for thermally driven and PV driven cooling. The simulations undertaken in this section concern the systems displayed and the loads computed in chapter 2. The different parts of the schemes are detailed in the following paragraphs.

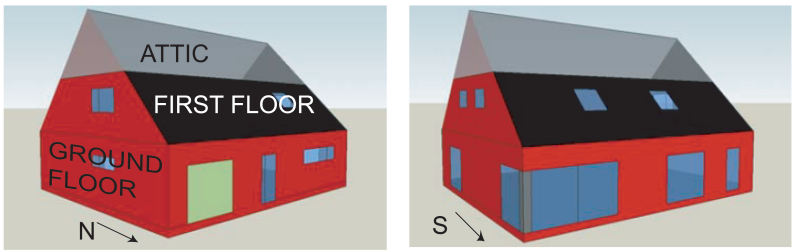

Figure 3.17: Detached house geometry (EPICOOL, 2009)

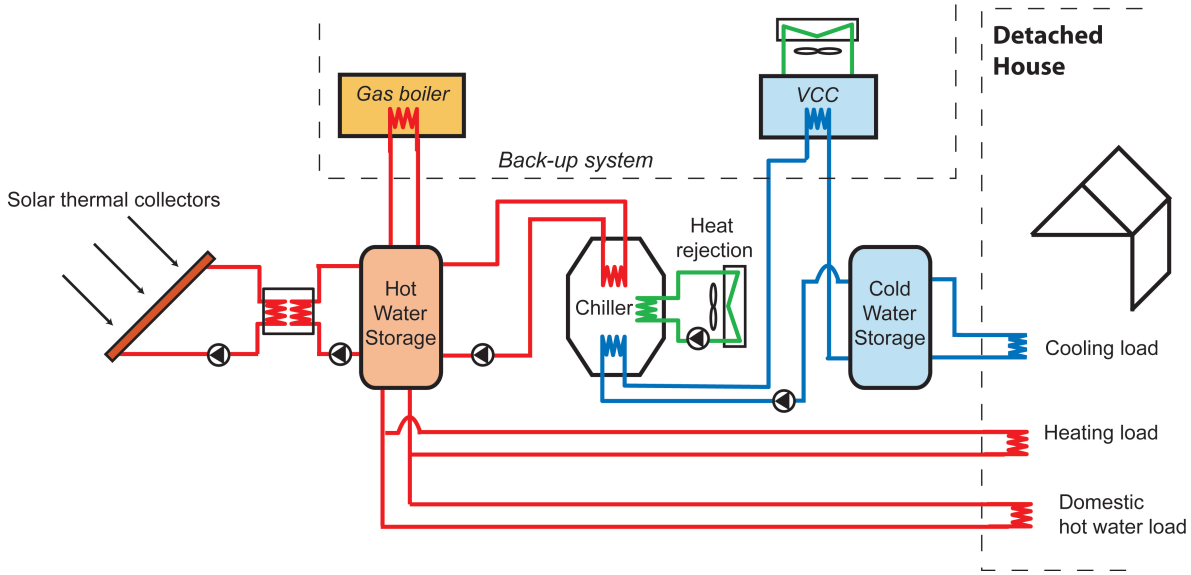

Figure 3.18: Detached house thermally driven solar air-conditioning scheme

3.3.2 Thermal collector field

Flat-plate collectors are used as they reach lower temperature but are a little bit less expensive. This kind of collector is suited to a residential building with adsorption technology requiring lower hot water temperature. TRNSYS Type 1 has been chosen to implement the manufacturer's data including the collector efficiency (see table 3.11), incidence angle modifier and mass flow variation. The general thermal collector efficiency is given in equation 3.18.

$$\eta_{thermal\ collector} = k(\theta)a_0 - a_1\frac{(T_{coll} - T_{amb})}{I_{tot}} - a_2\frac{(T_{coll} - T_{amb})^2}{I_{tot}} \qquad (3.18)$$

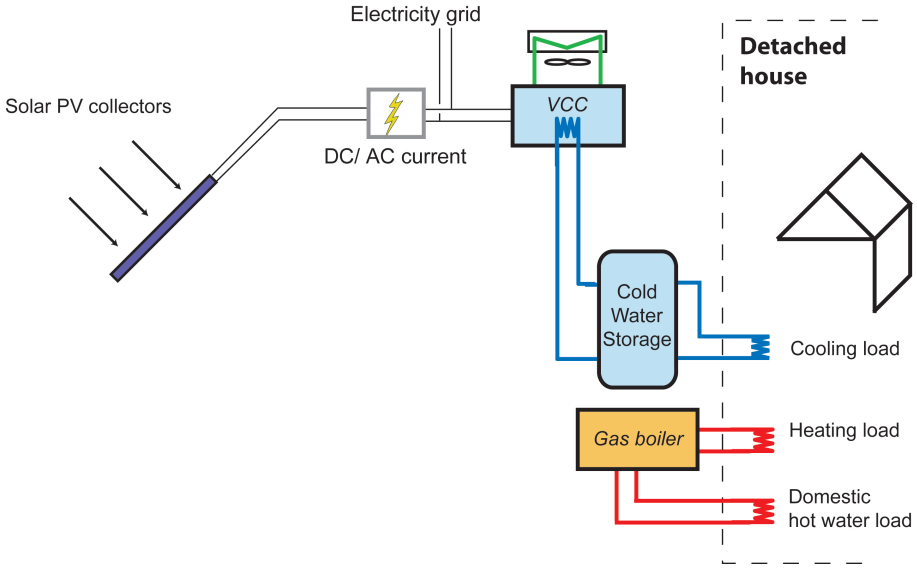

Figure 3.19: Detached house PV driven solar air-conditioning scheme

Collector type	a_0 $[-]$	a_1 $[W/(m^2K)]$	a_2 $[W/(m^2K^2)]$
ESE2.32	0.773	1.09	0.0094

Table 3.11: Flat-plate collector efficiency numerical values (DINCERTO, 2008a)

The design criteria of the collector field are the same as for the new office building (section 3.1). The collector field is restricted to the south oriented roof (45° slope) leading to an area of around 100 m^2. To reach 350 kWh per collector area per year, both locations need 8 collectors, which corresponds to a total absorber area of 18.56 m^2. The roof surface is absolutely not a restrictive criterion for this detached house. The main parameters of the collector field are presented in table 3.12.

As for the office building, the solar loop is connected to the storage tank via a heat exchanger with 95% constant effectiveness. The collectors mass flow has also been set to 30 kg/h per collector area.

In comparison with the evacuated tube collectors detailed in the previous section, the ratio between gross and net thermal collector area is quite high for the flat-plate collectors: 94% instead of 63%. For a given roof surface, the absorption area could be 30% larger for flat-plate collectors than for evacuated

tube (at least for the selected collectors).

	Unit	**Lisbon**	**Torino**
Thermal field			
Number of collectors	-	8	8
Net collector area	m^2	18.56	18.56
Minimal specific thermal prod.	$kWh/m^2_{absorber}$	350	350
Minimal specific thermal prod.	$kWh/m^2_{building}$	29.9	29.9
PV field			
Number of collectors		20	20
Net collector area	m^2	17.41	17.41
Specific elec.	kWh/m^2_{cells}	160.5	131.4
Specific elec.	$kWh/m^2_{building}$	15.0	12.3
Specific elec.	kWh/kW_p	1305	1060
Gross electricity prod.	kWh	3210	2628
Common data			
South roof use	%	20	20

Table 3.12: Detached house collector fields characteristics

3.3.3 PV collector field

The same collectors are modelled as in the new office building (keeping same hypothesis). The available roof size for PV collectors is equivalent to the one reserved to thermal collectors. It leads to 20 PV collectors on south roof for both locations. The electricity production of this 2.46 kW_{peak} field is summarized in table 3.12.

3.3.4 Adsorption chiller modelling

It is modelled in the same way as it was done for the absorption chiller in previous section. Type 255 is also reading manufacturer's data to compute the thermal COP and cooling capacity of the chiller at current conditions.

One house cooling load is not suited to the lowest capacity adsorption chiller. Among the adsorption chiller manufacturers it has been decided to consider half of the cooling power of INVENSOR LTC 09 chiller. It involves cooling power up to 5.23 kW (this fits one house needs). This chiller is the subject of chapter 4 dealing with solar cooling experimental studies. Its performance map is displayed in figure 4.16 on page 167. The main characteristics for the modelling are displayed on table 3.13, where the cooling power of the

real chiller is already divided by two.

	Manufacturer's rated conditions	**Model rated conditions**
$COP_{thermal}$	0.610	0.633
$\dot{Q}_{C\,rated}$	4.5 kW	5.23 kW
Temperature range		
$T_{H\,in}$	55-100 °C	
$T_{M\,in}$	22-37 °C	
$T_{C\,out}$	8-15 °C	

Table 3.13: Adsorption chiller thermal specifications

3.3.5 Other devices

Heat storage

The hot water storage tank (type 534) showed in figure 3.18 is connected in a different way from the new office building. There is still no heat exchanger in the tank. The system has to deal with domestic hot water but should remain as simple as possible to be suitable for a residential application.

The selected solution gathers all the heat consumption fields in the hot storage tank. It has now two energy sources (solar collectors and gas boiler) and three possible uses: adsorption chiller operation, building heating, domestic hot water. The system control described below tries to eliminate any energy waste due to multiple heat sources and uses.

A 0.2 m thick rock wool insulation has been modelled. The storage volume is 2 m^3 for each location, which corresponds to 100 litres per square meter solar absorber area. It is quite high compared with the previous section (55 l/m^2). Two reasons promote this decision of hot storage over sizing:

- The storage tank is now used for domestic hot water, heating and cooling, which raises the need for heat storage.
- At least 20% of the cooling load occurs during the night, which also raises the need for energy storage.

Cold storage

This new device is installed in order to avoid transient cold water temperatures caused by the intermittent adsorption chiller operation. Moreover, it allows an additional energy storage to cool the building during the night. A thinner insulation (5 cm rock wool) is required because of the lower temperature difference between the cold water and the ambient temperature. The cold water storage volume is 0.5 m^3 which does not impact greatly the system performance.

Cooling tower

The adsorption chiller requires a rejection circuit to evacuate the medium temperature energy flow. The model used is type 511 representing a closed circuit dry cooling tower. This kind of rejection device is generally installed in a small scale solar cooling system because of the costs and reasonable maintenance. Indeed, the dry cooling tower has no water treatment for health (legionella) nor cleansing reasons.

The dry cooling tower design point has been found for the device installed in the laboratory (figure 4.4 page 148) with a nominal rejection thermal power of 24 kW. The design point is based on the measurement made in chapter 4 (see page 183). The control of outlet water temperature is done by modifying the cooling tower fan speed. The internal control of type 511 tries to reach 27°C as outlet temperature. As it is a dry cooler, it will not achieve this set point when the outside temperature is above 27°C. In this case, the adsorption chiller operates at a lower thermal COP.

Vapour compression chiller

The same vapour compression chiller is used as in the previous section. It is however virtually downscaled to a nominal cooling power fitting with the building: 6 kW_C.

Gas boiler

The same gas boiler is used as in the previous section. It is also virtually downscaled to a nominal heating power fitting with the building heat demand and domestic hot water production: 10 kW.

3.3.6 Electricity consumption

The hypotheses are kept from section 3.1:

- 0.02 kWh electricity per kWh thermal energy collected for the solar system,
- 0.03 kWh electricity per kWh thermal energy rejected for the cooling tower,
- 0.01 kWh electricity per kWh cold energy produced for the adsorption chiller,
- 0.02 kWh electricity per kWh heat energy produced for the gas boiler,

3.3.7 Heating and cooling loads management

The heating and cooling loads are handled almost as they were in the new office section. However, the domestic hot water energy use profile (figure 2.15 on page 83) is purely added to the building heating load. The equation 3.9 is slightly

modified (where $\dot{Q}_{DHW}$ represent the current load required by domestic hot water):

$$T_{bui\ heat\ out} = T_{bui\ heat\ in} - \frac{\dot{Q}_{bui\ heat} + \dot{Q}_{DHW}}{\dot{m}_{bui\ heat} \cdot c_{p\ water}} \tag{3.19}$$

This quite straightforward domestic hot water load handling does not take any supplementary losses of the domestic hot water network into account.

3.3.8 System control

For the PV or classical air-conditioning systems, the heating and cooling loads are respectively satisfied by the gas boiler and vapour compression chiller. These cases do not require any particular control but the management of the cold storage. For the thermally driven solar air-conditioning, the control additionally affects three parts of the system.

Solar collectors

The solar collectors are operated when the collector temperature is 5°C higher than the bottom tank temperature. A hysteresis controller is implemented, the collectors stop collecting solar energy if the difference drops below 2°C. Finally, the maximum operating outlet collector temperature is set to 100°C. In this way, the system doesn't have to be pressurized (simpler and cheaper for residential application).

Heating

The same heating curve is kept for the detached house simulation (figure 3.7). The gas boiler heats up the water storage to attain the heating curve value on its top. In addition, the top temperature never falls below 50°C. A 5°C gap is maintained to make sure the tap hot water remains at 45°C.

Compared to the previous section, this strategy involves higher storage losses because it is heated permanently.

Cooling

The cooling devices (adsorption chiller and vapour compression chiller) can only be operated if there is a cooling load. As seen in figure 3.18, the two cold production devices are connected in series to the cold storage tank. Firstly, if available, the adsorption chiller cools down the cold water to 15°C. If this temperature is not reached, the cold water flow is cooled down to 15°C by the VCC. For PV driven and classical air-conditioning cases, the VCC is the only device cooling down the water to 15°C.

Previous work about this kind of adsorption cooling (Dubois, 2011) and investigations on the experimental setup in the laboratory gave advice about the chiller control strategy. So, the adsorption chiller starts if the hot water

tank top temperature reaches 65°C and stops if it drops below 62°C. This is a compromise between the amount of cold produced and the system global performance.

Besides, this strategy avoids the use of a gas boiler for driving the adsorption chiller. The cooling loads occur when the outside temperature is high, thus at low heating curve temperature (below 50°C). The adsorption chiller stops at 62°C storage temperature, there is at least a 12°C gap. The gas boiler will therefore not start to heat the tank.

3.3.9 Simulation results

The yearly simulation of the systems described below is carried out. It computes the key energy performance indicators for the different systems mentioned in the introduction:

- Thermally driven solar air-conditioning named *SAC therm*
- Classical air-conditioning named *Classical A-C*
- PV driven solar air-conditioning named *SAC PV*

In the next pages, the term heating load includes the building heating and domestic hot water loads.

Comfort model influence

As for the new office, the comfort model can influence the possible energy savings of the thermally driven system. The impact is especially encountered for Lisbon case. For example, Lisbon 'good' case encounters 17% higher fraction of energy savings with ACA model than with PMV model. Herealso, the implementation of the adaptive set point wins on both ways: building load and better solar system operation. For other cases, the comfort model does not impact much the fraction of energy savings. The analysis now deals with the ACA model only.

The PV driven system is not mentioned in this paragraph as the collector field operation is independent of the comfort model.

Cold production system performance

Globally, the same hypotheses are kept as for the new office building. The simulated mean thermal COP is 0.5 whatever the case. This is sligthly lower than the nominal value ($COP_{rated} = 0.61$), mainly for the following reason: the use of a dry cooling tower instead of a wet cooling tower increases the chiller rejection temperature and thus decreases the performance. Also in this case, the target given by Nowag *et al.* (2012) (mean thermal COP $\geq 0.8 \cdot COP_{rated}$) is a reachable goal for this thermally driven cooling system.

The electrical COP ($COP_{elec\,tot}$) ranges from 21 to 33. High values are encountered for cases where solar heat is mainly used for heating. By focusing on cooling only, the order of magnitude of the electrical COP is 10.

The VCC chiller yearly simulated COP ranges from 4.1 to 4.4 (COP_{VCC}). In comparison with the new office building simulation, the VCC chiller has a slightly higher COP because of the higher cold water temperature to reach (15°C instead of 7°C).

Primary energy use

The numerical results described in the following paragraphs are gathered in table 3.14.

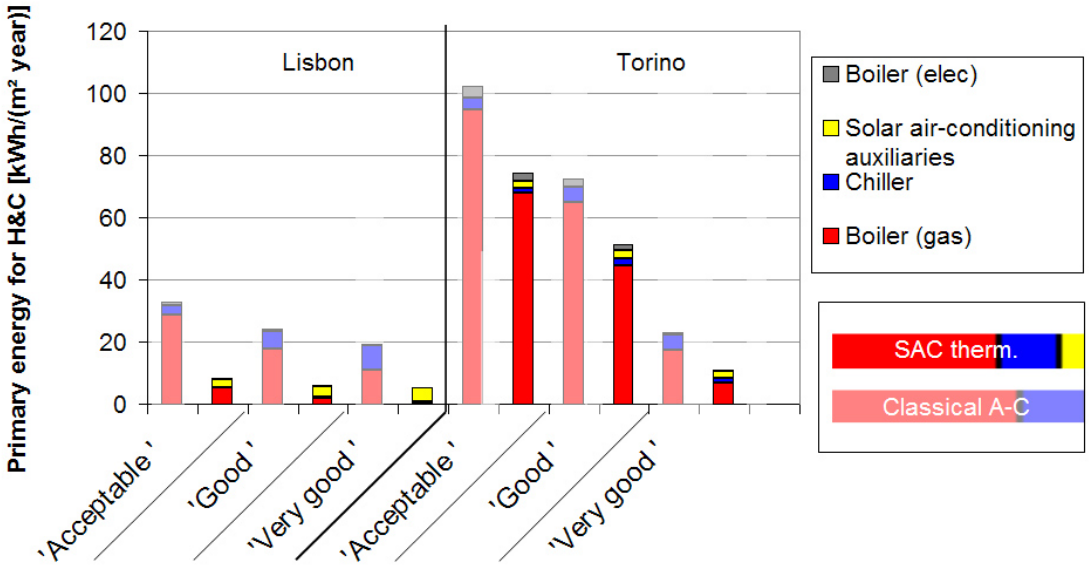

Figure 3.20: Yearly primary energy use for heating and cooling (three building performance levels)

The yearly primary energy use for heating and cooling per building area is displayed in figure 3.20 for classical air-conditioning and thermally driven solar air-conditioning (SAC therm.). Solar air-conditioning auxiliaries stand for collectors, adsorption chiller and cooling tower electricity consumption while the boiler consumption is separated into two parts: gas and electrical consumption.

In Lisbon, the primary energy use falls below 6 kWh/m^2 with *SAC therm* for two best building levels. The "very good" building increases the cooling load but the classical air-conditioning primary energy use remains lower than for the two other levels. In the three Lisbon levels the residual VCC consumption is so low that it could reasonably be avoided in the system implementation.

Moreover, the "very good" case does not require any significant back-up heat or cold sources. The energy use mainly comes from the solar air-conditioning auxiliaries apart 0.17 and 0.48 kWh/m^2 respectively for gas and VCC electricity consumption. These low values promote the back-up systems removal.

In Torino "acceptable" and "good" levels, where heating is important, thermally driven air-conditioning shows a saving of at least 22 kWh/m^2. The best building level reaches 10 kWh/m^2 primary energy use. Depending on the occupants' comfort requirements, the vapour compression chiller could be removed.

Fraction of energy savings

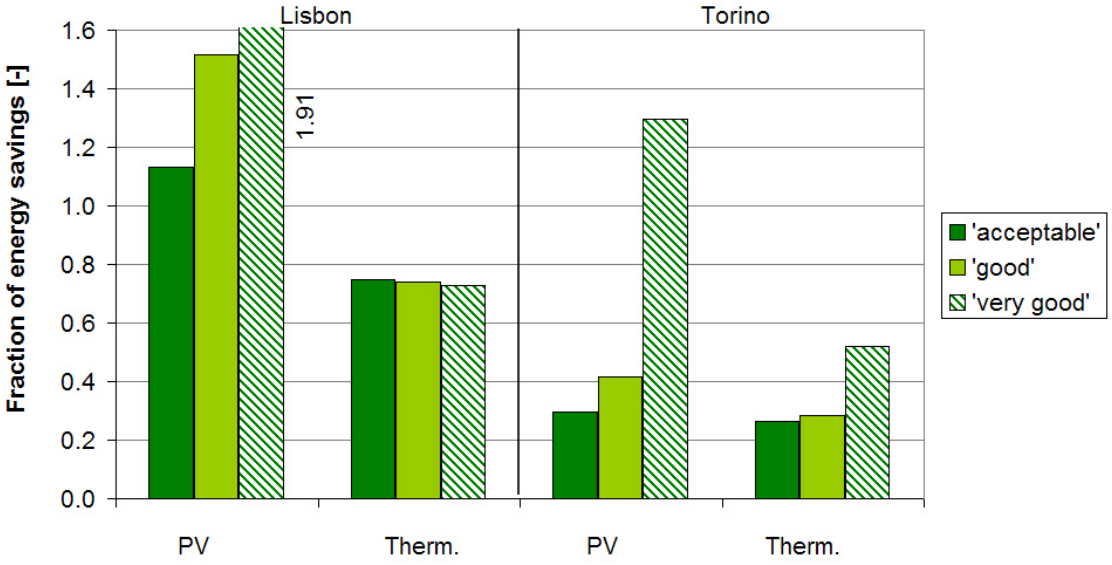

Figure 3.21: Fraction of energy savings for solar air-conditioning

The fraction of energy savings (f_{sav}) allows the comparison of both solar air-conditioning systems with classical air-conditioning. It is displayed in figure 3.21 for all the detached house ACA cases. The savings higher than one entail cases where the PV field compensates for the heating and cooling primary energy use on a yearly basis.

The thermally driven air-conditioning system reaches around 75% energy savings for Lisbon cases while it ranges from 25 to 50 % for Torino. These figures are a little higher than for the office building because of a general higher ratio between heating and total (heating and cooling) load. Moreover, the use of a larger storage improves this index.

The energy savings for PV system exceed 100% for the 4 cases. The difference between the PV system and thermally driven system is really significant,

except for Torino "acceptable" and "good" levels, which reach lower PV system energy savings. In these two cases, the solar thermal energy is much more used for heating or domestic hot water than for cooling.
Whatever the case, the PV system reaches higher savings.

Solar fraction

Lisbon location reaches a solar fraction of around 90% whatever the building (figure 3.22). This fact exhorts the potential removing of back-up cooling system as mentioned before. The back-up system is still used for peak loads, days without high solar radiation and late night cooling loads. For Torino, a solar fraction of around 60% is reachable. For the detached house, the building level does not affect greatly the solar fraction.

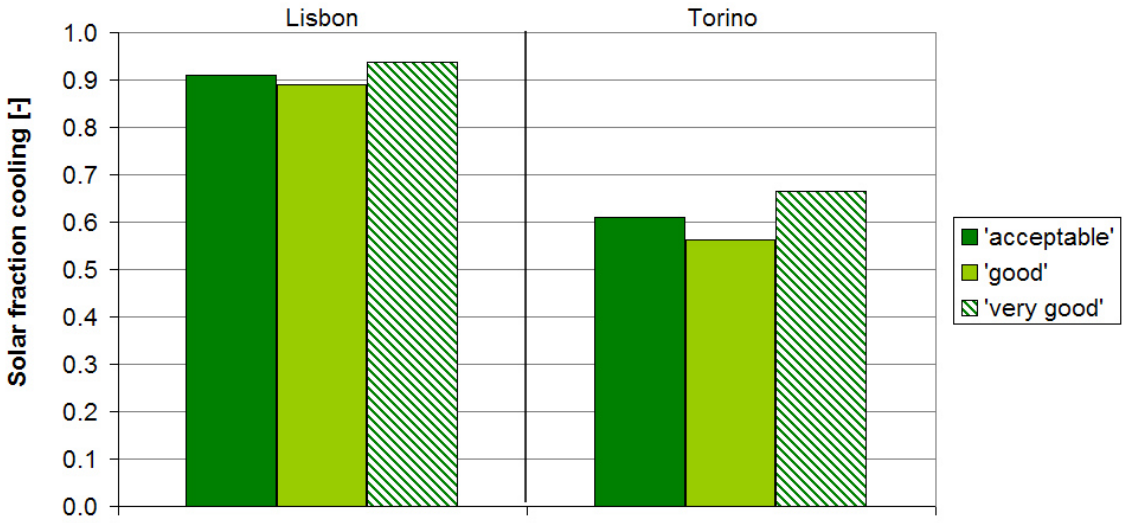

Figure 3.22: Solar fraction cooling for thermally driven solar air-conditioning

Primary energy savings per collector area

The primary energy savings per collector area represent the real primary energy benefits for each square meter collector (the absorption area is considered). The values are showed in table 3.14 for each case. Firstly, the PV collectors generally have a better efficiency than the thermal (between 1.75 and 3.16 times more energy savings per collector area for PV). The building level impacts the thermal collectors efficiency. The use of solar heat for heating load satisfaction is much more interesting than for cooling load.

	'Acceptable'			'Good'			'Very good'		
	Cl AC	*SAC therm.*	*SAC PV*	*Cl AC*	*SAC therm.*	*SAC PV*	*Cl AC*	*SAC therm.*	*SAC PV*
Primary energy use for heating and cooling $E_{prim\ tot}[kWh/m^2]$									
Lisbon	33.0	8.2	-4.0	24.2	5.9	-12.8	19.3	5.1	-17.7
Torino	103.2	75.1	72.9	73.2	51.6	42.9	23.1	10.9	-7.1
Fraction of energy savings $f_{sav}[-]$									
Lisbon	0	0.75	1.13	0	0.74	1.52	0	0.73	1.91
Torino	0	0.26	0.30	0	0.28	0.42	0	0.52	1.30
Primary energy savings per collector absorption area $[kWh/m^2_{coll.}]$									
Lisbon	0	285	461	0	189	461	0	162	461
Torino	0	186	377	0	152	377	0	119	377
Primary Energy Ratio $PER[-]$									
Lisbon	0.83	3.35	-6.37	0.98	4.14	-1.88	1.15	4.33	-1.26
Torino	0.79	1.21	1.13	0.82	1.30	1.42	0.96	2.21	-3.22

Table 3.14: Detached house building results for ACA comfort model

Storage efficiency

The hot and cold storages include supplementary losses that are not included in the building energy balance. First of all, the large hot water tank (2 m^3) involves 500 kWh and 850 kWh thermal losses respectively in Torino and Lisbon. This leads to a hot tank storage efficiency $\eta_{hot\ sto}$ (defined in equation 1.38 on page 49) of around 90% for all cases. This does no affect considerably the gas consumption because a high fraction of the heat stored comes from the collector (free energy except the pump consumption). This fraction ranges from 36% in Torino "acceptable" case to 99% in Lisbon "very good" case.

Secondly the small cold storage (0.5 m^3) losses count for maximum 36 kWh with a minimum storage efficiency of $\eta_{cold\ sto}$ (defined in equation 1.39 on page 49) 97%. The small difference bewteen the water temperature and room temperature assumption (22°C) ensures low losses.

3.3.10 Economical analysis

The analysis achieved in this paragraph is nearly the same as the new office building economical analysis, it aims to compare the two options of solar air-conditioning. Some of the detached house specificities are however handled and detailed below.

Hypothesis

As for the new office building the energy cost must firstly be selected. The energy prices in Europe (25 countries) for year 2011 have been recorded (EUROSTAT, 2011) for domestic use, the three selected scenarios also deal with mean and extreme values encountered. The highest energy prices recorded in Europe are named as **High** price energy scenario. They were respectively encountered in Sweden and Denmark for gas and electricity. The cheaper energy prices were encountered in Romania for gas and Bulgaria for electricity, they set the **Low** price energy scenario. The **Medium** energy scenario deals with the mean values of the 25 countries. The scenarios are detailed in table 3.15.

The investment costs must be set to achieve the system comparison. The hypotheses hold are described in table 3.16 where all the prices are tax included, they mainly deal with real manufacturer prices. They differ slightly from large scale application, the specific price of small systems is higher.

The considered cooling power for adsorption cooling is 4.5 kW (half of the nominal chiller power) while it is 5 kW for VCC cooling. The additional costs of solar air-conditioning are mentioned in table 3.16, they depend on the building case:

- Thermally driven Lisbon cases reach a solar fraction over 90%, the analysis no more considers any VCC machine. Comfort requirements are considered to be met in the building despite the lack of cold water production. The thermally driven supplementary costs are then decreased by the price of the VCC chiller.
- Thermally driven Lisbon 'Very good' case does not require any boiler as the entire heating and cooling load is satisfied by the solar collector field. The supplementary costs are consequently lower.
- All PV cases deal with the same supplementary costs (same peak power installed for both locations).

Globally, the other hypotheses are kept from new office analysis. The economical indexes computation is carried out in the same way as for the new office building.

Results

The economical analysis results are presented in table 3.17 and in figure 3.23 for discounted payback period.

Firstly, as for the new office building the installation of PV system is cheaper whatever the case. This also disadvantages the thermally driven system that had already reached a lower energy performance (see previously in this section).

The PV system reaches 11-13 years payback time while the thermal system has economically unrealistic values. The discounted payback period showed in figure 3.23 details the economical profitability of three price scenarios. The

energy price scenario	Symbol	**High**	**Medium**	**Low**	**Source**
Gas [€/kWh]	$€_{gas}$	0.117	0.064	0.028	EUROSTAT (2011)
Electricity [€/kWh]	$€_{elec}$	0.298	0.184	0.087	EUROSTAT (2011)
Yearly parameters			**Value**		
Inflation HICP	λ		1.84 %		Global-rates (2013)
Interest rate	δ		3 %		Own guess
Deduced annuity factor	i		1.1 %		
Gas price increase	i_{gas}		6.3 %		APERE (2012)
Electricity price increase	i_{elec}		4.5 %		APERE (2012)

Table 3.15: Detached house economical analysis parameters

Investment by field	**Amount**	**Unit**	**Source**
Adsorption chiller, dry cooler and hydraulic module	2350	$€/kW_C$	Invensor commercial doc.
Solar thermal field	280	$€/m^2$	Hartmann *et al.* (2011)
PV collectors	2500	$€/kW_p$	Belgian PV installer
Inverter substitution	500	$€/kW_p$	Belgian PV installer
VCC	500	$€/kW_C$	Laboratory investment cost
Gas boiler	350	$€/kW_{therm}$	Belgian heater installer
Cold storage tank	500	€	Laboratory investment cost
Hot water tank	1000	$€/m^3$	Belgian heater installer
Total investment	**Amount [€]**	**Extra costs (I) compared to Classical A-C [€]**	
Classical A-C	6 500	0	
SAC therm Torino	22 190	15 690	
SAC therm Lisbon 'Acceptable' and 'Good'	18 690	13 190	
SAC therm Lisbon 'Very good'	18 690	9 690	
SAC PV	12 650	6 150	

Table 3.16: Detached house investment costs

high price scenario reaches lower than 20 years payback period for both thermal and PV systems in 'acceptable' building. Despite a more efficient building, the energy savings in 'good' and 'very good' building are lower and thus the solar air-conditioning is less profitable. As for new office building, the discounted payback time computation leads to values between 2 and 4 times higher for the thermal system than for PV. For a given case the payback time of a thermally driven system is never lower than a PV system. In fact, the results are the same as for new office building economical analysis. The differences stand in lower investment costs for residential case (boiler or VCC are not required depending on the case) and lower energy price for industrial customer. Besides, the domestic energy price encounters a higher variation from lowest to highest energy price in Europe.

The Net Present Value gives for example the value of the investment of a PV system. For medium energy price scenario, the PV system gets at least 1 time the initial investment. Here also, the installation of a PV system does not require any subsidies to be highly profitable.

Concerning the thermally driven system, the cost of primary energy savings is lower for Lisbon because of the VCC removal and higher radiation. For thermal system in Lisbon 'acceptable' case, the cost stands around 2.6 c€ per kWh primary energy savings (medium energy price scenario). For PV systems, the cost of primary energy savings is generally positive due to high primary energy savings and lower investment. The gain is about the same as the cost of best thermally driven system.

Finally, if the additional costs of both solar cooling systems were similar and equal to the PV price (meaning a thermally driven system at 220 € per kW_C), the net present value is still at least two times higher for the $SAC\ PV$ case (in medium energy price scenario). Besides, the $SAC\ PV$ has always a shorter payback time.

	'Acceptable'			**'Good'**			**'Very good'**			*PV*		
	SAC therm			*SAC therm*			*SAC therm*			*SAC PV*		
Energy price	*High*	***Med.***	*Low*	*High*	***Med.***	*Low*	*High*	***Med.***	*Low*	*High*	***Med.***	*Low*
Payback period [*year*]												
Lisbon		**42**			**54**			**50**			**11**	
Torino		**45**			**58**			**100**			**13**	
Discounted payback period [*year*]												
Lisbon	16	**24**	36	20	**28**	41	22	**27**	42	6	**11**	20
Torino	17	**25**	37	20	**28**	42	28	**38**	53	8	**13**	23
Net present value (20 years operation) [k€]												
Lisbon	5.7	**-2.8**	-8.6	1.0	**-5.3**	-9.7	-1.3	**-3.6**	-11.8	18.8	**8.7**	0.2
Torino	5.5	**-4.1**	-10.6	0.5	**-6.7**	-11.8	-6.5	**-10.6**	-13.4	14.0	**5.8**	-1.2
Cost of primary energy savings (20 years operation) [c€/*kWh*]												
Lisbon	-5.3	**2.6**	8.0	-1.2	**6.5**	11.9	2.1	**5.7**	12.7	-11.7	**-5.4**	-0.1
Torino	-4.5	**5.0**	8.8	-0.6	**7.3**	12.7	12.3	**20.0**	25.4	-10.7	**-4.4**	0.9

Table 3.17: Detached house solar air-conditioning economical profitability

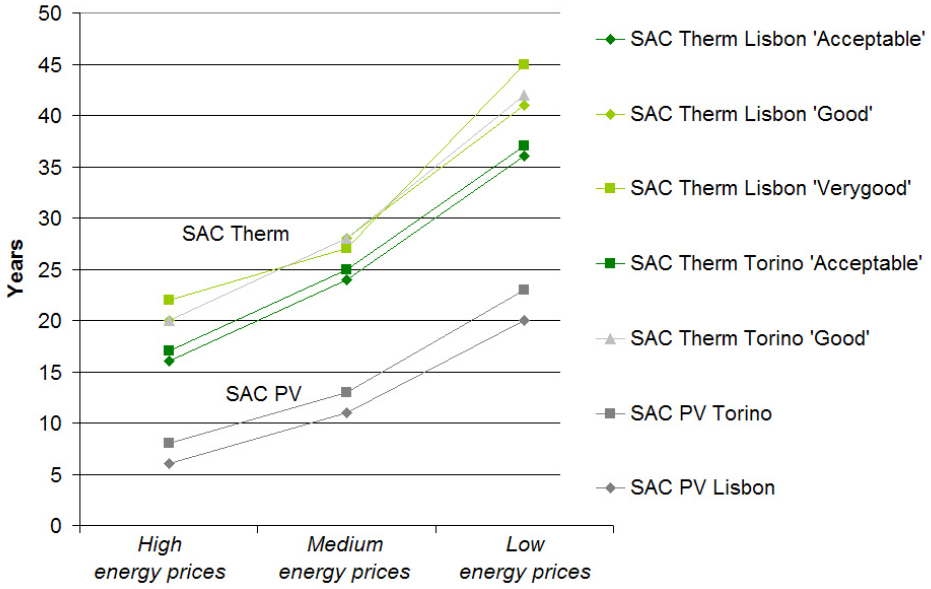

Figure 3.23: Detached house solar air-conditioning payback time

3.4 Discussions

The simulations based on the hypotheses detailed throughout the chapter reveal energy savings for both solar air-conditioning systems in each case. From both energy and economical point of view, the PV system seems to be the best solution. Some points need to be discussed before going deeper into the experimental analysis carried out in the following chapter.

3.4.1 Vapour compression chiller

Compared to the reference system detailed in chapter 1 (equation 1.12), the computed seasonal COP is really higher (around 4). When comparing the systems, it can be observed that a high vapour compression chiller COP disadvantages thermally driven systems. According to the certification company (EUROVENT, 2012), a vapour compression chiller COP of 4-5 is commonly encountered in steady state operation. The seasonal performance of such a chiller is described by the European Seasonal Energy Efficiency Ratio (Fatteh, 2011). The ESEER is calculated as a weighted average of EER (same as COP) at four part load conditions. The ESEER is generally even higher than the chiller COP in nominal conditions (EUROVENT, 2012). The yearly simulated COP seems to be consistent with highly efficient chillers. The reference value often used in the literature is more for comparison with an (old) existing vapour compression chiller.

The vapour compression chiller high COP also explains the high value of the Primary Energy Ratio encountered, even in classical air-conditioning. Tables 3.5, 3.14, 3.10 show PER higher than 1 in case of significant cooling load (all cases but new office in Stockholm). A PER of 1 is the minimal requirement for solar air-conditioning (Nowag *et al.*, 2012). The thermally driven system PER always increases in comparison to the classical air-conditioning; it is therefore never a problem to reach 1. The PER criterion is not a guarantee of quality, a higher value could be set.

3.4.2 Thermally driven system thermal and electrical performance

The thermal and electrical COP's are certainly a little bit overestimated as already discussed on page 107. The simulated system can be considered as a perfect system without any performance decrease due to part load or start-stop cycling effect. From the thermal point of view, the adsorption chiller has lower performance due to the dry cooling tower. It would have been lower by implementing the two effects mentioned above. On the electrical point of view, the $COP_{elec\,tot}$ reaches around 10 for all cases when speaking about cooling. The real systems such as the one detailed in next chapter scarcely accomplish $COP_{elec\,tot}$ higher than 5. There is clearly a big gap between the auxiliaries consumption fixed values generally chosen and the experimental values. Standby consumptions and part load operation could explain a part of this gap (see

next chapter).

The definition of the system electrical COP (equation 1.23 on page 46) does not distinguish the heating from the cooling operation. So, the yearly value could hide the real performance of the heating or the cooling system. The monthly value of the $COP_{elec\,tot}$ does distinguish (at least for office building without domestic hot water load) the heating from the cooling operation. As mentioned above, the cooling operation involves more electricity consumption, thus a lower $COP_{elec\,tot}$. The target of 10 detailed by Wiemken *et al.* (2010) is related to the cooling operation only.

3.4.3 Thermal collector field design

The sizing of the collector field is based on the "350 kWh per net collector area per year" given by Nowag *et al.* (2012). It makes the collector field smaller in northern locations. The size of the solar collector field is a crucial parameter for the solar air-conditioning system. The energy savings are directly linked to the collector size. The criterion selected guarantees to have an important use of solar collectors, but does not guarantee anything about the system operation performance.

3.4.4 Sorption chiller cooling power choice

Firstly, the detached house needs a low cooling power. The smallest available sorption chiller could be installed for two semi-detached houses sharing the same cold production device. The selected building is not currently adapted to the implementation of thermally driven solar air-conditioning. New chillers could fulfil the low peak cooling load buildings (Boudéhenn *et al.*, 2012).

Secondly, the office buildings have a significant higher load. The selected absorption chiller has a 105 kW_C nominal cooling power whatever the case. Generally, in larger thermally driven cooling systems, the sorption chiller power does not cover the peak load (Henning, 2007a). It is used in parallel or in series with vapour compression chillers designed to satisfy the peak load. The choice of sorption chiller size is based on an economical or feasibility criterion. For Lisbon case, the choice of a 105 kW_C nominal capacity is not really damaging the energy benefits of solar air-conditioning despite a high peak load (around 200 kW_C for ACA comfort model): 85 % of the cooling load is satisfied by the absorption chiller. The remaining 15% stand for peak loads and periods when sun is not shining enough meaning a higher cooling capacity could not reach significantly higher solar fraction. A monotonic curve could be set on to find out the appropriate cooling power of the sorption chiller (figure 3.24). This curve is not the only parameter, the solar energy availability affects the cold effectively produced by the sorption chiller. The hot water temperature and rejection temperature at current conditions are modifying considerably the chiller capacity as seen on figure 3.24.

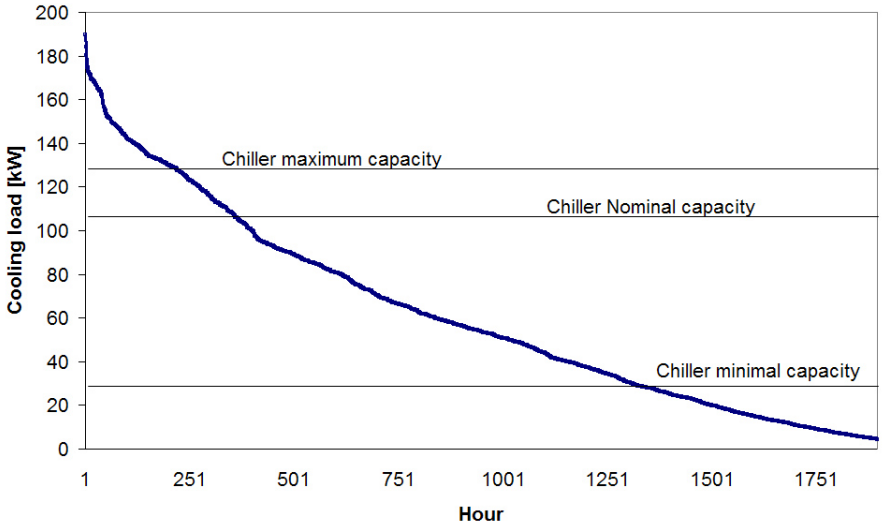

Figure 3.24: New office cooling load monotonic curve and chiller capacity limits for Lisbon 'acceptable' *ACA* comfort model case

In the cases analysed, Paris and Stockholm could have a lower chiller cooling power to decrease the very long payback period (3 times longer than the PV system). Even with a lower investment cost due to lower chiller price, the thermally driven chiller is not competitive with PV system. Besides, in the simulations, the chiller high cooling power does not impact the thermal performance (no chiller part load is handled).

3.4.5 Storage temperature limit

The storage temperature in an office building can be raised up to 140°C because of the efficiency curve of the evacuated tube collectors. This implies a pressurized system which is more restrictive in terms of regulations about safety. In the residential case where the system must be simpler and safer, the allowed temperature is below 100°C. This is suitable for the temperature usually reached in flat-plate collectors. It nevertheless reduces the stored heat per storage tank volume.

3.4.6 Electricity grid energy flows

The strongest hypothesis about PV profitability and primary energy savings is the use of electricity grid as perfect (no energy losses) and free of charge energy storage. Compared to the thermal system involving a limited storage with energy losses, this is clearly an advantage.

First of all, the **annual energy balance** reveals the PV production does not exceed the electricity consumed by the building. For the residential building, the PV system installed produces less than the household electricity consumption (3600 kWh). For the new office building, the electricity consumption for ventilation, appliances and light reaches 38 kWh/m^2 building surface. This is also less than the total electricity produced by PV (< 26 kWh/m^2 in table 3.2). Besides, the electricity consumption of office building has been investigated for the typical office building, it reaches 25.6 kWh/m^2 for appliances and 20.4 kWh/m^2 for lighting. Moreover, those internal gains have a double impact on energy utilization: their own consumption and the increase in cooling energy required.

Secondly, the **instantaneous electricity balance** reveals discrepancies between both kinds of buildings.

On the one hand, the maximum PV power (87 kW_p for Lisbon, 57 kW_p for Torino) of the new office building has the same order of magnitude as the building consumption for the week days (> 55 kW). Except for a possible day in Lisbon where sun is shining and there are no cooling loads, the weekday PV production is entirely consumed in the building. This does not involve grid for PV excess production. The weekend raises this problem, there is no building consumption and possible PV production. The worst scenario would be an obligation of PV switch off during the weekend leading to a decrease of PV production of around 29% (2/7). This worst case keeps nevertheless the advantage to PV system from an energy and economical point of view.

On the other hand, the residential building has to cope with a 2.48 kW_p power and a mean household consumption of $400W$ (without VCC). Energy exchange with the grid plays therefore an important role. Depending on the electricity grid injection taxes, the PV system could be economically less attractive than mentioned in table 3.17. Moreover, if the electricity cannot be injected on the grid, the energy profitability decreases as well.

In Walloon region, according to the energy regulator (CWAPE), the domestic PV installations below 3 kW_p do not require any grid reinforcement. In spite of this, a tax will be implemented to each residential installation. It costs around 55 €/kW_p to pay to the distribution network operator. Moving this tax to the residential case of Lisbon and Torino, it implies an increase of the discounted payback time of respectively 2 and 3 years. Perhaps, the current situation of Walloon residential sector is not representative of European countries. In a southern region context, it seems to be easy to convince the distribution network operator to accept PV production on a grid which is subject to peak loads due to air-conditioners.

3.4.7 Total primary energy use of buildings

In Paris, the yearly primary energy use for the offices buildings without any solar system ranges from around 130 to 240 kWh/m^2 for the new office and the typical office respectively. The part dedicated to the heating and cooling production remains low for those building meaning (35-40%) meaning the main part of the energy is used for other needs: lighting, ventilation, appliances, pumps. This work emphasizes the energy use for heating and cooling, it does no claim to evaluate the possible savings of efficient lighting or other electrical devices.

The work of Thewes (2011) presents some measurement of real air-conditioned office buildings in Luxembourg (climate similar to Paris), the total primary energy use ranges from 200 to 1500 $kWh/(m^2\ year)$ with a mean value of 727 $kWh/(m^2\ year)$. The electricity consumption takes the most important part. The large difference between simulation and reality raises two main questions:

1. Does it make sense to take the defined electricity consumption profiles in the simulations?
2. The thermal loads are there computed correctly ?

Firstly, the office building electricity consumption depends largely on the company activity. The awareness of office building activity is crucial for simulating it accurately. Moreover, the heat and cold distribution and emission systems electrical consumption should be taken into account (their net electricity consumption is 12.8 $kWh/(m^2\ year)$ for typical office building). Secondly, the load computation is based on some occupancy and set point temperatures profiles. These could be not met in the reality, this aspect has been studied by Hoos (2012) for residential buildings. The difference between simulation and reality seems to be lower in recent buildings that are more insulated. In old buildings (that are not well insulated), the set point used in simulation is generally higher than the mean temperature reached in the building.

3.4.8 Conclusions

Following the comment about the $COP_{elec\,tot}$ computation for heating and cooling, the results clearly show that the use of solar heat for heating the building instead of cooling is better as far as primary energy savings are concerned. For a thermally driven system in a temperate climate, the building energy performance level is inversely proportional to the efficient use of solar energy. In a hot climate with a slight heating load, a sufficient solar collector field could satisfy both total heating and cooling load if this last one is mainly linked to solar energy. The office building, where load depends largely on the internal gains, is not adapted to a 100% thermally driven solar air-conditioning.

From an economical point of view, the thermally driven system has more expensive investment costs. Apart from the fact that chiller costs are higher, the thermally driven system in office building still needs a back-up. So it implies the investment of two devices doing the same thing. In the detached house

where the load is more influenced by solar gains, the solar fraction cooling is higher, the eventuality of removing the vapour compression chiller is investigated in case of thermally driven system.

The PV system has great advantages compared to the thermal systems from both economical and energy point of views. The hypothesis about grid connection remains important even if its impact will no grab the huge gap between thermal and PV systems for cooling.

Chapter 4

In situ evaluation of solar cooling systems

This chapter describes the results of monitoring campaigns performed on two solar air-conditioning systems. Firstly, a small scale adsorption chiller coupled with a solar collector field, a cooling tower, storages and emissions systems is analysed. Secondly, a vapour compression chiller and an on-grid photovoltaic field is investigated. The energy performance figures are computed and some models are tuned with measured values. The comparison of energy benefits of the two systems is also undertaken.

Both cooling systems are installed in a laboratory building (figure 4.1) in Arlon, South of Belgium. This location belongs to the 4^{th} climatic zone defined in chapter 2 which is characterized by a medium heating load and a low cooling load. The yearly solar radiation on an optimal plane reaches around 1200 kWh/m^2 for this location. The monitoring periods take place during the cooling season which runs mainly from May to September.

4.1 Adsorption cooling system

4.1.1 Installation description

A small-scale adsorption chiller has been installed in the laboratory building in 2011. This building was previously equipped with a fully monitored heat and cold production and distribution system. Besides, a solar collector field is used for building heating and domestic hot water production. The building has the shape and size of a small residential house, its cooling load led to the choice of one of the smallest market available adsorption chiller. As described in chapter 3, the solar cooling system common ratio between solar collector size and cooling power ranges from 2.5 to 3.5 m^2/kW_C. The installed system has 14 m^2 net solar collector area for a nominal cooling power of 9 kW_C. Both economical and architectural limits made it difficult to enlarge the existing solar collector field. Some electrical resistances are set up to compensate the lack of collectors.

The general scheme of the installed system is displayed in figure 4.2. By operating and measuring this cooling system in real scale conditions, it is pro-

Figure 4.1: Jacques Geelen laboratory at University of Liège in Arlon

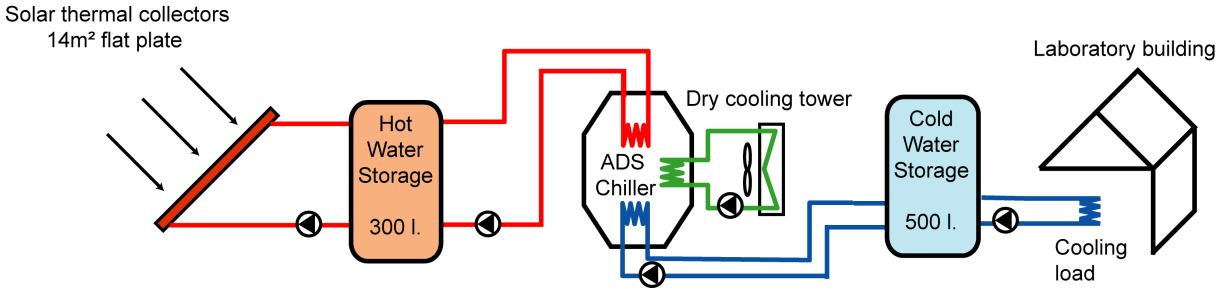

Figure 4.2: Scheme of the installed adsorption cooling system

posed to assess its thermal and electrical performance. The main components dedicated to solar air-conditioning are listed below (from left to right in figure 4.2):

- The hot water loop containing flat-plate solar collectors and hot water storage (300 litres with 7.2 kW electrical heater). The main "South" roof has an azimuth of 43° to East and a slope of 42°,
- The adsorption chiller (ADS) containing two reactors with a total cooling nominal power of 9 kW_C,
- The recooling loop and its dry cooling tower,
- The cold water loop including the cold water storage (500 litres),
- Cold emission devices to cool the laboratory building: cooling floor, cooling ceiling, air handling unit

.

The pumps driving water to the adsorption chiller as well as the cooling tower fans are internally controlled by the adsorption chiller. The laboratory computer controls the other parts of the systems (cold water temperature, adsorption chiller start-up ...). The installed system is shown by figures 4.3 and 4.4 on which the hydraulics module contains the three pumps driving water into the chiller.

Figure 4.3: Installed adsorption cooling system with hot water tank (left), adsorption chiller (bottom) and hydraulics module (top)

The fluid used in all loops is water except for solar collector loop. A water-glycol mix flows into the collectors, the heat is transferred to the hot water storage aided with two heat exchangers in series. The collector loop also includes a drain back storage where the water-glycol mix is kept when the pump is not in use.

Figure 4.4: Dry cooling tower

Adsorption chiller

The selected sorption chiller has to satisfy the following requirements in order to be installed in the laboratory building:

- A cooling power to meet the building cooling load (< 10 kW)
- Good performance at part load conditions
- Low driving temperature due to the collectors technology and small area

Through the thermally driven cooling solutions available on the market, an adsorption chiller with zeolite-water couple has been selected to satisfy the previous requirements. Its thermal specifications are listed on table 4.1. The thermal COP given by the manufacturer keeps high value even with low driving temperature. For example, the announced thermal COP is 0.55 for 60°C driving heat, 27°C recooling and 18°C cooling water (chiller inlets).

4.1.2 Monitoring description

In accordance to section 1.4 in chapter 1, some measurements must be undertaken to compute the energy performance indexes. The relevant energy flows (heat, cold, electricity...) are computed based on the measurements to be able to derive key figures such as Primary Energy Ratio (PER), thermal COP, electrical COP... The measurements picked up every 10 seconds in the installed solar air-conditioning system enable the computation of those indexes.

As the building is considered as an infinite heat source, the whole cold energy produced can be consumed by the building. This explains why the adsorption cooling system monitoring focuses on cold production. The measurements on the cold distribution or emission will therefore not be presented in this work.

Characteristics	Unit	Cold loop	Rejection loop	Hot loop
COP_{therm} max	[-]	0.69		
Capacity range	$[kW_C]$	3-11		
Temperature range	[°C]	10-25	20-37	45-100
Nominal point				
COP_{therm}	-		0.61	
Capacity	[kW]	9	24	15
Temperature chiller IN	[°C]	18	27	72
Volume flow	[l/min]	38	75	37

Table 4.1: Adsorption chiller thermal specifications (INVENSOR, 2010)

The graphical user interface developed to monitor the system is displayed in figure 4.5. The probes can be split into three groups: thermal and electrical measurements and meteorological data. All probes displayed in figure 4.5 have real time measurements except for thermal and electrical COP's that are previous hour mean values. This monitoring screen makes possible the instantaneous visualization of each thermal flow and of the electrical consumption of the main devices. Moreover, the past 30 minutes thermal flows are plotted dynamically to be aware of the adsorption cycle duration (not mentioned in figure 4.5).

Thermal measurements

The thermal measurements consist of temperature and mass flow sensors. They are mainly used to evaluate the chiller, solar collector and dry cooler thermal behaviours. The most important measurements and computed variables are described in table 4.2. The maximum error (heat flows and COP's computation) is based on the mass flow meter specifications and the calibration of temperatures probes. Due to the short difference between the supply/return flow temperatures, the probe accuracy of 0.2°C which is given by the probe manufacturer is not sufficient. For example, an error of 0.4°C on the temperature difference would have led to a thermal COP error of 22%. The probes T89 to T94 were put in a temperature calibrator bath matching the temperature range of the solar cooling system (10-80°C). The maximum difference of each probe couple is used to compute for further error computations of heat flows. The biggest difference among 500 measurements gives +/- 0.06 ; 0.02 ; 0.11°C respectively for the hot water loop (T89-T90), the rejection loop (T93-T94), the cold loop (T91-T92). Besides, a calibrated temperature probe proofed the maximum bias error (+/- 0.2°C) of the other probes.

Electrical measurements

To analyse the electrical behaviour of the system, it is necessary to measure the consumption of each device. Measurements only concern components dedi-

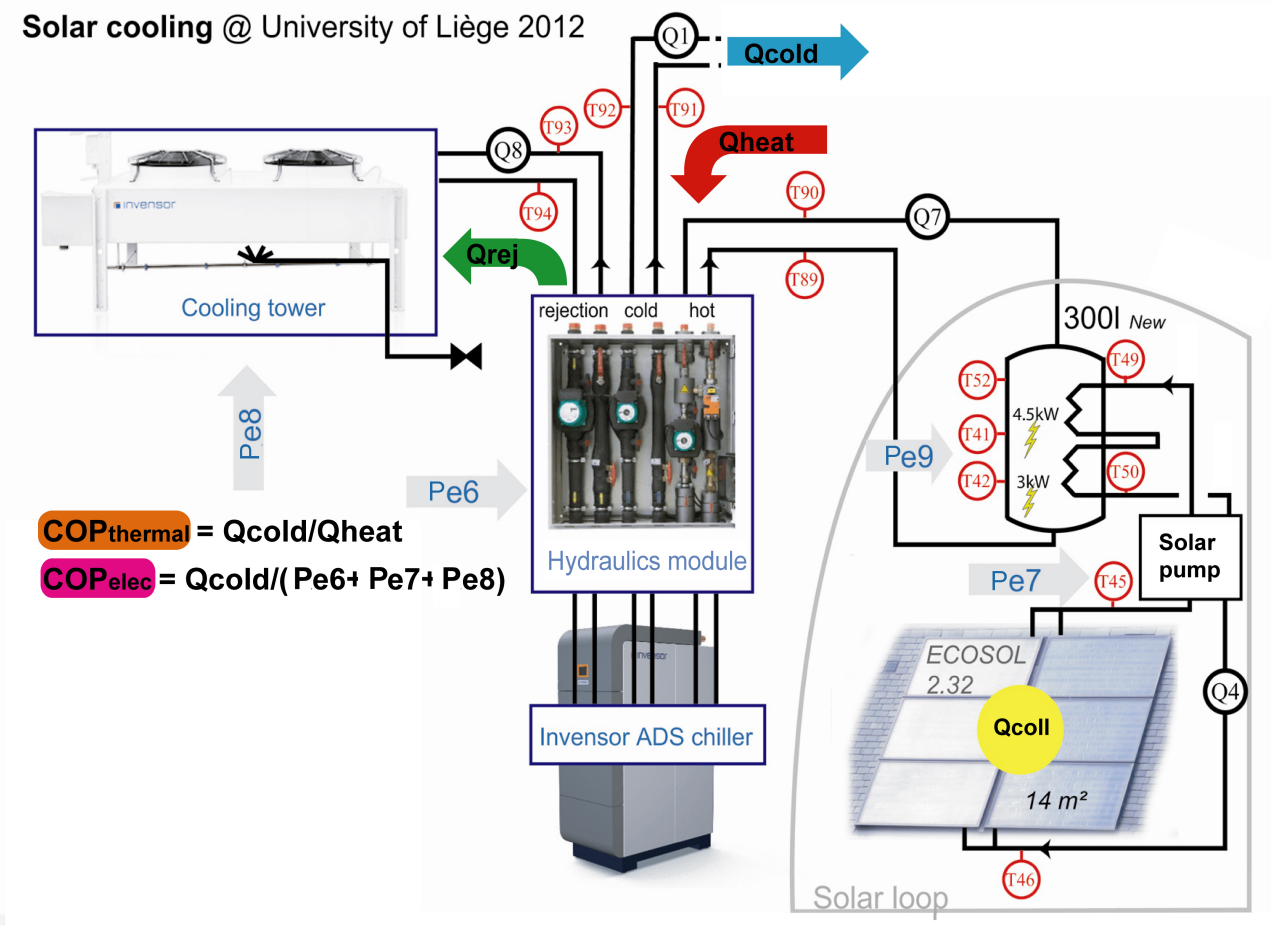

Figure 4.5: Solar air-conditioning system monitoring screen

cated to solar air-conditioning. The electrical consumptions due to the emission devices for example are not included as they would be present whatever the installed air-conditioning system. The electrical measurements are shown in table 4.3. The solar drain back system includes a solar pump which has a constant electrical consumption of 83W. The electrical COP computation shown in figure 4.5 does not take the auxiliary heater into account.

Meteorological data measurements

Two pyranometers placed respectively in the collector plane and on horizontal plane have an uncertainty of 4.5 % under clear sky conditions. They are used to evaluate the solar collector yield. The external temperature is measured within an accuracy of +/- 0.2°C, this measurement is useful to analyze the cooling tower behavior.

Measurement	**Probe number**	**Unit**	**Probe accuracy**
Temp. supply/return for each chiller water flow	T89-T94	[°C]	+/- 0.2 [°C]
Solar collector supply/return temp.	T45-T46	[°C]	+/- 0.2 [°C]
Solar heat exchanger supply/return temp.	T49-T50	[°C]	+/- 0.2 [°C]
Storage tank temp.	T41-T42-T52	[°C]	+/- 0.2 [°C]
Chiller mass flows rates	Q1-Q7-Q8	[l/min]	2%
Solar loop mass flow rate	Q4	[l/min]	2%
Computations based on measurements	**Variable name**	**Unit**	**Maximum error**
Chiller heat consumption	$\dot{Q}_{heat}$	[kW]	3% +/- 395 [W]
Chiller heat rejected	$\dot{Q}_{rej}$	[kW]	3% +/- 466 [W]
Chiller cold produced	$\dot{Q}_{cold}$	[kW]	7% +/- 412 [W]
Solar collector field heat produced	$\dot{Q}_{coll}$	[kW]	4% +/- 70 [W]
Hourly thermal COP	COP_{therm}	[-]	10%

Table 4.2: Adsorption cooling: thermal measurements and computed values

Measurement	**Probe number**	**Unit**	**Range**	**Accuracy**
Hydraulics module (including three pumps) and chiller	Pe6	[W]	18-450	1%
Solar loop pump power	Pe7	[W]	0-83	10%
Cooling tower consumption	Pe8	[W]	0-1100	0.6%
Hot water tank electrical heating	Pe9	[W]	0-7234	5%
Computations based on the measurements	**Variable name**	**Unit**		**Maximum error**
Hourly electrical COP	COP_{elec}	[-]		10%

Table 4.3: Adsorption cooling: electrical measurements and computed values

Adsorption chiller control

The chiller is switched on if the hot water storage reaches 65°C while it stops if its temperature drops below 55°C (60°C for *back-up heating* period). The chiller cold water set point is 15°C. The results will show that the chiller continues operation even if the set point is reached. The switching off temperature during the experimentations is slightly lower than for the simulations (62°C), it has been implemented to have a larger operation temperature range. Moreover, the switching off temperature of 55°C maximizes the cold water production and decreases a little bit the thermal COP.

Dry cooling tower control

During chiller operation, the dry cooling tower receives a constant water flow. The control of the fan power is made by the chiller to reach 27°C as inlet chiller recooling temperature. It is governed by a proportional-integral controller using cooling tower outlet temperature measurement. A 0-10V signal from chiller sets the fan speed, thus the electricity consumption. Three main cases are encountered:

- Low outdoor temperature (lower than 18°C) implies a very low fan consumption ($<$ 50W),
- High outdoor temperature (higher than 27°C) implies fan at full load (950W),
- Intermediate outdoor temperature where the fan controller is useful.

4.1.3 Monitoring results

Measurement periods

Some preliminary measurements were carried out in 2011 but were not kept for this analysis because of a non nominal flow was encountered on the hot water loop. This was due to a wrong pipe network design and to a narrow connection on the hot water tank. This problem was solved and the measurement period lasted for 82 days during spring and summer 2012.

The first measurement period (28 days from April 17^{th} to May 29^{th} and 30^{th}August) is carried out with **back-up heating** (electrical resistances in the hot water tank in figure 4.5) driving the adsorption chiller. It allows running the adsorption chiller for long periods with various hot water driving temperatures. The cold production has consequently no link with solar radiation. This period handles low external temperature (thus a low electricity consumption of the dry cooling tower) and building non infinite heat source. This last fact involves a rather low water temperature in the cold water tank (10-15°C).

The second period (17 days from May 30^{th} to June 13^{th} June and August 4^{th}) is **solely solar air-conditioning** (without back-up). It implies a shorter chiller operation duration and multiple chiller start-ups per day.

The third period (36 days from June to August) copes with **emulated solar collector**. As mentioned before, the available collector surface on the laboratory roof is not sufficient to run the adsorption chiller in nominal operation. The proposed solution was to use the 14 m^2 solar collector and add 14 m^2 emulated collectors with electrical resistances. The chiller operation is now in real scale conditions but driven by a combination of real and emulated collectors. More information about collector emulation is given in the following paragraph.

Collector emulation

This paragraph details the collector emulation implementation for the third measurement period. Two electrical resistances (3 and 4.5 kW) are installed in the hot water storage as seen in figure 4.6(a), their control makes possible the emulation of the 14 m^2 collectors. The energy flow from the collector to the hot water tank is measured and the "same" thermal power is provided by electrical resistances. These two resistances can be switched ON or OFF each minute while the collector energy flow is measured with two minutes interval. This implies seven power possibilities for the collector emulation. The control law of the resistance in relation to the measured collector energy is displayed in figure 4.6(b). For the whole test, this control leads to 5% variation between the collector energy flow and the electrical consumption by resistances.

The position of heat exchangers is not set to reach any stratification in the tank. The tank stratification is unwanted in our case because of the high water flow rate to the chiller (35 litres per minute). Stratification occurs when the solar energy is available trough collectors and chiller is not operating, it represents a short period before chiller starts up.

Global results

The main global results of the three operation periods are presented in table 4.4. The performance indexes have been defined in chapter 1 section 1.4 starting on page 43.

There are some important remarks about table 4.4:

The energy provided by the electrical heater is not taken into account in the electrical consumptions. It is considered as a "free" energy input for the *back-up heating* period. For the *collector emulation* period, it is also not taken into account in the electrical consumptions. Nevertheless, the measured solar pump consumption is multiplied by 2 to do as if the electrical heater was solar energy.

The *back-up heating* period works with a higher driving temperature. The chiller is switched off if the driving temperature is lower than 60°C. For the other periods, this value is set at 55°C to take advantage of a maximum cold production. The threshold for starting the machine ranges from 65 to 70°C.

(a)

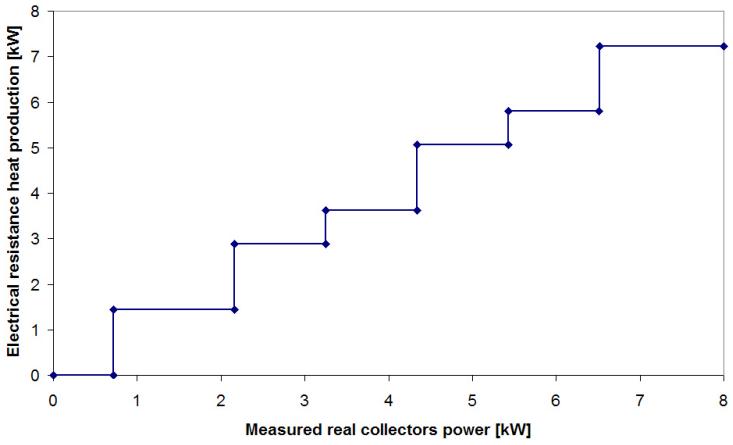

(b)

Figure 4.6: electrical resistances in hot water storage (a) and the control law in relation to the measured collector power (b)

Period	**Back-up heating**	**Solar only**	**Collectors emulation**
duration *[days]*	29	17	36
$\eta_{thermal\ collector}$	0.29	0.30	0.31
COP_{therm}	0.60	0.47	0.55
$COP_{el\ chill\ pump}$	10.1	5.6	9.3
$COP_{el\ cold\ chill}$	8.2	4.3	6.5
$COP_{elec\ tot}$	7.4	3.3	4.7
$COP_{solar\ loop}$	32.8	39.8	38.6
COP_{rej}	111.2	53.0	57.5
PER_{therm}	-	1.31	1.88
f_{sav}	-	0.15	0.40

Table 4.4: Adsorption cooling installation global results for 2012

The thermal collector efficiency is 30% whatever the case, it is a commonly encountered value for a collector summer operation. The flat-plate collectors have a lower yield because of high operating temperature. As clouds often covers the Belgian sky, the diffuse radiation is not high enough to operate the collectors at high temperatures. These two reasons explain mainly the apparently low thermal yield value.

The thermal COP is higher with a longer chiller operation duration which was met in *back-up heating* period. It reaches the chiller nominal value. The

thermal COP decreases during the other periods due to lower driving temperature and intermittent operation. Even with the 14 m^2 solar collector field the thermal COP satisfies the minimal requirements given by Nowag *et al.* (2012) in table 1.7 on page 51. The value of 0.55 measured during the *collectors emulation* period is good, part load and lower driving temperature do not affect significantly the thermal performance compared to the nominal one.

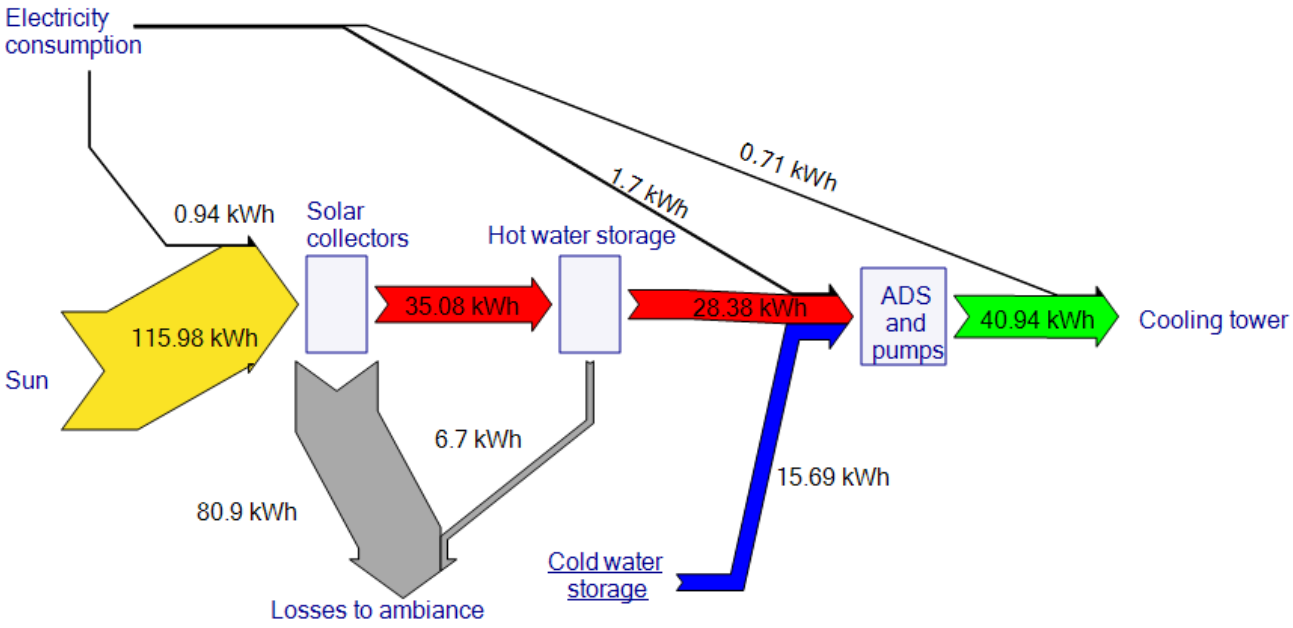

Figure 4.7: Daily mean thermal and electrical energy flows for *collectors emulation* period. Black arrows stand for electricity.

The energy flows (thermal and electricity) for the *collectors emulation* period are represented in figure 4.7. The main losses are encountered at the collector level, the storage and solar loop efficiency ($\eta_{thermal\ collector} \cdot \eta_{hot\ sto}$) is around 80%. The total amount of thermal flows to drive in order to produce 15 kWh cold energy (useful effect) is nearly 106 kWh (40.3+15.4+28+34.2).

The electrical performance is depicted by the various electrical COP's on table 4.4. The solar air-conditioning system electrical COP ($COP_{elec\ tot}$) does not meet the targeted value of Wiemken *et al.* (2010) whatever the period. The electricity sharing is displayed in figure 4.7 for *collectors emulation* period. Besides, the stand-by consumption is about 30 W for the adsorption chiller (21W) and the cooling tower (9W). It counts for 17% of the total electricicty consumption for this period.

If this system were operating in favourable conditions (see *optimal conditions* below) to reach an electrical COP of 10, the mean electrical COP of the rejection device (COP_{rej}) should be 240. Such high values have been measured when the outdoor temperature was lower than 17°C. Obviously, this outdoor temperature is not representative of a period requiring cooling energy. So, for this system, an electrical COP of 10 is unreachable.

The *optimal conditions* assumptions to compute COP_{rej} with $COP_{elec\,tot} = 10$ are:

- Stand-by power: 30 W (measured)
- Pump + chiller power in operation: 400 W (measured)
- Operating period: 8 hours per day
- Solar loop COP: 50 (order of magnitude for good systems)
- Chiller thermal COP: 0.6 (met for the best testing period)
- Chiller cold power: 8 kW_C (lower than the nominal power to take variable driving temperature into account)

In spite of the low electrical performance, some primary energy savings are encountered compared to a classical air-conditioning system. The fraction of energy savings (f_{sav}) reaches 15 to 40% in the third period which is more representative of a well designed solar air-conditioning system. The reference system energy performance is defined in equations 1.11 and 1.12 on page 18.

The rejection COP (COP_{rej}) quantifies the cooling tower performance. It is strongly linked with the external temperature which is higher for the second and third period. More details are given about the cooling tower electricity consumption following in the text.

Daily results

The cold production and the energy performance of the system depend on the daily available radiation. Figure 4.8 represents the daily cold production results in order of decreasing solar radiation. The first period *back-up heating* is less affected by the solar radiation because of permanent back-up heating. It is also the sunniest period (solid line higher). This graph tells interesting things about the two other periods.

For those days with quite important solar radiation, there is sometimes no cold production. It means the collector energy is not enough to reach the threshold value for chiller start-up (storage tank losses through the night decrease its temperature by roughly 5°C). Generally, before starting the adsorption chiller in the morning, the storage tank needs 3.5 kWh thermal energy.

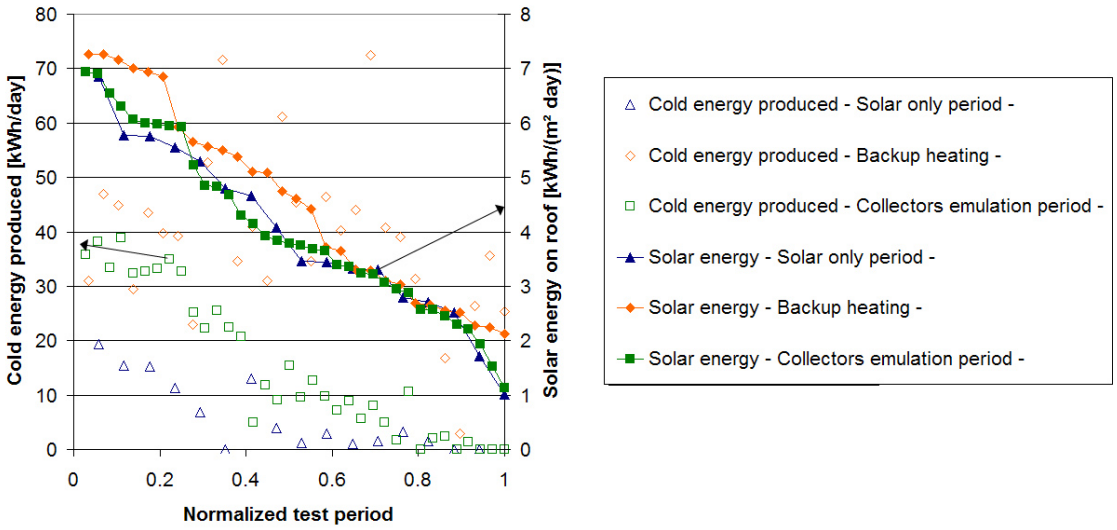

Figure 4.8: Daily cold energy produced and available solar energy for the 3 monitoring periods (normalized)

The *collectors emulation* period shows a good linear correlation (empty markers in figure 4.8) of daily cold produced in relation to the available solar energy in sunny days. It allows to evaluate the cooling load met by the solar air-conditioning system aided by radiation prediction. This gives for sunny days (higher than 3 kWh/m^2) the following correlation achieving R^2= 0.93:

$$Q_{cold}\,[kWh] = 9.0876 \cdot Radiation\,on\,coll.\,plane\,[kWh/m^2] - 22.541 \qquad (4.1)$$

Two typical days are selected to analyse the solar air-conditioning system behaviour. One sunny day for *solar only* and *collectors emulation* periods. Figures 4.10 and 4.9 show the energy flows, chiller supply temperatures and thermal COP for those two days. Table 4.5 summarizes these two days energy indexes and add a hotter day to emphasize the heat rejection electricity consumption.

The sunny days show high collector efficiency because of the important part of direct radiation. The thermal COP gets closer to the nominal one and electrical COP's are larger than the mean period values. Less stand-by power and better operating conditions are encountered throughout sunny days. Those sunny days with warm outdoor temperature reach around 50% energy savings compared to classical air-conditioning.

August 11th (*Solar only*) is characterized by a four-hour chiller operation. Figure 4.9 shows three chiller starts ($\dot{Q}_{cold}$ means cold water energy flow). The chiller starts when the hot water storages reaches 70°C. The collector energy

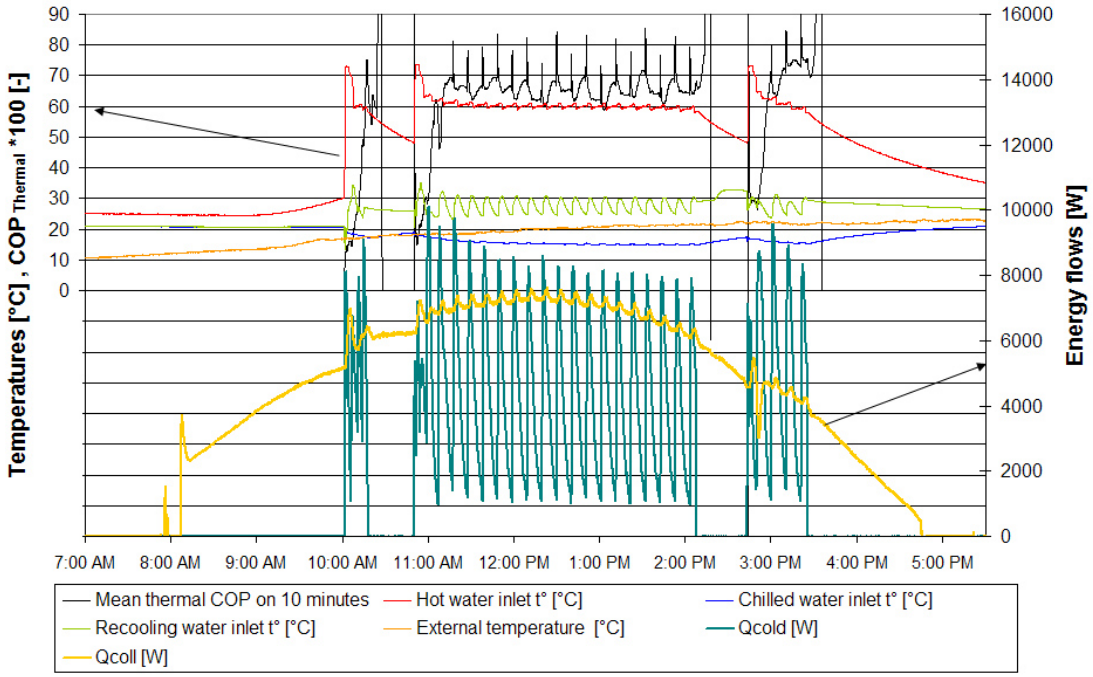

Figure 4.9: Daily energy flows and temperature for a sunny day in the *solar only* period (11^{th} August)

Period	**Solar only**	**Collectors emulation**	**Collectors emulation - Hot day**
Date	August 11^{th}	August 10^{th}	August 21^{st}
Max external temp. [°C]	23	24	30
Q_{cold} $[kWh]$	19.3	38.2	22.5
$\eta_{thermalcollector}$	0.46	0.44	0.39
COP_{therm}	0.58	0.55	0.52
$COP_{el\ chill\ pump}$	9.0	10.7	11.6
$COP_{el\ cold\ chill}$	7.4	8.8	4.9
$COP_{elec\ tot}$	5.8	6.7	3.8
$COP_{solar\ loop}$	60.7	61.3	39.0
COP_{rej}	106.0	128.4	23.5
PER_{therm}	2.32	2.67	1.53
f_{sav}	0.52	0.58	0.27

Table 4.5: Solar cooling installation daily results for three hot days

is not sufficient to keep it in operation, the inlet temperature falls below 57°C. The second start occurs when the collector power is around 7kW which is suffi-

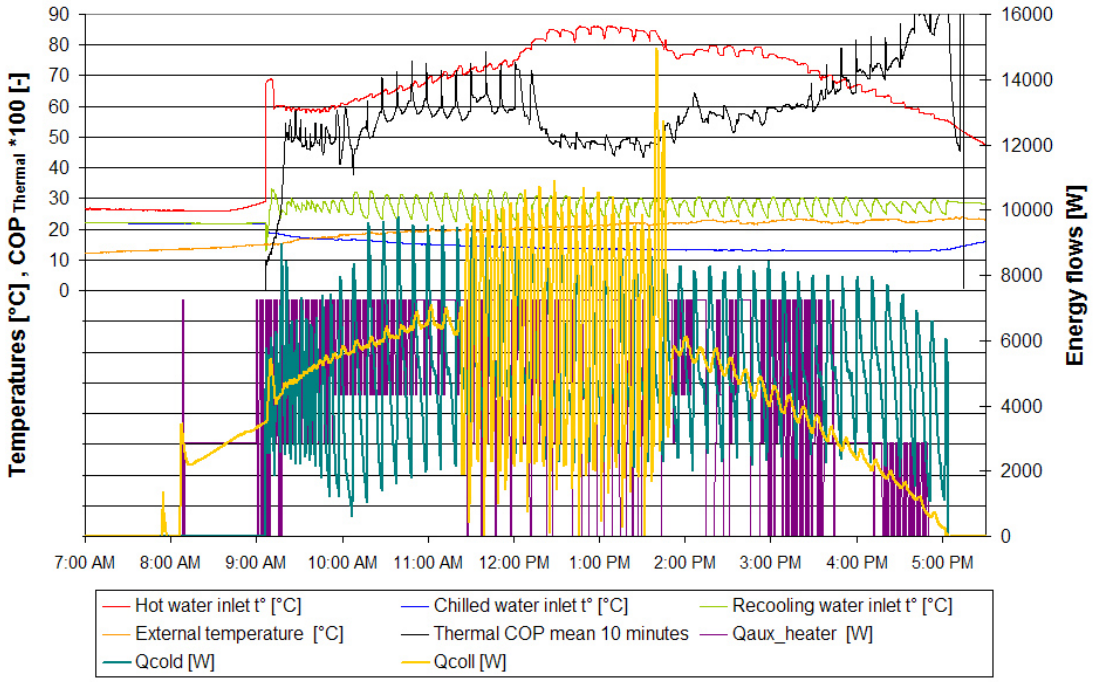

Figure 4.10: Daily energy flows and temperature for a sunny day in the *collectors emulation* period (August 10^{th})

cient to drive the adsorption chiller. When the collector power drops below 6-7 kW, the machine does not operate any more. It has to wait until the storage charges up to 70°C to do the third start. Due to the cycling of adsorption machine, the cold energy produced is varying throughout the cycle. This is also the case for driving and recooling energy flows (not mentioned in figure 4.9).

The thermal COP is shown on a 10-minute basis to filter peaks. It is quite low for the beginning of the operation periods and varies between 0.6 and 0.7 for the remaining time. The hot water temperature is quite constant (60°C) during the longest operation period, the chiller driving energy is balanced with the collector power. The machine is switched off in the middle of a cycle, the mean 10-minute thermal COP has no sense in this case (high thermal COP values are encountered as shown on black curve of figure 4.9).

The outdoor and chiller recooling inlet temperatures are also shown in figure 4.9. The system controls the fans power to reach the 27°C mean temperature on one cycle. The rejection heat flow is also varying a lot which implies changes in recooling temperature. Nevertheless, the system manages to have a mean

value of 27°C when the outdoor temperature is below 27°C.

The chiller cold water inlet should be constant (the result of an infinite load). However, the laboratory building was not able to manage a 8 kW cooling load with a 18°C water temperature supply. Consequently the chiller inlet temperature starts at 18°C at the beginning and decreases down to 15°C. The chiller cold energy produced is very sensitive to the cold inlet temperature, this explains the relatively low (4.5 kW) daily mean cold power. Taking into account a mean COP of 0.65 during the longest operation period, the cold power is consistent with the hot water power required to drive the machine ($4.5/0.65 \approx 7$ kW).

August 10^{th} (*Emulated collectors*) is characterized by a longer chiller operation: seven hours and a half. figure 4.10 shows one operation period. The chiller starts in the morning when the hot water storage reaches 65°C. The collector energy added to the auxiliary heater (14 m^2 emulated collectors) is sufficient to operate the chiller up to 5 pm, at that time the solar radiation is too low on the collector roof. The auxiliary heater power is also displayed, the seven power possibilities manage to reach 85% of the collector measured power. This difference comes mainly from the ON-OFF cycles of the solar loop pump from 11:30 am to 1:40 pm. The solar loop pump stops and restarts every two minutes when there is overheating in the collectors (this hardware security could no be supressed during the tests). The peak collector power at pump start (around 10 kW in figure 4.10) cannot be reached by the auxiliary heaters (limited to 7.2 kW).

The beginning of the day has a low driving temperature (60°C). Chiller start-up has low thermal COP as main feature. Then, a thermal COP of 0.5 is nearly reached for the period where two conditions are met: the driving temperature is low (60°C) and the cold water inlet is quite high (18°C). This differs from the August 11^{th} analysis which also deals with a low driving temperature but lower cold water temperature (15°C) and higher thermal COP (0.65). Later during August 10^{th}, the driving temperature increases as well as the thermal COP. At around midday, the driving hot water temperature reaches 85°C for one hour and a half. The chiller is equipped with a 3 way valves to avoid a temperature higher than 75°C in the chiller even if the hot storage temperature is higher. The thermal COP achieves low values for that period despite the more optimistic manufacturer's data. The rest of the day sees a decrease of the driving temperature (down to the threshold storage tank temperature of 55°C) and an increase of thermal COP. This increase comes from the delay between the charging and discharging of the adsorption chiller. The cold power produced at a certain time depends on the heat provided during the previous cycle. So the thermal COP computation shown on daily figures 4.10 and 4.9 does not consider this delay, it is the ratio between cold and heat energy flows on moving 10 minutes.

As for August 11^{th}, the system manages to have a mean chiller recooling inlet temperature of 27°C. The variation between the rejection COP for both days comes mainly from the outdoor temperature conditions.

The chiller cold water inlet also drops during this day. It drops down to 13°C implying a decreasing cold power from midday to chiller switch off. The mean cold power is 5.2 kW, a little bit higher than the other day. Here also, the chiller cold water inlet temperature affects considerably the cold energy produced. Considerations about the influence of cold water inlet of system performance are detailed hereunder.

The energy balance of August 10^{th} is displayed in figure 4.11. As for the entire period diagram, it treats the emulated and real collectors altogether. The cold energy produced is two times higher than the average produced on the whole period. The System Thermal Ratio (defined on equation 1.40 on page 49) describes the conversion quality of solar energy into cold energy. It amounts around 20% (38.24/193.15) for August 10^{th}. The storage losses have also less impact, the heat is able to be used directly in the adsorption chiller. It leads to a storage efficiency of 88%. Finally the adsorption chiller energy balance is not closed, 12 kWh thermal energy are missing on the cooling tower side. This means a certain quantity of thermal energy is brought to the adsorption but not released by the cooling tower. The measurement error put aside, this is due to the chiller heat losses. It happens when the machine is producing cold but also after its operation. When chiller stops, one of the rejection loop probe has a big temperature step (up to 50°C). There is probably the natural convection involving a water mass flow cooling the machine. Unfortunately, it was not possible to measure this flow. Anyway, there is a certain amount of heat which is not released by the cooling tower.

The outdoor temperature peaks up to 30°C during **August 21**st. The rejection COP (table 4.5) falls down to 23.5 in this hot day. The chiller controls the cooling tower fans to reach a mean inlet rejection temperature of 27°C. When the outdoor temperature is closed to or higher than 27°C, the fans consume their maximum power (1kW). It explains the very high fan consumptions for days with high outdoor temperatures leading to a decrease of energy savings by 50%. The rejection COP can be scaled by a factor 10 depending on external temperature. To decrease the fans electricity consumption, a water sprincklage device, controlled by the chiller itself, was installed below the cooling tower. Unfortunately, the measurement did not show any sprincklage operation during the testing periods.

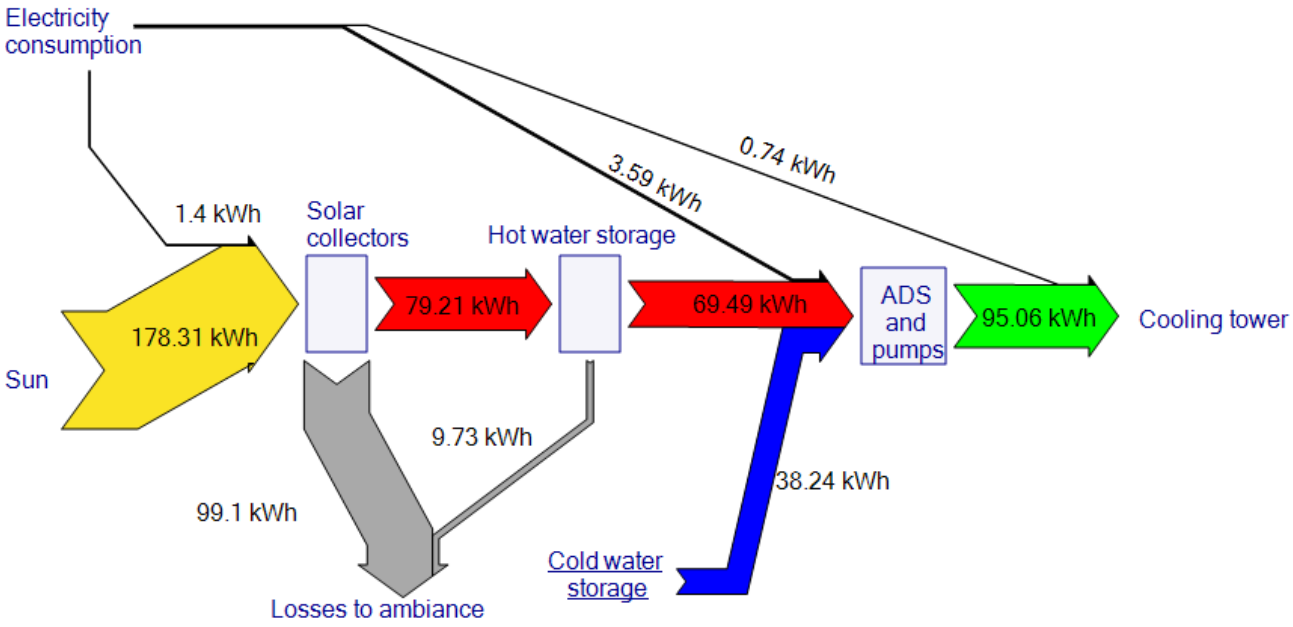

Figure 4.11: Thermal and electrical energy flows for August 10^{th} (*collectors emulation* period). Black arrows stand for electricity.

Shorter periods

This paragraph focuses on the adsorption chiller operation and its dynamics. The adsorption chiller contains two reactors and thus two cycles in phase opposition involving simultaneous charging and discharging of the adsorbers A and B (figure 4.12). This kind of chiller operation was described in chapter 1 in figure 1.23 (page 29). **Representative chiller operation** thermal flows and supply temperatures are displayed in figure 4.12 where the beginning of a cycle has been set to the rejection flow peak. It corresponds respectively to the beginning of adsorption and desorption phases of the two adsorbers. The peak encountered is the consequence of the valve moving: the recooling circuit is connected to the hot circuit for a few seconds.

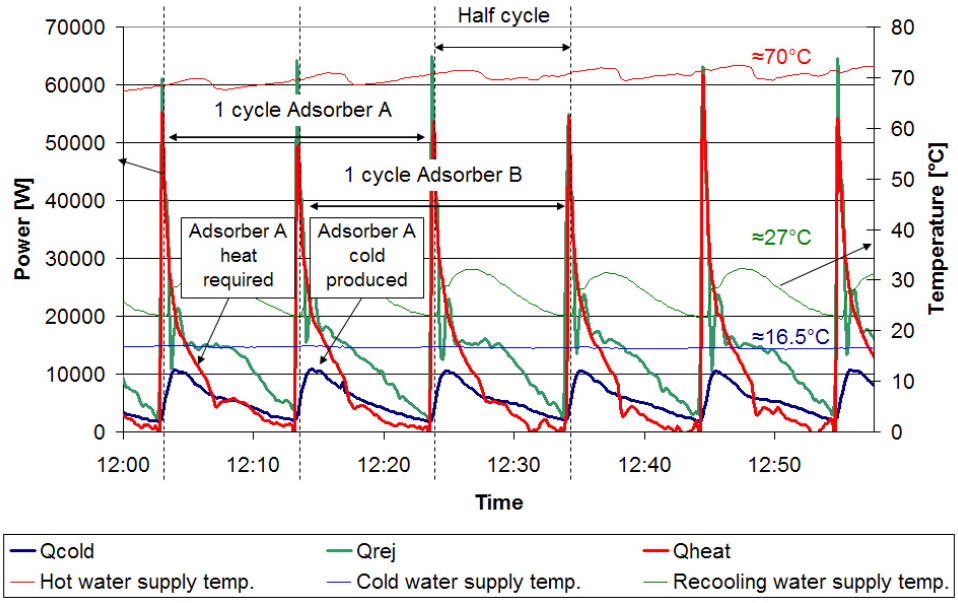

Figure 4.12: Heat flows in the adsorption chiller and three source/sink temperatures at midday on August 22^{nd}

All cycles have the same shape because of the constant supply temperatures over the cycles. The rejection temperature is not constant (maximum 10°C variation) due to high rejection flow variation and cooling tower low inertia. The mean temperature is however constant (27°C) for each cycle (outdoor temperature below 26°C). The 300 litres hot water storage has significantly more inertia, some small variations of the hot water chiller inlet (+/- 1°C) are encountered. The cold water supply temperature remains constant thanks to the cold water storage inertia. Thus, the mean supply temperatures are taken into account to characterise the half-cycle thermal behaviour.

The 10-second sampling interval makes it possible to capture the quick flows variations. Within a 10-second interval at the beginning of the cycle, the chiller hot water temperature could be decreased by 20°C. Even though the thermal COP deals with mean energy flows values, their huge variations require a high sampling frequency.

The temperature conditions met in figure 4.12 involve a cycle duration of 20 minutes, a 5.7 kW mean cold power and a 0.63 thermal COP. The **influence of chiller supply water temperatures on a cycle shape** is displayed in figure 4.13. Compared to the previous example, the cold supply temperature is higher (18.5 instead of 16.5); results shown in figure 4.13 deal with two driving temperatures 60 and 65°C. The left side of figure 4.13 shows the cycle shape for a relatively high hot water supply temperature, it gives a cycle time of 8 minutes, a 7 kW mean cold power and a thermal COP of 0.58. Those values are very closed to nominal chiller operation. The right side deals with a lower hot water temperature giving a shorter cycle duration of 6 minutes and affecting the cold power and thermal COP which drop respectively to 5.3 kW and 0.44.

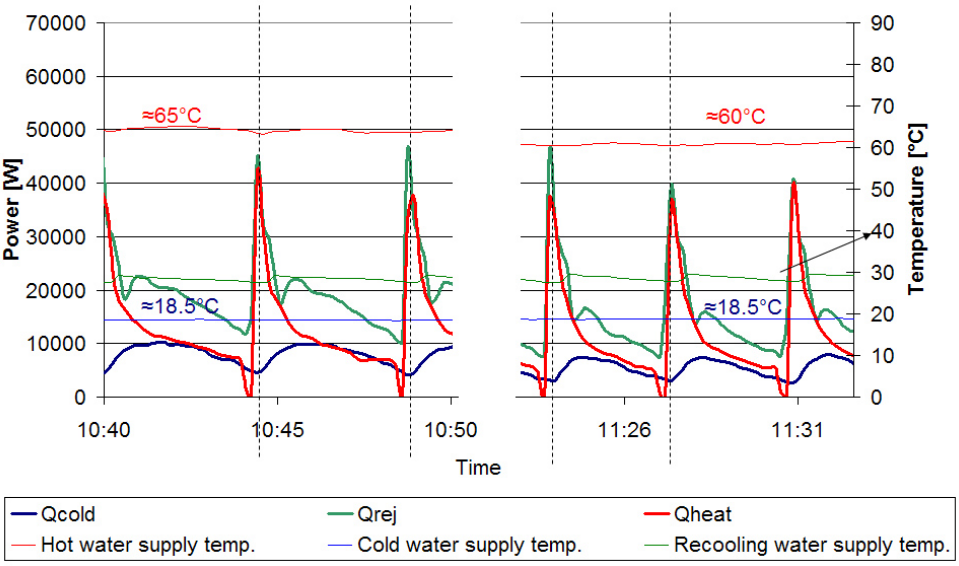

Figure 4.13: Heat flows in the adsorption chiller and three source/sink temperatures near midday on August 20^{th}

In this example, the hot water temperature influences the thermal COP while the cold water temperature affects the cold power. During the measurement periods, the mean rejection temperature was quite constant, the fan control was always able to set a 27-29°C mean temperature. Performances decrease considerably for short cycles of which driving temperature falls below 60°C. The impact of the temperatures on cycle duration and thermal COP is

analysed later in the text.

The steady state operation of chiller has been described here above, the focus is now put on the chiller start-up. A typical start-up is displayed in figure 4.14 and represents 20 minutes chiller operation since start-up. The adsorbers are loaded during the first minutes of the operation implying a low cold production, high heat consumption and short cycle duration. The steady state operation comes generally at the fourth or fifth cycle which means a time period of around 10 minutes. This will be important to handle it for chiller modelling purpose.

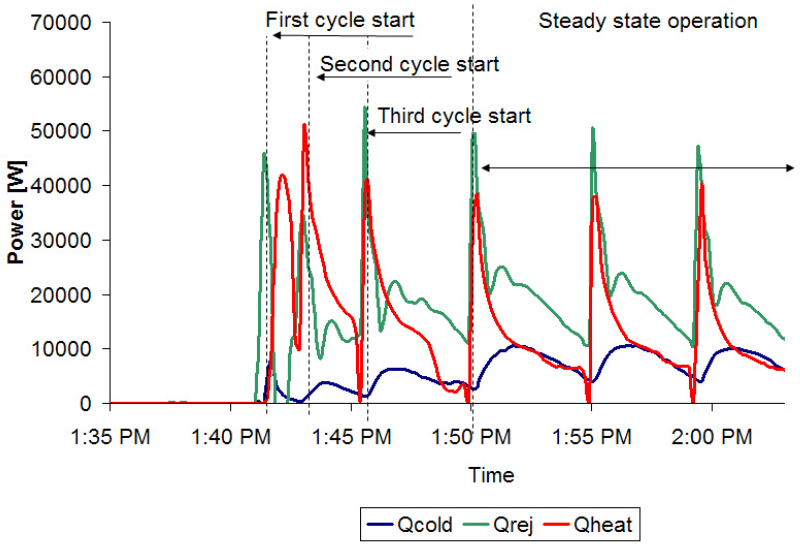

Figure 4.14: Chiller start-up on August 20^{th}

The cooling tower control is illustrated in figure 4.15. The fans power, the cooling tower supply and the return temperatures are plotted during a period involving short and long cycles. It is showed on the left side that the fan power is quite constant over the short cycle period and it manages to maintain 27°C as maximum outlet temperature. When the chiller operates with long cycles (part load operation), the fan power cycles. The fan power is high when the rejection heat flow is low, this is something which is unexpected. The moment when the chiller needs to reject a huge amount of heat (largest difference between supply and return cooling tower temperatures) reaches 31°C as cooling tower return temp. The fan control reaches a mean chiller inlet temperature of 27°C. However, it is not able to reach a constant temperature over the cycle for long cycles operation. This could impact the chiller energy performance. It seems to be a delay of the fan speed control which is not adapted to long cycles. Deeper investigations on cooling tower behaviour are done later in the

text (cooling tower modelling paragraph).

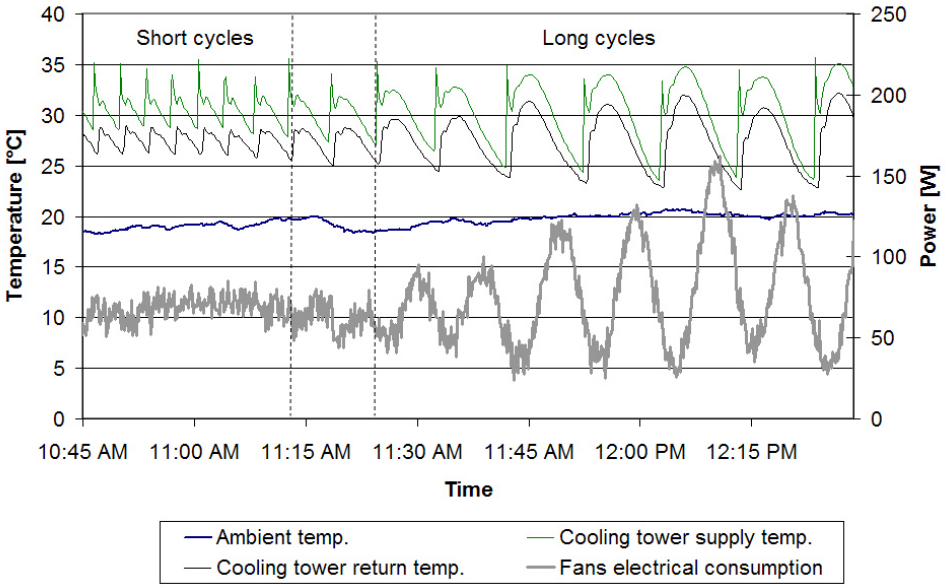

Figure 4.15: Cooling tower fans consumption near midday on August 22^{nd}

4.1.4 Adsorption model validation

The monitoring results emphasize the performance of adsorption chiller regarding the inlet temperatures and also shows a different thermal behaviour occurring at start-up. This paragraph explains the thermal modelling of the adsorption chiller. The analysis deals with the heat flows measurement outside the machine to determine its thermal COP and cooling capacity. The objective is to create a simple model to evaluate as accurately as possible the thermal performance of the adsorption chiller. It could be used afterwards in an energy simulation software to evaluate the performance of a solar cooling system throughout the cooling season.

Existing adsorption chiller models

The existing simulation models for adsorption chillers can be separated into two categories according to Döll (2011):

- Dynamic models that try to represent the actual physical phenomena inside the machine as described by Schicktanz *et al.* (2012) or Wang and Chua (2007)
- Static models that simplify the physical phenomena (they are often using performance map) as described by Albers and Römmling (2002)

Both approaches have their drawbacks. Since dynamic models can reveal the real adsorption phenomenon, they can be used for optimization of operation or materials characteristics evaluation. Those models are generally high computer resources consuming which makes annual system simulation infeasible. The static models are more flexible but less accurate. Yearly simulations overestimate commonly the energy performance of systems (Thomas *et al.*, 2012).

The results of a model using a performance map is shown in figure 4.16 for the studied adsorption chiller, it highlights the importance of a wide range of measured performance points. The large operation temperature range given in manufacturer's data sheet (summarized in table 4.1) is not fully described in the performance map. For example, it is not possible to know the machine behaviour at higher rejection temperature combined with lower cold water temperature.

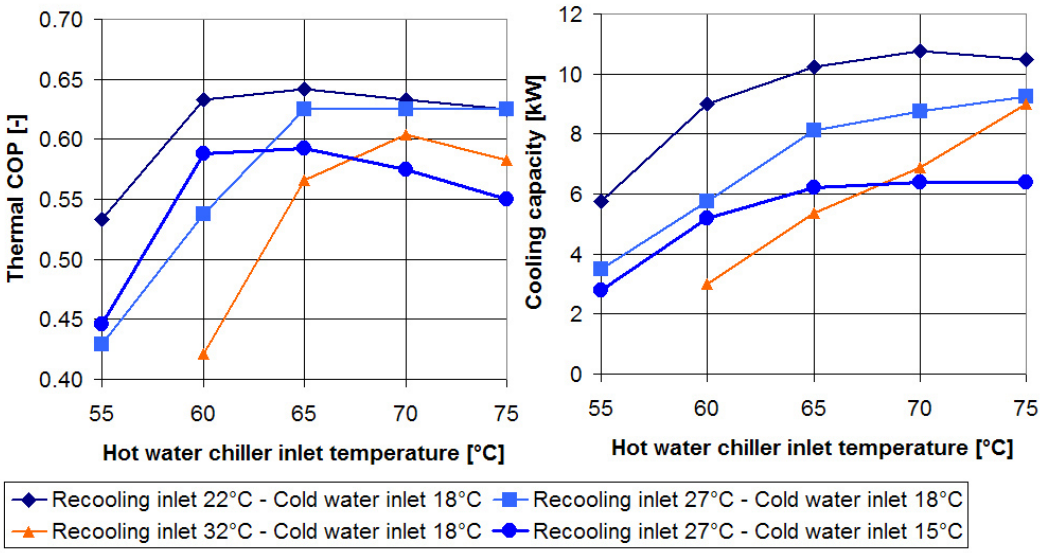

Figure 4.16: Manufacturer performance map for thermal COP and cooling capacity (INVENSOR, 2010)

Another approach has been recently chosen by Döll (2011) and Frey (2011); they have developed a dynamic model without entering into the physical phenomenon. Their Artificial Neural Network models predict the machine behaviour depending on the three temperatures and the mass flow rates. The model is calculated by learning the experimental data. They found a really good agreement between the model and the experimental data with this technique (less than 1% error on COP for 8-hour test period).

This kind of model uses a short sampling data series (30 seconds) that is not compatible with yearly building simulations. The data recorded on the machine studied in this work shows heat flows huge variations within a shorter period than 30 seconds (especially for the hot water energy flow in figure 4.12). Moreover, there is clearly a lack of physical sense in this model.

New adsorption chiller model

The idea of the new model developed in the following paragraphs is to take the dynamics of the system in a long time scale into account (longer than cycle duration) and filter short time dynamics (shorter than cycle duration). One cycle has its own dynamics, it is repeated each time. Otherwise, in figure 4.14, a transient start-up period and a steady-state period can be determined. The proposal is to create a model based on some mean half cycle values (half cycle is represented in figure 4.12). The model is based on measurements and not on the machine physical properties; consequently, it could be exploited only for this kind of machine.

The main assumptions for this model are:

- The thermal behaviour of the adsorption chiller can be split into two parts: start-up and steady-state
- Inlet temperatures are nearly constant throughout the cycle
- There are no mass flow modifications (the nominal mass flows are used)
- The steady-state half-cycles are only influenced by the previous half-cycle

The last assumption needs more explanation: one cycle entails the succession of heating and cooling of an adsorber (cycle description in figure 1.23), there is no energy storage on a longer time scale. The cold energy produced during the adsorption phase depends on the cold water inlet temperature and recooling inlet temperature **within this phase** and on the hot water temperature charging the adsorber during **the two previous phases** (namely the Constant volume compression and Desorption). This interpretation leads to forget all information about cycle operation before the previous adsorber loading to model the adsorption chiller. This assumption is not taken for the chiller start-up because it handles the first charge of the adsorbers.

On the one hand, the model proposes a performance map of cooling capacity and heat input (thermal COP can be deducted) for the chiller in steady-state operation. That will be compared to the manufacturer static performance map. On the other hand, it provides coefficients to modify the performance map to handle the start-up period.

Data processing

It has been decided to use mean half cycle measurements. To split the data into the half-cycles, the rejection heat flow peak is taken as the beginning. As

mentioned before, it corresponds respectively to the beginning of adsorption and desorption phases of the two adsorbers. In fact there are two peaks (figure 4.12) but the second one is not significant for the half cycle splitting. A peak detection routine is implemented to split the half-cycles correctly. Initially, the hot water heat flow peak was chosen but there is a delay between the two curves during the beginning period (figure 4.14). The rejection peak was finally found to be more representative of the process start. The last half-cycle before switching off the chiller is removed from the analysis handling with the entire half-cycles.

The data processing stores useful information about each half-cycle, the most important variables are presented in table 4.6. Around 2900 half-cycles were recorded during the 2012 test period.

Variable name	**Unit**	**Explanation**
Cycle Start	[s]	Time stamp of half-cycle beginning
Cycle End	[s]	Time stamp of half-cycle ending
$\dot{Q}_H$	[W]	Mean hot water energy flow
$\dot{Q}_C$	[W]	Mean cold water energy flow
$\dot{Q}_M$	[W]	Mean cooling water energy flow
$T_{H\ in\ mean}$	[°C]	Mean hot water t° entering the chiller (T90)
$T_{M\ in\ mean}$	[°C]	Mean cooling water t° entering the chiller (T94)
$T_{C\ in\ mean}$	[°C]	Mean cold water t° entering the chiller (T92)
$T_{H\ in\ max}$	[°C]	Max hot water t° (T90)
$T_{H\ in\ min}$	[°C]	Min hot water t° (T90)
Cycle Time	[s]	half-cycle duration
Time machine operating	[s]	Time elapsed between the last machine start-up and half-cycle beginning

Table 4.6: Most important variables stored for each half-cycle

Steady-state operation modelling

First of all, it is important to distinguish the beginning period and the steady-state one. To do this, the comparison is carried out between measured thermal COP and manufacturer steady-state performance curves. Half-cycles are sorted by time elapsed since machine start in figure 4.17. The beginning period stands for measurements that do not meet the manufacturer's data at all: 10 minutes is kept as beginning period, it is avoided in the steady-state analysis (around 2200 half-cycles remaining). Döll (2011) says that adsorption chillers need around two hours to reach steady-state operation. This assertion is not verified with our measurements, there are no thermal COP modifications due to the time operating machine.

Around 1700 half-cycles are kept for the steady-state analysis, they all meet the following requirements:

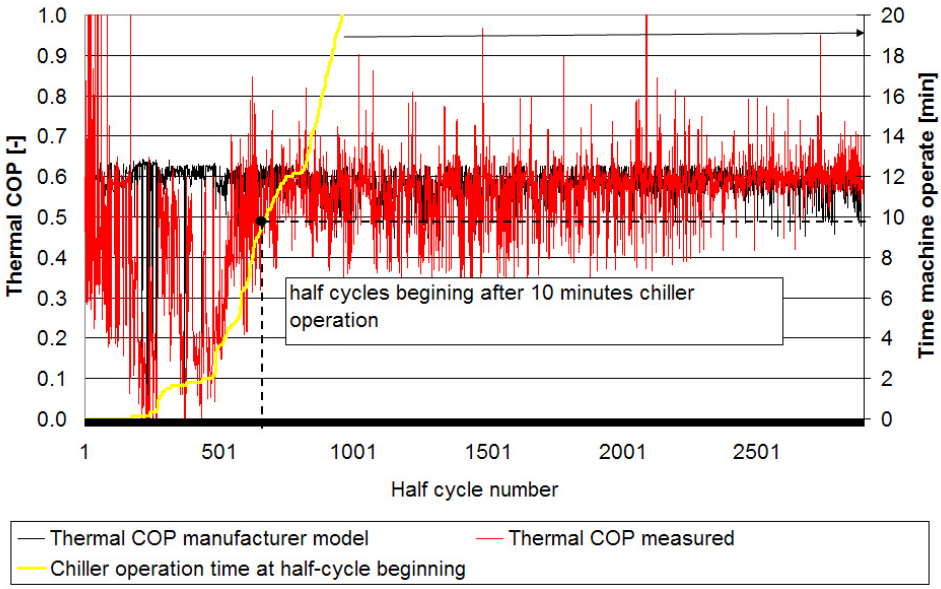

Figure 4.17: Half-cycle COP measured and computed sorted by chiller operating duration

- They begin at least 600 seconds after the chiller start-up (steady-state operation)
- They have a mean driving temperature between 55 and 75°C (consistent with the manufacturer temperature range)
- They have a slight hot temperature variation through the cycle < 4°C (consistent with the mean temperature hypothesis)
- They don't have a too low cold inlet temperature >10°C (consistent with the manufacturer temperature range)

The manufacturer model (performance map) has a good agreement with the mean measured COP on the total measurement period (2.4% error with the mean thermal COP = 0.574). Otherwise, the standard deviation of the thermal COP variation (manufacturer and measured) is high as pictured in figure 4.18. In other words, the performance map gives meanly the correct COP but there are important variations between half-cycle thermal COP measured and modelled with the performance map. The error is much more important on the cooling capacity, the measured one is 30% lower than the manufacturer model. The cooling capacity measured and computed with manufacturer performance map is presented in figure 4.19 for the two modes emphasized before: short cycles ($<$ 10 minutes) when the cold supply temperature is above 17°C and long cycles (20 minutes) in other cases. A very few other intermediate duration cycles can be found in figure 4.20, they involve a cold water temperature

close to 17°C.

Two kinds of operation can be distinguished. As a reminder, the chiller cold water set point is 15°C on the whole measurement period. When the outlet chiller cold temperature gets closer to 15°C, the chiller starts to operate in part load conditions. **Short cycles entail full load operation while long ones describe part load operation**. The manufacturer model does not indicate whether it is full load (short cycles) or part load (long cycles) operation. As shown on figure 4.19, the manufacturer capacity data seems to be closer to the full load operation one. The part load operation does normally not reach the maximum cooling capacity. The chiller control ranges the cycle duration between 3 and around 10 minutes to satisfy the cold water set point. It does not stop when the cold water set point is achieved but still operates at its lower capacity.

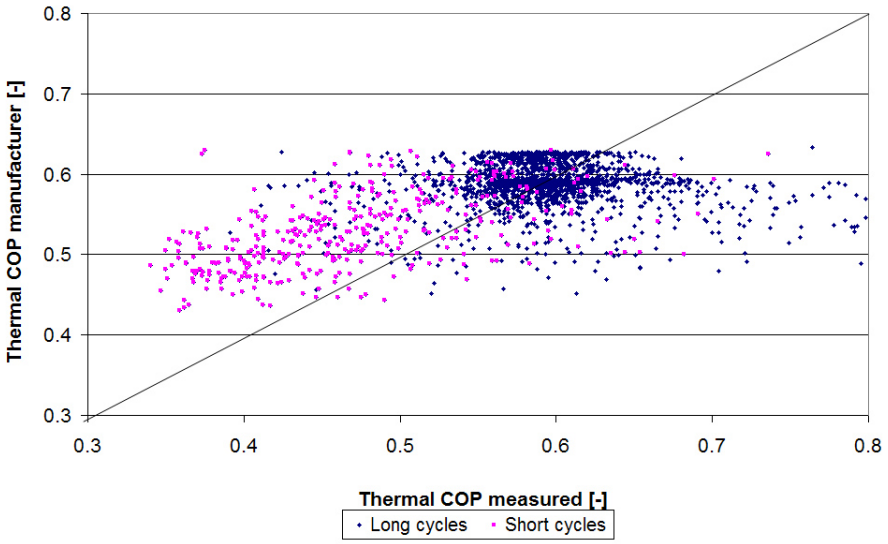

Figure 4.18: Half-cycle thermal COP measured and computed with manufacturer performance map

The model is a correlation between the cold energy measured and some other measured variables that do not directly depend on the chiller behaviour. Those variables are the mean chiller inlet temperatures in the current half-cycle or previous half-cycles. Moreover, they include the difference between those temperatures levels. A stepwise linear regression is achieved with those variables.

The two most significant variables to explain the cold energy produced ($\dot{Q}_{cold}$) are $T_{H\ in\ mean}$ at previous half-cycle and ($T_{M\ in\ mean} - T_{C\ in\ mean}$). This corroborates the influence of the previous cycle on cold production. The heat energy input ($\dot{Q}_{heat}$) most significant variables are $T_{H\ in\ mean}$ and ($T_{M\ in\ mean} -$

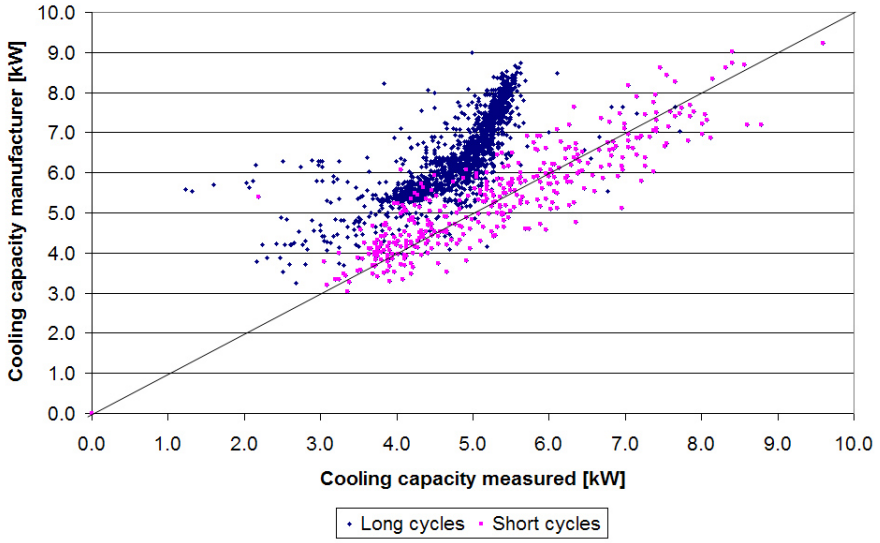

Figure 4.19: Half-cycle cooling capacity measured and computed with manufacturer performance map

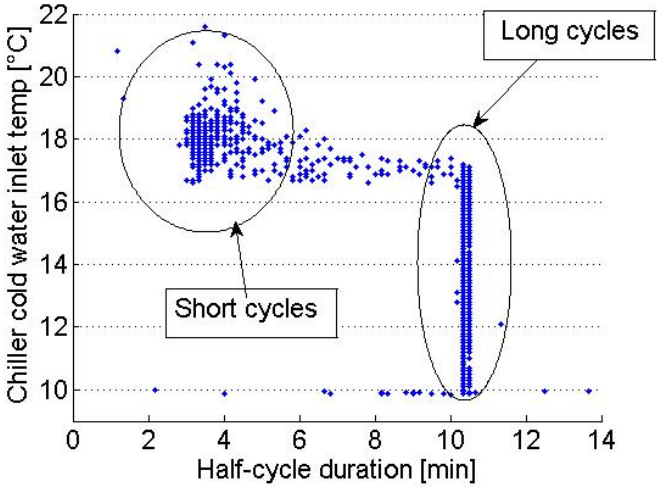

Figure 4.20: Duration of half-cycles in relation to the chiller cold water inlet temperature

$T_{C\,in\,mean}$).

As the rejection temperature was around 27°C and did not vary a lot, the analysis is only valid for the mean chiller inlet rejection temperatures ranging from 26°C to 29°C. The relatively low upper bound is due to the low outdoor

temperature during the testing period while the lower bound is a consequence of the fan control trying to reach 27°C.

Knowing the important variables, it is now interesting to investigate the correlation functions. Taking the theoretical sorption cycle into account (chapter 1, figure 1.21 on page 27), the cold production depends on the amount of sorbent adsorbed. The x-axis is in fact -1/T while the pressure depends on the temperature with an exponential law. The best estimation (least square method) of the cold and heat production is given by the functions detailed in equations 4.2, 4.3 and table 4.7 where the temperatures are expressed in °C.

$$\dot{Q}_C = a{\cdot}exp(b{+}c{\cdot}T_{H\ in\ mean\ -1}){+}\frac{d}{T_{H\ in\ mean\ -1}}{+}\frac{e}{T^2_{H\ in\ mean\ -1}}{+}\frac{f}{(T_{M\ in\ mean} - T_{C\ in\ mean})}{+}g\ [kW] \tag{4.2}$$

$$\dot{Q}_H = a \cdot exp(b + c \cdot T_{H\ in\ mean}) + \frac{d}{T_{H\ in\ mean}} + \frac{e}{T^2_{H\ in\ mean}} + \frac{f}{(T_{M\ in\ mean} - T_{C\ in\ mean})} + g\ [kW] \tag{4.3}$$

Where $T_{H\ in\ mean\ -1}$ means $T_{H\ in\ mean}$ at previous half-cycle.

The distinction between short and long cycles is carried out by two threshold values. The long cycles are characterized by a low input temperature ($<$ 17 °C) and a long duration ($>$ 450 seconds). The short cycles are characterized by a high input temperature ($>$ 17°C) and a short duration ($<$ 450 seconds). The error is also mentioned in table 4.7 (RMSE means Root Mean square Error) for both sets of data. 80% of the data are used for building the model while 20% is used for testing it. The global error describes the total error on the whole operation duration.

The graphical view of equations 4.2 and 4.3 is then displayed in figure 4.21 for both models: short and long cycles. Moreover, the ratio of the cooling capacity and the heat energy input functions (thermal COP) curve are mentioned. This last curve considers that $T_{H\ in\ mean\ -1}$ equals $T_{H\ in\ mean}$ for graphical purposes. This figure reveals the influence of hot water inlet temperature on cold production.

For the long cycles, the maximum cold energy produced is encountered for an inlet temperature near 68°C, the horizontal distance between >5 kW curves decreases when the temperature difference between rejection and cold flows increases (the chiller has to fill a higher temperature difference between condenser and evaporator). Besides, in the case of long cycles, the thermal performance of the machine is nearly constant (thermal COP $>$ 0.5) over the entire temperature range while it varies a lot in case of short cycles. To obtain a thermal COP of 0.5, the hot source temperature has to reach 61-63°C for short cycles, 55-56°C for long cycles. During a long cycle, the adsorption and desorption

periods are longer involving a higher quantity of water adsorbed/desorbed in the beds. Nevertheless, the cooling capacity is lower because of the longer cycle. The higher thermal COP compared to the short cycle is due to the fewer switches heating/recooling of the adsorber for a given period.

The short cycles take advantage of the first minutes of the adsorbers loading/unloading leading to a high rate of refrigerant adsorption/desorption and thus a high cooling capacity. The disadvantage is the thermal losses of the numerous heating/recooling cycles of the adsorbers involving a lower thermal COP. In this operation mode, the hot water temperature has a considerable impact on the chiller performance (cooling capacity and thermal COP).

Generally the cooling capacity and the thermal COP decrease as well as the temperature lift ($T_M - T_C$) increases. The adsorbers design and operating pressures of the chiller lead to an optimal hot water inlet temperature of 65-70°C as foreseen by the manufacturer performance map (figure 4.16). Beyond this point, the losses become greater and the thermal COP lower.

	Long cycles		**Short cycles**	
Parameter	$\dot{Q}_C$	$\dot{Q}_H$	$\dot{Q}_C$	$\dot{Q}_H$
a	0.032	0.099	0.143	0.041
b	-0.900	-0.721	0.357	-2.897
c	0.084	0.074	0.019	0.024
d	18175	25580	-6314	-167
e	-565935	-790308	142685	-48951
f	16.129	30.739	28.874	37.384
g	-144.788	-206.258	67.177	23.828
Model accuracy				
RMSE test data	0.172	0.299 [kW]	0.273 [kW]	0.603 [kW]
RMSE all data	0.171	0.285 [kW]	0.158 [kW]	0.293 [kW]
Global error	0.1 [%]	1.9 [%]	0.3 [%]	-1.8 [%]
Global COP_{therm} error	1.8 [%]		1.5 [%]	

Table 4.7: Steady-state model parameters and accuracy

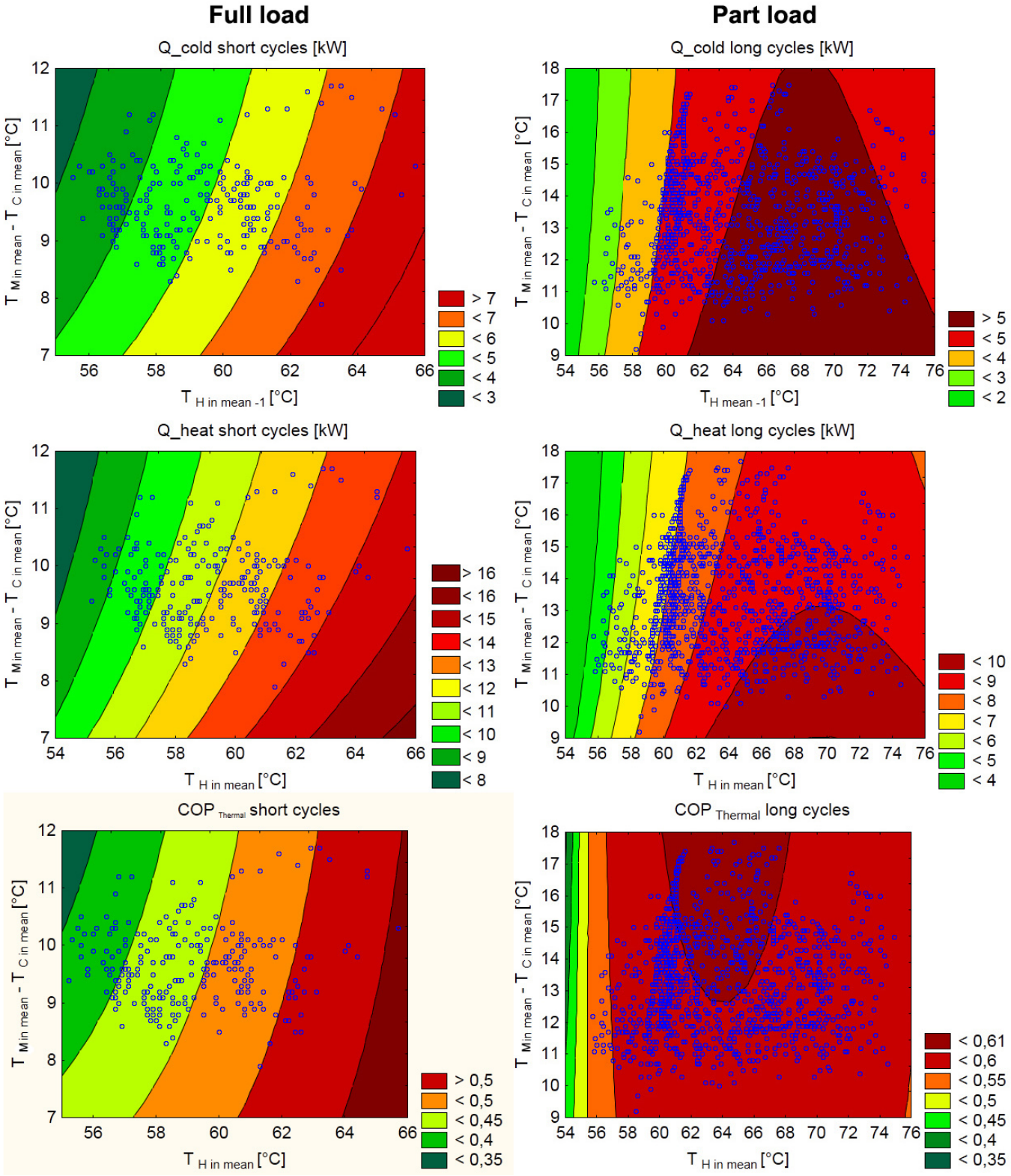

Figure 4.21: Steady-state model cold produced, heat consumed and thermal COP

Figure 4.21 also shows the measured half-cycles (blue points). This points out the representativeness of the model. Much more long half-cycles have been recorded (right graphs) while there are only low hot temperatures short half-cycles. This gives in table 4.8 the new created model validity temperature ranges. Unfortunately, the new model cannot describe the chiller energy performance on the whole temperature range. In comparison with the manufacturer's data, high hot water temperature combined with high cold water temperature is not handled in the new model. However, low cold water temperature operation is wider handled in the new model.

Criteria	**Short cycles Full load** $T_{C\,in\,mean} > 17$°C	**Long cycles Part load** $T_{C\,in\,mean} \leq 17$°C
$T_{H\,in\,mean}$	55-65 °C	55-75 °C
$T_{R\,in\,mean}$	26-29 °C	26-29 °C
$T_{C\,in\,mean}$	17-19 °C	10-17 °C
$T_{R\,in\,mean} - T_{C\,in\,mean}$	8-12 °C	9-18 °C
$T_{H\,in\,max} - T_{H\,in\,min}$	< 4°C	< 4°C

Table 4.8: Steady-state model temperature validity ranges

The comparison between the manufacturer's data and the model gives the curves shown in figure 4.22. As mentioned below, the validity range of the model is restricted to the measured half-cycles. So, for chiller full load (inlet temperature > 17°C), there are no measurements above 65°C. Besides, the model is obviously valid for a cold water set point of 15°C.

The trend of the manufacturer curve is confirmed by the new model based on the measurements. The two operation modes (short and long cycles) give respectively a good agreement with the cooling capacity and the thermal COP. Square and diamond markers curves in figure 4.22 represent the short cycle (full load) operation. The left graph shows a lower measured COP than the manufacturer's data (- 0.06) while the measured power on the right graph is close to the manufacturer value. It is the opposite for the part load (triangle and circle markers): the COP is closer to manufacturer while the chilled cooling capacity is decreased by at least 1 kW. Given our measurement results dealing with full load operation for high cold water inlet temperatures (> 17°C) and part load operation for colder water inlet, **it seems that the manufacturer's data shows the cooling capacity of full load operation and the COP of part load operation**. Indeed, full load operation gives more cold production but does not operate in optimal conditions (decreasing the thermal COP).

The measurement error is mentioned in figure 4.22. The large thermal COP error (10%) is the same for the full load and part load curves (not mentioned for the part load for readability purpose). Despite its high value, the COP measurement error does not explain the difference between the manufacturer's

data and the computed values for full load operation. Moreover, the measured cooling capacity error in part load is lower than the difference between the manufacturer curve and the model. The manufacturer's curves are not reproduced even if the maximum errors are taken into account.

Focusing on thermal COP at part load and cooling capacity at full load reveal some small differences between the curves in figure 4.22. These differences are lower than the maximum error. The probe location could also be source of additional differences between measured and manufacturer's data: the probes for temperature measurements are located at the outlet of the hydraulics module while the manufacturer curve deals only with the chiller itself. Our measurements include losses in the hydraulics module and the thermal influence of pumps. Nevertheless, the impact is not important: the hydraulics module is well insulated and pumps for hot and cold loops consume less than 150 W each. What is measured in our case is the real energy flow consumed/produced by the system (including chiller and hydraulics module).

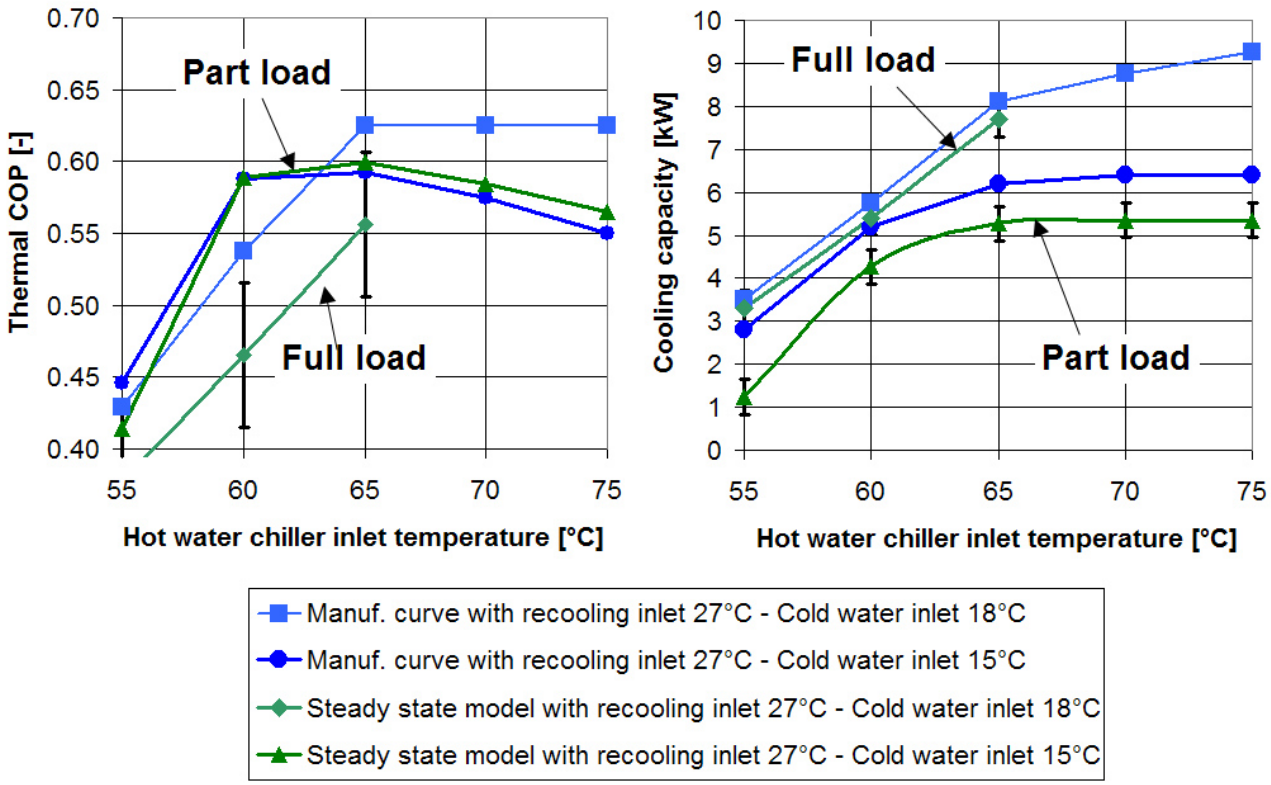

Figure 4.22: Manufacturer performance map comparison with the steady-state model of the chiller

Start-up operation modelling

As seen in figure 4.14 on page 165, the start-up period entails uncommon half-cycles. The shape of the energy flows can be different each time the chiller starts. The variables impacting the chiller thermal behaviour can be split into two parts: the current supply temperatures of the three flows and the past chiller activity. The first part deals mainly with the steady-state model developed before, while the second part emphasizes the following phenomena:

- The duration since last operation
- The adsorbers state (charging-discharging) at last chiller switch off
- The chiller energy flows and temperature levels through the last cycle.

The sensible heat or cold energy stored in the different parts of the chiller decreases with stand-by duration. The last two items suggest to handle the energy stored in the adsorbers. The two adsorbers operate in phase opposition, they are respectively being loaded and unloaded when chiller is turned off. The chiller can be turned off whatever the cycle status, it is then very difficult to know the loading/unloading level of the two adsorbers. Moreover, the data treatment deals with complete half-cycles and it does not include the thermal behaviour of the last initiated half-cycle before turn off.

Despite the very little available information about the last operation adsorber loading/unloading it is proposed to model the chiller start-up operation. As a reminder, the start-up period was set to 10-minute operation according to figure 4.17. As the purpose of the model is to evaluate the yearly performance of a solar cooling system, it implies simulation time step with an order of magnitude of 10 minutes. In other words, it is not necessary to analyse each half-cycle of the start-up period (they have particularly short duration). The start-up period is then summarized by a mean operation representative of all half-cycles starting sooner than 10 minutes after the chiller switches on. Moreover, a start-up period occurs if there is at least 20 minutes stand-by period, otherwise the chiller operation is considered as continuous.

Given this mean Start-up behaviour, a comparison with the steady-state model is made. The comparison includes 114 chiller start-ups within the temperature range (see table 4.8) of steady-state model. Figure 4.23 emphasizes the ratio between the measured cooling or heating power and the computed one with steady-state model in relation to the time elapsed since last turn off.

Firstly, for any start-up which occurs at least one hour after turn off, the heat energy consumed during start-up is higher than heating power given in steady-state model. It is the opposite for cold energy produced. During the start-up period, the chiller needs more energy and produces less than during the steady-state mode. Heat and cold sensible energy of the chiller is especially lost when the stand-by period is long.

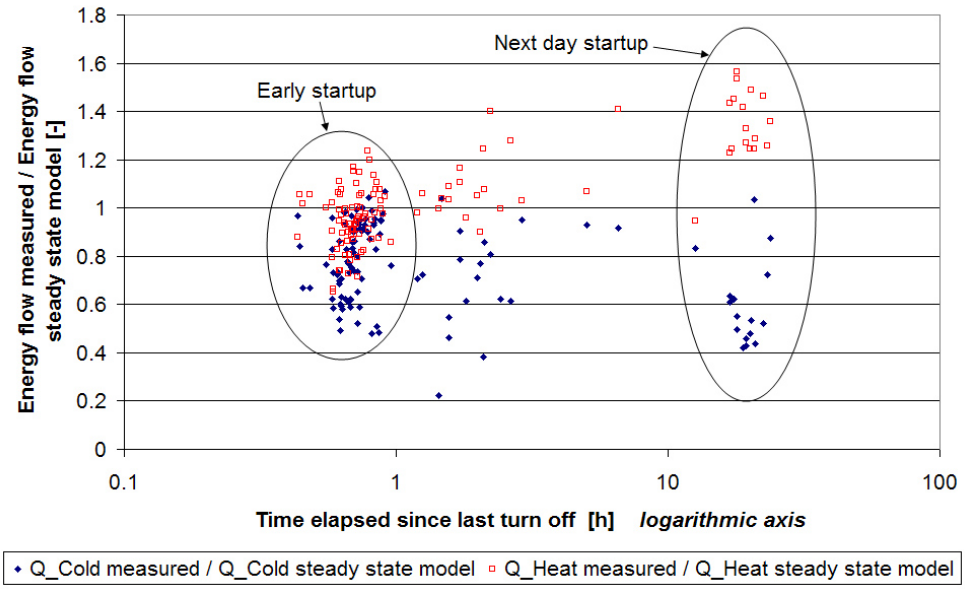

Figure 4.23: Start-up behaviour compared to steady-state model

Secondly, the early start-up points show high variability. There is globally a lower cold energy produced but no significant extra heat consumed. Within one hour stand-by, the chiller sensible energy is not much lost. In both cases, the variability of points is due to the chiller load before last turn off. It is proposed to take one of the last operation variable into account to explain this variability: the mean supply hot temperature of last recorded half-cycle ($T_{H\ in\ mean\ -1}$).

A non linear estimation of the ratio between start-up and steady-state heat and cold energy mean power is carried out. The functions are chosen according to the physical phenomenon: the decrease of sensible energy follows a logarithmic curve in relation to the time; the extra energy available at current start-up is proportional to the difference between the hot temperature supply during last half-cycle and the mean hot temperature during the current start-up. The model equation is presented in equation 4.4 (same equation for the mean heat consumed) while the model accuracy and parameters are written in table 4.9. The root mean square error expressed is considerably high while the seasonal error is low. All measured points have been used to build the model which

represents consequently a mean measured behaviour. The high variability due to the unknown chiller load at switch off is not handled.

$$\frac{\dot{Q}_{C\ start-up}}{\dot{Q}_{C\ Steady\ State}} = a{\cdot}ln(stand{-}by\ Duration){+}b{\cdot}(T_{H\ in\ mean}{-}T_{H\ in\ mean\ -1}){+}c\ [-] \tag{4.4}$$

Where *stand-by Duration* is expressed in hours between the beginning of last complete half-cycle and the current chiller start-up.

Parameter	$\frac{\dot{Q}_{C\ start-up}}{\dot{Q}_{C\ Steady\ State}}$	$\frac{\dot{Q}_{H\ start-up}}{\dot{Q}_{H\ Steady\ State}}$
a	-0.0344	0.1106
b	0.0133	-0.0089
c	0.8149	0.9639
Model accuracy		
RMSE all data	0.880 [kW]	1.120 [kW]
Global error	0.37 [%]	0.41 [%]

Table 4.9: Start-up model parameters and accuracy

Some comments must be added about this new start-up model:

- There is no significant difference between both models (short and long cycles), the steady-state cycle duration does not influence the start-up energy performance.
- It is difficult to evaluate the chiller inertia because of the lack of measurement inside the chiller itself. The measurements at the machine boundary do not allow to better understand its transient operation during starting period.
- There are not enough start-ups to build a robust model, the trend is shown but no precise evaluation can be carried out.
- The heat balance of the chiller is not met for start-up periods as it is loaded with thermal energy. It has no sense to compute directly the rejection thermal flow as the sum of heat and cold flows. The model does not currently involves the heat rejection thermal flow computation.
- The knowledge of the adsorption beds state at last switch-off is an interesting thing to investigate for futur researches.

4.1.5 Dry cooling tower modelling

The performance of solar air-conditioning systems strongly depends on the chosen heat rejection system and its control strategy. The control affects the system electrical COP ($COP_{elec\ tot}$) by around 50% for wet and dry cooling

towers (Eicker *et al.*, 2012). The fan speed control present in the installed system appears to be a good solution for energy savings.

Besides, the influence of dry cooling tower on the measured system performance is emphasized in daily results (table 4.5 on page 158) where the energy savings can be diminished by 50% on a hot day. The outdoor temperature has therefore a huge impact on electricity consumption.

The electricity consumption of a cooling tower is generally given in terms of fan nominal power divided by the rejection power (inverse function of the COP_{rej} already defined in equation 1.20). Various values are encountered in the literature, some of them are presented in table 4.10. There is a wide range of measured values, a nominal value is not enough to evaluate the cooling tower electrical consumption. It is consequently proposed to model the dry cooling tower behaviour.

	$kW_{elec\ fan}/kW_{rej}$	COP_{rej}	**Reference**
Literature			
Open cooling tower with axial fan	0.018	56	DIN18599-7 (2007)
Closed cooling tower with axial fan	0.033	30	DIN18599-7 (2007)
Dry cooler	0.045	22	DIN18599-7 (2007)
Dry cooler	0.008-0.01	100-125	Measured Sparber *et al.* (2009a)
Installed system			
Dry cooler	0.04	25	Nominal value
Dry cooler	0.002-0.07	14-500	Measured value

Table 4.10: Cooling tower fan consumption

Measured electrical consumption

The measurements also deal with the mean half-cycles duration measurements (data sampling: 10 seconds). The fan control manages to reach 27°C as mean cooling tower outlet temperature, whatever the external temperature (< 26.5°C). Besides, the cooling tower mass flow rate is constant (75 l/min). The cooling tower electrical COP (defined in equation 1.20 on page 46) is then correlated with the external temperature. This variable is adequate to explain the electrical COP variability. Figure 4.24 shows the electrical COP and the fan power for each measured half-cycle in relation with the external temperature.

The start-up operation half-cycles are not included in the analysis. High electrical COP is encountered for low external temperature while it falls to 15 when the outside temperature is higher than 27°C. The electrical COP is quite linear below 27°C outside temperature. The variability of the electrical COP for a given outdoor temperature could be attributed to the measurement error

and other effects such as the delay of the fan control seen in figure 4.15 (page 166). Nevertheless, the trend of electrical COP is clearly depicted by figure 4.24.

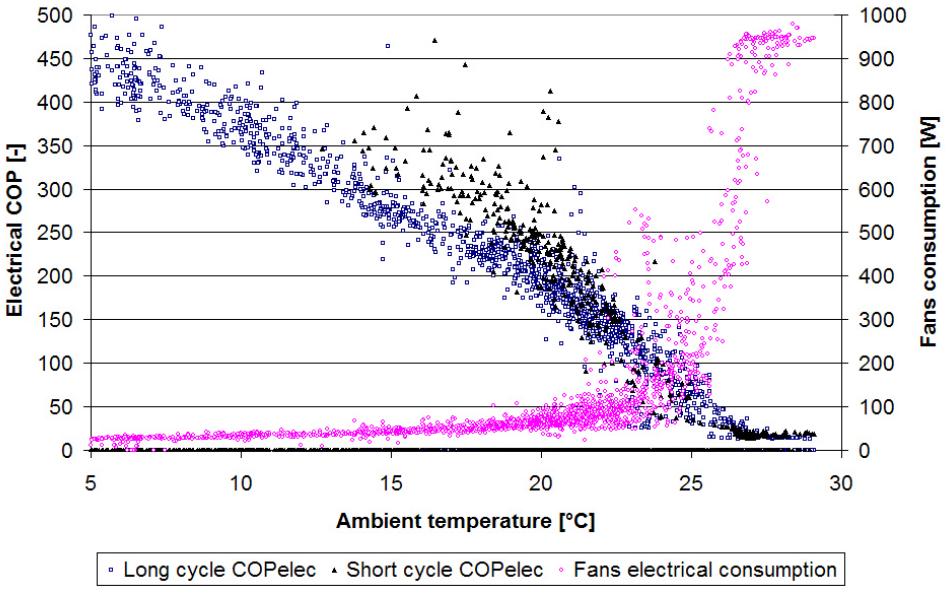

Figure 4.24: Measured cooling tower electrical COP and fans consumption

The strange control of fans for a long cycle operation (mentioned in figure 4.15) affects a little bit the electrical COP of the cooling tower. The electrical COP of long and short cycles is distinguished in figure 4.24. The long cycles have a slightly lower electrical COP for the same external temperature. Despite this difference, the analysis deals with one cooling tower model for both short and long cycles.

As a first approximation, between 15 and 26°C outdoor temperature the electrical COP decreases by 25 for each outdoor temperature degree decrease. For outdoor temperatures above 27°C, an electrical COP value of 15 could be considered. This shows the influence of outdoor temperature, a COP value of 25 is commonly accepted for a wet cooling tower (Henning and Döll, 2012), it corresponds to an outdoor temperature of around 26°C for the dry cooling tower.

From the electrical consumption point of view, three regions can be distinguished:

- Low outdoor temperature (<15°C) involving low fan consumption <50W. The fans are operating at their minimal power.
- Intermediate temperature involving fans control to reach 27°C.

- High outdoor temperature (> 26°C) where maximum fan power is encountered (950 W).

Thermal model

To go deeper in the cooling tower analysis it is proposed to model its thermal and electrical behaviour. The objective is also to achieve seasonal evaluation of solar cooling system performance. An existing model (Thornton, 2010) is tuned with measured power.

The model already implemented into TRNSYS computes the fan control signal to reach a desired cooling tower outlet temperature. This involves a heat transfer computation based on design conditions. As mentioned below, the cooling tower fan consumption (which has a cubic relation to the air volumetric flow rate) is greatly affected by the external temperature. The model handles therefore variable air flows.

The cooling tower nominal heat flow measured is 21.5 kW ($\dot{Q}_{DCT\,design}$). Even if the cooling tower comes from the manufacturer, it does not reach the same cooling capacity as the provided data. Discussions with the manufacturer are still in progress to find out what is the real cooling capacity of our cooling tower. Nevertheless, the nominal behaviour has been approximated by the maximal heat rejected during summer 2012 addressing these conditions:

- Fluid temperature: 32.4 (in) - 28.3 (out) [°C],
- Fluid mass flow rate: 74.5 [l/min],
- Dry air temperature: 26.3 (in) [°C],
- Air mass flow rate: 10500 [m^3/h] (manufacturer's data).

The maximum rejection heat flow is given by equation 4.5 where $T_{water\ inlet}$ is the cooling tower water supply ($T93$ in figure 4.5 page 150). C_{min} means the minimum capacitance (product of specific heat and flow rate) of the two fluids.

$$\dot{Q}_{DCT\,design\,max} = C_{min} \cdot (T_{water\ inlet} - T_{outdoor}) \tag{4.5}$$

The design conditions heat flow $\dot{Q}_{DCT\,design}$ allows to compute the heat exchanger efficiency:

$$\epsilon = \frac{\dot{Q}_{DCT\,design}}{\dot{Q}_{DCT\,design\,max}} \tag{4.6}$$

The fluid mass flow rate is constant in our case while the air flow rate variation modifies the heat transfer and thus the heat exchanger efficiency. The $\epsilon - NTU$ method links the heat transfer to the heat exchanger efficiency (Rohsenow *et al.*, 1998). The heat transfer coefficient h_{air} is defined by the following equation where d is the pipe diameter.

$$h_{air} = Nu\,\frac{\lambda_{air}}{d} \tag{4.7}$$

Mac Adams correlation (ASHRAE, 2001) handles the air flow impact on Nusselt number:

$$Nu = cst \cdot Re^{0.6} \cdot Pr^{1/3} \tag{4.8}$$

As the $Prandtl$ number is independent of air velocity, the ratio between the convection coefficient in current and design conditions becomes:

$$\frac{h_{air}}{h_{air\ design}} = \gamma_{air}^{0.6} \tag{4.9}$$

Where γ_{air} is the percentage of nominal air flow. The model iterates to find the correct γ_{air} to reach the outlet water set point.

The fan power is then computed using the following correlation:

$$P_{fan} = P_{fan\ nominal}(b_0 + b_1(\gamma_{air}) + b_2(\gamma_{air})^2 + b_3(\gamma_{air})^3)\ [W] \tag{4.10}$$

For each half-cycle, the cooling tower model computes the fan control signal to reach the measured outlet cooling tower temperature (given the measured inlet temperature and the oudoor temperature). Then, the coefficients b_0 to b_3 are tuned with the measured power on installed variable speed fans. The minimum error between the computed and the measured fan power gives the values in table 4.11. The root mean square error is very low, it implies a total electrical consumption error of around 1% on the whole season.

$P_{fan\ nominal}$	950 [W]
b_0	-0.086
b_1	1.161
b_2	-3.034
b_3	2.958
RMSE	24.72 [W]

Table 4.11: Fan power curve coefficients

The May 25^{th} measurements have been removed from the analysis because of a high cooling tower consumption linked with a low outdoor temperature. For some unknown reason, this day encounters a cooling tower behaviour that was different from other days. Despite the same water temperatures, outdoor temperature and water mass flow rate, May 25^{th} (solid markers in figure 4.25) reaches a much higher fan consumption than May 26^{th} (empty markers). Neither solar radiations nor wind speed effects can explain this discrepancy.

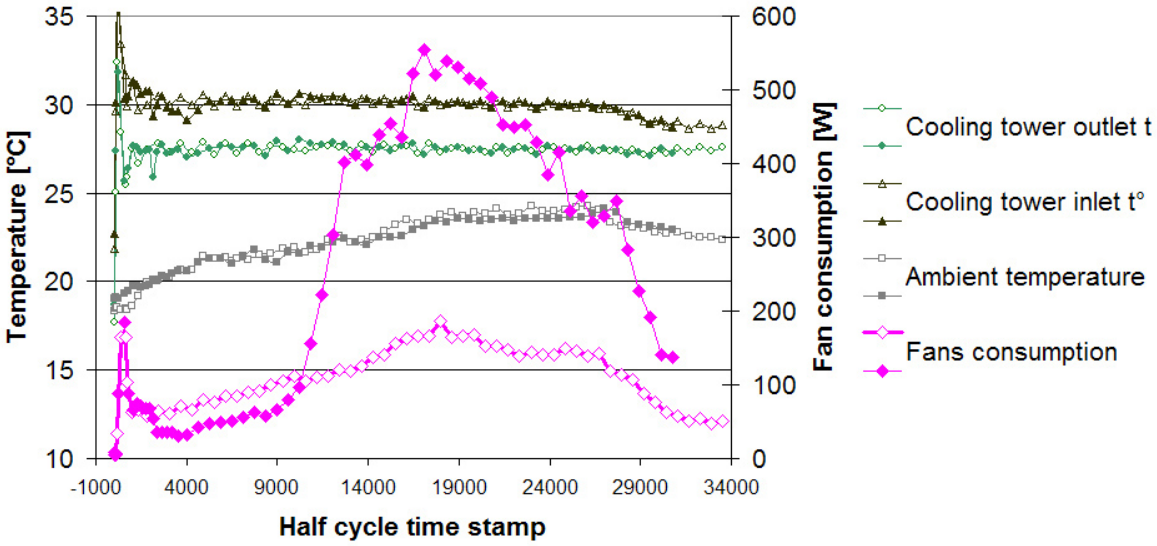

Figure 4.25: Cooling tower temperatures and fans consumption for May 25^{th} (solid markers) and 26^{th} (empty markers)

4.2 PV connected with vapour compression chiller

4.2.1 Installation description

A reversible air cooled heat pump has been installed in the laboratory building in 2010. A grid connected PV collector field (collector net area 9.3 m^2 - 1200 W_{peak}) is also installed with the same roof orientation as the thermal collectors (figure 4.1). This small scale heat pump (around 10 kW heat-cold) is used to satisfy the building heating and cooling loads. In the following analysis, the heat pump is named vapour compression chiller (VCC) because of the exclusive use in cooling mode.

The PV collectors area is not sufficient to satisfy the heat pump energy needs, the main part of energy supply comes from the electrical network. The general scheme of the installed system is displayed in figure 4.26. By operating and measuring this cooling system in real scale conditions, it is proposed to assess its energy performance. The main components dedicated to solar air-conditioning are listed below (from left to right in figure 4.26):

- 9.3 m^2 building integrated Mono-crystalline silicon PV collectors in series. The South roof has an azimuth of 43° to East and a slope of 42°.
- The inverter
- The vapour compression chiller (VCC) with embedded air-cooler
- The cold water loop including the cold water storage (500 litres)

- Cold emission devices for cooling the laboratory building: cooling floor, cooling ceiling, air handling unit

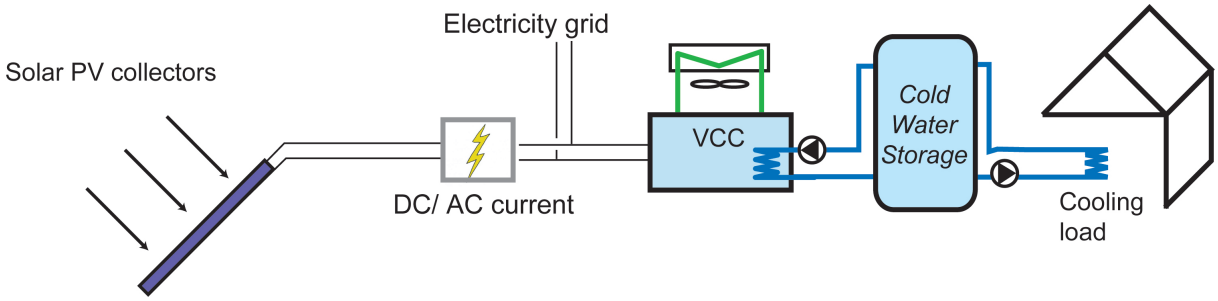

Figure 4.26: Installed PV driven cooling system scheme

The internal and external units are represented in figure 4.27. The Mitsubishi Zubadan reversible heat pump is split into two parts: the internal unit (MODZU80EH6V-2) contains an electrical heater (for heating mode only), the evaporator (in cooling mode) and circulation pump, while the external unit (PUHZ-HRP100VHA-2) takes in the compressor, the condenser (in cooling mode) and all other devices. This chiller has direct expansion, it does not have any water circuit on the condenser side.

Figure 4.27: Installed vapour compression chiller internal (left) and external unit (right)

4.2.2 Monitoring description

As for thermally driven cooling, the energy performance indexes must be computed. The relevant energy flows are computed based on the measurements to be able to derive key figures. The measurements are also picked up every 10 seconds in the system. Here also the monitoring focuses on cold production, the measurements on the cold distribution or emission are not presented in this work.

The graphical user interface developed to monitor the system is displayed in figure 4.28 for the chiller monitoring and in figure 4.29 for the PV collectors. The chiller monitoring screen is the same for both heating (black arrows and text) and cooling modes (blue arrows and text). The probes can be split into three groups: thermal, electrical measurements and meteorological data.

Thermal measurements

The thermal measurements consist in temperature and mass flow rate sensors. They are mainly used to evaluate the vapour compression chiller performance. The most important measurements and computed variables are described in table 4.12. The maximum error mentioned in table 4.12 is based on the temperature probes and mass flow rate sensors specifications and calibration.

Electrical measurements

To analyse the electrical behaviour of the system, it is useful to measure the consumption of each device. As for the adsorption cooling system analysis, the electrical consumptions due to the emission devices are not included as they would be present whatever the installed air-conditioning system. Miscellaneous chiller consumption consists of electricity used for electronic cards and compressor body heating.

Meteorological data measurements

The same measurements are made as for the adsorption cooling system experimentation: solar radiation on collector plane and external temperature.

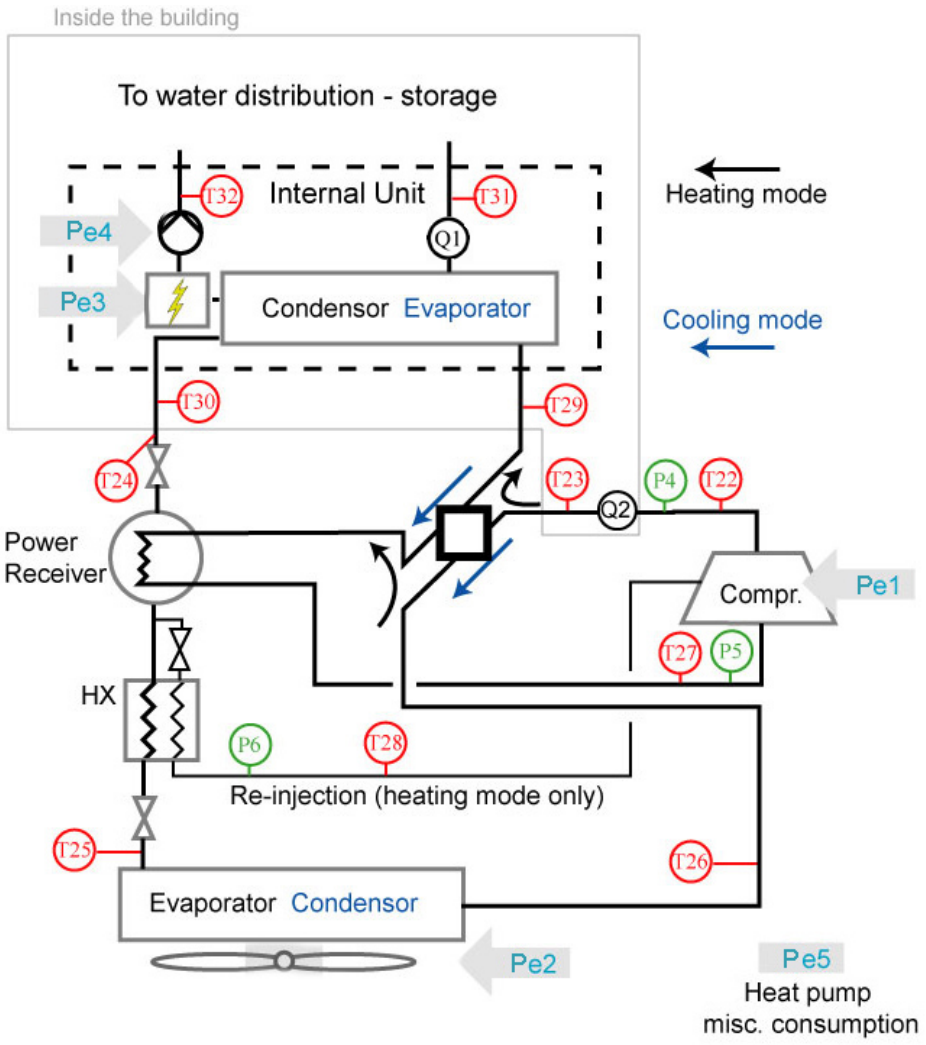

Figure 4.28: Vapour compression chiller monitoring screen

Comments about table 4.12

The COP's and collector efficiency yield are detailed in the following equations using the units of the table:

$$COP_{rej} = \frac{\dot{Q}_{cold} \cdot 1000 + Pe1}{Pe2} \tag{4.11}$$

$$COP_{VCC} = \frac{\dot{Q}_{cold} * 1000}{Pe1 + Pe2 + Pe4 + Pe5} \tag{4.12}$$

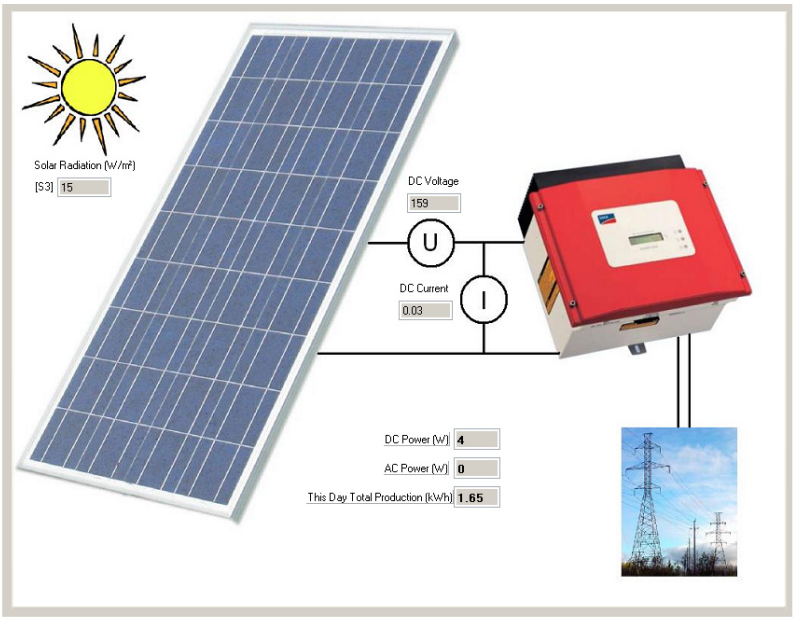

Figure 4.29: PV collectors monitoring screen

$$\eta_{PV} = \frac{AC_{Power}}{S3 * 9.3} \tag{4.13}$$

The general VCC chiller COP definition is described in equation 1.24 (page 47) while the collector efficiency refers to equation 1.7 (page 13). This last definition must be explained more precisely: the reference electricity produced is AC power at the inverter boundary and the reference surface is the net collector area (10·0.93 m^2). The collector efficiency definition therefore includes all possible losses from solar energy to grid electricity. The accuracy is given for clear sky conditions.

VCC chiller control

During these experimentations, the VCC chiller operation is controlled by the cold water storage tank temperature. The reference temperature threshold is 15-19°C, measured at the top of the tank. Compared to the adsorption cooling, the constant cold water mass flow rate is low (22.5 instead of 38 l/min). For a given cold production, it implies a higher temperature increase (around 5°C) between the inlet and outlet temperature. Even with a storage temperature at 15°C, the VCC chiller produces water at 10°C. The temperature levels are consistent with the adsorption cooling experiments. Moreover, the compressor speed is internally controlled, the useful stages for our tests can be defined as follows:

- Outlet water temperature >12°C: compressor speed is 100%

Measurement	**Probe number**	**Unit**	**Probe accuracy**
Thermal measurements			
Chiller water inlet Temp.	T31	[°C]	+/- 0.2 [°C]
Chiller water outlet Temp.	T32	[°C]	+/- 0.2 [°C]
Chiller water mass flow	Q1	[l/min]	2%
Electrical measurements			
Compressor consumption	Pe1	[W]	1.6%
Fans consumption	Pe2	[W]	2%
Pump consumption	Pe4	[W]	0.6%
Miscellaneous consumption	Pe5	[W]	2%
PV collector AC power	AC_{Power}	[W]	10%
Meteorological measurements			
Solar radiation	S3	[W/m^2]	4.5%
Computations based on the measurements	**Variable name**	**Unit**	**Maximum error**
Chiller cold produced	$\dot{Q}_{cold}$	[kW]	4% +/- 379 [W]
Rejection COP	COP_{rej}	[-]	6 %
Chiller COP	COP_{VCC}	[-]	6 %
Collector efficiency	η_{PV}	[-]	14.5%

Table 4.12: Vapour compression chiller cooling: measurements and computed values

- Outlet water temperature from 11 to 12°C: compressor speed is 80%
- Outlet water temperature from 10 to 11°C: compressor speed is 50%

Finally the fan power is also internally controlled to get the refrigerant complete condensation. As mentioned below, the cold water storage is used to satisfy a cooling load which depends on the outdoor temperature and solar radiation.

4.2.3 Monitoring results

Measurements periods

The two cooling devices (the vapour compression chiller and the adsorption chiller) could not operate together. Thus the VCC cooling measurement periods are not simultaneous to the adsorption cooling. The measurements were taken in July 2011 and July 2012. The results of 2011 monitoring campaign revealed some control improvements to have a better electrical COP. Besides, July 2011 was quite cold, and thus not representative of a typical summer in our region. The analysed period deals with 27 days in July 2012. During this period the chiller cold production was linked with the building cooling load and solar energy availability. The amount of cold energy produced cannot be compared to the adsorption chiller cold produced. This last was only linked with the solar energy availability.

Global results

The 27 days in 2012 measurements revealed the energy performance detailed in table 4.13. The performance indexes have been defined in chapter 1 section 1.4 on page 43 and followings.

Index	Unit	Value
duration	days	27
η_{PV}	-	0.099
COP_{VCC}	-	3.91
Q_{cold}	kWh/day	28.7
$E_{elec\,PV}$	kWh/day	4.33
COP_{rej}	-	289
PER_{VCC}	-	1.56
PER_{PV}	-	3.40
$f_{sav\,VCC}$	-	0.28
$f_{sav\,PV}$	-	0.67

Table 4.13: VCC cooling installation global results for July 2012

Two kinds of indexes are built depending on the PV collectors inclusion. Firstly, PER_{VCC} and $f_{sav\,VCC}$ handle only the benefits of using a more efficient chiller as the reference one ($SPF_{ref} = 2.8$). Secondly PER_{PV} and $f_{sav\,PV}$ follow chapter 1 definitions where PV production is involved in energy savings computation.

Photovoltaic system yield (including collectors, cable and inverter) stands in the order of magnitude of 10%. Some installed system characterictics affect the yield compared to a common domestic non tracking PV system: the collectors are building-integrated which increases their temperature and thus decreases their yield. Unfortunately, no collector temperature was recorded to evaluate this effect. Moreover, due to inverter overheating, some sunny days encounter inverter short switch off periods. Finally, the installation is quite old (installed in 2002), the installed collectors have 12.9% yield in standard conditions (Soltech, 1998) while more recent collectors reach 17.5% (Green *et al.*, 2011). Those explanations justify the fact that the measured system is less efficient than a more recent well designed and well installed collector field.

The electrical COP of the chiller during the whole period is in the order of magnitude of the instantaneous values given by EUROVENT (2012). The measured COP on the 27 days can be compared to the seasonal performance factor. The 2.8 reference value (Napolitano *et al.*, 2011) is much lower than the measured one. The measured one (3.9) follows the Eurovent test data (4.1) in steady-state conditions; it means the start-up, stand-by and part load operation do not affect greatly the chiller performance. The Eurovent steady-state conditions are defined in standard EN14511 (2004). The outdoor air dry and

wet bulb temperatures are respectively 35 and 24°C. The cold side conditions are dealing with a cold emitting device. The indoor air temperature conditions are then relevant for testing (27°C dry bulb - 19°C wet bulb).

The amount of cold energy produced is higher than for the adsorption cooling system (28.7 instead of 15.7). As mentioned below, the cooling load comparison between both tests is not relevant. More than half (55%) of the electricity consumed to produce 28.7 kWh is met by the 10 square meter solar PV collector field. For adsorption cooling comparison the Only Solar Ratio is computed in section 4.3.

The measured system reaches high primary energy ratios and thus high energy savings. The VCC machine is more efficient than the reference one and implies 28% energy savings ($f_{sav\,VCC}$). Adding PV production achieves 67% energy savings $f_{sav\,PV}$ which is the highest figure reached in all testing periods. By considering a reference chiller with a SPF of 3.91, the energy savings would have reached 55%.

The Sankey diagram showing the energy flows for the recorded period is displayed in figure 4.30. The only losses are encountered at the collector level. As the only electricity consuming device is the VCC machine, the electricity performance computation is straightforward. In relation to the adsorption cooling system where many thermal flows must be driven by pumps (106 kWh for 15.6 kWh useful effect), the PV connected VCC system has to manage only the cold water flow to water storage.

The VCC electricity sharing between the different devices shows main consumption for the compressor 84%. The stand-by consumption reaches 9% while the pump counts for 5%. The fans consumption closes the electricity sharing with 2%. It is really low compared to the dry cooling tower detailed before which leads to a rejection COP of nearly 300. A higher temperature difference between the condenser and the outside temperature leads to an air mass flow rate (and thus fan consumption) decrease. Otherwise, a low flow rate (22.5 l/min) in the cold water loop leads also to lower electricity consumption. The pump consumption could be even lower (it is effectively a class B pump).

Daily results

As for the adsorption cooling, two typical days are selected. They give details about a warm and a hot sunny day, the main results are presented in table 4.14. Moreover, figure 4.31 highlights the temperatures and energy flows for the hottest day.

The PV collectors reach nearly the same yield whatever the day. The maximum inverter AC power achieves 890 Watts (figure 4.31) while its nominal value is 850 Watts (Soltech, 1998). Some inverter failures appear clearly at certain times of the day. During this recorded period, the outside temperature

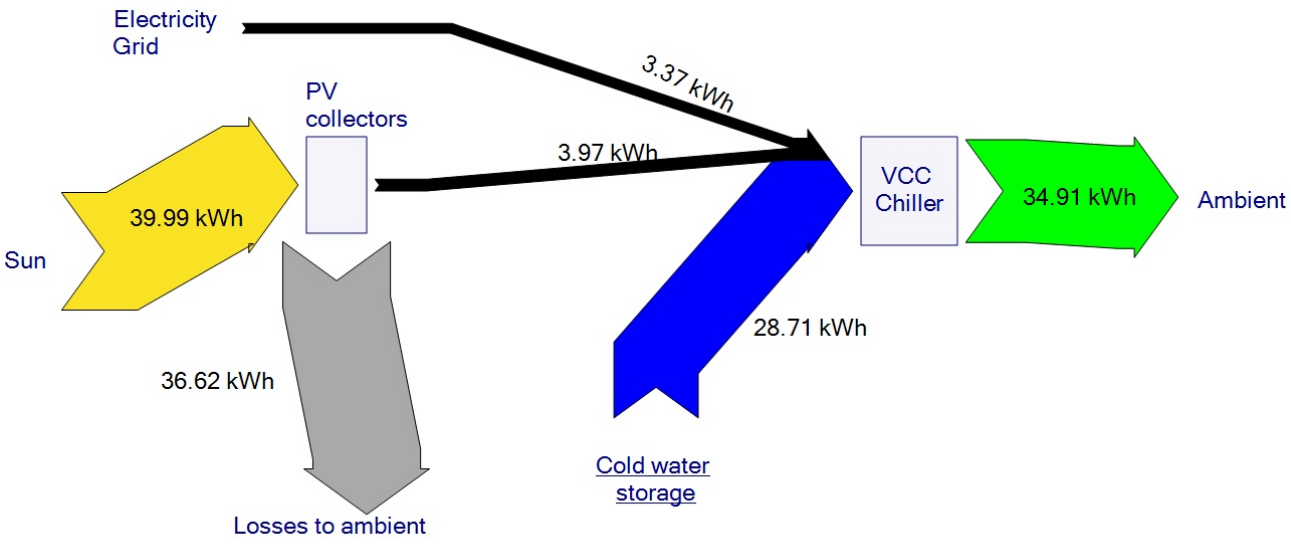

Figure 4.30: Mean daily thermal and electrical energy flows for PV collectors connected with VCC chiller (27-day period)

Period	Unit	**Warm day**	**Hot day**
Date		July 23^{rd}	July 26^{th}
Max outdoor t°	°C	24	32
η_{PV}	-	0.104	0.904
COP_{VCC}	-	4.26	4.02
Q_{cold}	kWh	53.9	70.8
$E_{elec\,PV}$	kWh	6.98	5.89
COP_{rej}	-	350	180
PER_{VCC}	-	1.70	1.61
PER_{PV}	-	3.79	2.41
$f_{sav\,VCC}$	-	0.34	0.30
$f_{sav\,PV}$	-	0.70	0.54

Table 4.14: VCC driven installation daily results for two sunny days

does not affect significantly the PV system efficiency while the inverter failures appear especially when the hot temperature is reached in the technical room (where inverter is located).

The VCC machine has high COP values for both days. The inlet cold temperature during July 26^{th} is high (>20°C) due to high cooling load at that period. Other days with lower cold water inlet temperature did not show a

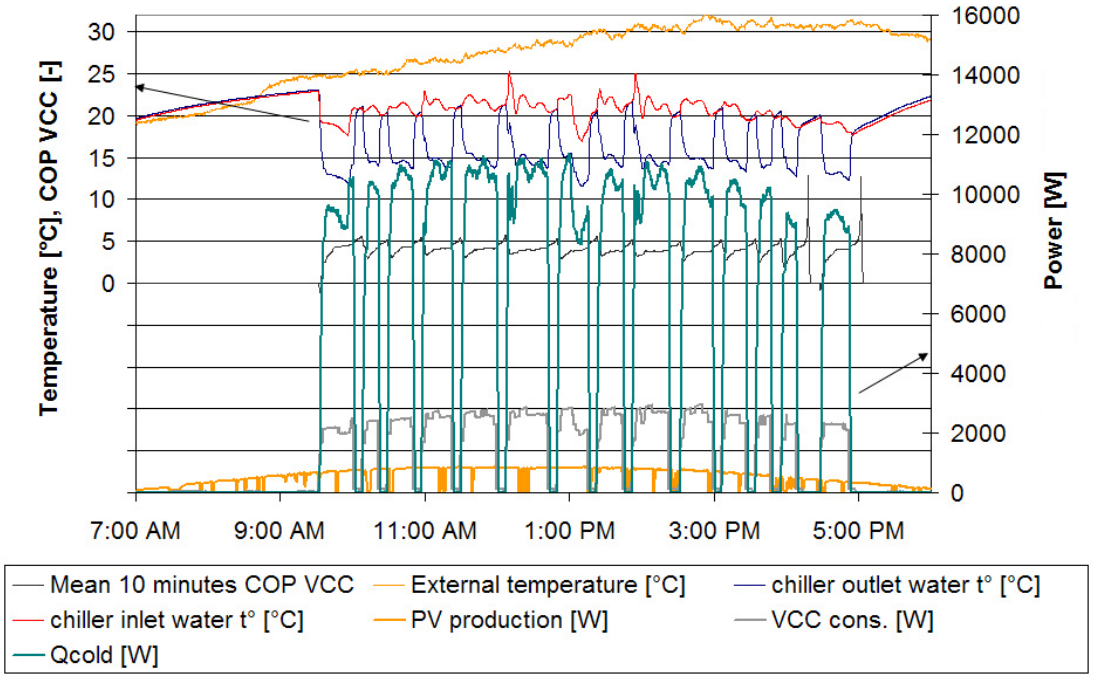

Figure 4.31: Daily energy flows and temperatures for a hot and sunny day (July 26^{th})

significant decrease in chiller performance but a slight decrease in chiller cold produced. In the same way, numerous start-up periods do not appear to involve a significant performance decrease. Besides, the water pump operates two minutes after the compressor switch off, this produces cold nearly for free! Better energy performance of those two days are more correlated with longer operation period and thus lower stand-by duration (62% for July 26^{th} instead of 87% for the whole test). Apart from stand-by consumption, the electricity sharing between the different fields is very similar to global results.

The Primary energy ratio (PER) and the fraction of energy savings (f_{sav}) follow the trend of the global results. However, $f_{sav\,PV}$ is lower for July 26^{th} than for the global results. This is due to the high load met this day (around 71 kWh). PV and VCC work fine but the PV field is not sufficient at all to satisfy the cooling load.

The rejection COP (COP_{rej}) is really impacted by the outdoor temperature. Nevertheless, the fans involve so low electricity consumption that the temperature influences on daily COP_{VCC} and energy savings are not important (respectively 0.2 [−] and 4%).

To conclude this part about daily results, it is proposed to compare the thermal collectors and the PV system yields for a summer period. In 2011, both kinds of collectors performances were recorded, it appeared that the PV yield is constant over the period while the thermal yield is proportional to the daily solar radiation. The results are showed in figure 4.32 where $PV\ yield = \eta_{PV}$ and $Solar\ thermal\ yield = \eta_{thermal\ collector}$. 32 days of adsorption cooling application were recorded (high temperature in collectors), they are sorted in global solar radiation decreasing order ($S3$ probe). Some days with low radiation on collectors (days 30 to 32), the thermal panels did not reach a temperature high enough to heat the storage, their yield is 0. Care should be taken because the comparison deals with thermal energy and electricity. For days with high solar radiation, thermal panels collect around four times more energy than PV ones.

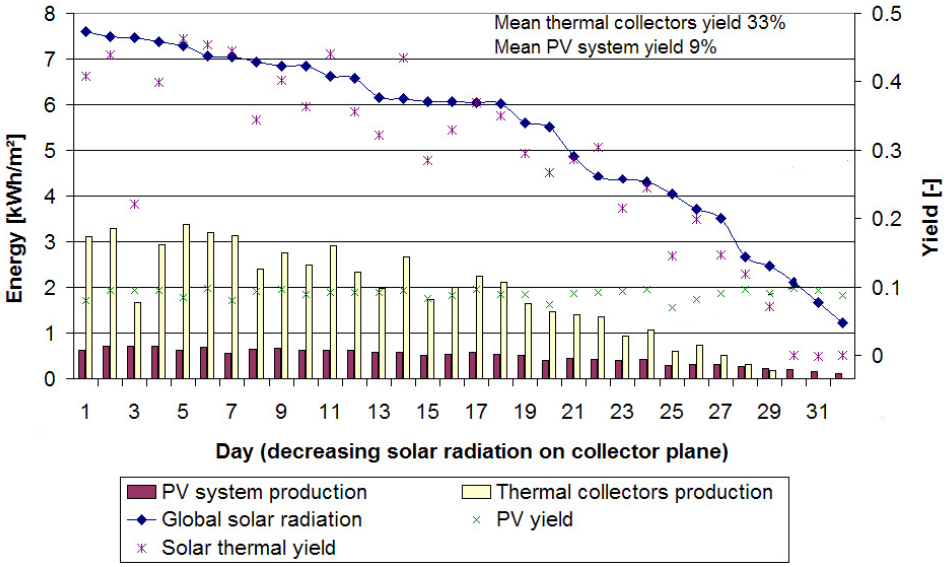

Figure 4.32: Daily incident radiation, PV system and thermal collectors yield during 2011 measurements

Shorter periods

Shorter periods of less than one day are useful to describe some system special features. First of all, the VCC stand-by consumption includes a compressor electric heating for better lubrication in case of low outside temperature. This protection can not be removed, even though it is useless in summer and energy consuming. In measurements, the compressor heating occurs when the VCC is in stand-by mode. It starts nearly every hour for 20-25 minutes. The stand-by consumption with compressor electric heating reaches 50-55 W while the normal stand-by consumption is 15 W. On the whole period it counts for

7.85 kWh which counts for 45% of stand-by consumption and 4% of total VCC consumption.

The start-up period appears to have a short duration (around 5 minutes). This is showed in figure 4.33 representing typical chiller operation (30 minutes). One minute after the start-up, the chiller produces cold, it lasts 4 more minutes to reach a nominal cold production. The cold production is nearly constant over the steady-state operation, it depends only on the cold water temperature level which decreases through time. The electrical COP is constant during the steady-state operation period (4:22 to 4:47). At VCC switch off, the water pump still operates for two minutes. It is enough to evacuate the cold energy stored in the heat exchanger as showed in figure 4.33 between 4:47 and 4:49. This delay was previously ten minutes (manufacturer value) which is too long because the water circulation was heating the cold storage!

Short start-up period combined with appropriate pump operation after compressor switch off achieves a good chiller performance. The mean COP during operation is 4.43 which is very close to the instantaneous COP measured during steady-state operation. The global COP on the 27 days period is getting close to the nominal one, stand-by power is the main effect involving global COP decrease. Without any stand-by power, the mean COP would have reached 4.28.

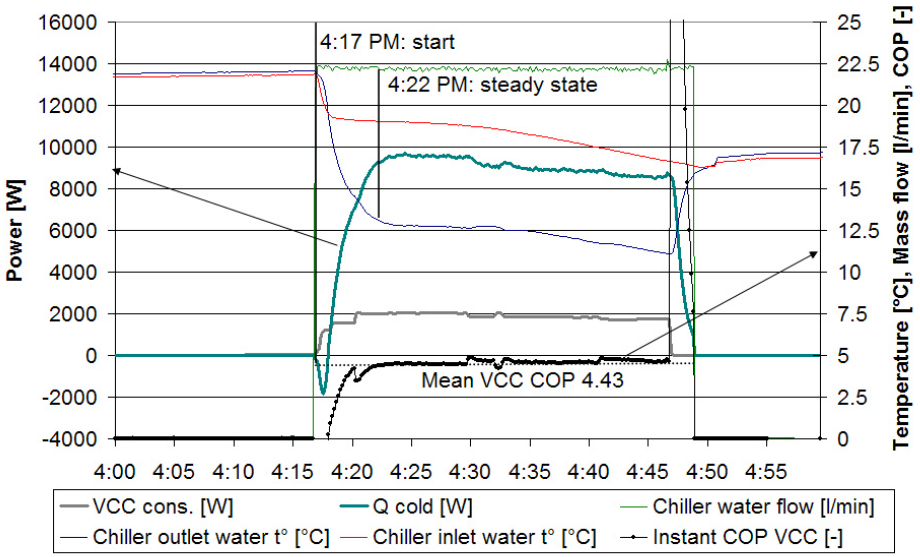

Figure 4.33: Typical VCC operation on July 18^{th} afternoon

The low fan consumption in comparison with adsorption cooling is linked to the temperature of rejected heat. In the VCC case, the steady-state operation mean difference between outdoor temperature and condenser inlet ($T26$ in figure 4.28) is 35°C while the useful temperature difference between external temperature and cooling tower inlet was 5-10°C for adsorption cooling. The condensation temperature reaches +/− 15°C temperature difference with the external temperature. For VCC cooling, the influence of external temperature on fan power and COP_{VCC} is displayed in figure 4.34 where each point represents a 5-minute steady-state operation. The fan power is controlled level by level (15-30-50-140 W) as the external temperature rises.

The influence of external temperature on refrigerant cycle is not significant in the measurements. Moreover, the cold water outlet temperature variation did not impact the COP. Thus, the condenser and evaporator temperature do not influence considerably the refrigerant cycle. This applies to the temperature ranges encountered during the measurement periods: external temperature <32°C and cold water produced between 10 and 18°C.

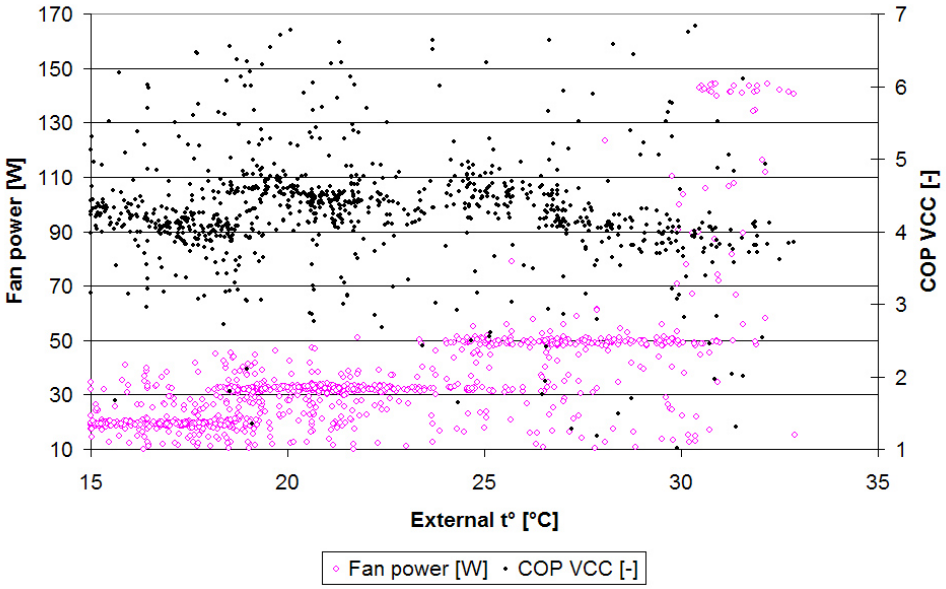

Figure 4.34: Influence of external temperature on fans consumption and VCC COP for steady-state operation

The cold water outlet influences the compressor power as mentioned in the manufacturer's documentation. Low outlet temperature leads to a compressor speed decrease and thus to lower cold produced (10-12°C outlet cold water is correlated with 8 kW cold power instead of 10 kW nominal). It has however

no great impact on energy performance. Besides, each chiller start-up has a progressive compressor speed up to the nominal one at current outlet temperature conditions. This is clearly seen in figure 4.33 where lower compressor electricity consumption is measured during the first three minutes.

4.3 Energy performance comparison

Thermally and PV driven solar air-conditioning systems monitoring revealed the energy performance on a representative summer period.

We should keep in mind that no cooling back-up system is used. Both systems are grid connected, meaning exchanges between the electricity grid and the system. For the PV system, there is currently no evaluation of the electricity which is exchanged with the electricity grid.

The key indexes for both cooling systems are written in table 4.15. This table gives the results for a complete period and for a typical day which presents good results (sunny but not so hot). The PV connected with the vapour compression chiller system (namely PV+VCC) reaches more energy savings (f_{sav}) in any case. The electrical performance of the adsorption cooling system could be higher to reach the targeted value of 10 (Nowag *et al.*, 2012). For PV+VCC system, the energy savings are sensitive to the cooling load and PV area. To compare the systems, it is proposed to use the *System Thermal Ratio* and *Only Solar Ratio* defined in equations 1.40 to 1.45 in chapter 1 (page 49 and followings). The *System Thermal Ratio* (STR) is the ratio of the cold energy produced to the solar incident radiation. The *Only Solar Ratio* (OSR) is similar but includes the mandatory solar energy used to run the electrical equipments. Those two indexes allow the comparison of the entire cooling systems fed only by solar energy.

A graphical overview of the energy flows in a purely solar-driven system is showed in figures 4.35 and 4.36 respectively for adsorption cooling system and VCC system (black arrows stand for electricity). For a given irradiation (100 kWh), these Sankey diagrams display the global energy balance of a cooling system of which the only source is solar energy. The system is still connected to the electricity grid but its global energy balance is zero. The OSR can be found easily: it is **cold energy produced related to the solar radiation** (around 11% for adsorption cooling, 39% for VCC system). For the adsorption cooling system, the *Thermal Fraction* is 77% which means that 23% of solar energy must be dedicated to satisfy the system electrical consumption by PV collectors. For VCC system, no thermal collectors are used, the vapour compression chiller is the only electricity consuming device.

Those ratios are sensitive to the period chosen to measure the performance. Table 4.15 presents the results for both long period and typical days. Those sunny days show that OSR increased by 0.05 for each system meaning the adsorption cooling is more impacted by a sunny day than the VCC system.

In other words the OSR remains more constant over the period for VCC system. Moreover, the monitoring campaign revealed a PV constant yield whatever daily solar radiation. As mentioned before, cloudy days do not encounter enough radiation to operate the thermal collectors.

Cold production device	**Adsorption cooling**		**VCC + PV**	
Period	**Collectors emulation**	**August 10^{th}**	**July 2012**	**July 23^{rd}**
duration [days]	36	1	27	1
$\eta_{thermal\ collector}$	0.31	0.44	-	-
η_{PV}	-	-	0.099	0.104
COP_{therm}	0.55	0.55	-	-
$COP_{elec\,tot}$	4.69	6.68	3.91	4.22
COP_{rej}	58	128	289	350
PER	1.88	2.67	3.40	3.79
f_{sav}	0.40	0.58	0.67	0.70
STR	0.14	0.22	0.39	0.44
OSR	0.11	0.17	0.39	0.44

Table 4.15: Measured cooling systems performance comparison

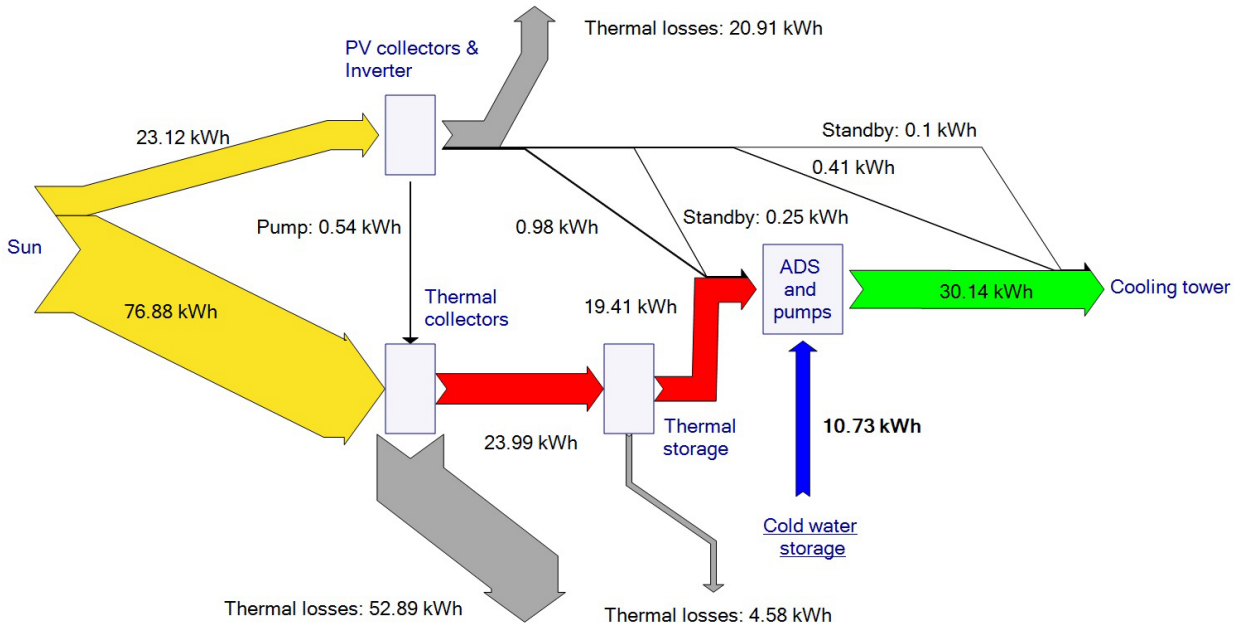

Figure 4.35: Adsorption cooling energy flows with solar energy as only energy source (performance recorded during *collector emulation* 36-day period)

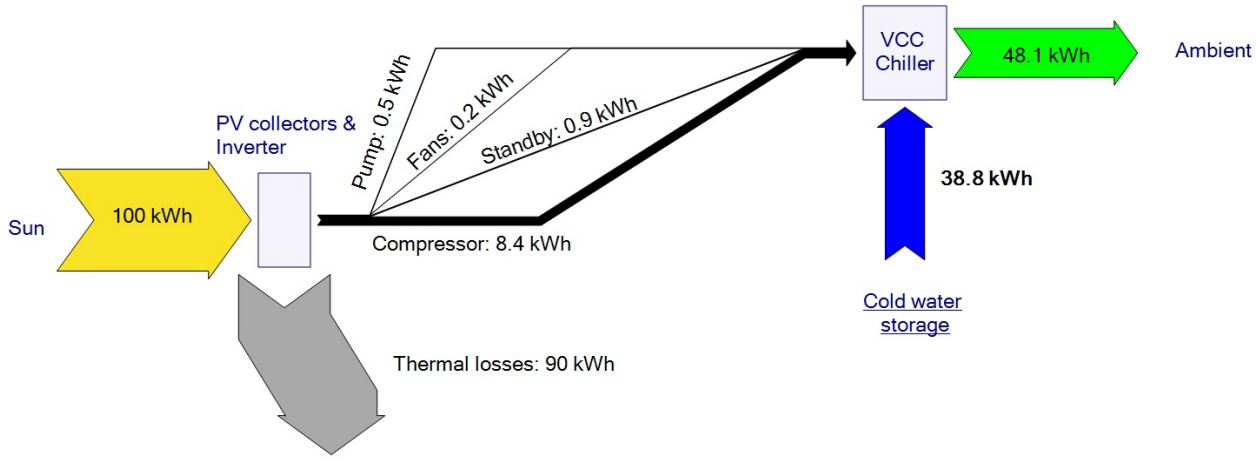

Figure 4.36: VCC cooling energy flows with solar energy as only energy source (performance recorded during 27-day period)

On the one hand, some limitations of the adsorption cooling system have been described previously in the text (section 4.1). On the other hand, the VCC system has showed extremely good energy performance. To have a fairly comparison of both solar cooling systems (thermally driven and PV driven), the comparison is extended to some theoretical cases in table 4.16. The comparison addresses OSR and STR (the PER and f_{sav} cannot be compared, the entire cold production is met by solar energy involving f_{sav}=100%). The four cases are detailed:

1. **Targeted system** consists in an ab or adsorption chiller operation in very efficient conditions.

2. **Measured case** is the PV+VCC system measured through last summer with a slightly higher PV yield (9.9% to 10%).

3. **Reference VCC** is a PV+VCC system of which VCC has the reference seasonal performance: 2.8 (Napolitano *et al.*, 2011).

4. **Double effect** is a thermally driven system driven with a double effect absorption chiller also in very efficient conditions.

For each case, a 10% global yield for PV is assumed. This could be considered as a good approximation of a PV system integrating losses in cables, inverter, a common shading (Suri *et al.*, 2007). The thermally driven systems have a collector yield of 60% that is the nominal yield achieved by highly efficient collectors (figure 1.14 on page 18). The thermal COP has been chosen in the range given by Henning (2011) to handle the mean value over the cooling period. The thermal loop efficiency is the maximum encountered during the tests run in the lab. Finally, the total electrical COP of the thermally driven systems has been chosen in accordance to the target proposed by Wiemken *et al.* (2010) despite it is very difficult to reach in the monitored systems (Thomas and André, 2012).

The single effect thermally driven chillers (case 1) reach half of the cold produced with the VCC+PV system measured (case 2) for a given collector area. Nevertheless, case 1 and reference VCC+PV system have about the same ratios. A highly efficient double effect system (case 4) reaches the same OSR as case 2. To handle more cases, figure 4.37 presents the OSR computation for various thermal COP and collector yields.

Case number	1	2	3	4
Name Cold production device	Target system Adsorption	Measured case VCC+PV	Reference VCC VCC+PV	Double effect Absorption
$\eta_{thermal\ collector}$	0.6			0.6
$\eta_{thermal\ loop}$	0.9			0.9
η_{PV}	0.1	0.1	0.1	0.1
COP_{therm}	0.6			1.2
$COP_{elec\ tot}$	10.00	3.91	2.80	10.00
STR	0.32	0.39	0.28	0.65
OSR	0.24	0.39	0.28	0.39

Table 4.16: Theoretical cases performance comparison

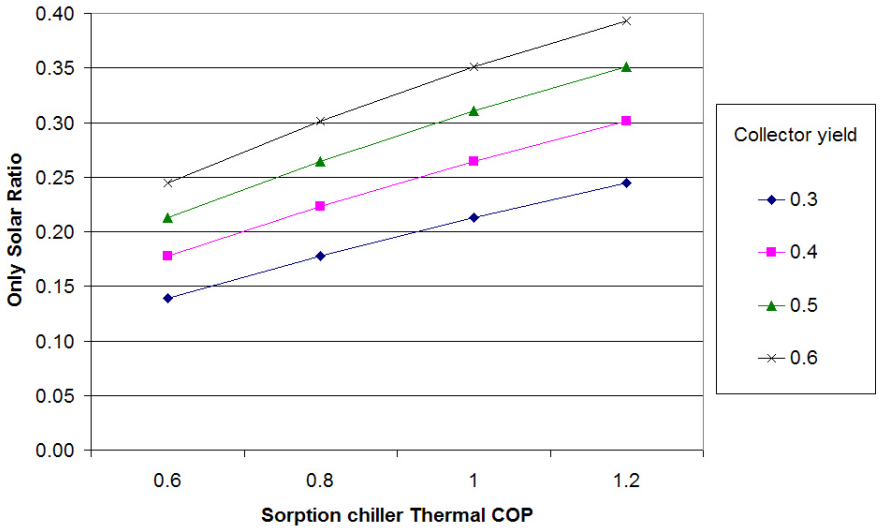

Figure 4.37: Thermally driven cooling OSR computation with the following parameters: $\eta_{PV} = 0.1$; $COP_{elec\ tot} = 10$; $\eta_{thermal\ loop} = 0.9$

4.4 Discussions

This chapter detailed the performance measurement of two solar cooling system in operation during summer. The results obtained from the monitoring campaigns corroborate the simulation results about system comparison. Moreover, some of the measured devices have also been modelled.

4.4.1 Adsorption cooling system performance

The performance figures discussed below address the *collectors emulation* period which is representative of a real system. The *solar only* period does not meet nominal operation while the *back-up heating* period deals partially with the solar radiation.

The adsorption cooling system considered has no back-up system, it is an **autonomous** system. Generally, the thermally driven cooling system is coupled with a VCC system which is used for back-up and peak loads. The system energy performances computed in this chapter are consistent with a real thermally driven solar cooling system but there is no consideration on cold production sharing between multiple cold production devices.

Firstly, considering the flat-plate collector area, 28 m^2 (or $\approx$ 3 m^2/kW_C) is enough to feed an adsorption chiller during the day. For a longer operation during the day or in the night, some additional storage and collector capacities must be installed. With thermally driven cooling, the thermal storage could be present on both sides: hot and cold. It increases the flexibility of the cooling system compared with PV cooling which allows the cold energy storage only.

Then, the adsorption cooling system operation analysis emphasized two modes: the part load and the full load implying a cycle duration modification. The manufacturer's data does not mention what kind of operation is figured out in their curves. This is nevertheless important because of the significant thermal COP and cooling capacity variations between the two modes. In the studied case, the full load operation stands only for high cold water supply of the chiller ($>$ 17°C). It would have been interesting to compare the full and the part loads with the same temperature levels.

From the thermal performance point of view (thermal COP), the global period measurements rely to the manufacturer's data (model implemented in chapter 3). However, the cooling power is not the same as the manufacturer's data mainly because of the part load operation. The influence of start-up performance decrease was emphasized but does not significantly affect the global performance. Numerous chiller start-ups per day would modify this statement.

Finally, on the electrical point of view, the measured consumption is substantially higher in measurement than the results of the hypothesis taken in chapter 3 (ranging from 150% to more than 250% depending on the day). The $COP_{solar\ loop}$ must achieve 50 to cope with the good practice hypothesis. This

value encountered in sunny days but is decreased for less sunny days. Globally the solar loop achieves a $COP_{solar\ loop}$ of 40. The chiller consumption is 400 W (it includes 3 pumps), thus it is able to reach a $COP_{el\ chill\ pump}$ of around 20. It nevertheless achieves a value of 10 due to the part load operation and stand-by consumption. The rejection involves the most electricity consumption variability (COP_{rej} ranging from 23 up to 130 depending on the day). On a representative summer period in Belgium, the COP_{rej} reached around 55, it could be ever lower in hotter locations. Despite the separation between pumps and fans consumption measurements in our analysis, both are sometimes gathered to entail the total electricity consumption of rejection system. While comparing the results, care should be taken to check what is included in the rejection electricity consumption. The consumptions detailed hereunder are significantly affected by the stand-by power (17% of the total consumption), a night switch off of solar systems would be useful. The measurements lead to a global $COP_{elec\ tot}$ of 5 which is in the range of the systems studied by Wiemken *et al.* (2010).

4.4.2 Adsorption chiller thermal modelling

Despite the narrow temperature validity range of the developed adsorption chiller model, some particularities of the chiller operation have been pointed out.

For steady-state operation, the adsorbers cycles depend mainly on the heat flows during the previous cycle. Moreover, the thermal performance and cooling capacity are mainly influenced by the hot water inlet temperature and the temperature difference between the cold and the rejection heat flows. The importance of cycle duration on chiller capacity is also emphasized. The performance decrease during the start-up phase (10-minutes period) could be more investigated although it scarcely impacts the global energy performance.

A more detailed adsorption model implying physical parameters to handle dynamic effects could be investigated as it has been done for absorption (Bourdoukan, 2009). This kind of model involves many chiller data such as the mass and size of the heat exchangers. The manufacturers really want to prevent copying their chillers, it would be therefore difficult to fill the models with those informations.

4.4.3 Use of adsorption chiller steady-state thermal modelling in simulations

As mentioned above, the new created model has a narrow validity range. Nevertheless, there is a great temptation to inject the values in the performance map model detailed in chapter 3. Some hypotheses should be made about extrapolation of the full load and part load data to fill a new performance map. First of all, the full load operation has to be extended to higher hot water inlet temperatures. Secondly, the part load thermal behaviour modelled only consid-

ers a set point of 15°C. It would be hazardous to run a yearly simulation with such incomplete data. Nevertheless, the yearly performance of the adsorption chiller will certainly be lower than the expected one due to the explanations of figure 4.22.

A rough approximation of a full load operation with 65°C constant supply temperature would lead to a thermal COP yearly decrease of 0.06 compared to the manufacturer data. Besides, the electrical consumptions would also be decreased regarding higher thermal flows in required to produce the same cold energy. A global decrease of the $COP_{elec\ tot}$ of around 4% would be encountered taken the global results of *collectors emulation* period into account.

4.4.4 Dry cooling tower behaviour

The analysis of the dry cooling tower behaviour revealed discrepancies between the measured and manufacturer's data. In this case, three companies play an important role: the fan manufacturer, the dry cooler assembler and finally the system integration company which implements the fan control. The data provided by these three companies was not consistent. The design of thermally driven air-conditioning systems must really pay more attention to this high electricity consumer device.

4.4.5 Electricity grid energy flows

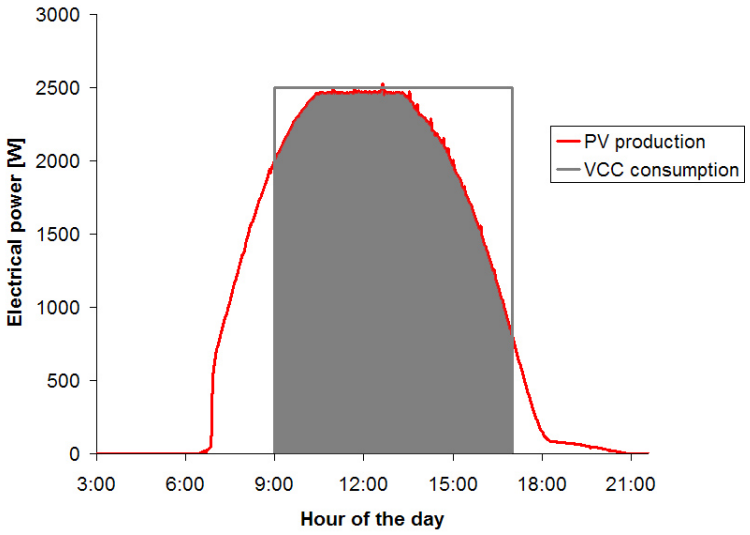

Figure 4.38: Electricity production of a solar PV field and consumption of a VCC chiller during a sunny day

The electricity grid connection hypotheses are important. The amount of electrical energy as well as its time dependency is crucial at least in terms of grid stability. Both systems (PV driven or thermally driven) cannot be operated without any help of the electricity grid. For a thermally driven system, the entire electricity consumption comes from the grid, it is linked to the cold produced and the $COP_{elec\,tot}$.

For the PV driven system, it depends mainly on the coincidence of the solar radiation and the chiller operation. A simplified example of a sunny day is displayed in figure 4.38. A 8-hour full operation of a VCC machine is considered. Taking a COP_{VCC} of 4 and a power of 2.5 kW into account, the machine will provide 80 kWh cold energy during the day (the chiller and the operation are similar to those encountered on July 26^{th}). Besides, the PV field is designed to cover the daily electricity consumption of the chiller (20 kWh). The laboratory PV field efficiency is used but 26 m^2 are considered instead of 9.3 m^2. 85% of the electricity is shared between the PV collectors and the chiller which is represented by the grey shape in figure 4.38. A shift of one curve (the PV curve can be shifted by modifying the collector azimuth) could even reach 90%. A cleverly controlled chiller and cold storage could be implemented to provide the cooling load entirely fed by PV to a building throughout the day.

The other days with lower or intermittent solar radiation would involve more electricity consumption from the grid. This is the case for both assisted thermally driven or PV driven solar air-conditioning systems.

Despite the simplicity of this example, we could easily imagine that a PV system could really decrease the electricity consumption from the grid during the sunny days.

Conclusions and perspectives

Whereas in the past the major challenge was to keep our buildings sufficiently warm, nowadays the challenge is in guaranteeing reasonable comfort conditions in summer without (or with minimum) cooling energy. It is therefore important that building designers and other stakeholders understand the thermal behaviour of a building and its occupants and are aware of the available alternative techniques that substantially improve the comfort in the building and significantly decrease the energy consumption (BUILDUP, 2012).

This last sentence summarizes the main interest of this work. The impact of solar air-conditioning systems implementation on the energy use has been evaluated for some residential and office buildings in Europe.

Conclusions

The work began with a description of the solar cooling technologies available on the market and at a laboratory level. It is important to distinguish the cold production device (absorption chiller for example) and the entire cooling system. The energy performance indexes definition allows to understand the thermally driven systems complexity and puts forward two main concerns: the electricity use and the thermal performances. The thermal performance of the chiller and the global performance (thermal and electrical) of the cooling system depend mainly on the choice of the three temperature levels and the proper design of devices managing to reach these temperatures. These last devices are mainly influenced by the weather conditions, it is therefore important to evaluate the systems performance on the whole cooling season for a given location.

For some theoretical residential and office buildings, the building yearly thermal loads (heating, cooling, domestic hot water) revealed the great influence of the comfort model, the building energy performance level and the climate. The cooling load will be decreased by a larger comfort tolerance of the occupants. Besides, a high building energy performance level, which is linked to a higher envelope insulation, increases the cooling load whatever the climate. Despite this increase, all conventional heating and cooling device simulations reached lower total primary energy use for well insulated buildings. Furthermore, the residential building analysed does not need any active cooling system for Paris and Stockholm. For these locations, some passive techniques are supposed to lower the little computed discomfort to an acceptable level.

The cooling system involving an absorption or adsorption cooling machine is simulated for the previously defined building cases on a yearly basis. The use of solar energy through thermal collectors for heating meets higher primary energy savings as for cooling. In all cases, the thermally driven system achieves a lower energy and economical performance than a vapour compression chiller partially supplied with a PV field. The PV connected system compensates the energy used for cooling the buildings in some of the Lisbon and Torino cases. The PV system results are influenced by the strong hypothesis which is the use of electricity grid as perfect (no energy losses) and free of charge energy storage. Coming back to the thermally driven systems, they are generally not sufficient to cover the entire building load meaning a back-up chiller is installed. This involves supplementary costs coming to a very low profitability.

To compare solar air-conditioning with a conventional system, a reference case has been computed. The seasonal COP of the vapour compression chiller implemented in the reference system impacts greatly the energy savings reached by a thermally driven system. **The common COP value taken in the literature (2.8) is lower than the real encountered in the experimentations or in the certificate (around 4)**. The use of the higher COP value consequently gives lower energy savings.

The last part of the work involved real scale testing of solar air-conditioning systems in Arlon (Belgium). A small scale thermally driven adsorption chiller and a vapour compression chiller with grid-connected photovoltaic field were operated during the cooling season. For the thermally driven system, the monitoring revealed higher electricity consumption in real scale than in simulations. **Stand-by power, part load operation and high fan consumption lead to a total electrical COP of 5 although the target as well as the simulated values are 10.** These three items must be investigated to increase the electrical performance.

The adsorption chiller thermal performance analysis revealed a good agreement between the performance map model and the measurements. Generally, the steady-state analysis is precise enough but **care should be taken to specify the kind of adsorption chiller operation: part load or full load**. The manufacturer does not mention what kind of operation is figured out in its performance curves.

In the frame of the experimentations, a new energy performance index has been formulated. The *Only Solar Ratio* (OSR) depicts the conversion quality of a cooling system using solar energy as the only energy source. Thus, for thermally driven systems, this index takes the electrical consumption of auxiliaries into account; it considers that electricity comes from a PV field. For both systems, it answers the question: What is the cold energy produced with 1 kWh solar energy? The system comparison leads to a lower OSR for every single effect sorption chiller than for PV driven systems. A highly efficient double effect system would reach the same value as the measured PV driven

system. Apart from this case, this means that the **photovoltaic system is probably the best way to convert solar energy into cold energy for building air-conditioning purposes. The results obtained from the monitoring campaigns corroborate the simulation results about this statement.**

Perspectives

The results presented above favour the installation of PV driven systems instead of the solar thermally driven ones. These lasts have nevertheless a great interest when waste heat is used instead of solar heat to drive the ab- or adsorption chillers. The waste heat promotion at least in summer is probably an economically feasible and an energy efficient solution.

The buildings, locations and system investigated give an overview of the impact of solar air-conditioning in a limited number of cases. The analysis of thermally driven systems could be extended to other kinds of buildings: hotels, rest homes and hospitals are especially interesting because they meet high heating and cooling loads during summer periods. Furthermore, the use of double, triple effect chillers or desiccant cooling systems could modify the energy and economical conclusions of this work.

The thermal behaviour of the adsorption chiller could be deeper investigated by extending the model presented in this work to a larger temperature range of driving flows. Besides, the evaluation of the electricity consumption of such a thermally system is crucial to reach energy savings. An efficient system control should be able to minimize the electricity consumption of pumps and fans in operation and the stand-by modes. Concretely, the various devices could be really switched off if no operation (without any parasite consumption) and the fans, pumps could be controlled according to the chiller operating phases (sorption/desorption) and load (part or full).

The evaluation of the energy flowing between the electricity grid and the building should be addressed to take advantage of the solar cooling technology (thermally or PV driven). The cooling system control has a key impact on these exchanges. This could be optimized by good knowledge of the occupants and the building thermal behaviour as well as by an accurate weather forecast.

Appendices

Bibliography

Abbas, R., Montes, M., Piera, M., and Martinez-Val, J. 2012. Solar radiation concentration features in Linear Fresnel Reflector arrays. Energy Conversion and Management, 54(1):133 – 144.

Abdulateef, J., Sopian, K., Alghoul, M., and Sulaiman, M. 2009. Review on solar-driven ejector refrigeration technologies. Renewable and Sustainable Energy Reviews, 13(6):1338 – 1349.

AEC. 2007. Heat & Cool FG cooling tower. Technical report, AEC.

Agyenim, F., Knight, I., and Rhodes, M. 2010. Design and experimental testing of the performance of an outdoor LiBr/H2O solar thermal absorption cooling system with a cold store. Solar Energy, 84:735–744.

Ait-Taleb, L. 2002. *Contribution à l'étude des machines à froid à sorption solide par bi-régénération en fonctionnement semi continu*. Ph.D. thesis, Université Henry Poincarré, Nancy 1.

Albers, J. and Römmling, U. 2002. TRNSYS Type107 Part load simulation of single staged absorption chillers in quasi steady states. Technical report, IEA SHC TASK25 Subtask B.

Alessandrini, J.-M., Fleury, E., Filfi, S., and Marchio, D. 2006. Impact de la gestion de l'éclairage et des protections solaires sur la consommation d'énergie de bâtiments de bureaux climatisés (in French). In *Climamed, 3ème congrès méditerranéen des climaticiens, Lyon, France.*.

APERE. 2011. Energie solaire en 2010. Renouvelle, 37:12.

APERE. 2012. Prix d'achat de l'énergie par les ménages. Renouvelle, 49:12.

ASHRAE. 2001. *2001 ASHRAE Handbook: Fundamentals*. ASHRAE handbook. American Society of Heating, Refrigerating & Air Conditioning Engineers, Incorporated.

Bales, C. and Nordlander, S. 2005. TCA Evaluation, Lab measurements, Modelling and system simulations. Technical report, SERC, Solar Energy Reseach Center, Dalarna, Sweden.

Besana, F., Fernandez, R., Nienborg, B., and Franchini, G. 2009. Solar Combi+ with a 4.5 kW absorption chiller : best choice for different cases. In *Proceedings of the 3rd International Conference Solar Air-Conditioning, Palermo, Italy*.

Bolocan, S. and Boian, I. 2010. Solar cooling for energy saving, can we afford not to use the heat of the sun? Bulletin of the Transilvania University of Brasov, Series I: Engineering Sciences, 3:313–322.

Boudéhenn, F., Demasles, H., Wyttenbach, J., Jobard, X., Chèze, D., and Papillon, P. 2012. Development of a 5 kW Cooling Capacity Ammonia-water Absorption Chiller for Solar Cooling Applications. Energy Procedia, 30(0):35 – 43.

Bourdoukan, P. 2009. Description of simulation tools used in solar cooling: New developments in simulation tools and models and their validation. Technical report, IEA-SHC Task 38 Report, Solar Air-Conditioning and Refrigeration.

BP. 2012. BP Statistical Review of World Energy June 2012. Technical report, BP British Petroleum.

BUILDUP. 2012. What does the EPBD stipulate for summer comfort and how does this affect energy use and building design? http://www.buildup.eu/faq/european-countries/6645?CommunityId=8100 Visited on April 1^{st}2013
.

Canada, S., Cohen, G., Cable, R., Brosseau, D., and Price, H. 2005. Parabolic Trough Organic Rankine Cycle Solar Power Plant. In *DOE Solar Energy Technologies Program Review Meeting, Denver, Colorado*.

Castaing-Lasvignottes, J. 2001. Aspects thermodynamiques et technico-économiques des systèmes à absorption liquide. Technical report, Conservatoire national des arts et métiers, institut français du froid industriel.

Chunnanond, K. and Aphornratana, S. 2004. Ejectors: applications in refrigeration technology. Renewable & Sustainable Energy Reviews, 8:129–155.

Clean-Energy-Council. 2012. Consumer guide to buying household solar panels (photovoltaic panels). 21.

CLIMASOL. 2002. Technical overview of active techniques. Technical report, CLIMASOL project.

Conde-Petit, M. 2007. Liquid desiccant based air-conditioning systems - LDACS. In *1st European Conference on Polygeneration, Tarragona, Spain*.

Daou, K., Wang, R., and Xia, Z. 2004. Desiccant cooling air conditioning: a review. Renewable & Sustainable Energy Reviews, 10:55–77.

Deng, J., Wang, R., and Han, G. 2011. A review of thermally activated cooling technologies for combined cooling, heating and power systems. Progress in Energy and Combustion Science, 37(2):172 – 203.

DIN18599-7. 2007. Energy efficiency of buildings - Calculation of the energy needs, delivered energy and primary energy for heating, cooling, ventilation, domestic hot water and lighting - Part 7: Delivered energy for air handling and air conditioning systems for non-residential building.

DINCERTO. 2008a. Summary of EN12975 Test Results, annex to Solar Keymark Certificate for Collector "ESE Ecosol 2.32". Technical report, DINCERTO.

DINCERTO. 2008b. Summary of EN12975 Test Results, annex to Solar Keymark Certificate for Collector "Viessmann Vitosol 200-T". Technical report, DINCERTO.

DINCERTO. 2011. Summary of EN12975 Test Results, annex to Solar Keymark Certificate for Collector "AS Solar FK2.3". Technical report, DINCERTO.

Döll, J. 2011. Simulation of Adsorption chiller Using Artificial Neural Networks. In *Proceedings of the 4th International Conference Solar Air-Conditioning, Larnaca, Cyprus*.

Dubois, R. 2011. *Modélisation et simulation du fonctionnement d'une climatisation solaire à adsorption*. Master's thesis, University of Luxembourg.

Duffie, J. and Beckman, W. 1991. *Solar Engineering of Thermal Processes*. A Wiley-Interscience Publication. John Wiley & Sons.

ECOHEATCOOL. 2006. The European Cold Market, ECOHEATCOOL work package 2. Technical report, ECOHEATCOOL project.

Eicker, U. and Pietruschka, D. 2009. Design and performance of solar powered absorption cooling systems in office buildings. Energy and Buildings, 41:81–91.

Eicker, U., Huber, M., Seeberger, P., and Vorschulze, C. 2006. Limits and potential of office building climatisation with ambient air. Energy and Buildings, 38:574–581.

Eicker, U., Pietruschka, D., and Pesch, R. 2012. Heat rejection and primary energy efficiency of solar driven absorption cooling systems. International Journal of Refrigeration, 35(3):729 – 738.

EN14511. 2004. Air conditioniers, liquid chilling packages and heat pumps with electrically driven compressors for space heating and cooling.

EN15251. 2007. Indoor environmental input parameters for design and assessment of energy performance of buildings addressing indoor air quality, thermal environment, lighting and acoustics.

Energieplus. 2012. Energie+, version 7, réalisé par l'université Catholique de Louvain avec le soutien de la Wallonie - DGO4 - Département de l'Énergie et du Bâtiment Durable.

EPICOOL. 2009. Definitie en simulatie van referentiegebouwen, WP1 R02. Technical report, ULG & KULeuven.

EUROSTAT. 2011. Website
http://epp.eurostat.ec.europa.eu/statistics_explained/index.php
/Energy_price_statistics
visited on April 15^{th}2013
.

EUROVENT. 2012. Eurovent certification database. Available at : http://www.eurovent-certification.com/. Technical report, Eurovent Certification.

Evliya, H. 2007. Energy storage for sustainable future: a solution to global warming. In Paksoy, H., editor, *Thermal Energy Storage for Sustainable Energy Consumption*, volume 234 of *NATO Science Series*, pages 87–99. Springer Netherlands.

Evola, G., Pierrès, N. L., Boudehenn, F., and Papillon, P. 2013. Proposal and validation of a model for the dynamic simulation of a solar-assisted single-stage LiBr/water absorption chiller. International Journal of Refrigeration, 36(3):1015 – 1028.

Fanger, P. 1970. *Thermal comfort: Analysis and applications in environmental engineering*. Danish Technical Press.

Fatteh, A. 2011. RATING STANDARD for LIQUID CHILLING PACKAGES. Eurovent Certificatoin Company, RS 6/C/003-2011.

Ferrari, S. and Zanotto, V. 2012. Adaptive comfort: Analysis and application of the main indices. Building and Environment, 49(0):25 – 32.

Fischer, S., Müller-Steinhagen, H., Perers, B., and Bergquist, P. 2001. Collector test method under quasi-dynamic conditions according to the European Standard EN 12975-2. In *ISES World congress, Adelaide, Australia*.

Florides, G., Kalogirou, S., Tassou, S., and Wrobel, L. 2003. Design and construction of a LiBr water absorption machine. Energy Conversion and Management, 44:2483–2508.

Frey, P. 2011. Development of artificial neural network models for sorption chillers. In *ISES2011 conference Kassel*.

Gail Brager, G. and Baker, L. 2008. Occupant satisfaction in mixed-mode buildings. In *Air Conditioning and the Low Carbon Cooling Challenge, Windsor, UK*.

Givoni, B. 2011. Indoor temperature reduction by passive cooling systems. Solar Energy, 85(8):1692 – 1726.

Global-rates. 2013. Website: http://www.global-rates.com/
Visited on April 1^{st}2013
.

Green, M. A., Emery, K., Hishikawa, Y., and Warta, W. 2011. Solar cell efficiency tables (version 37). Progress in Photovoltaics: Research and Applications, 19(1):84–92.

Haller, M. 2012. TRNSYS Type 832 v4.00 Dynamic Collector Model by Bengt Perers Updated Input-Output Reference. Technical report, HSR Hochschule für Technik Rapperswil and SPF Institut für Solartechnik.

Hallström, O., Rupp, J., Koch, L., Wiemken, E., and Nienborg, B. 2010. WP4 Determination of standard applications & most promising markets. Technical report, SolarCombi+ project.

Hartmann, N., Glueck, C., and Schmidt, F. 2011. Solar cooling for small office buildings: Comparison of solar thermal and photovoltaic options for two different European climates. Renewable Energy, 36(5):1329 – 1338.

Hatamipour, M. and Abedi, A. 2008. Passive cooling systems in buildings: Some useful experiences from ancient architecture for natural cooling in a hot and humid region. Energy Conversion and Management, 49(8):2317 – 2323.

Helm, M., Hagel, K., Hiebler, S., Mehling, H., and Schweigler, C. 2009. Performance of a Solar Heating and Cooling System with Absorption Chiller and Latent Heat Storage. In *Proceedings of the 3rd International Conference Solar Air-Conditioning, Palermo, Italy*.

Henning, H. 2007a. *Solar-assisted air conditioning in buildings: a handbook for planners*. Springer.

Henning, H.-M. 2007b. Solar assisted air conditioning of buildings - an overview. Applied Thermal Engineering, 27:w1734–1749.

Henning, H.-M. 2008. Solar Cooling Components and Systems - an Overview. In *in proceedings of OTTI Solar air-conditioning Seminar, Munich, Germany*.

Henning, H.-M. 2011. Solar cooling position paper. Technical report, IEA SHC Task 38 Solar Air-Conditioning and Refrigeration.

Henning, H.-M. and Döll, J. 2012. Solar Systems for Heating and Cooling of Buildings. Energy Procedia, 30(0):633 – 653.

Henning, H.-M., Erpenbeck, T., Hindenburg, C., and Santamaria, I. 2000. The potential of solar energy use in desiccant cooling cycles. International journal of refrigeration, 24:220–229.

Holter, C. 2012. Solar Thermal Cooling in MW Scale. In *SHC2012 : International conference on solar heating and cooling for buildings and industry*.

Hoos, T. 2012. *Einsparpotential und ökonomische Analyse der energetischen Sanierung staatlicher Gebäude in Luxemburg*. Ph.D. thesis, University of Luxembourg.

Huld, T., Müller, R., and Gambardella, A. 2012. A new solar radiation database for estimating PV performance in Europe and Africa. Solar Energy, 86(6):1803 – 1815.

Hung, T., Shai, T., and Wang, S. 1997. A review of organic rankine cycles (ORCs) for the recovery of low-grade waste heat. Energy, 22(7):661 – 667.

IBGE. 2006. Bilan énergétique de la région Bruxelloise 2004. Technical report, Institut bruxellois pour la gestion de l'environnement IBGE.

ICOGEN. 2009. Product description ICOGEN-ClimateWell DB220. Technical report, ICOGEN company.

IEA-PVPS. 2011. TRENDS IN PHOTOVOLTAIC APPLICATIONS Survey report of selected IEA countries between 1992 and 2010. Technical report, IEA-PVPS Task 1 report.

IMT-Solar. 2009. Standard Test Conditions (STC) in the Photovoltaic(PV) Industry. Technical report, IMT-Solar company.

INVENSOR. 2010. Adsorption Chiller InvenSor LTC 09. Technical report, INVENSOR Company.

ISO7730. 2005. Ergonomics of the thermal environment - Analytical determination and interpretation of thermal comfort using calculation of the PMV and PPD indices and local thermal comfort criteria.

ISO/FDIS13370. 2007. Thermal performance of buildings - Heat transfer via the ground - Calculation methods.

Jalalzadeh-Azar, A. A. 2005. Thermally activated desiccant technology for heat recovery and comfort. ASME Advanced Energy Systems Division Newsletter.

Kalogirou, S. 1998. Use of parabolic trough solar energy collectors for sea-water desalination. Applied Energy, 60(2):65 – 88.

Kalogirou, S. 2009. Thermal performance, economic and environmental life cycle analysis of thermosiphon solar water heaters. Solar Energy, 83(1):39 – 48.

Kohlenbach, P. and Dennis, M. 2010. Solar cooling in Australia: The future of air-conditioning? In *9th IIR Gustav Lorentzen Conference, Sydney, Australia*.

Kou, Q., Klein, S., and Beckman, W. 1998. A method for estimating the long-term performance of direct-coupled PV pumping systems. Solar Energy, 64(1?3):33 – 40.

Lachance, D., Bernier, M., and Castaing-Lasvignottes, J. 2002. Simulation dynamique d'une machine à adsorption : application à un cycle bi-étagé. In *E-Sim 2002 : the Canadian Conference on Building Energy Simulation.*, page 7.

Liu, H. 2010. *Stockage inter-saisonnier d'énergie solaire pour l'habitat par absorption*. Ph.D. thesis, Université de Grenoble, France.

Marc, O., Lucas, F., Sinama, F., and Monceyron, E. 2009. Experimental investigation of a solar cooling absorption system operating without any backup system under tropical climate. Energy and Buildings, 42:774–782.

Mavroudaki, P., Beggs, C., Sleigh, P., and Halliday, S. 2002. The potential of solar powered single-stage desiccant cooling in southern Europe. Applied Thermal Engineering, 22:1129–1140.

McCartney, K. J. and Nicol, J. F. 2002. Developing an adaptive control algorithm for Europe. Energy and Buildings, 34(6):623 – 635.

Menberg, K., Bayer, P., Zosseder, K., Rumohr, S., and Blum, P. 2013. Subsurface urban heat islands in German cities. Science of The Total Environment, 442(0):123 – 133.

Mugnier, D. 2002. *Rafraîchissement solaire de locaux par sorption : optimisation théorique et pratique*. Ph.D. thesis, Ecole des Mines Paris.

Mugnier, D. 2011. Quality assurance and support measures for Solar Cooling. Technical report, IEA SHC Task 48.

Napolitano, A., Sparber, W., Thür, A., Finocchiaro, P., and Nocke, B. 2011. Monitoring Procedure for Solar Cooling Systems. Technical report, Task 38 Report, Solar Air-Conditioning and Refrigeration.

NBN-EN13779. 2004. Ventilation dans les bâtiments non résidentiels - Exigences de performances pour les systèmes de ventilation et de climatisation.

NBN-EN442. 2004. - Radiateurs et convecteurs - Partie 1: spécifications et exigences techniques.

Neyer, D. and Streicher, W. 2011. Monitoring and simulation results of two small scale solar cooling plants. In *Proceedings of the 4th Solar Air-Conditioning Conference, Larnaca, Cyprus*.

Nowag, J., Boudéhenn, F., Denn, A. L., Lucas, F., Marc, O., Raduslescu, M., and Papillon, P. 2012. Calculation of Performance Indicators for Solar Cooling, Heating and Domestic Hot Water Systems. Energy Procedia, 30(0):937 – 946.

Onda, N., Yokoyama, T., Oka, M., Homma, R., and Kajiyama, K. 2009. Demonstration and field test of a solar air conditioning system with an absorption chiller/heater operated with solar thermal energy and/or fuel fas for commercial buildings. In *Proceedings of the 3rd International Conference Solar Air-Conditioning, Palermo, Italy*.

Ortiz, O., Bonnet, C., Bruno, J. C., and Castells, F. 2009. Sustainability based on LCM of residential dwellings: A case study in Catalonia, Spain. Building and Environment, 44:584–594.

Pagliano, L. 2010. Sustainable summer comfort: Comfort models. Technical report, Austrian Energy Agency.

Pink, W. 2010. Pink Absorption chiller. In *OTTI Solar ai-conditioning seminar, June 2010*.

Pollerberg, C., Kauffeldb, M., Oezcanb, T., Kofflerb, M., Hanua, L., and Doetscha, C. 2012. Latent heat and cold storage in a solar-driven steam jet ejector chiller plant. In *Proceedings of the International Conference on Solar Heating and Cooling for buildings and Industry, San Francisco, USA*.

Preisler, A. 2008. Reduction of costs of Solar Cooling systems - Final Report - Publishable Part.

Pridasawas, W. 2006. *Solar-Driven Refrigeration Systems with focus on the Ejector Cycle*. Ph.D. thesis, KTH Royal Institute of Technology, Sweden.

Quoilin, S. 2007. *Experimental Study and Modeling of a Low Temperature Rankine Cycle for Small Scale Cogeneration*. Master's thesis, University of Liège.

Riepl, M., Loistl, L., Gurtner, R., Helm, M., and Schweigler, C. 2011. Energetic and Economic Analysisof a Solarthermal Assisted Energy System for Flexible Cooling and Heating. In *Proceedings of the 4th International Conference Solar Air-Conditioning, Larnaca, Cyprus*.

Riepl, M., Loistl, L., Gurtner, R., Helm, M., and Schweigler, C. 2012. Operational Performance Results of an Innovative Solar Thermal Cooling and Heating Plant. In *Proceedings of the International Conference on Solar Heating and Cooling for buildings and Industry, San Francisco, USA*.

Rohsenow, W., Hartnett, J., and Cho, Y. 1998. *Handbook of Heat Transfer*. McGraw-Hill Handbook. McGraw-Hill Companies,Incorporated.

Rosiek, S. and Batlles, F. J. 2009. Integration of the solar thermal energy in the construction: Analysis of the solar-assisted air-conditioning system installed in CIESOL building. Renewable Energy, 34:1423–1431. 0960-1481 doi: 10.1016/j.renene.2008.11.021.

SACE. 2003. Solar Air Conditioning in Europe : evaluation report (NNE5/2001/25). Technical report, SACE project.

Saelens, D., Leenknegt, S., Jansens, A., Goethals, K., Feldheim, V., Altdorfer, B., De Paepe, M., and Lemort, V. 2009. Implementatie aanpassingen energieprestatiebeschrijving voor koeling, WP5 R15, deliverable EPICOOL project. Technical report.

Sajonz, M., Zeine, C., and GmbH, A. 2001. *Verbrauchskennwerte 1999: Energie- und Wasserverbrauchskennwerte in der Bundesrepublik Deutschland ; Forschungsbericht der ages GmbH Münster*. ages.

Santamouris, M. 2003. *Solar Thermal Technologies for Buildings: The State of the Art*. Buildings, Energy, Solar Technology. James & James.

Santamouris, M. 2012. Cooling the cities ? A review of reflective and green roof mitigation technologies to fight heat island and improve comfort in urban environments. Solar Energy, (0).

Schaefer, L. A. 2000. *Single Pressure Absorption Heat Pump Analysis*. Ph.D. thesis, Georgia Institute of Technology.

Schicktanz, M., Hügenell, P., and Henninger, S. 2012. Evaluation of methanol/activated carbons for thermally driven chillers, part II: The energy balance model. International Journal of Refrigeration, 35(3):554 – 561.

SCHOTT. 2003. Schott Evacuated Tube Collector ETC16. Technical report, SCHOTT-Rohrglas Gmbh.

SHARP. 2006. SHARP NDL3E62 data sheet. Technical report, SHARP.

Singh, P. L., Sarviya, R., and Bhagoria, J. 2010. Thermal performance of linear Fresnel reflecting solar concentrator with trapezoidal cavity absorbers. Applied Energy, 87(2):541 – 550.

Soltech. 1998. Système photovoltaïque pour les instituts d'enseignement: Manue d'utilisation pour le système photovoltaïque raccordé au réseau. Technical report.

SONNENKLIMA. 2002. Desiccant Cooling system: Description of the technology. Poster from the workshop at AIRCONTEC trade fair, Frankfurt (Germany), April 2002.

SORTECH. 2008. SorTech Adsorptionskältemaschine : Planungsanleitung. Technical report, SorTech company.

SORTECH. 2009. Adsorption chiller ACS08/ACS15. Technical report, SORTECH AG company.

Sourbron, M. and Helsen, L. 2011. Evaluation of adaptive thermal comfort models in moderate climates and their impact on energy use in office buildings. Energy and Buildings, 43(2?3):423 – 432.

Sparber, W., Napolitano, A., Besana, F., Thür, A., Nocke, B., Finocchiaro, P., Nujedo Nieto, L., Rodriguez, J., and Núnez, T. 2009a. Comparative results of monitored solar assisted heating and cooling installations. In *Proceedings of the 3rd International Conference Solar Air-Conditioning, Palermo, Italy*.

Sparber, W., Napolitano, A., Eckert, G., and Preisler, A. 2009b. State of the art on existing solar heating and cooling systems. Technical report, IEA-SHC Task 38 Report, Solar Air-Conditioning and Refrigeration.

Stabat, P., Sarrade, L., Rogiest, C., Franck, P.-Y., Caciolo, M., Bertagnolio, S., and André, P. 2011. Analysis of building heating and cooling demands in the purpose of assessing the reversibility and heat recovery potentials. Technical report, IEA ECBCS Task 48 Heat Pumping and Reversible Air Conditioning.

Stryi-Hipp, G., Weiss, W., and Mugnier, D. 2012. Strategic Research Priorities for Solar Thermal Technology. Technical report, European Solar Thermal Technology Panel.

Suri, M., Huld, T. A., Dunlop, E. D., and Ossenbrink, H. A. 2007. Potential of solar electricity generation in the European Union member states and candidate countries. Solar Energy, 81(10):1295 – 1305.

Syed, A., Izquierdo, M., Rodriguez, P., Maidment, G., Missenden, J., Lecuona, A., and Tozer, R. 2005. A novel experimental investigation of a solar cooling system in Madrid. International Journal of Refrigeration, 28:859–871.

Tatsidjodoung, P., Pierrès, N. L., and Luo, L. 2013. A review of potential materials for thermal energy storage in building applications. Renewable and Sustainable Energy Reviews, 18(0):327 – 349.

THERMAX. 2012. Specifications of Themax Model HD10ACU http://www.thermax-europe.com/french/hot-water-spec-high-temp.aspx Visited on December 27^{th}2012.

Thewes, A. 2011. *Energieeffizienz neuer Schul- und Bürogebäude in Luxembourg basierend auf Verbrauchsdaten und Simulationen*. Ph.D. thesis, University of Luxembourg.

Thomas, S. and André, P. 2009. Control strategies study of a complete solar assisted air conditioning system in an office building using TRNSYS. In *Proceedings of the 3rd International Conference Solar Air-Conditioning, Palermo, Italy*.

Thomas, S. and André, P. 2010. Numerical simulation and performance assessment of an absorption solar air-conditioning system coupled with an office building. In *Proceedings of 8th International Conference on System Simulation in Buildings, Liège, Belgium,*.

Thomas, S. and André, P. 2012. Numerical simulation and performance assessment of an absorption solar air-conditioning system coupled with an office building. Building Simulation, 5 Issue 3:243–255.

Thomas, S., Hennaut, S., Maas, S., and André, P. 2012. Experimentation and Simulation of a Small-Scale Adsorption Cooling System in Temperate Climate. Energy Procedia, 30:704 – 714.

Thornton, J. 2010. *TRNSYS TYPE 511: Dry fluid cooler*. TESS Thermal Energy Specialists.

Tozer, R. M. and James, R. W. 1997. Fundamental thermodynamics of ideal absorption cycles. International Journal of Refrigeration, 20(2):120 – 135.

TRNSYS. 2012. *TRNSYS simulation studio, Version 16 to 17.1 Licensed to University of Liège*.

Vitte, T. 2007. *Le froid solaire par dessication appliqué au bâtiment : Proposition d'un stratégie de régulation du système*. Ph.D. thesis, Institut national des sciences appliquées de Lyon.

Vukits, M., F, F. A., and Thür, A. 2011. Operation and energy performance as well as simulation results of two solar cooling plants in Gleisdorf. In *4th Solar Air-Conditioning Conference, Larnaca, Cyprus.*.

Wall, M. and Bülow-Hübe, H. 2003. Solar Protection in Buildings. Technical report, Lund Institute of Technology.

Wang, R. and Oliveira, R. 2006. Adsorption refrigeration - An efficient way to make good use of waste heat and solar energy. Progress in energy and combustion science, 32:424–458.

Wang, X. and Chua, H. T. 2007. Two bed silica gel-water adsorption chillers: An effectual lumped parameter model. International Journal of Refrigeration, 30:1417–1426.

WESPER. 2005. Pompes à chaleur réversibles air-eau VLH 504 1204. Technical report, WESPER.

Wiemken, E., Petry-Elias, A., Wewior, J., Koch, L., and Nienborg, B. 2010. Performance and Perspectives of Solar Cooling. In *Proceedings of Eurosun 2010, International Conference on Solar Heating, Cooling and Buildings, Graz, Austria*.

YAZAKI. 2008. Water Fired Chiller/Chiller-Heater WFC-S Series. Technical report.

Zahler, C., Berger, M., and Louw, J. 2011. Largest Solar Cooling System in the Middle East for a Showcase Football Stadium in Qatar. In *Proceedings of the 4th International Conference Solar Air-Conditioning, Larnaca, Cyprus*.

Zambrano, D., Bordons, C., Garcia-Gabin, W., and Camacho, E. F. 2008. Model development and validation of a solar cooling plant. International Journal of Refrigeration, 31(2):315 – 327.

Zetzsche, M., Koller, T., Brendel, T., and Müller-Steinhagen, H. 2009. Solar cooling with an ice-storage back-up system. In *Proceedings of the 3rd International Conference Solar Air-Conditioning, Palermo, Italy*.

Zhai, X. Q., Qu, M., Li, Y., and Wang, R. Z. 2011. A review for research and new design options of solar absorption cooling systems. Renewable and Sustainable Energy Reviews, 15:4416–4423.

Ziegler, F. 2002. State of the art in sorption heat pumping and cooling technologies. International journal of refrigeration, 25:450–459.

Zweifel, G., Dorer, V., Koschenz., M., and Weber, A. 1995. Building energy and systems simulation programs : model development, coupling and integration. In *proceedings of Building Simulation 1995, Madison, USA*.

Building properties

.1 Typical existing European office building

This paragraph comes mainly from the published work *Numerical simulation and performance assessment of an absorption solar air-conditioning system coupled with an office building* (Thomas and André, 2012). The building is inherited from the IEA ECBCS Task 48 project (Stabat *et al.*, 2011) and is representative of the European building stock. It is a twelve identical floors, 15000 m^2 building with an average of 1000 persons occupancy. From the modelling point of view, only one floor is modelled but all floors can be treated similarly. A three floor building is considered for the solar collector field design.

.1.1 Geometrical description

Geometrical description of one floor is presented on figure A.1. Five zones are considered for a total of 1250 m^2. The room surfaces and glazed surfaces are defined in table A.1

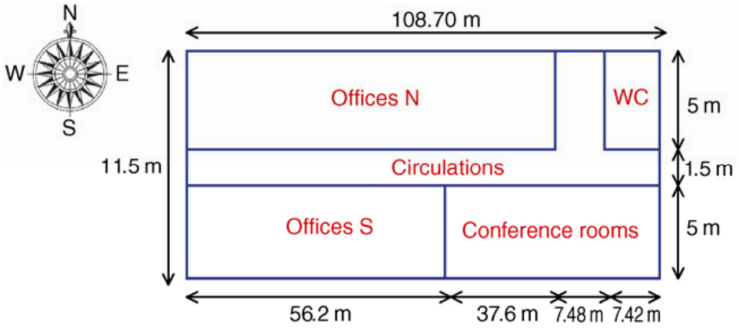

Figure A.1: Office building floor geometry (Stabat *et al.*, 2011)

.1.2 Envelope

The building studied is representative of existing buildings, the insulation is thus not very efficient. North and South façade are similarly largely glazed while East and West are blind walls. Rooms are 3 meters high while windows take up 2 meters. Wall constitution and U values are described in table A.2.

Zone	Surface area for one floor (m^2)	Glazed surface (m^2) N	S	E	W
Toilets	37	11.1	0	0	0
offices S	281	0	84.3	0	0
offices N	469	140.7	0	0	0
meeting room	262.5	0	78.7	0	0
circulations	200.5	11.2	0	0	0
Totals	1250	163	163	0	0

Table A.1: Zones surfaces and glazed surfaces

	Constitution	U value ($W/m^2/K$)
Outside wall	Outside layer : Cement 0.13m (ρ=1900 kg/m^3 λ=0.58 W/(m K) c_p= 1000 J/(kg K)) Insulating material 0.024m (ρ=56 kg/m^3 λ=0.029 W/(m K) c_p= 1220 J/(kg K)) Inside layer: plaster 0.012m (ρ=1860 kg/m^3 λ=0.72 W/(m K) c_p= 840 J/(kg K))	0.8
Windows	Double glazing of 0.004 m width for each glazing and 0.008 m air space.	2.95
Floor & ceiling	Cement 0.1m c_p= 1000 J/(kg K)) (ρ=1900 kg/m^3 λ=0.58 W/(m K)	5.8
Roof	Outside layer : Cement 0.13m (ρ=1900 kg/m^3 λ=0.58 W/(m K) c_p= 1000 J/(kg.K)) insulating material 0.06m (ρ=56 kg/m^3 λ=0.029W/(m K) c_p= 1220 J/(kg.K)) Inside layer: plaster 0.012m (ρ=1860 kg/m^3 λ=0.72W/(m K) c_p= 840 J/(kg.K))	0.4
Inner wall	plaster 0.02 m (ρ=1860 kg/m^3 λ=0.72W/(m K) c_p = 840 J/(kg K))	36

Table A.2: Office building wall constitution

.1.3 Internal heat gains

People

Offices and conference room have two different schedules and occupancy rates. The sizing of the offices is defined as one person per 12 m^2 (1 person per 3.5 m^2 for conference room). The sensible heat released by each person is supposed to be 105 W and the moisture release is 0.09 kg/h (Stabat *et al.*, 2011). Occupancy profile are defined in figure A.2. The ratio is the current occupancy divided by the sizing value. No consideration about holiday is taken into account. During weekend, appliances gains as well as occupancy are zero.

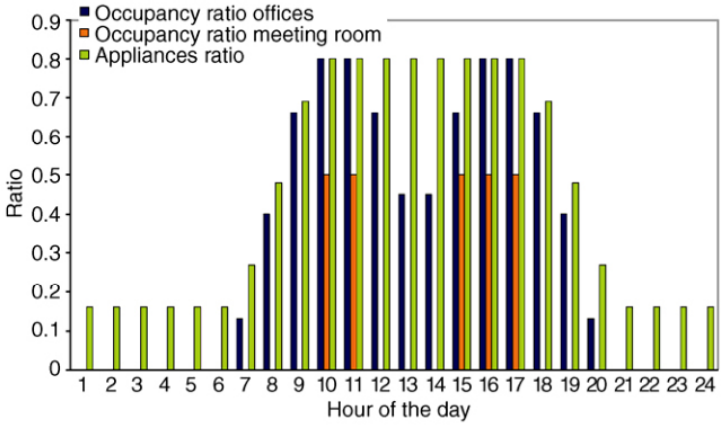

Figure A.2: Office building occupancy profile (Stabat *et al.*, 2011)

Appliances

Similarly to previous paragraph, appliances gains are defined. Figure A.2 notifies that the appliances ratio for a sizing value is 15 W/m^2. The appliances are essentially computers; these gains exist only in the offices zones.

Lighting system

The lighting power is set to 18 W/m^2 in offices and conference rooms, 12 W/m^2 in the circulations and 6W/m^2 in the toilets. Based on the work of Alessandrini *et al.* (2006) the use of artificial lighting depends on natural light available for workers. Between 0 and 100 Lux, the use of artificial lighting is 90% ; between 100 and 700 Lux, it drops linearly to 30% ; it falls to 0% when the available natural light is higher than 2500 Lux. The implemented curve is represented in figure A.3. The available light is computed with TRNSYS regarding the solar energy through the windows. A basic law is implemented and considers luminous efficacy of solar radiation equal to 100 lm/W. Lights are switched on only during occupancy, in toilets and circulation zone it is always on from 6 am to 7 pm. Two typical simulated days (summer and winter) are represented

in figure A.4. The glazed façades decrease significantly the artificial lighting needs.

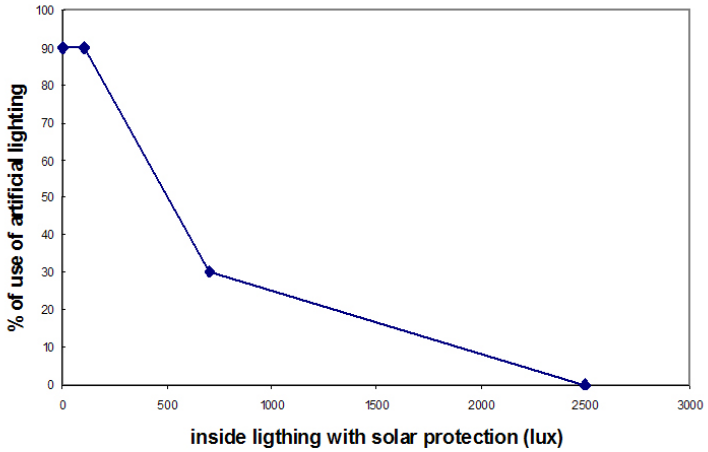

Figure A.3: Average use of artificial lighting (Alessandrini *et al.*, 2006)

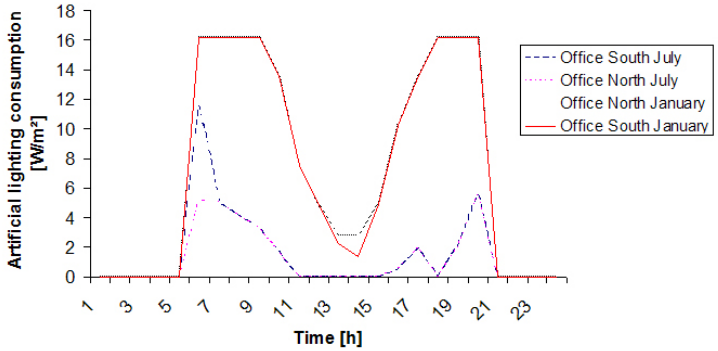

Figure A.4: Artificial lighting consumption for two days in January and July

Solar protections

Some manual external solar protections are modelled. They implement the behaviour of the people in the zones (Alessandrini *et al.*, 2006). When the solar protections are completely closed, the energy transmission is 20% (in other words the efficiency of solar protections is 80%). The opening of solar protections is made by the user; depending on the outside luminance, the solar protections are closed from 7 to 45%. The implemented curve is shown in figure A.5. The position of solar protections during non occupancy is defined as equal

to those in the last hour of occupancy. An example of curves for two summer days is represented in figure A.6. This correlation based on a mean user implies a low shaded radiation.

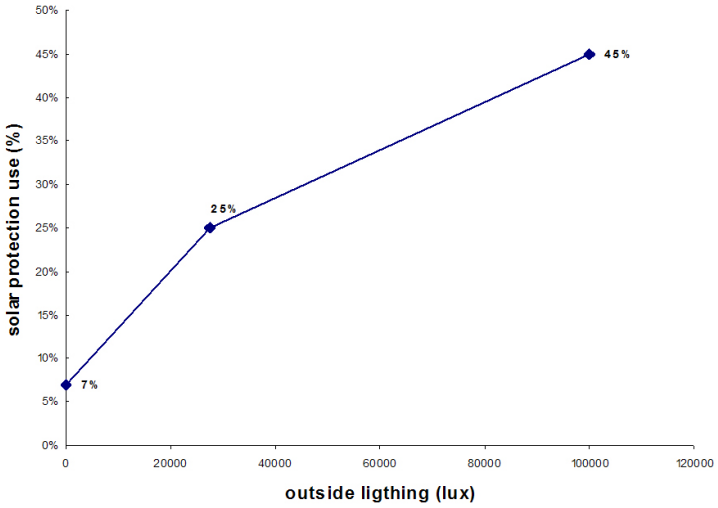

Figure A.5: Average use of solar protections (Alessandrini *et al.*, 2006)

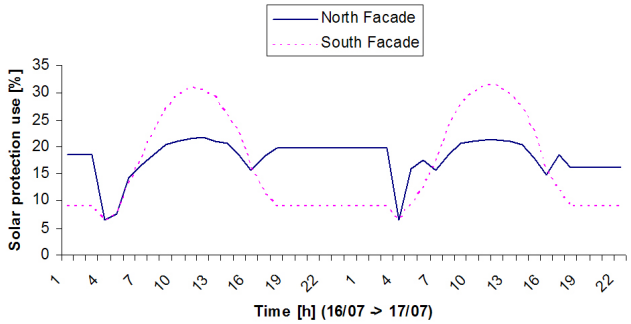

Figure A.6: Use of solar protections during a summer period (16^{th} to 17^{th} of July)

.1.4 Ventilation and infiltration

Constant mass flow rate is blown in the building during occupancy (figure A.7), it corresponds to 25 m^3/h fresh air per person for offices and 30 m^3/h per person for conference room. No heat recovery is implemented. When there is no occupancy, the mechanical ventilation is switched off; infiltration is then

equal to 0.373 volume per hour. For all zones except conference room the power of ventilator is 330W (single flux ventilation). For conference room, a double flux ventilation without recovery is implemented, it leads to fan power 2 times 470 W (0.21 W/(m^3.h)). This specific consumption leads to SPF class 3 (NBN-EN13779, 2004).

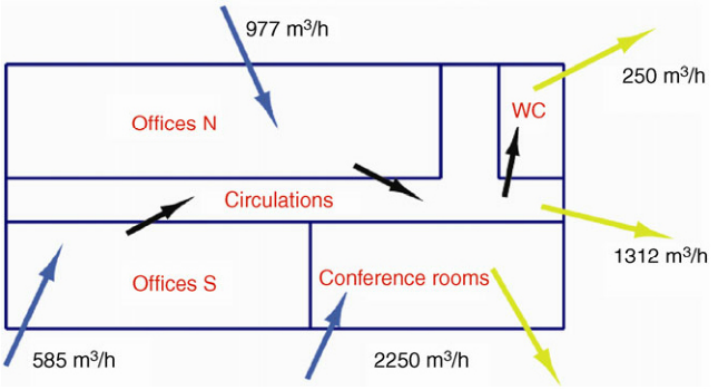

Figure A.7: Ventilation mass flows for one floor

.2 Belgian small office building

This building has been defined in the frame of the EPICOOL project (EPICOOL, 2009). It is an office building representative of what could be built in Belgium today. Three levels of energy performance are defined : "acceptable, good, very good". The "acceptable" case is the minimal requirements of the Brussels region energy performance directive translation. The main characteristics are picked up from EPICOOL (2009) and detailed hereunder. The heating and cooling systems have also been defined in the EPICOOL but are not used in this work.

.2.1 Geometry

This paragraph comes from EPICOOL (2009) and refers to figure A.8.

The small office building consists of three floors and has main orientations north and south. The ground floor is 50% glazed (vertical full height windows) and contains cafeteria (E-side), lobby (W-side) and central dark zone with technical and storage area and sanitary. The first and second floor are identical: open plan office at the area near the façade and central dark zone with sanitary and meeting rooms. It is a stand-alone building. The geometry can be seen in figure A.8.

The zoning is defined as follows:

- cafeteria (orange): ground floor, 3 façades N, E and S (380 m^2)

- lobby (light green): ground floor, 3 façades N, W and S (831 m^2)
- technical and storage (brown): mainly ground floor (under meeting rooms), with vertical channels through 1st and 2nd floor, flanked by sanitary zone, no façade (205 m^2)
- sanitary (blue): identical over three floors, two sanitary blocks per floor in the dark zone, no façade (238 m^2)
- open plan office (dark green): 1st and 2nd floor, area surrounding dark zone, 4 façades N, E, W and S (2415 m^2 altogether)
- meeting rooms (red): 1st and 2nd floor, inside dark zone, flanked by sanitary blocks, no façade (372 m^2)

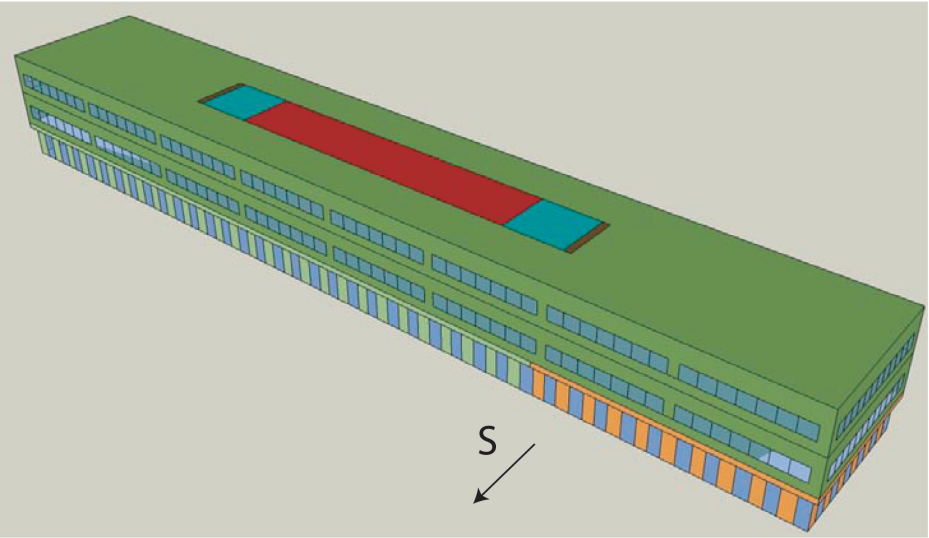

Figure A.8: Small office geometry (EPICOOL, 2009)

The total available area is 4403 m^2 (volume 18350 m^3) while the percentage of windows area is 19.8 % of available floor area, it is shared on all façades without any orientation considerations. All the zones can be heated or cooled.

.2.2 Walls and windows

The walls U-Values are defined in the following table as well as the windows characteristics for the three energy performances. The constitution of the walls is not detailed here. The external walls have an insulating layer on the external side of the wall. The U values are given taking the external thermal resistances (internal and external surfaces).

	Unit	Building energy performance level		
U value	$[W/(m^2.K)]$	ACCEPTABLE	GOOD	VERY GOOD
External wall		0.37	0.28	0.2
Floor-ground		0.33	0.18	0.16
Roof		0.29	0.25	0.19
Window frame		2.40	1.8	0.9
Glazing		1.17	1.17	0.64
Mean U value		**0.55**	**0.45**	**0.32**
Glazing g-value	[–]	0.38	0.38	0.46

Table A.3: U and g values for the small office building (EPICOOL, 2009)

.2.3 Ventilation - infiltrations

About the infiltrations, the three energy level cases are defined in the following table A.4. The fresh air flow rate equals the extracted air flow rate for each zone. There are no air flow rate transfer between zones. It implies higher mass flows and thus higher fan consumption. The heat recovery on the ventilation air flow rate is implemented whatever the building energy level. One heat exchanger is installed for the entire building, it recovers 65% of sensible energy. The heat exchanger is no more used if the extracted air flow rate is higher than 24°C and the external temperature is lower than the extracted flow temperature. The ventilation is switched on two hours before occupancy and stops at 8 pm.

The ventilation flow comes from the designed number of people per zone surface and the required air flow rate for each person. The designed values are given:

- offices: 1 person per 15 m^2.
- meeting room: 1 person per 3.5 m^2.
- lobby: 1 person per 10 m^2.
- cafeteria: 1 person per 1.5 m^2.

The air mass flow rate is 36 m^3/h per person, the total mass flow for each zone is described in table A.4.

.2.4 Internal gains

The internal gains in office building is split into three parts: people, light, equipments (including fans).

People

Their are internal gains due to people only during weekdays, the occupancy profile of the zones is presented in figure A.9 where the fraction of designed

		Building energy performance level		
Infiltrations	Units	ACCEPTABLE	GOOD	VERY GOOD
Infiltrations in test conditions	n_{50} $[h^{-1}]$	3.85	3	0.6
Infiltrations in use				
Cafeteria	h^{-1}	0.222	0.173	0.034
Offices	h^{-1}	0.1462	0.114	0.022
Lobby	h^{-1}	0.233	0.181	0.036
Technical	h^{-1}	0.132	0.103	0.02
Meeting	h^{-1}	0.058	0.045	0.009
Sanitary	h^{-1}	0.082	0.064	0.012
Ventilation mass flow		Same for each performance level		
Cafeteria	m^3/h	5500		
Offices	m^3/h	5800		
Lobby	m^3/h	1850		
Technical	m^3/h	261		
Meeting	m^3/h	2290		
Sanitary	m^3/h	3400		
Total	m^3/h	19101		

Table A.4: Small office infiltrations and ventilation flow rates (EPICOOL, 2009)

occupancy is displayed as well as the total number of people in the building. The designed occupancy for the zones is then defined:

- Cafeteria: 107 persons
- Lobby: 136 persons
- Office: 161 persons
- Meeting room: 103 persons

The activity of people is set to 1.2 met whatever the zone meaning a sensible gain of 81.7 W and a latent gain of 44 W.

Lights

Efficient lights have been selected for this building, the installed power is defined in the table A.5.

According to the required illumination between 150 and 500 LUX (depending on the zone), the installed power is 1.84 W/m^2 for 100 LUX for each zone and achieves 1.58 W/m^2 for 100 LUX for the "very good" level.

Appliances

During the occupancy period (from 9 am to 6 pm), the computers and other devices counts for a mean value of 7.52 and 9.43 W/m^2 respectively for offices and meeting room. There are no equipment considered in the other zones.

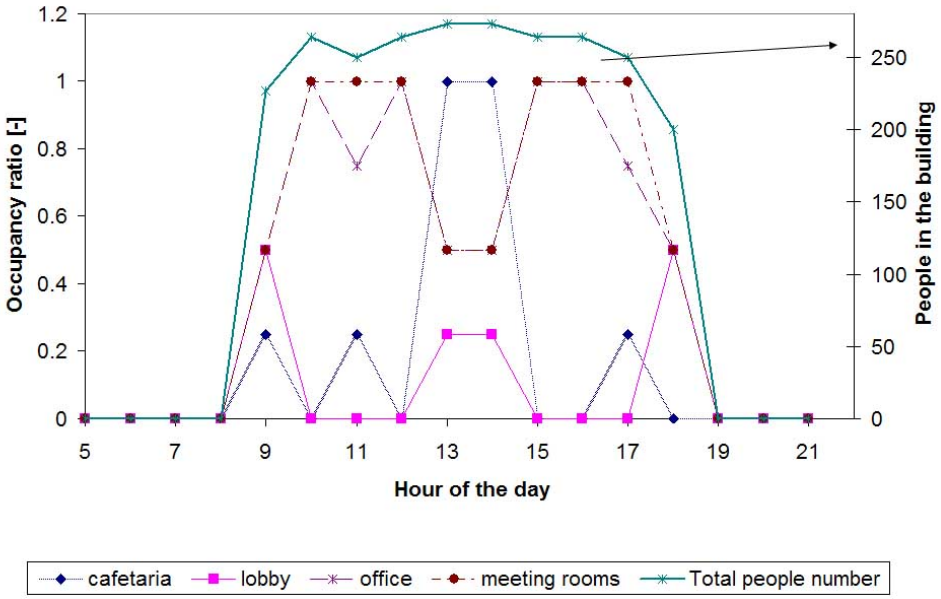

Figure A.9: Small office occupancy (EPICOOL, 2009)

		Building energy performance level		
Light installed power	Units	ACCEPTABLE	GOOD	VERY GOOD
Cafeteria	W/m^2	3.68	3.16	3.16
Lobby	W/m^2	3.68	3.16	3.16
Technical	W/m^2	3.68	3.68	3.16
Sanitary	W/m^2	2.76	2.76	2.37
Office	W/m^2	9.19	7.9	7.9
Meeting	W/m^2	9.19	7.9	7.9

Table A.5: Small office light installed power (EPICOOL, 2009)

The **fans** power is not transmitted in the air flow rate. Nevertheless, their consumption is interesting for the whole building consumption analysis. The supply fans have a specific power of 0.35 $W/(m^3.h)$ while the extract fans have 0.25 $W/(m^3.h)$ which means a SFP class 3. It involves a total of 9047 W for building fans consumption.

More information about energy performance classification of fans can be found in standard NBN-EN13779 (2004). The SFP classes are mentioned in the table A.6.

Fan class	Fan power $[W/m^3.s]$	Fan power $[W/m^3.h]$
SFP 1	< 500	< 0.139
SFP 2	500 750	$0.139 - 0.208$
SFP 3	750 1250	$0.208 - 0.347$
SFP 4	1250 2000	$0.347 - 0.556$
SFP 5	> 2000	> 0.556

Table A.6: Fan energy efficiency classification (NBN-EN13779, 2004)

.2.5 Shading

The house has a shading mask taking into account its surroundings. The elevation of this shading mask is 7.5° on every azimuth.

.2.6 Ground temperature

The studied building does not contain any cellar, it is directly in contact with the ground. Its temperature and heat flow through the basement is computed according to the standard ISO/FDIS13370 (2007). Taking into account the shape of the building, the properties of the ground wall, a virtual layer is defined in addition to the existing layer. This computation is more accurate, it handles a variable ground temperature and the thermal influence of the building on the basement.

.3 Belgian residential building

This building has also been defined in the frame of the EPICOOL project (EPICOOL, 2009). The shape and size of this building are representative of Belgian stock family houses (4 people). Three levels of energy performance are defined : "acceptable, good, very good". The "acceptable" case is the minimal requirements of the Brussels region energy performance directive translation. The "very good" case get closer to the passive house standard. The main characteristics are picked up from EPICOOL (2009) and detailed hereunder. The heating and cooling systems have also been defined in the EPICOOL project but are not used in this work.

.3.1 Geometry

The building is a two floors detached house with an attic. The geometry is displayed in figure A.10. The available area of ground floor is 143 m^2 while the useful area for first floor is 74 m^2 (part of the zone which has not a Mansard roof). The total glazing area is 29.6 m^2 corresponding to 14.1 % of available floor area, mainly installed on the south facade. There are three thermal zones, both ground and first floor are heated-cooled.

.3.2 Walls and windows

The walls U-Values are defined in the following table as well as the windows characteristics for the three energy performances. The constitution of the walls is not detailed here. The external walls have an insulating layer between two

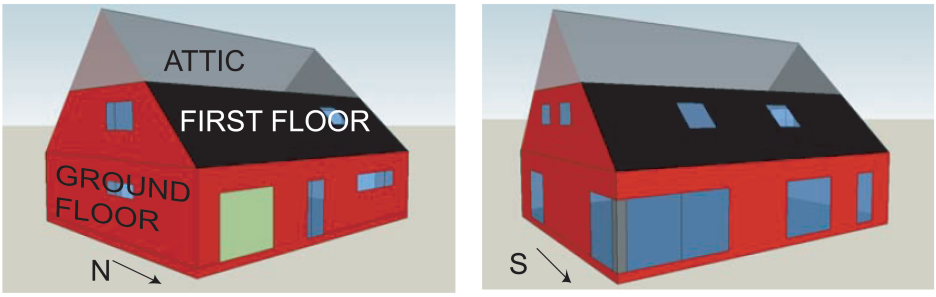

Figure A.10: Detached house geometry (EPICOOL, 2009)

masonries. The U values are given taking the external thermal resistances (internal and external surfaces).

	Unit	Building energy performance level		
U-value	$W/(m^2.K)$	ACCEPTABLE	GOOD	VERY GOOD
External wall		0.27	0.17	0.14
Door		1.55	1.55	0.55
Floor-ground		0.33	0.16	0.13
Roof-attic walls		0.20	0.20	0.13
Window frame		2.40	1.8	0.9
Glazing		1.17	1.17	0.64
Mean U value		**0.38**	**0.29**	**0.19**
Glazing g-value	–	0.58	0.58	0.38

Table A.7: U and g values for the residential building (EPICOOL, 2009)

.3.3 Ventilation - infiltrations

The ventilation and infiltrations are also defined (see table A.8). Mechanical ventilation is used to set the specified mass flow according to the Belgian standard NBN D 50 001. Besides, the "very good" case includes a heat recovery (95% efficiency on sensible load) on the ventilation air flow rate. It will decrease the heating load but not increase the cooling because of the bypass implementation. The heat exchanger is no more used if the extracted air flow is higher than 24°C and the external temperature is lower than the extracted flow temperature. The ventilation is permanently switched on.

.3.4 Internal gains

The internal gains are representative of a residential building. Some schedules are defined for weekdays and weekend. The day period lasts from 8 am to 10 pm during the week and from 8 am to 11 pm during the weekend.

		Building energy performance level		
Infiltrations	Units	ACCEPTABLE	GOOD	VERY GOOD
Infiltrations in test conditions	$n_{50}\,h^{-1}$	8.3	4	0.6
Infiltrations in use				
Ground zone	h^{-1}	0.310	0.15	0.021
First floor	h^{-1}	0.361	0.173	0.028
Ventilation mass flow				
Fresh air	m^3/h	561	561	580
Extracted air	m^3/h	355	355	580

Table A.8: Ventilation and infiltrations for the residential building (EPICOOL, 2009)

People

During the day, the four people have an activity of 1.2 met (81.7 W sensible and 44 W latent) and stand in the ground floor zone. The other period is the night period, the four people stay on the first floor with an equivalent activity of 1 met (68.09 W sensible and 36.67 W latent). It implies a vapour production of 63.3 g/h per people for the day and 52.8 g/h for the night.

Appliances & lights

A mean value for equipment and lighting devices is set. The gains are uniformly distributed along the period (day or night). The heat gain values are defined in table A.9. The total electricity consumption involved by this gains is around 3600 kWh per year (considering an electricity to heat conversion of 100%). The equipments are considered 50% convection - 50 % radiation gains.

	Weekday		**Weekend**	
	Day period *9 am-10 pm*	Night period	Day period *9 am-11 pm*	Night period
Daily sensible load	10.67	6.88	10.42	6.12
Total	17.56		16.54	
People load				
sensible	4.90	2.45	5.23	2.18
latent	2.64	1.32	2.82	1.17
Total people load	11.31		11.40	
Equipment	10.20		9.13	

Table A.9: Residential building internal gains in [kWh/day] (EPICOOL, 2009)

.3.5 Shading

The house has a shading mask taking into account its surroundings. The elevation of this shading mask is 7.5° on every azimuth. Solar protections can be defined depending on the simulation case.

.3.6 Ground temperature

The studied building does not contain any cellar, it is directly in contact with the ground. Its temperature and heat flow through the basement is computed according to the standard ISO/FDIS13370 (2007). Taking into account the shape of the building, the properties of the ground wall, a virtual layer is defined in addition to the existing layer. This computation is more accurate, it handles a variable ground temperature and the thermal influence of the building on the basement.

Publications and Conferences

Publications in international journals

- Thomas, S. André, P. Franck, P-Y. Model validation of a dynamic embedded water base surface heat emitting system for buildings, *Building Simulation: An International Journal*, **2011**, 4, 41-48.
- Thomas, S and André, P. Numerical simulation and performance assessment of an absorption solar air-conditioning system coupled with an office building, *Building Simulation: An International Journal*, **2012**, 5, 243-255.

Publications in national journals

- Hennaut, S. Thomas, S. Davin, E. Skrylnyk, A. Frère, M. André, P. Dynamic simulations of solar combisystems integrating a seasonal sorption storage: Influence of the combisystem configuration, *Strojarstvo (Croatian journal), Journal for Theory and Application in Mechanical Engineering*, **2012**, 54-6.

International Conferences

- Thomas, S and André, P. Simulation based energy consumption calculation of an office building using solar-assisted air conditioning, *Proceedings of Eurosun 2008,1stInternational Conference on Solar Heating, Cooling and Buildings* , Lisbon, Portugal, October 2008.
- Thomas, S and André, P. Dynamic simulation of a complete solar assisted air-conditioning system in an office building using TRNSYS, *Proceedings of Building Simulation 2009*, Glasgow, United Kingdom, July 2009.
- Thomas, S and André, P. Control strategies study of a complete solar assisted air conditioning system in an office building using TRNSYS, *Proceedings of the 3rdInternational Conference Solar Air-Conditioning*, Palermo, Italy, September 2009.
- Thomas, S. Franck, P-Y. André, P. Optimization of dynamic embedded, Water based surface heat (and cold) emitting system for buildings, *Proceedings of the Comsol Conference Europe*, Milano, Italy, October 2009.
- Thomas, S. Hennaut, S. André, P. Combination of experimental and simulated small scale solar air-conditioning system, *Proceedings of EUROSUN 2010, International Conference on Solar Heating, Cooling and Buildings*, Graz, Austria, October 2010.

- Thomas, S and André, P. Numerical simulation and performance assessment of an absorption solar air-conditioning system coupled with an office building, *Proceedings of 8^{th} International Conference on System Simulation in Buildings*, Liège, Belgium, December 2010.

- Hennaut, S. Thomas, S. André, P. Courbon, E. Le Berigot, T. Frère, M. Pré-dimensionnement par simulations dynamiques d'un réacteur de stockage thermochimique assurant l'autonomie d un système solaire combiné, *Proceedings of "Congrès Français de Thermique 2011"*, Perpignan, France, May 2011.

- Hennaut, S. Thomas, S. Davin, E. André, P. Dynamic simulation of residential buildings with seasonal sorption storage of solar energy - parametric analysis, *Proceedings of ISES solar world congress 2011*, Kassel, Germany, September 2011.

- Thomas, S. Maas, S. André, P. Performance assessment of a small-scale adsorption chiller integrated to an already existing solar heating system, *Proceedings of the 4^{th} International Conference Solar Air-Conditioning*, Larnaca, Cyprus, October 2011.

- Thomas, S. Hennaut, S. Maas, S. André, P. Experimentation and Simulation of a Small-Scale Adsorption Cooling System in Temperate Climate, *Proceedings of the International Conference on Solar Heating and Cooling for buildings and Industry SHC2012*, San Francisco, USA, July 2012.

- Hennaut, S. Thomas, S. Skrylnyk, A. Frère, M. André, P. Dynamic simulations of solar combisystems integrating a seasonal sorption storage: Influence of the combisystem configuration, *Proceedings of EUROSUN 2012, International Conference on Solar Heating, Cooling and Buildings*, Rijeka, Croatia, September 2012.

- Carton, J. Thomas, S. Scholzen, F. Energy performance assessment of an existing double-skin façade: measurements and simulation, *Proceedings of the Energy Forum 2012*, Bressanone, Italy, December 2012.

- Thomas, S. Hennaut, S. Maas, S. André, P. Experimentation and modelling of a small-scale adsorption cooling system in temperate climate, Accepted paper for *Building Simulation 2013*, Chambéry, France, August 2013.